Magnetite
–
environmental biogeobattery and heavy metal remediator

Dissertation

der Mathematisch-Naturwissenschaftlichen Fakultät
der Eberhard Karls Universität Tübingen
zur Erlangung des Grades eines
Doktors der Naturwissenschaften
(Dr. rer. nat.)

vorgelegt von
M.Sc. Timm Bayer
aus Berlin

Tübingen
2024

Gedruckt mit Genehmigung der Mathematisch-Naturwissenschaftlichen Fakultät der Eberhard Karls Universität Tübingen.

Tag der mündlichen Qualifikation:	17.05.2024
Dekan:	Prof. Dr. Thilo Stehle
1. Berichterstatter:	Assoc. Prof. Dr. James Byrne
2. Berichterstatter:	Prof. Dr. Stefan Haderlein

What does the world need with just another [scientist]?
What the world needs is good people.

Victor (*1964) and Dorothy Wooten (1934-2011)

Contents

Summary

Iron (Fe) is an essential element widely distributed throughout planet Earth, and is interconnected with various geochemical cycles, such as oxygen, nitrogen, and carbon, because it can be redox cycled between reduced and oxidized states. Due to the abundance of Fe in the environment, as one of the most abundant elements in the crust, microorganisms have developed ways to harvest the energy of the transfer of one electron between reduced and oxidized iron (ferrous Fe(II) and ferric Fe(III), respectively). Ferrous iron can be an electron donor for Fe(II) oxidation, and ferric iron can be an electron acceptor for Fe(III) reduction. This cycling between Fe(II) and Fe(III) has significant consequences for the stability and identity of Fe minerals. Additionally, it can affect the (bio-)availability of the Fe minerals and the contaminants and nutrients associated with the minerals' surface areas. Mixed-valent Fe minerals are unique because they contain both forms of Fe in their crystal structure. Magnetite (Fe_3O_4 or $Fe(II)Fe(III)_2O_4$) is one of the most prominent mixed-valent Fe minerals.

Recent studies have demonstrated that certain microorganisms can utilize Fe(II) or Fe(III) in magnetite as a source or sink for electrons, respectively. This rather unique ability of magnetite to enable electron transport and storage for Fe-metabolizing microorganisms has earned it the name *biogeobattery*. However, the impact of prolonged redox cycling on magnetite's properties and its function as an electron source and sink it not yet clear. Additionally, it is uncertain how the magnetite nanoparticles' interactions with heavy metal contaminants, commonly associated with the surface area, change due to biotic oxidation or reduction of the mineral. Therefore, the goals of this thesis were: (1) to determine the extent of magnetite oxidation and reduction during continued redox cycles by Fe-metabolizing microorganisms, (2) to understand how this process affects the properties of magnetite's ability to be used by Fe-metabolizing microorganisms, (3) to examine whether magnetite nanoparticles can indefinitely serve as a biogeobattery or to determine which factors lead to a decrease in biogeobattery capacity, and lastly, (4) to examine the importance of microbially-driven magnetite oxidation and reduction on the adsorption capacity and efficiency towards environmentally relevant heavy metal contaminants.

Firstly, we discovered that the nitrate-reducing Fe(II)-oxidizing enrichment culture, 'culture KS', could utilize synthesized magnetite nanoparticles as an electron source.

Afterwards, we successfully demonstrated that magnetite was utilized as a biogeobattery for 41 days in two consecutive cycles of oxidation by culture KS and reduction by *Geobacter sulfurreducens*. The Fe(III) reduction by *G. sulfurreducens* resulted in reductive dissolution of the mineral, followed by a re-precipitation of secondary minerals, mainly vivianite, an Fe(II)-phosphate mineral ($Fe(II)_3(PO_4)_2,8H_2O$). This dissolution-reprecipitation process was more pronounced during the second reduction. Interestingly, the electron-charged magnetite benefited the oxidizers, as shown by a greater change in the Fe(II)/Fe(III) ratio during the second oxidation. During oxidations, a lower threshold of the Fe(II)/Fe(III) ratio was determined, possibly reflecting the thermodynamic limitations for microbial magnetite oxidation in our system. A slight passivation of the surface due to maghemitization of magnetite was expected, which was, however, not recorded in any performed measurements.

These findings have significant implications for understanding the role of magnetite as a biogeobattery in the environment. Repeated redox cycles caused magnetite to become less stable due to reductive dissolution but more favourable as an electron source for Fe(II) oxidation due to increased electron load after reduction. This suggests that magnetite nanoparticles will no longer function as biogeobattery if they undergo multiple redox cycles and reductive dissolution. Enhanced oxidation (after reduction) might cause maghemitization, which could passivate the surface area. The biogeobattery-loss could be attenuated by additional processes that produce magnetite, such as Fe(II) oxidation or Fe(III) reduction. These findings have demonstrated the intricacy of magnetite-biogeobattery cycling and highlighted the complexity of the process, providing valuable insights into the biogeobattery phenomenon.

Due to the oxidation and reduction of magnetite by microorganisms, the surface properties will significantly change, thereby impacting magnetite's capacity to adsorb heavy metal contaminants. Industrial and agricultural activity are increasingly endangering the environment through heavy metals pollution. The presented work showed that magnetite nanoparticles, oxidized by culture KS and reduced by *G. sulfurreducens*, had unique adsorption capacities and efficiencies for the two heavy metals copper (Cu^{2+}) and cadmium (Cd^{2+}). For Cu^{2+}, reduced magnetite nanoparticles

had the highest adsorption capacity, followed by oxidized and unmodified nanoparticles. For Cd^{2+}, the greatest adsorption capacities were exhibited by reduced magnetite nanoparticles, followed by native and oxidized magnetite nanoparticles. Here, the unmodified nanoparticles exhibited superior performance compared to their oxidized counterparts, showing that biomodification can yield unfavourable outcomes. A change in the redox potential of the different types of magnetite nanoparticles could explain the differences in adsorbed heavy metals. Larger Cd^{2+} ions were supposedly more strongly repulsed from the positively charged (oxidized) surface area than smaller Cu^{2+} ions. Notably, the change in the mineral's redox potential (and therefore Fe(II)/Fe(III)) could be at least as important as a change in pH, as shown for Cd^{2+} adsorption at high pH values. This work demonstrated that the activity of Fe-metabolizing microorganisms can significantly influence the adsorption behaviour of magnetite with heavy metals. The presented work, therefore, demonstrated that in locations with high levels of heavy metal concentrations, such as industrial sites and agricultural fields, the activity of Fe-metabolizing microorganisms could greatly impact the (bio)availability and the resulting mobility and toxicity of heavy metal contaminants.

Finally, the aggregation of biogenic and abiotic magnetite nanoparticles was studied. Biogenic particles tended to form larger aggregates with less density, possibly due to organic matter associated with or incorporated into the biogenic magnetite. The influence of particle aggregation on magnetite nanoparticles' bioavailability and adsorption interactions is a non-negligible factor to consider.

In summary, this work has expanded our understanding of the roles that the mixed-valent Fe mineral magnetite can have in the environment and provided evidence for the importance of microbial activity for the fate of magnetite and associated contaminants. It showed that magnetite can serve as a biogeobattery in consecutive redox cycles that will, however, be lost over time. Furthermore, it highlighted the significance of magnetite's redox state for interactions with heavy metal pollutants; and lastly indicated the importance of the particle aggregation depending on the type of investigated magnetite.

.

Zusammenfassung

Eisen (Fe) ist ein essenzielles Element, welches auf der Erde weit verbreitet ist und mit verschiedenen geochemischen Kreisläufen wie Sauerstoff, Stickstoff und Kohlenstoff verbunden ist. Dies entspringt der Eigenschaft, dass Fe redox-aktiv ist und zwischen reduziertem und oxidiertem Zustand (Fe(II) und Fe(III)) wechseln kann. Da Fe in der Natur sehr häufig vorkommt, haben Bakterien Wege entwickelt, um Energie aus dem Transfer von einem Elektron zwischen Fe(II) und Fe(III) zu gewinnen. Zweiwertiges Fe(II) kann als Elektronendonator für die Fe(II)-Oxidation und dreiwertiges Fe(III) als Elektronenakzeptor für die Fe(III)-Reduktion verwendet werden. Dieser Kreislauf zwischen Fe(II) und Fe(III) hat große Auswirkungen auf die Stabilität und Identität der Fe-Minerale. Ebenso wichtig ist, dass er sich auf die (Bio-)Verfügbarkeit von den Fe-Mineralen selbst, und von Schad- und Nährstoffen auswirken kann, welche gewöhnlich mit den Mineraloberflächen assoziiert sind. Gemischtvalente Fe-Minerale sind einzigartig, weil sie in ihrer Kristallstruktur beide Formen von Eisen enthalten (Fe(II) und Fe(III)). Magnetit (Fe_3O_4 bzw. $Fe(III)_2Fe(II)O_4$) ist mit das bekannteste gemischtvalente Fe-Mineral. Es wurde gezeigt, dass bestimmte Mikroorganismen Fe(II) und Fe(III) in Magnetit respektive als Elektronenquelle bzw. -senke nutzen können. Diese ziemlich einzigartige Fähigkeit von Magnetit, den Elektronentransport und die Elektronenspeicherung zwischen Fe-metabolisierende Mikroorganismen zu ermöglichen, hat ihm den Namen *Biogeobatterie* eingebracht. Unklar ist jedoch, welche Folgen fortgesetzten Redoxzyklen für die Eigenschaften des Magnetits haben und ob es grundsätzlich bei längerer Exposition in Redoxzyklen kontinuierlich als Elektronenquelle und -senke dienen kann. Außerdem ist unklar, inwiefern sich die Interaktionen von Magnetit-Nanopartikeln mit Schwermetallen, welche Verunreinigungen in der Umwelt darstellen, durch die biotische Magnetite-Oxidation oder Reduktion ändern. Dementsprechend waren die Ziele dieser Arbeit, (1) das Ausmaß der Magnetit-Oxidation und Reduktion während fortgesetzter Redoxzyklen zu bestimmen, (2) die Folgen dieser Oxidation und Reduktion für die allgemeinen Eigenschaften des Magnetits und die Bioverfügbarkeit für die Fe-metabolisierenden Bakterien festzustellen, (3) festzustellen, ob Magnetite Nanopartikel für unbegrenzte Zeit als Biogeobatterie dienen können, oder herauszufinden, welche Prozesse zum Verlust der Biogeobatterie Eigenschaften führten und zuletzt, und zuletzt, (4) den Einfluss der mikrobiellen Oxidation und

Reduktion auf die Adsorptionskapazität und -Effizienz gegenüber umweltrelevanten Schwermetallverunreinigungen zu untersuchen.

Zunächst entdeckten wir, dass die nitratreduzierende Fe(II)-oxidierende Anreicherungskultur „culture KS“ synthetisierte Magnetit-Nanopartikel als Elektronenquelle nutzen konnte. Daraufhin konnte erfolgreich demonstriert werden, dass Magnetit-Nanopartikel in zwei aufeinanderfolgenden Oxidation-Reduktions-Zyklen über 41 Tage als Biogeobatterie von culture KS und *Geobacter sulfurreducens* verwendet werden konnte. Die Fe(III) Reduktion durch *G. sulfurreducens* führte zu einer reduktiven Auflösung des Minerals, gefolgt von einer sekundären Wiederausfällung, vor allem als Vivianit, ein Fe(II)-Phosphat Mineral ($Fe(II)_3(PO_4)_2$, 8H2O). Dieser Auflösungs- und Ausfällungsprozess war während der zweiten Reduktion ausgeprägter. Interessanterweise kam der elektronengeladene Magnetit den Fe(II)-oxidierenden Bakterien zugute, was sich in einer größeren Veränderung des Fe(II)/Fe(III)-Verhältnisses während der zweiten Oxidation zeigte. Während den Oxidationen wurde ein unterer Schwellenwert des Fe(II)/Fe(III)-Verhältnisses festgestellt, womöglich das thermodynamische Limit der mikrobiellen Magnetit-Oxidation. Eine Passivierung der Oberfläche durch Maghemitisierung des Magnetits wurde erwartet, jedoch in keiner der durchgeführten Messungen erfasst.
Diese Ergebnisse haben eine große Bedeutung für das Verständnis von Magnetit als Biogeobatterie in der Umwelt. Wiederholte Redox-Zyklen führten dazu, dass Magnetit durch reduktive Auflösung weniger stabil wurde, aber gleichzeitig, aufgrund der erhöhten Elektronenmenge, die Fe(II)-Oxidation nach der Reduktion begünstigte. Diese Studie legt daher nahe, dass Magnetit-Nanopartikel nicht mehr als Biogeobatterien fungieren können, wenn sie mehrere Redox-Zyklen durchlaufen haben, und die reduktive Auflösung das Mineral zunehmend zersetzt. Zusätzlich könnte die begünstigte Oxidation (nach den Reduktionen) vermehrt zur maghemitisierung des Magnetits führen, welche womöglich die Oberfläche passiviert. Dieser Biogeobatterie-Verlust könnte durch zusätzliche Prozesse wie Fe(II) Oxidation Fe(III) Reducktion, die Magnetit erzeugen, abgeschwächt werden. Die hier vorgestellten experimentellen Ergebnisse haben die Komplexität des Magnetit-Biogeobatterie-Zyklus Prozesses verdeutlicht, was wertvolle Einblicke in das

Phänomen der Biogeobatterie ermöglichte. Diese Beobachtungen dienen dazu, unser Verständnis zu vertiefen und weitere Forschung in diesem Bereich zu ermöglichen.

Durch die Oxidation und Reduktion von Magnetit durch Mikroorganismen verändern sich die Oberflächeneigenschaften erheblich, was sich auf die Fähigkeit von Magnetit auswirken wird, Schwermetallverunreinigungen zu adsorbieren. Industrielle und landwirtschaftliche Tätigkeiten gefährden die Umwelt zunehmend durch Verursachung von Schwermetallverunreinigungen. Die vorgestellte Arbeit zeigte, dass Magnetit-Nanopartikel, die von culture KS oxidiert und von *G. sulfurreducens* reduziert wurden, einzigartige Adsorptionskapazitäten und Effizienzen für die beiden Schwermetalle Kupfer (Cu^{2+}) und Cadmium (Cd^{2+}) aufwiesen. Für Cu^{2+} zeigten reduzierte Magnetit-Nanopartikel die höchste Adsorptionskapazität, gefolgt von oxidierten und unveränderten Nanopartikeln. Für Cd^{2+} wiesen reduzierte Magnetit -Nanopartikel die größten Adsorptionskapazitäten auf, gefolgt von nativem und oxidiertem Magnetit-Nanopartikeln. Hier zeigten die unveränderten Nanopartikel interessanterweise eine bessere Leistung als ihre oxidierten Gegenstücke, was zeigte, dass die Biomodifizierung auch unerwünschten Auswirkungen haben kann. Die Änderungen des Redoxpotentials führte vermutlich zu einer Änderung der Oberflächenladung, und größere Cd^{2+}-Ionen wurden stärker von der positiv geladenen (oxidierten) Oberfläche abgestoßen als kleinere Cu^{2+}-Ionen. Insbesondere konnte gezeigt werden, dass die Änderung des Redoxpotentials des Minerals (und damit von Fe(II)/Fe(III)) mindestens ebenso wichtig sein kann wie eine Änderung des pH-Werts; was für die Cd^{2+}-Adsorption bei hohen pH-Werten gezeigt wurde. Die Ergebnisse demonstrierten, dass das Adsorptionsverhalten von Magnetit durch die Aktivität von Fe-metabolisierenden Mikroorganismen erheblich beeinflusst werden konnte. Sie erlaubt daher die Schlussfolgerung, dass die Aktivität von Fe-metabolisierenden Mikroorganismen an Standorten mit hohen Schwermetallkonzentrationen, wie z.B. an Industriestandorten und auf landwirtschaftlichen Feldern, die (Bio)Verfügbarkeit und die daraus resultierende Toxizität von Schwermetallverunreinigungen stark beeinflussen kann.

Schließlich wurde die Aggregation von biotischen und abiotischen Magnetit-Nanopartikeln untersucht. Biogene Partikel neigten dazu, größere Aggregate

mit geringerer Dichte zu bilden, was auf organische Stoffe zurückzuführen ist, die mit ihnen assoziiert sind. Der Einfluss der Partikelaggregation auf die Bioverfügbarkeit und die Adsorptionswechselwirkungen von Magnetit-Nanopartikeln ist ein nicht zu vernachlässigender Faktor, den es zu berücksichtigt gilt. Daher haben wir den ersten Schritt getan, um die Aggregation von Magnetit-Nanopartikeln aus verschiedenen Quellen zu verstehen.

Zusammenfassend lässt sich sagen, dass diese Arbeit unser Verständnis der Rollen, die das gemischtvalente Fe-Mineral Magnetit in der Umwelt spielen kann, erweitert hat. Darüber hinaus erbrachte sie Beweise für die Bedeutung der mikrobiellen Aktivität für das Schicksal von Magnetit und den assoziierten Schadstoffen. Sie zeigte, dass Magnetit in aufeinander folgenden Redoxzyklen als Biogeobatterie dienen kann, jedoch im Laufe der Zeit verloren geht. Außerdem wurde die Bedeutung des Redox-Zustandes von Magnetit für die Interaktion mit Schwermetallschadstoffen in der Umwelt hervorgehoben; und sie zeigte zuletzt die Bedeutung der Partikelaggregation in Abhängigkeit von der Art des untersuchten Magnetits auf.

Chapter 1: Introduction

Iron (Fe) is the fourth most abundant element in Earth's crust[1] and is essential for almost all known living organisms[2, 3]. It is essential due to its abundant use in cellular compounds and as the metallic center of many proteins[4], such as haemoglobin[5]. In the environment, Fe occurs as reduced ferrous (Fe(II)) or as oxidized ferric (Fe(III)) iron. Microorganisms have evolved to use Fe as an energy source by transferring one electron between ferrous and ferric Fe[6]. Fe(II), readily soluble at neutral pH in anoxic conditions, is used as an electron source by Fe(II)-oxidizing bacteria. Fe(III) is poorly soluble at neutral pH and, therefore, readily precipitates as Fe(III) (oxyhydr)oxides (short for oxides, oxyhydroxides, and hydroxides) minerals[7-9]. Fe(III) is an electron sink for Fe(III)-reducing microorganisms. Microorganisms using Fe as an electron source or sink have to deal with poor solubility of Fe^{3+} and the rapid oxidation of Fe^{2+} at circumneutral pH by oxygen[10], both leading to rapid precipitation of Fe(III) (oxyhydro)oxides[11], as shown by low solubility products in the range of 10^{-38}–10^{-42} [9, 11]. Furthermore, abiotic processes also affect the oxidation state of Fe in the environment, which ultimately determines the bioavailability, solubility, and adsorption properties[12]. The cycling of Fe depends on the abundance of Fe-metabolizing bacteria and geochemical parameters such as pH, oxygen (O_2) concentration, and redox potential (E_h).

1.1 Abiotic and biotic Fe cycling in the environment

Various abiotic reactions that reduce or oxidize Fe can occur in the environment. Under circumneutral pH, ferrous Fe(II) can be oxidized by oxygen and reactive oxygen species (ROS)[13, 14]. It can also be oxidized when reacting with manganese oxides (MnO_2), nitrite (NO_2^-), and nitric oxide (NO)[11, 15-17]. On the other hand, Fe(III) can be reduced by reduced organic matter like humic substances, by superoxide ($O_2^{-\cdot}$) by interacting with light ($h\nu$) while associated with organic compounds, and reactive sulfur species (H_2S)[12, 18, 19]. Concurrent with the abiotic processes, different microorganisms can use Fe as an electron acceptor or electron donor for energy generation and growth.

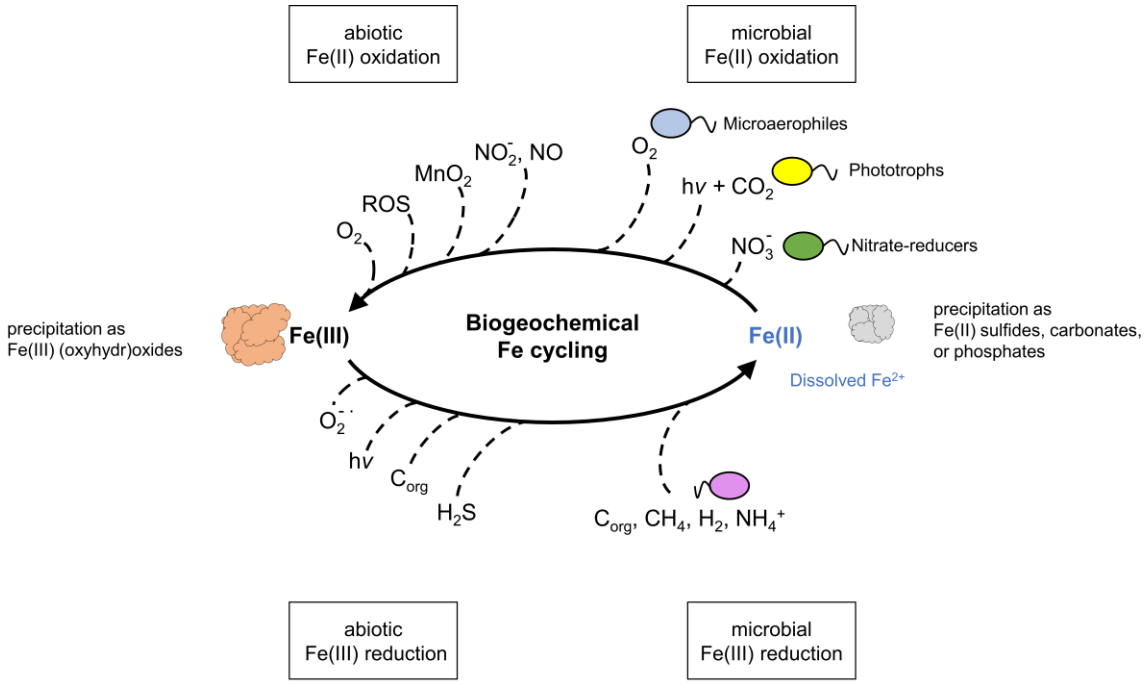

Figure 1. Iron cycling in the environment. *Fe(III) can be reduced microbially by Fe(III)-reducing bacteria (purple bacterium), coupling it to the oxidation of organic carbon (C_{org}), methane (CH_4), dihydrogen (H_2), or ammonium (NH_4^+). Fe(III) can abiotically be reduced by superoxide ($O_2^{-\cdot}$), by light when Fe(III) is in an organic complex, by reduced organic carbon, and by sulfide (H_2S). Fe(II) can be microbially oxidized by microaerophilic Fe(II)-oxidizers (blue bacterium), using O_2 as the electron acceptor, by phototrophic Fe(II)-oxidizers (yellow bacterium) using CO_2 as the electron acceptor and light (hv) as the energy source, and by nitrate-reducing Fe(II)-oxidizers (green bacterium) by using nitrate (NO_3^-) as the electron acceptor.*

At circumneutral pH, microorganisms must deal with rapid precipitation of Fe^{3+} as (oxyhydr)oxides and rapid oxidation of Fe^{2+} with oxygen. To avoid abiotic oxidation by O_2, acidophilic Fe(II)-oxidizing microorganisms grow in low pH environments, using it as an electron acceptor[20]. At circumneutral pH (pH 5.0 – 8.0), microaerophilic Fe(II)-oxidizers can outcompete the abiotic oxidation of Fe(II) by O_2 by growing in environments of low O_2 concentrations (<40 µmol L^{-1}), using O_2 as the electron acceptor[21-23]. To prevent encrustation in Fe(III) (oxyhydr)oxides, microaerophiles produce organic structures like twisted stalks or sheets that serve as a template for the precipitation[24, 25]. In anaerobic environments, phototrophic Fe(II)-oxidizers and

nitrate-reducing Fe(II)-oxidizers can use Fe(II) as an electron source. Phototropic Fe(II)-oxidizers use CO_2 as the electron acceptor, fixing it into biomass using light (hν) as an energy source[26]. Fe(II)-oxidizing nitrate-reducers can connect Fe oxidation to stepwise reduction of nitrate (NO_3^-) to dinitrogen (N_2) or ammonium (NH_4^+)[27, 28]. Meanwhile, Fe(III)-reducers that live in anoxic environments can use ferric Fe(III) as an electron acceptor. The reduction is coupled to the oxidation of organic fatty acids like acetate and lactate[29, 30], or inorganic dihydrogen (H_2)[31]. Furthermore, microorganisms use Fe(III) as an electron acceptor and couple it to the oxidation of ammonium (NH_4^+, Fe-Ammox)[32, 33], sulfides (H_2S)[18], or methane (CH_4)[34]. Figure 1 provides an overview of both microbial and abiotic Fe redox reactions. When studying the Fe cycle, it can be challenging to distinguish microbial activity and abiotic reactions, as the processes can be closely intertwined. Thus, it is essential to be cautious to prevent errors and artifacts that might occur during the investigations.

1.2 Fe mineral (trans)formation

Microbial activity and abiotic reactions majorly impact the (trans-)formation of Fe minerals. New minerals can be formed due to the precipitation of previously dissolved Fe species, while previously solid minerals can also be dissolved. These processes have important consequences for elements and compounds commonly associated with Fe minerals or used as redox partners during reactions. Fe(II) oxidation will lead to the formation of (possibly) dissolved Fe^{3+}, which will form Fe(III) (oxyhydr)oxides like ferrihydrite ($Fe_{10}O_{14}(OH)_2$), goethite (α-FeOOH), and hematite (α-Fe_2O_3). The formation of Fe(III) minerals can be influenced by the rate of oxidation/reduction and the presence of ions and organics[35, 36]. Fe(III) reduction, on the other hand, can lead to reductive dissolution of a Fe(III) mineral into a dissolved Fe^{2+} phase, which could stay in solution, associate with already present Fe minerals, or precipitate as secondary Fe(II)-minerals. Depending on the types of anions and Fe phases present, different Fe(II) minerals can be formed. Some examples of formed Fe(II) minerals are siderite ($FeCO_3$)[37], mackinawite ($(Fe,Ni)_9S_8$)[38], and vivianite ($Fe^{II}_3(PO_4)_2$, $8H_2O$)[39]. Mixed-valent Fe minerals containing both Fe(II) and Fe(III) like green rust (i.e., carbonate green rust $Fe(II)_4Fe(III)_2(OH)_{12}[CO_3]$, $3H_2O$) or magnetite (Fe_3O_4 or $Fe(II)Fe(III)_2O_4$) can also be formed[40, 41].

1.3 Mixed-valent Fe minerals, magnetite formation and general properties

Magnetite and green rust, the naturally occurring mixed-valent Fe oxides, are unique because they contain both Fe oxidation states within their crystal structure, making them highly reactive. Therefore, they play a vital role in the mobility, redox transformation, and availability of toxic compounds and nutrients[40]. While green rusts are layered double hydroxides,[42] magnetite is a member of the spinel group[43]. As the name suggests, magnetite is the most magnetic, naturally occurring compound known. This can be demonstrated by values of the spontaneous magnetization, which is 480 kA m^{-1} for magnetite, 380 kA m^{-1} for maghemite, and about 2 kA m^{-1} for goethite[44]. It has, therefore, been used for navigation of early humans in lodestone[45] and as a means to explain the reversal of Earth's magnetic field[46].

Magnetite can be formed through biological, geological, and anthropogenic processes. Anthropogenic processes that lead to the formation of magnetite are combustion of fossil fuel in vehicles and industry derived air pollution[47, 48], which may present a neurotoxicant and therefore a risk factor for Alzheimer's disease[49]. Weathering and serpentinization are geological processes of magnetite formation[44, 50]. Magnetite derived from microbial activity is differentiated by biologically controlled formation and biologically induced formation of magnetite[44]. The biologically controlled formation of magnetite was described for magnetotactic bacteria (MTB)[51]. MTB can produce organelle-like structures, the so-called magnetosomes, which contain crystallites of magnetite or its sulfur counterpart, greigite (Fe_3S_4)[52]. Magnetosomes are essential for MTB, as they allow alignment along the earth's magnetic field and mobility along the field lines to ideal geochemical conditions[53]. Therefore, the formation of magnetosomes is controlled by a series of proteins[54]. On the other hand, the biologically induced formation of magnetite is only a result of the oxidation or reduction of Fe in geochemical surroundings that support the formation/precipitation of magnetite. The formation of magnetite due to Fe(II) oxidation has scarcely been described for nitrate-reducing Fe(II)-oxidizing *Acidovorax* sp. BoFeN1[41] and *Dechlorosoma suillum*[55], and the phototrophic Fe(II)-oxidizing *R. palustris* TIE-1[56]. On the other hand, magnetite formation during the reduction of ferrihydrite was already described by Lovley et al. in 1987[57]. It has since been frequently observed that magnetite is produced as a byproduct during the reduction of Fe(III)[58]. Stoichiometric

magnetite has a Fe(II)/Fe(III) ratio of 0.5. Structurally, magnetite consists of eight Fe(II) and eight Fe(III) atoms in octahedral coordination, and eight Fe(III) atoms in tetrahedral coordination. As nanoparticle, magnetite can have a specific surface area of up to 100 m^2g^{-1} [59], which enables ad- and desorption interactions with trace elements like phosphates[60], adsorption and redox interactions with heavy metals like cadmium[61], and redox interactions with organic contaminants[62].

1.4 Magnetite reactivity and magnetic properties

As the reactivity of magnetite is dependent on the amount of Fe(II) and Fe(III)[63, 64], it can be described as a function of the Fe(II)/Fe(III) ratio. This ratio was classically described within a range from 0.5 (stoichiometric magnetite) down to the completely oxidized form with a ratio of 0. Reaching a Fe(II)/Fe(III) ratio of 0 in magnetite is described as maghemitization, since maghemite (γ-Fe_2O_3) is the fully oxidized version of magnetite, with a Fe-deficiency to maintain charge balance[65], and ratios greater than 0.5 for reduced magnetite were reported[66]. Depending on the Fe(II)/Fe(III) ratio of magnetite, its properties, such as surface charge, point of zero charge, redox potential, and reactivity, will change. Due to this variability of the Fe(II)/Fe(III) ratio, the redox potential of the mineral can change from positive to negative values[64, 67].

Due to the antiparallel magnetic alignment of the octahedrally and tetrahedrally coordinated Fe(III) atoms, their magnetic moments cancel each other, leaving the magnetic moments of Fe(II) atoms uninfluenced, and thus making them the main component of magnetite's magnetization. Therefore, magnetite's magnetic properties are tightly linked to the Fe(II)/Fe(III) ratio. Due to the alignment, but not equal strength, of magnetic fields, magnetite is a ferrimagnet. The magnetic properties of magnetite can be used for non-invasive measurements of magnetic susceptibility. Here, a weak magnetic field is applied to a sample, and the response is measured[68]. The greater the magnetic susceptibility of a material, the stronger its response to a magnetic field and, therefore, the results of magnetic susceptibility measurements. For diamagnetic materials it is in the order of 10^{-8} m^3kg^{-1}, for paramagnetic materials like rock forming silicates about 10^{-7} m^3kg^{-1} and for ferro(i)magnetic materials like magnetite in the order of 10^{-4} m^3kg^{-1}. Results of magnetic susceptibility measurements depend on factors like concentration of magnetic materials, grain size[44], and the applied frequency[69].

Changes in magnetic susceptibility were correlated to Fe(II)/Fe(III) ratio, therefore allowing non-invasive investigation of magnetite stoichiometry[66, 68]. Further approaches of using magnetic susceptibility measurements were the investigations of anthropogenic impact on Danube river sediments[70], of heavy metal pollution in the Linfen basin of China[71] and for magnetoclimatic analysis of loess layers in China where magnetic susceptibility measurements that closely match with marine oxygen isotopes measurements[44].

1.5 Microbial magnetite oxidation and reduction

For Fe-metabolizing microorganisms, magnetite can be of interest as both an electron acceptor (i.e., a Fe(III) source for Fe(III)-reducing microorganisms) and as an electron donor (i.e., a Fe(II) source for Fe(II)-oxidizing microorganisms). While the reduction of magnetite by microorganisms has been known for more than 20 years[58, 72], the oxidation of magnetite by microorganisms has first been proposed indirectly by demonstrating the oxidation of magnetite by the purified c-type cytochrome MtoA of the microaerophilic strain *Siderooxydans lithotrophicus*[73]. Thereafter, it was demonstrated that magnetite could serve as an electron donor and acceptor for Fe-oxidizing and Fe-reducing microorganisms, respectively[66]. It was demonstrated that the phototrophic Fe(II)-oxidizing *Rhodopseudomonas palustris* TIE-1, isolated from an iron-rich mat in Woods Hole (Massachusetts)[56], could oxidize magnetite, which could then, in turn, be reduced by Fe(III)-reducing *Geobacter sulfurreducens*[74], thus being called biogeobattery. It was additionally shown that further microorganisms (nitrite-producing *Paracoccus denitrificans* ATCC 19377, Fe(III)-reducing *Shewanella oneidensis* MR1, Fe(II)-oxidizing *Acidovorax sp*. BoFeN1) could oxidize/reduce iron[66]. Magnetite, as a biogeobattery, could store and donate electrons to Fe-metabolizing bacteria depending on the redox conditions. It has been shown that a surface layer of oxidized magnetite, resulting in the formation of maghemite, can form during oxidations with a depth of 2 nm[75]. Therefore, the oxidation of magnetite is suggested to be more dependent on the surface area of the mineral. This oxidation results in lower reactivity with redox-active pollutants like chromium (Cr(VI))[75].

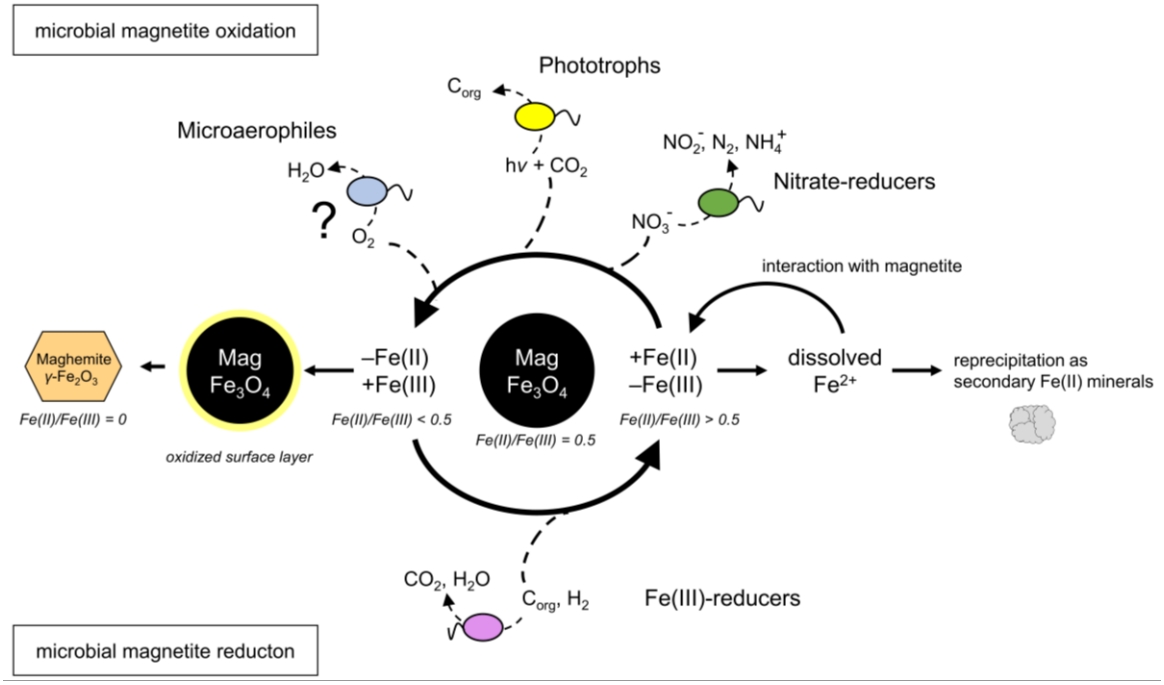

Figure 2. Magnetite cycling in the environment. *Magnetite can be reduced by Fe(III)-reducing bacteria by oxidizing biotic fatty acids or abiotic dihydrogen (H_2). Dissolved Fe^{2+} can associate with the surface of magnetite, stay in solution, or reprecipitate as secondary Fe(II) minerals. Magnetite can be oxidized by nitrate-reducing or phototrophic Fe(II)-oxidizers and possibly (marked with **?**) by microaerophilic Fe(II)-oxidizers, as it has been shown that proteins isolated from microaerophiles could oxidize magnetite. Oxidation can cause surface passivation of magnetite due to the formation of an oxidized surface layer of maghemite. Complete oxidation of magnetite yields maghemite.*

Contrarily, it was suggested that the Fe(III) reduction is less dependent on the surface area of magnetite and more of a bulk-dependent process, driven by an electron-hopping process throughout the particles[76]. Therefore, in analogy to Figure 1, the Fe-cycling can be re-interpreted with magnetite as the electron donor and acceptor. This 'magnetite-iron' cycle is depicted in Figure 2.

If magnetite is to be cycled in the environment by microbial activity, it occurs in depths allowing both oxidation and reduction, depending on water level and O_2 saturation. Magnetic susceptibility measurements can reveal this depth of magnetite biogeobattery redox cycling. In preliminary experiments of measuring magnetic susceptibility of course collected from a pond in the Schönbuch forest (Tübingen, Germany: 48°32'55.1"N, 9°04'57.8"E) and a rice paddy in Italy (Vercelli, Italian Rice Experiment Station) we could determine a peak in magnetic susceptibility in a depth of between 3 to 8 cm (Figure 3). This is the depth of sediments and soils that, hence, should be investigated for the magnetite biogeobattery. The peak value of $80x10^{-6}$ SI collected from the Vercelli rice paddy soil (Figure 3) would correlate to a rough concentration of 10 mg L^{-1}, compared to a pure magnetite reference (data not published).

However, this peak in magnetic susceptibility can not be solely attributed to magnetic minerals such as magnetite. This is due to magnetic signals that can be caused by airborne pollution of magnetic particles in the upper layers of soils[77], which could be caused by industrial pollution[78].

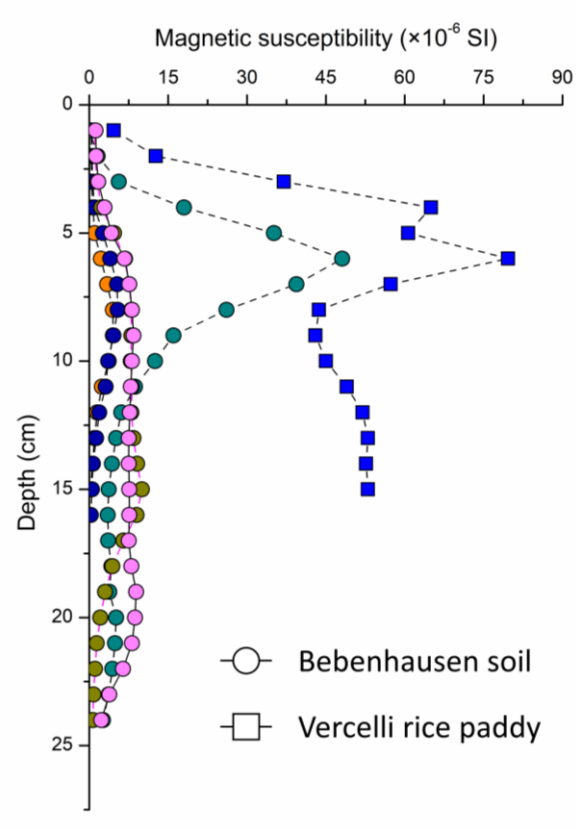

Figure 3. Magnetic susceptibility profiles of soil cores. *Measured magnetic susceptibility of soil cores collected close to Bebenhausen, Tübingen, Germany (coloured circles) and in the rice paddy fields of the Italian Rice Experiment Station, Vercelli, Italy (squares). If an increase in magnetic susceptibility was detected, it was usually confined to a particular depth range. This depth suggests an increased presence of magnetic minerals (magnetite), which could be redox cycled as a biogeobattery depending on redox conditions.*

However, even if magnetite particles are not of biological or geogenic origins, they could likely be used as an electron donor and acceptor in the layers of peak magnetic susceptibility for biogeobattery processes. Therefore, independent of their origin, magnetite particles in the environment could be used as biogeobatteries by Fe-metabolizing bacteria with extensive consequences for the Fe and associated element cycles and heavy metal contaminants (Figure 4).

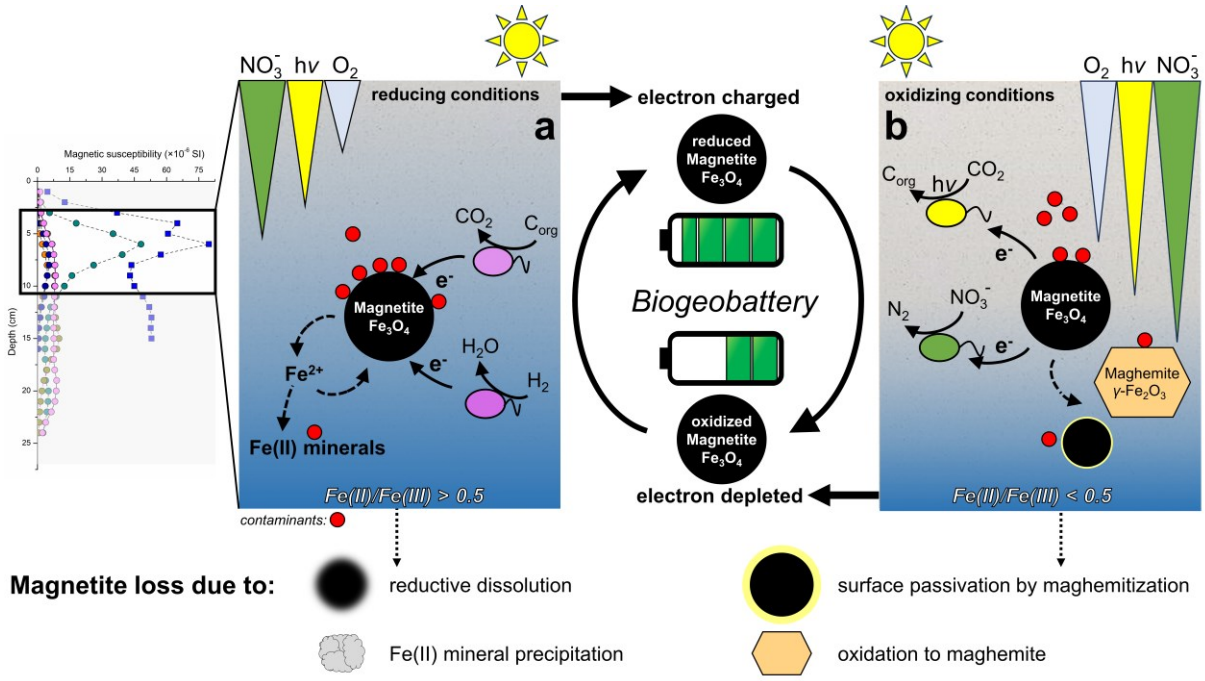

Figure 4. Magnetite as an environmental biogeobattery. *Elevated concentrations of magnetite are expected in a vertical depth, in which an increase in magnetic susceptibility was measured. Here, magnetite can serve as a biogeobattery. Depending on the present redox conditions (water saturation and oxygen penetration) magnetite can be "charged" by Fe(III)-reducing microorganisms (left panel a), and after a decrease in water level and hence increase in O_2 saturation, magnetite can be "discharged" by Fe(II)-oxidizing microorganisms like phototrophic Fe(II)-*oxidizers or nitrate-reducing Fe(II)-oxidizers *(right panel b). Magnetite and its biogeobattery capacities of it can possibly be lost over time due to surface passivation by maghemitization, oxidation to maghemite and reductive dissolution and re-precipitation of secondary Fe(II) minerals, which represents a biogeobattery loss. Interactions with contaminants (red circles) are highly dependent on the Fe(II)/Fe(III) rato of magnetite*

1.6 References

1. Taylor, S. R. Abundance of chemical elements in the continental crust: a new table. *Geochim. Cosmochim. Acta* **1964**, *28* (8), 1273-1285.
2. Konhauser, K. O.; Kappler, A.; Roden, E. E. Iron in microbial metabolisms. *Elements* **2011**, *7* (2), 89-93.
3. Taylor, S. R.; McLennan, S. M. The continental crust: its composition and evolution. **1985**.
4. Andrews, S. C.; Robinson, A. K.; Rodríguez-Quiñones, F. Bacterial iron homeostasis. *FEMS Microbiol. Rev.* **2003**, *27* (2-3), 215-237.
5. Sheftel, A. D.; Mason, A. B.; Ponka, P. The long history of iron in the Universe and in health and disease. *Biochim. et Biophys. Acta-General subjects* **2012**, *1820* (3), 161-187.
6. Weber, K. A.; Achenbach, L. A.; Coates, J. D. Microorganisms pumping iron: anaerobic microbial iron oxidation and reduction. *Nat. Rev. Microbiol.* **2006**, *4* (10), 752-764.
7. Kappler, A.; Bryce, C.; Mansor, M.; Lueder, U.; Byrne, J. M.; Swanner, E. D. An evolving view on biogeochemical cycling of iron. *Nat. Rev. Microbiol.* **2021**, *19* (6), 360-374.
8. Bird, L. J.; Bonnefoy, V.; Newman, D. K. Bioenergetic challenges of microbial iron metabolisms. *Trends Microbiol.* **2011**, *19* (7), 330-340.
9. Becker, S.; Enright, A.; Kappler, A. Living on iron. *Metals Microb Minerals Biogeochem Side Life* **2021**, *21*, 185.
10. Weber, K. A.; Urrutia, M. M.; Churchill, P. F.; Kukkadapu, R. K.; Roden, E. E. Anaerobic redox cycling of iron by freshwater sediment microorganisms. *Env. Microbiol.* **2006**, *8* (1), 100-113.
11. Cornell, R. M.; Schwertmann, U. *The iron oxides: structure, properties, reactions, occurrences and uses*; John Wiley & Sons, 2003.
12. Melton, E. D.; Swanner, E. D.; Behrens, S.; Schmidt, C.; Kappler, A. The interplay of microbially mediated and abiotic reactions in the biogeochemical Fe cycle. *Nat. Rev. Microbiol.* **2014**, *12* (12), 797-808. DOI: 10.1038/nrmicro3347.
13. Stumm, W.; Lee, G. F. Oxygenation of ferrous iron. *Indust. Engin. Chem.* **1961**, *53* (2), 143-146.
14. Weiss, J. Elektronenübergangsprozesse im Mechanismus von Oxydations-und Reduktionsreaktionen in Lösungen. *Naturwissenschaften* **1935**, *23*, 64-69.
15. Postma, D. Concentration of Mn and separation from Fe in sediments—I. Kinetics and stoichiometry of the reaction between birnessite and dissolved Fe (II) at 10 C. *Geochim. Cosmochim. Acta* **1985**, *49* (4), 1023-1033.
16. Wullstein, L.; Gilmour, C. Non-enzymatic formation of nitrogen gas. *Nat.* **1966**, *210* (5041), 1150-1151.
17. Tamura, H.; Goto, K.; Nagayama, M. Effect of anions on the oxygenation of ferrous ion in neutral solutions. *J. Inorg. Nucl. Chem.* **1976**, *38* (1), 113-117.
18. Dos Santos Afonso, M.; Stumm, W. Reductive dissolution of iron (III)(hydr) oxides by hydrogen sulfide. *Langmuir* **1992**, *8* (6), 1671-1675.
19. Lovley, D.; Fraga, J.; Blunt-Harris, E.; Hayes, L.; Phillips, E.; Coates, J. Humic substances as a mediator for microbially catalyzed metal reduction. *Acta Hydrochim. Hydrobiol.* **1998**, *26* (3), 152-157.

20. Bonnefoy, V.; Holmes, D. S. Genomic insights into microbial iron oxidation and iron uptake strategies in extremely acidic environments. *Env. Microbiol.* **2012**, *14* (7), 1597-1611.
21. Druschel, G. K.; Emerson, D.; Sutka, R.; Suchecki, P.; Luther III, G. W. Low-oxygen and chemical kinetic constraints on the geochemical niche of neutrophilic iron(II) oxidizing microorganisms. *Geochim. Cosmochim. Acta* **2008**, *72* (14), 3358-3370.
22. Emerson, D.; Moyer, C. Isolation and characterization of novel iron-oxidizing bacteria that grow at circumneutral pH. *Appl. Environ. Microbiol.* **1997**, *63* (12), 4784-4792.
23. Lueder, U.; Druschel, G.; Emerson, D.; Kappler, A.; Schmidt, C. Quantitative analysis of O_2 and Fe^{2+} profiles in gradient tubes for cultivation of microaerophilic Iron(II)-oxidizing bacteria. *FEMS Microbiol. Ecol.* **2018**, *94* (2).
24. Chan, C. S.; Fakra, S. C.; Emerson, D.; Fleming, E. J.; Edwards, K. J. Lithotrophic iron-oxidizing bacteria produce organic stalks to control mineral growth: implications for biosignature formation. *The ISME J.* **2011**, *5* (4), 717-727.
25. Koeksoy, E.; Bezuidt, O. M.; Bayer, T.; Chan, C. S.; Emerson, D. Zetaproteobacteria pan-genome reveals candidate gene cluster for twisted stalk biosynthesis and export. *Front. Microbiol.* **2021**, *12*, 679409.
26. Widdel, F.; Schnell, S.; Heising, S.; Ehrenreich, A.; Assmus, B.; Schink, B. Ferrous iron oxidation by anoxygenic phototrophic bacteria. *Nat.* **1993**, *362* (6423), 834.
27. Canfield, D. E.; Glazer, A. N.; Falkowski, P. G. The evolution and future of Earth's nitrogen cycle. *Sci.* **2010**, *330* (6001), 192-196.
28. Straub, K. L.; Benz, M.; Schink, B.; Widdel, F. Anaerobic, nitrate-dependent microbial oxidation of ferrous iron. *Appl. Environ. Microbiol.* **1996**, *62* (4), 1458-1460.
29. Lovley, D. R.; Phillips, E. J. Novel mode of microbial energy metabolism: organic carbon oxidation coupled to dissimilatory reduction of iron or manganese. *Appl. Environ. Microbiol.* **1988**, *54* (6), 1472-1480.
30. Richter, K.; Schicklberger, M.; Gescher, J. Dissimilatory reduction of extracellular electron acceptors in anaerobic respiration. *Appl. Environ. Microbiol.* **2012**, *78* (4), 913-921.
31. Lovley, D. R.; Ueki, T.; Zhang, T.; Malvankar, N. S.; Shrestha, P. M.; Flanagan, K. A.; Aklujkar, M.; Butler, J. E.; Giloteaux, L.; Rotaru, A.-E. Geobacter: the microbe electric's physiology, ecology, and practical applications. *Adv. Microb. Physiol.* **2011**, *59*, 1-100.
32. Kuenen, J. G. Anammox bacteria: from discovery to application. *Nat. Rev. Microbiol.* **2008**, *6* (4), 320-326.
33. Oshiki, M.; Ishii, S.; Yoshida, K.; Fujii, N.; Ishiguro, M.; Satoh, H.; Okabe, S. Nitrate-dependent ferrous iron oxidation by anaerobic ammonium oxidation (anammox) bacteria. *Appl. Environ. Microbiol.* **2013**, *79* (13), 4087-4093.
34. Cai, C.; Leu, A. O.; Xie, G.-J.; Guo, J.; Feng, Y.; Zhao, J.-X.; Tyson, G. W.; Yuan, Z.; Hu, S. A methanotrophic archaeon couples anaerobic oxidation of methane to Fe (III) reduction. *The ISME J.* **2018**, *12* (8), 1929-1939.
35. Dippon, U.; Schmidt, C.; Behrens, S.; Kappler, A. Secondary Mineral Formation During Ferrihydrite Reduction by Shewanella oneidensis MR-1 Depends on Incubation Vessel Orientation and Resulting Gradients of Cells, Fe^{2+} and Fe Minerals. *Geomicrobiol. J.* **2015**, *32* (10), 878-889.

36. Han, X.; Tomaszewski, E. J.; Sorwat, J.; Pan, Y.; Kappler, A.; Byrne, J. M. Effect of Microbial Biomass and Humic Acids on Abiotic and Biotic Magnetite Formation. *Environ. Sci. Technol.* **2020**, *54* (7), 4121-4130.
37. Jimenez-Lopez, C.; Romanek, C. S. Precipitation kinetics and carbon isotope partitioning of inorganic siderite at 25°C and 1 atm 1 1Associate editor: J. Horita. *Geochim. Cosmochim. Acta* **2004**, *68* (3), 557-571.
38. Wolthers, M.; Gaast, S. J. V. D.; Rickard, D. The structure of disordered mackinawite. *Am. Min.* **2003**, *88* (11-12), 2007-2015.
39. Miot, J.; Benzerara, K.; Morin, G.; Bernard, S.; Beyssac, O.; Larquet, E.; Kappler, A.; Guyot, F. Transformation of vivianite by anaerobic nitrate-reducing iron-oxidizing bacteria. *Geobiol.* **2009**, *7* (3), 373-384.
40. Usman, M.; Byrne, J.; Chaudhary, A.; Orsetti, S.; Hanna, K.; Ruby, C.; Kappler, A.; Haderlein, S. Magnetite and green rust: synthesis, properties, and environmental applications of mixed-valent iron minerals. *Chem. Rev.* **2018**, *118* (7), 3251-3304.
41. Miot, J.; Li, J.; Benzerara, K.; Sougrati, M. T.; Ona-Nguema, G.; Bernard, S.; Jumas, J.-C.; Guyot, F. Formation of single domain magnetite by green rust oxidation promoted by microbial anaerobic nitrate-dependent iron oxidation. *Geochim. Cosmochim. Acta* **2014**, *139*, 327-343.
42. Hansen, H. C. B.; Rives, V. Environmental chemistry of iron (II)-iron (III) LDHs (green rusts). *Layered Double Hydroxides: present and future* **2001**, 469-493.
43. Bragg, W. The structure of magnetite and the spinels. *Nat.* **1915**, *95* (2386), 561-561.
44. Evans, M.; Heller, F. *Environmental magnetism: principles and applications of enviromagnetics*; Elsevier, 2003.
45. Kirschvink, J. L.; Walker, M. M.; Diebel, C. E. Magnetite-based magnetoreception. *Current opinion in neurobiology* **2001**, *11* (4), 462-467.
46. Pétrélis, F.; Fauve, S.; Dormy, E.; Valet, J.-P. Simple mechanism for reversals of Earth's magnetic field. *Phys. Rev. Lett.* **2009**, *102* (14), 144503.
47. Matzka, J.; Maher, B. A. Magnetic biomonitoring of roadside tree leaves: identification of spatial and temporal variations in vehicle-derived particulates. *Atmos. Environ.* **1999**, *33* (28), 4565-4569.
48. Maher, B. A. Rain and dust: magnetic records of climate and pollution. *Elements* **2009**, *5* (4), 229-234.
49. Maher, B. A. Airborne magnetite-and iron-rich pollution nanoparticles: potential neurotoxicants and environmental risk factors for neurodegenerative disease, including Alzheimer's disease. *J. of Alzheimer's Disease* **2019**, *71* (2), 361-375.
50. Beard, J. S.; Frost, B. R.; Fryer, P.; McCaig, A.; Searle, R.; Ildefonse, B.; Zinin, P.; Sharma, S. K. Onset and progression of serpentinization and magnetite formation in olivine-rich troctolite from IODP Hole U1309D. *J. Petrol.* **2009**, *50* (3), 387-403.
51. Uebe, R.; Schüler, D. Magnetosome biogenesis in magnetotactic bacteria. *Nat. Rev. Microbiol.* **2016**, *14* (10), 621.
52. Byrne, J. M.; Amor, M. Biomagnetism: Insights Into Magnetic Minerals Produced by Microorganisms. *Elements* **2023**, *19*, 208-214. DOI: 10.2138/gselements.19.4.208.
53. Faivre, D.; Schuler, D. Magnetotactic bacteria and magnetosomes. *Chem. Rev.* **2008**, *108* (11), 4875-4898.
54. Schüler, D. The biomineralization of magnetosomes in Magnetospirillum gryphiswaldense. *International microbiology* **2002**, *5*, 209-214.
55. Chaudhuri, S. K.; Lack, J. G.; Coates, J. D. Biogenic magnetite formation through anaerobic biooxidation of Fe (II). *Appl. Environ. Microbiol.* **2001**, *67* (6), 2844-2848.

56. Jiao, Y.; Kappler, A.; Croal, L. R.; Newman, D. K. Isolation and characterization of a genetically tractable photoautotrophic Fe(II)-oxidizing bacterium, Rhodopseudomonas palustris strain TIE-1. *Appl. Environ. Microbiol.* **2005**, *71* (8), 4487-4496.
57. Lovley, D. R.; Stolz, J. F.; Nord Jr, G. L.; Phillips, E. J. Anaerobic production of magnetite by a dissimilatory iron-reducing microorganism. *Nat.* **1987**, *330* (6145), 252.
58. Kostka, J. E.; Nealson, K. H. Dissolution and reduction of magnetite by bacteria. *Environ. Sci. Technol.* **1995**, *29* (10), 2535-2540.
59. Sun, Z.-X.; Su, F.-W.; Forsling, W.; Samskog, P.-O. Surface Characteristics of Magnetite in Aqueous Suspension. *J. Colloid Interface Sci.* **1998**, *197* (1), 151-159.
60. Shahid, M. K.; Kim, Y.; Choi, Y.-G. Magnetite synthesis using iron oxide waste and its application for phosphate adsorption with column and batch reactors. *Chem. Eng. Res. Des.* **2019**, *148*, 169-179.
61. Babaei, A. A.; Bahrami, M.; Farrokhian Firouzi, A.; Ramazanpour Esfahani, A.; Alidokht, L. Adsorption of cadmium onto modified nanosized magnetite: kinetic modeling, isotherm studies, and process optimization. *Desalination and Water Treat.* **2015**, *56* (12), 3380-3392.
62. Elsner, M.; Schwarzenbach, R. P.; Haderlein, S. B. Reactivity of Fe (II)-bearing minerals toward reductive transformation of organic contaminants. *Environ. Sci. Technol.* **2004**, *38* (3), 799-807.
63. Byrne, J.; Telling, N.; Coker, V.; Pattrick, R.; Van Der Laan, G.; Arenholz, E.; Tuna, F.; Lloyd, J. Control of nanoparticle size, reactivity and magnetic properties during the bioproduction of magnetite by Geobacter sulfurreducens. *Nanotechnol.* **2011**, *22* (45), 455709.
64. Gorski, C. A.; Nurmi, J. T.; Tratnyek, P. G.; Hofstetter, T. B.; Scherer, M. M. Redox behavior of magnetite: Implications for contaminant reduction. *Environ. Sci. Technol.* **2010**, *44* (1), 55-60.
65. Gorski, C. A.; Scherer, M. M. Determination of nanoparticulate magnetite stoichiometry by Mossbauer spectroscopy, acidic dissolution, and powder X-ray diffraction: A critical review. *Am. Min.* **2010**, *95* (7), 1017-1026.
66. Byrne, J. M.; Klueglein, N.; Pearce, C.; Rosso, K. M.; Appel, E.; Kappler, A. Redox cycling of Fe(II) and Fe(III) in magnetite by Fe-metabolizing bacteria. *Sci.* **2015**, *347* (6229), 1473-1476.
67. Dong, H.; Zeng, Q.; Sheng, Y.; Chen, C.; Yu, G.; Kappler, A. Coupled iron cycling and organic matter transformation across redox interfaces. *Nat. Rev. Earth Environ.* **2023**, *4* (9), 659-673.
68. Porsch, K.; Dippon, U.; Rijal, M. L.; Appel, E.; Kappler, A. In-situ magnetic susceptibility measurements as a tool to follow geomicrobiological transformation of Fe minerals. *Environ. Sci. Technol.* **2010**, *44* (10), 3846-3852.
69. Van Berkum, S.; Dee, J. T.; Philipse, A. P.; Erné, B. H. Frequency-dependent magnetic susceptibility of magnetite and cobalt ferrite nanoparticles embedded in PAA hydrogel. *Int. J. Mol. Sci.* **2013**, *14* (5), 10162-10177.
70. Jordanova, D.; Veneva, L.; Hoffmann, V. Magnetic susceptibility screening of anthropogenic impact on the Danube river sediments in Northwestern Bulgaria-preliminary results. *Studia Geophys. et Geod.* **2003**, *47*, 403-418.
71. Yang, P.; Byrne, J. M.; Li, H.; Shao, H.-B. Evaluation of semi-arid arable soil heavy metal pollution by magnetic susceptibility in the Linfen basin of China. *Arid Land Research and Management* **2016**, *30* (3), 258-268.

72. Dong, H.; Fredrickson, J. K.; Kennedy, D. W.; Zachara, J. M.; Kukkadapu, R. K.; Onstott, T. C. Mineral transformations associated with the microbial reduction of magnetite. *Chem. Geol.* **2000**, *169* (3-4), 299-318.
73. Liu, J.; Pearce, C. I.; Liu, C.; Wang, Z.; Shi, L.; Arenholz, E.; Rosso, K. M. Fe3–x Ti x O4 Nanoparticles as Tunable Probes of Microbial Metal Oxidation. *J. Am. Chem. Soc.* **2013**, *135* (24), 8896-8907.
74. Methe, B.; Nelson, K. E.; Eisen, J.; Paulsen, I.; Nelson, W.; Heidelberg, J.; Wu, D.; Wu, M.; Ward, N.; Beanan, M. Genome of Geobacter sulfurreducens: metal reduction in subsurface environments. *Sci.* **2003**, *302* (5652), 1967-1969.
75. Peterson, M. L.; White, A. F.; Brown, G. E.; Parks, G. A. Surface passivation of magnetite by reaction with aqueous Cr (VI): XAFS and TEM results. *Environ. Sci. Technol.* **1997**, *31* (5), 1573-1576.
76. Byrne, J. M.; van der Laan, G.; Figueroa, A. I.; Qafoku, O.; Wang, C.; Pearce, C. I.; Jackson, M.; Feinberg, J.; Rosso, K. M.; Kappler, A. Size dependent microbial oxidation and reduction of magnetite nano- and micro-particles. *Sci. Rep.* **2016**, *6*, 30969.
77. Spiteri, C.; Kalinski, V.; Rösler, W.; Hoffmann, V.; Appel, E.; Team, M. Magnetic screening of a pollution hotspot in the Lausitz area, Eastern Germany: correlation analysis between magnetic proxies and heavy metal contamination in soils. *Environ. Geol.* **2005**, *49*, 1-9.
78. Zhang, W.; Yu, L.; Lu, M.; Hutchinson, S. M.; Feng, H. Magnetic approach to normalizing heavy metal concentrations for particle size effects in intertidal sediments in the Yangtze Estuary, China. *Environ. Pollut.* **2007**, *147* (1), 238-244.

Open questions and objectives of this study

Although the biogeochemical redox reactions involving Fe in the environment have been studied for many years, the interactions of microorganisms with mixed valent Fe minerals such as magnetite and their impact on the properties of the mineral and associated contaminants and nutrients remain important open questions. Magnetite has been shown to change its ratio of Fe(II)/Fe(III) depending on the activity of Fe-reducing and Fe-oxidizing microorganisms. However, further changes like mineral dissolution and possible precipitation of secondary minerals are to be expected in a dynamic biogeobattery system. Reductive dissolution of magnetite would result in a loss of the magnetite nanoparticles and therefore a loss of an electron source/sink for microbial activity. It is unknown if magnetite (nano)particles can serve as biogeobatteries indefinitely or if the capability to act as biogeobattery will be lost during consecutive redox cycles.

Fe oxides, and magnetite specifically, have been investigated as a way for heavy metal remediation. However, activity of Fe-metabolizing microorganisms will greatly alter the mineral's surface properties and hence the capacity to adsorb heavy metal nutrients.

The understanding of the capability of magnetite to serve as a biogeobattery for Fe-metabolizing microorganisms will expand our understanding of the Fe cycle and the consequences for the (bio)availability of Fe minerals, and nutrients and contaminants that commonly associated with the minerals' surface area. Therefore, to improve our understanding of the magnetite biogeobattery the objectives of this study are:

- To determine the extent of magnetite oxidation and reduction during continued redox cycles (**Chapter 2**).

- To elucidate the consequences of this redox cycling on the properties of magnetite and its bioavailability as electron source and sink for Fe-metabolizing microorganisms (**Chapter 2).**

- To investigate whether magnetite nanoparticles can serve as biogeobatteries indefinitely, or to reveal processes which could lead to a loss of the biogeobattery properties (**Chapter 2**).

- To study the influences of microbially driven oxidation and reduction of magnetite nanoparticles on the adsorption capacity and efficiency towards environmentally relevant heavy metal contaminants (**Chapter 3**).

- To understand differences between biotic and abiotic magnetite nanoparticles regarding the particle aggregation (**Chapter 4**).

.

Chapter 2 – Personal contribution

The conceptual background to this project was designed by Assoc. Prof. Dr. James Byrne and Prof. Dr. Andreas Kappler, extending this hypothesis for nitrate-reducing Fe(II)-oxidizing culture KS was suggested by myself. Together with Assoc. Prof. Dr. James Byrne I designed the experiment. I performed the research experiments. The research was supervised by Assoc. Prof. Dr. James Byrne and Prof. Dr. A. Kappler. Dr. Natalia Jakus performed μ-XRD measurements and helped with the data analysis and interpretation. Discussions with Jun. Prof. Dr. E. Marie Muehe improved the methodology of this work. Lars Grimm performed freeze-drying of magnetite particles and BET measurement. Dr. Bio Wan performed FTIR measurements and helped with data discussion. Franziska Schädler performed flow injection analysis (FIA) measurements for nitrate and nitrite data. Verena Nikeleit performed high-pressure liquid chromatography (HPLC) for acetate data. Dr. Jeremiah Schuster and Dr. Stefan Fischer enabled access to electron microscopy infrastructure. I interpreted the collected data and wrote the manuscript. All co-authors contributed to the manuscript revisions and/or wrote parts of the manuscript.

Chapter 2: Magnetite nanoparticles are metastable biogeobatteries in consecutive redox cycles driven by microbial Fe oxidation and reduction

T. Bayer[1], N. Jakus[1, †], A. Kappler[1,2] and J. M. Byrne[3]

[1]Geomicrobiology Group, Department of Geosciences, University of Tuebingen, Schnarrenbergstrasse 94-96, 72076 Tuebingen, Germany

[†]Current address: Environmental Microbiology Laboratory, École Polytechnique Fédérale de Lausanne, CE1 644, Lausanne CH 1015, Switzerland.

[2]Cluster of Excellence: EXC 2124: Controlling Microbes to Fight Infection, Tuebingen, Germany.

[3]School of Earth Sciences, University of Bristol, Queens Road BS8 1RJ, Bristol, United Kingdom

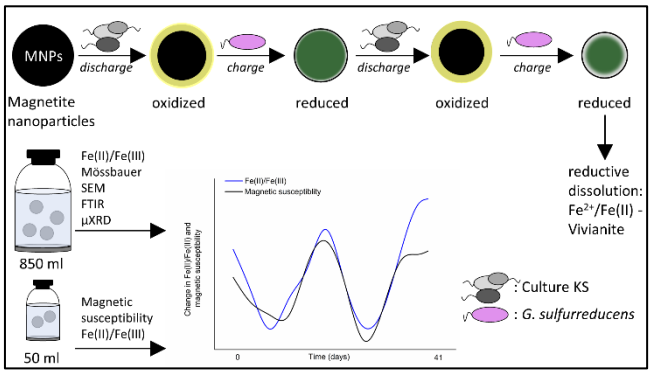

Manuscript submitted for publication to: *Geo-Bio Interfaces*

2.1 Abstract

Iron (Fe) minerals play a crucial role in biogeochemical cycles due to their ubiquity in nature, high adsorption capacity, and redox activity towards many other elements. Mixed-valent Fe minerals are unique since they contain Fe(II) and Fe(III). For example, magnetite (Fe(II)Fe(III)2O4) nanoparticles (MNPs) can affect the availability and mobility of nutrients and contaminants. This is due to the high surface area to volume ratio and the presence of Fe(II) and Fe(III), allowing redox transformation of (in-)organic contaminants. Recent studies have shown that magnetite can serve as an electron source and sink for Fe(II)-oxidizing and Fe(III)-reducing microorganisms, storing and releasing electrons; thus, it functions as a biogeobattery. However, the ability of MNPs to act as biogeobatteries over consecutive redox cycles and the consequences for mineral integrity and identity remain unknown. Here, we show MNPs working as biogeobatteries in two consecutive redox cycles over 41 days. MNPs were first oxidized by the autotrophic nitrate-reducing Fe(II)-oxidizing culture KS and subsequently reduced by the Fe(III)-reducing Geobacter sulfurreducens. In addition to reduced magnetite, we identified the Fe(II) mineral vivianite after reductions, suggesting partial reductive dissolution of MNPs and re-crystallization of Fe2+ with phosphate from the growth medium. Measurements of the Fe(II)/Fe(III) ratio revealed microbial oxidation and reduction for the first redox cycle (oxidation: 0.29±0.014, reduction: 0.75±0.023) and the second redox cycle (oxidation: 0.30±0.015, reduction: 1.64±0.10). Relative changes in magnetic susceptibility (∆κ in %) revealed greater changes for the second oxidation (–8.7±1.99%) than the first (–3.9±0.19%), but more minor changes for the second reduction (+14.29±0.39%) compared to the first (+25.42±1.31%). Our results suggest that MNPs served as biogeobatteries but became less stable over time, which has significant consequences for associated contaminants and nutrients and bioavailability for Fe-metabolizing microorganisms.

2.2 Introduction

Biogeochemical element cycles determine the distribution and availability of nutrients and contaminants in environmental systems. Iron (Fe) (oxyhydr)oxides are essential constituents in sediments and soils, as Fe is one of the most abundant elements in Earth's crust (Kendall, Anbar, Kappler and Konhauser, 2012) and is interlinked with the global carbon, nitrogen and oxygen cycles (Kappler, Becker and Enright, 2021). Fe is present in ferrous Fe(II) and ferric Fe(III) forms (Kappler, Bryce, Mansor, Lueder, Byrne and Swanner, 2021). As Fe is critical to almost all living organisms as a nutrient, it has a high turnover in the biosphere (Kappler and Straub, 2005) and can undergo redox cycling between oxidation states by abiotic or biotic processes (Kappler, Becker and Enright, 2021; Kappler, Bryce, Mansor, Lueder, Byrne and Swanner, 2021). At circumneutral pH, Fe(II) can be oxidized by photoautotrophic, nitrate-reducing, or microaerophilic bacteria (Widdel, Schnell, Heising, Ehrenreich, Assmus and Schink, 1993; Straub, Benz, Schink and Widdel, 1996; Emerson and Moyer, 1997; Bryce et al., 2018). Fe(III)-reducing bacteria use fatty acids or H2 as electron donors to reduce Fe(III) in anoxic conditions (Lies, Hernandez, Kappler, Mielke, Gralnick and Newman, 2005; Lovley et al., 2011). Mixed-valent Fe minerals are unique because they contain both Fe(II) and Fe(III) in their crystal structure (Usman, Byrne, Chaudhary, Orsetti, Hanna, Ruby, Kappler and Haderlein, 2018). Magnetite, an abundant mixed-valent Fe oxide (Maher and Taylor, 1988; Evans and Heller, 2003), contains two Fe(III) and one Fe(II) per unit cell in crystals with ideal stoichiometry, giving it the formula of Fe(II)Fe(III)2O4. While Fe(III) in magnetite is present in octahedral or tetrahedral coordination, Fe(II) is only in tetrahedral coordination. In the environment, magnetite can be formed through biological processes such as microbial Fe(II) oxidation (Miot, Li, Benzerara, Sougrati, Ona-Nguema, Bernard, Jumas and Guyot, 2014), microbial Fe(III) reduction (Lovley, Stolz, Nord Jr and Phillips, 1987; Kappler, Thompson and Mansor, 2023), and intracellularly by magnetotactic bacteria (Schüler, 2002; Uebe and Schüler, 2016; Amor, Tharaud, Gélabert and Komeili, 2020), which use magnetite crystals to navigate along the earth's magnetic field (Byrne and Amor, 2023). Abiotic processes that produce magnetite include weathering (Evans and Heller, 2003) and anthropogenic processes like combustion (Maher, 2009). When present as nanoparticles (MNPs), magnetite can have a specific surface area of up to 100 m2g–1 (Cornell and Schwertmann, 2003; Bayer, Wei, Kappler and Byrne, 2023) which

promotes interactions with nutrients and contaminants via adsorption (Sundman, Vitzhum, Adaktylos-Surber, Figueroa, van der Laan, Daus, Kappler and Byrne, 2020; Bayer, Wei, Kappler and Byrne, 2023) or redox reactions (Peterson, White, Brown and Parks, 1997). These interactions are heavily influenced by the Fe(II)/Fe(III) ratio, as it changes the redox properties, surface charge, magnetic properties, and hence the reactive surface of the mineral (Gorski, Nurmi, Tratnyek, Hofstetter and Scherer, 2010). Since there are two Fe(III) for every Fe(II), the Fe(II)/Fe(III) ratio for stoichiometric magnetite is 0.5. Maghemite (γ-Fe2O3) is the fully oxidized end member of magnetite with a deficiency in Fe to maintain charge balance (Usman, Byrne, Chaudhary, Orsetti, Hanna, Ruby, Kappler and Haderlein, 2018). It was previously shown that the ratio of MNPs can exceed the stoichiometry (≥ 0.5), in particular following microbial Fe(III) reduction (Byrne, Klueglein, Pearce, Rosso, Appel and Kappler, 2015; Bayer, Wei, Kappler and Byrne, 2023), as it was demonstrated that the Fe(II)/Fe(III) ratio can be altered through activity of Fe-metabolizing microorganisms. Fe(II) in MNPs was shown to be an electron source for the phototrophic Fe(II)-oxidizing strain Rhodopseudomonas palustris TIE-1 and Fe(III) as an electron sink for the Fe(III)-reducing Geobacter sulfurreducens and was therefore classified as a biogeobattery (Byrne, Klueglein, Pearce, Rosso, Appel and Kappler, 2015). Additionally, magnetite particles could play a crucial role in long-range electron transport (Liu, Rotaru, Shrestha, Malvankar, Nevin and Lovley, 2015; Byrne et al., 2016). During these previous experiments, the MNP-biogeobattery capabilities (i.e. the capability to serve as electron donor and acceptor for microbial metabolisms) were mainly tested with cell suspension experiments (high cell density of added microorganisms) in comparatively short time frames. Therefore, long-term effects and interactions between MNPs and microbes in consecutive cycles were not fully explored. We expect that consecutive redox cycles with lower numbers of added microorganisms have key effects on the stability and stoichiometry of MNPs and, hence, on the redox and magnetic properties. It was previously demonstrated that long-term incubations could reveal previously overlooked processes during Fe(II) oxidation (Bayer, Tomaszewski, Bryce, Kappler and Byrne, 2023). Therefore, to shed light on the importance of prolonged microbial Fe(II) oxidation and Fe(III) reduction on the properties of MNPs, long-term experiments with growing cultures (low volumes of added microbes) are key to understanding changes to MNPs properties, which will influence the (bio-)availability of contaminants

and nutrients in natural environments. In this study, we investigated microbial oxidation and reduction of MNPs over 41 days by nitrate-reducing Fe(II)-oxidizing culture KS and Fe(III)-reducing G. sulfurreducens. We quantified the Fe(II)/Fe(III) ratio and the relative change in magnetic susceptibility $\Delta\kappa$ in % during two full redox cycles driven by these microorganisms. Additionally, we analysed mineral properties, composition, and morphology by X-ray diffractometry (μXRD), Mössbauer spectroscopy, scanning electron microscopy (SEM), and Fourier-transform infrared spectroscopy (FTIR).

2.3 Experimental Methods

Magnetite synthesis

Magnetite nanoparticles were synthesized using a modified version of Pearce et al. (Pearce, Qafoku, Liu, Arenholz, Heald, Kukkadapu, Gorski, Henderson and Rosso, 2012). Specifically, a separating funnel was kept anoxic by sealing it with a rubber stopper and continuously flushing it with N2 in a fume hood. The funnel was connected to a rubber-stopper-sealed 1 L Schott bottle via rubber tubing. To ensure anoxia of the system, it was flushed for ≥ 5 min after adding anoxic Fe solution to the Schott bottle and anoxic NH4OH solution to the separating funnel. The synthesized magnetite was collected and washed four times with anoxic ultrapure water and then resuspended in a pH 7 bicarbonate (NaHCO3) buffer (22 mM).

Cultivation of microorganisms

The nitrate-reducing Fe(II)-oxidizing culture KS and the Fe(III)-reducing G. sulfurreducens were obtained from the culture collection of the Geomicrobiology group at the University of Tuebingen. Cells were cultivated before inoculation for seven days (culture KS) or five days (G. sulfurreducens) in replicate 50 ml serum bottles with a volume of 25 ml and 10% v/v inoculum. As previously described, incubations were performed in a bicarbonate-buffered medium (Tominski, Heyer, Lösekann-Behrens, Behrens and Kappler, 2018). Once fully grown, the bottles from each respective culture were pooled in a sterile, anoxic Schott bottle to ensure homogeneity. For culture KS, 4 mM of NaNO3 and for G. sulfurreducens, 20 mM of Na-acetate was added from sterile and anoxic stock solutions.

Experimental setup

Large volume 9 x 1 L Schott bottles and small volume 9 x 50 ml serum bottles (six replicates and three controls each) were amended with bicarbonate buffered growth medium, 30 mM magnetite (as total Fe concentration), and 4 mM NaNO3. Culture KS (10% v/v) was added to six bottles, while the same volume of buffered medium was added to three controls. The total volumes were 850 ml and 25 ml, respectively. Schott bottles were sealed with a rubber stopper and regular lid with an opening that allowed sampling. Serum bottles were sealed with a rubber stopper and heat-shrinking tube to avoid interferences of otherwise commonly used aluminium lids during magnetic susceptibility measurements (Porsch, Dippon, Rijal, Appel and Kappler, 2010). Large Schott bottles were sampled for geochemical and mineralogical analysis, while the smaller serum bottles were mainly used for magnetic susceptibility measurements. To ensure consistency with the larger Schott bottles, serum bottles were irregularly sampled for geochemical analysis. An overview of the sampling procedure is displayed in Fig. S1.

Oxidation and reduction cycles

At the end of each redox half-cycle MNPs were washed five times with anoxic and sterile bicarbonate buffer to remove cells. To retain MNPs in the bottles, two strong magnets were applied from the bottom and side before and during disposal of the washing solution. The bottles were kept anoxic through a constant stream of N2/CO2 gas and sterile by working next to Bunsen burners. After washing, new growth medium was added to the MNPs, followed by thorough shaking to guarantee well mixing. Microorganisms and stock solutions (NaNO3/Na-acetate) were added to achieve consistent volumes and concentrations of NaNO3/Na-acetate and 10% v/v inoculum of the respective bacteria.

Geochemical analyses

Samples for geochemical analyses were taken in the glovebox, centrifuged for 5 minutes at 10,000 g, and split into pellet and supernatant. The pellet was dissolved in the glovebox in 40 mM sulfamic acid in 6 M HCl (60 min) (Klueglein and Kappler, 2013; Schaedler, Kappler and Schmidt, 2017). The supernatant was used to quantify dissolved Fe, nitrate, and acetate (see Fig. S2 for nitrate and acetate). The 6 M HCl

extract was diluted with 1 M HCl, and the Fe concentrations were determined via the ferrozine assay (Stookey, 1970). Fe(III) was calculated as the difference between measurements for total Fe and Fe(II). This sampling was performed daily for Schott bottles. For the 50 ml serum bottles, it was performed exclusively before the first and after the last magnetic susceptibility measurement of each redox phase.

Magnetic susceptibility κ measurements

In-situ volume-specific magnetic susceptibility κ was measured with a KLY-3 Kappabridge (AGICO, Czech Republic). The 50 ml serum bottles were lowered into a coil, and the response to an applied magnetic field (peak magnetic field of 300 A/m and a frequency of 875 Hz) was measured. Each bottle of biological and control replicates was measured in triplicate.

^{57}Fe Mössbauer spectroscopy

Samples were taken for Mössbauer spectroscopy before addition of bacteria; after addition of culture KS; at the end of the first oxidation; after each subsequent redox half phase. In the glovebox, 12 ml liquid was filtered through a 0.45 µm pore-size syringe filter (Millipore membrane); filtered minerals were embedded in Kapton tape and stored at –20 °C until measurement. The samples were inserted into a closed-cycle exchange gas cryostat (SHI-650-5; Janis Research, USA). Spectra were collected at 140 K using a constant acceleration drive system (WissEl, Blieskastel, Germany). Gamma radiation was emitted by a 57Co-source embedded in a rhodium matrix. Spectra were calibrated against a 7-µm-thick Fe(0) foil at room temperature. Recoil (University of Ottawa, Canada) was used to fit spectra using the extended Voigt-based fitting model (xVBF). The Lorentzian half-width-half-maximum (HWHM) value was kept constant at either 0.124 mm/s or 0.140 mm/s, as two separate Mössbauer instruments were used for sample analyses, each with different instrumental broadening. Spectra were analysed with respect to the isomer shift (δ), quadrupole splitting (ΔEQ), and hyperfine magnetic field (Bhf).

X-ray diffractometry (XRD)

In an anoxic glovebox, samples for µXRD analysis were collected from batch incubations. Solid precipitates were washed with anoxic Milli-Q, dried, and stored in

Eppendorf tubes in an oven (28 °C). μXRD was performed using Bruker's D8 Discover GADDS XRD2 micro-diffractometer equipped with a standard sealed tube with a Co-anode (CoKα radiation, λ = 0.17903 nm, 30 kV/30 mA). The measurement time was 120 s at two detector positions (15° and 40°). Resulting diffractograms were analysed using the software Match! (version 3.6.2.121) using reference patterns from Crystallography Open Database (ver. COD-Inorg REV248644 2020.03.03). Before starting the measurement, samples were retained in an N2-filled Schott bottle for as long as possible to prevent oxidation. The average crystal size (nm) and the lattice parameter (ang) were calculated from the μXRD patterns by analysis of the most intense reflection of magnetite (311) at 2 Theta of 43.36° (Patterson, 1939).

Scanning electron microscopy

Samples for scanning electron microscopy (SEM) were prepared at the end of the second reduction. 2 ml sample were removed from different bottles with a syringe and needle in an anoxic glovebox, washed with Milli-Q water, and then carefully distributed on a glass slide covered with 0.1% w/v aqueous solution of Poly-L-Lysine, to provide a hydrophilic surface for cells. After drying in the glovebox, the samples were transported in an N2-filled Tupperware box to be coated with a Bal-Tec SCD005 sputter coater to prevent as much contact with O_2 as possible. Samples were coated with platinum for 120 s at 4×10^{-2} mbar, 30 mA, and a working distance of 35 mm, which yielded a platinum layer of 12 nm thickness. SEM was performed with a ZEISS Crossbeam 550/5502 L, an acceleration voltage of 5 kV, and the SESI (secondary electrons - secondary ions) detector.

Fluorescence microscopy

Culture KS collected after the first oxidation was imaged between repeated washing steps to determine the number of washes needed to remove bacterial cells. 10 μL of the sample were stained with 2 μL of Dead/Live stain to obtain a fluorescence signal (LIVE/DEAD BacLight bacterial viability kit, Molecular Probes) and investigated with a Leica DM 5500 B (Leica Microsystems).

Specific surface area determination

To determine the specific surface area (SSA), MNPs were freeze-dried and weighed out anoxically. For SSA determination, a Micromeritics Gemini VII surface area and porosity analyser (Micromeritics Instrument Cooperation, USA) equipped with a VacPrep 061, using N_2 as adsorbate, was used.

Infrared spectroscopy

Samples for Fourier-transformed infrared (FTIR) analysis were collected after the second oxidation and the second reduction. Samples were washed with anoxic MilliQ water and dried in Eppendorf tubes in an anoxic glovebox. Spectra were collected on a Bruker Vertex 70 FTIR spectrometer equipped with a deuterated triglycine sulfate (DTGS) detector (Bruker Optics, Inc., Ettlingen, Germany). Pellets were prepared by mixing 1 mg of the sample with 250 mg of KBr (spectrometry grade) and pressed into a pellet. Spectra were collected under vacuum from 400 to 4000 cm−1 for an average of 256 scans at an instrument resolution of 4 cm−1 (Wan, Yan, Liu, Tan, Chen and Feng, 2016).

2.4 Results & Discussion

MNPs characterization

The MNPs were analysed using a range of analytical techniques. BET measurements revealed a specific surface area of freeze-dried unaltered MNPs of 90.3 m2g–1. The Fe(II)/Fe(III) ratio of MNPs (Fe(II)/Fe(III)mag hereafter) before inoculation was determined with the ferrozine assay as 0.43±0.002. Both values closely agree with earlier studies (Pearce, Qafoku, Liu, Arenholz, Heald, Kukkadapu, Gorski, Henderson and Rosso, 2012; Bayer, Wei, Kappler and Byrne, 2023). 57Fe Mössbauer spectroscopy of a MNP sample before inoculation revealed pure magnetite with two characteristic sextets corresponding to octahedrally and tetrahedrally coordinated Fe (Fig. S3, light blue and grey). Analysis of the relative spectral areas of the two sextets resulted in a Fe(II)/Fe(III)mag of 0.45±0.01 (Table S1) (Gorski and Scherer, 2010), which is in good agreement with the ferrozine measurement. The average crystallite size of our MNPs from µXRD patterns was calculated to be 10.24 nm (Patterson, 1939; Klug and Alexander, 1974) and the Fe(II)/Fe(III)mag from µXRD data was calculated as 0.52 (Table S1) (Pearce, Qafoku, Liu, Arenholz, Heald, Kukkadapu, Gorski,

Henderson and Rosso, 2012). Partial adsorption of reduced Fe(II) to the inner-surface of the utilized glassware is a possible explanation for inconsistent results between chemical and spectroscopic methods, especially towards later stages of the experiment (Notini, Byrne, Tomaszewski, Latta, Zhou, Scherer and Kappler, 2019; Dong et al., 2020).

Measurements of the Fe(II)/Fe(III) ratio and magnetic susceptibility κ during redox cycling experiment

Measurements of the Fe(II)/Fe(III) ratio ($Fe(II)/Fe(III)_{total}$ hereafter) by ferrozine during the redox cycling experiments (Fig. 1a) showed that the MNPs were successfully oxidized by culture KS as previously described for this strain (Bayer, Wei, Kappler and Byrne, 2023).

Initially (t = 0), the $Fe(II)/Fe(III)_{total}$ determined by ferrozine seemed lower than expected for stoichiometric magnetite (0.404±0.005 for the experiments and 0.434±0.001 for controls). Stoichiometric magnetite is expected to have a Fe(II)/Fe(III) ratio of 0.5. However, slightly lower values have been previously seen for MNPs synthesized using this method (Byrne, Klueglein, Pearce, Rosso, Appel and Kappler, 2015; Sundman, Byrne, Bauer, Menguy and Kappler, 2017; Bayer, Wei, Kappler and Byrne, 2023). Additionally, about 1 mM Fe(III) was introduced due to inoculation of culture KS, that was pre-cultivated on Fe(II). Due to the additional Fe(III) introduced to the system, the average Fe(II)/Fe(III)total ratio determined by ferrozine is expected to have been 0.026±0.002 lower, as calculated for the initial six replicates in Schott bottles.

At the end of the first oxidation period (10 days), the Fe(II)/Fe(III)total decreased to 0.285±0.014 in biological replicates and remained at 0.436±0.003 in controls, demonstrating that culture KS successfully oxidized MNPs. After washing the MNPs, and less than 24 hours after adding G. sulfurreducens, the Fe(II)/Fe(III)total quickly increased to 0.448±0.023. At the same time, the controls showed a slight decrease to 0.402±0.003, presumably caused by the washing process. During the following eight days, the Fe(II)/Fe(III)total of the MNPs increased to 0.754±0.023, while it slightly decreased for abiotic controls to 0.384±0.006. This suggested that G. sulfurreducens successfully reduced the MNPs after the previous oxidation by culture KS.

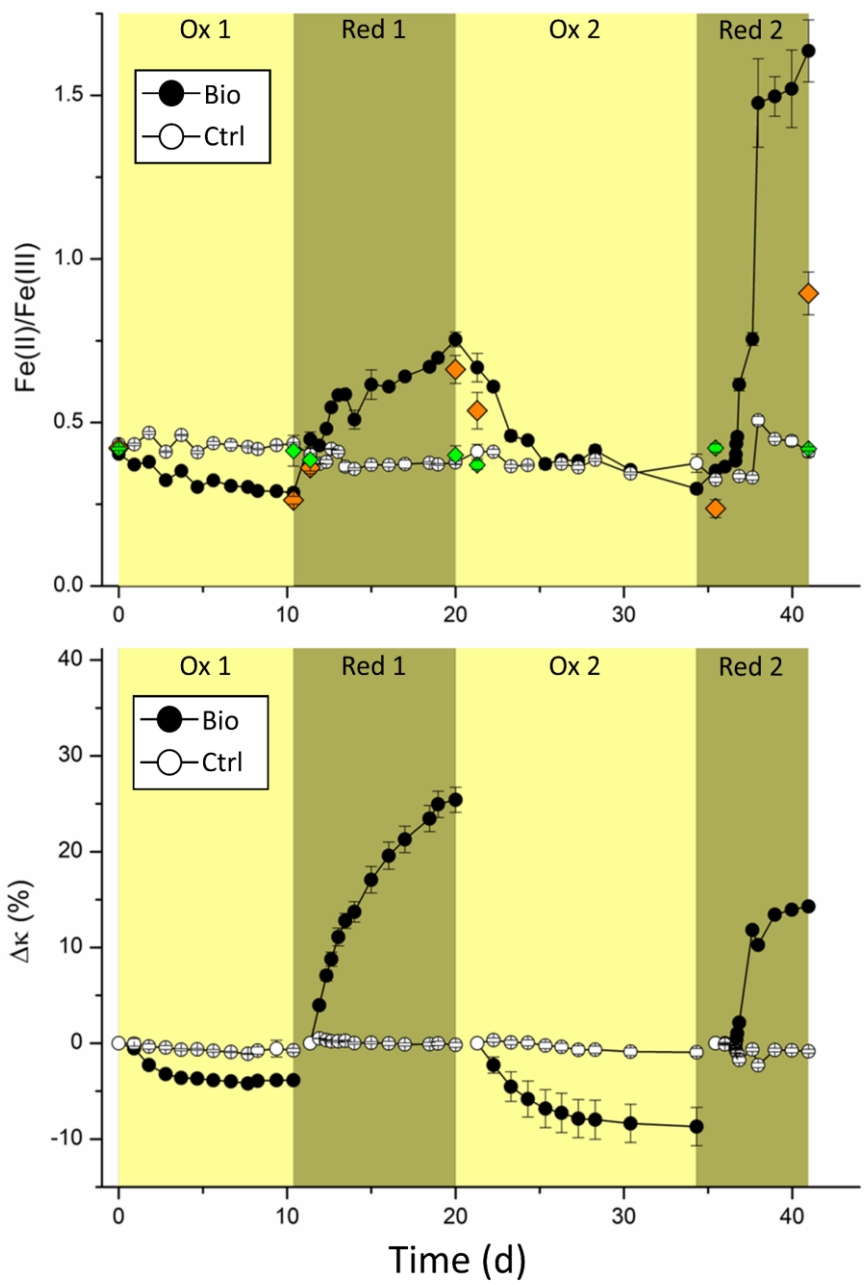

Figure 1. *(a) Changes in the Fe(II)/Fe(III) ratio determined by ferrozine assay over time and (b) relative changes of magnetic susceptibility (Δκ in %), with respect to the starting value of each oxidation or reduction cycle, of MNPs incubated with either culture KS (yellow background) or G. sulfurreducens (green background). Symbols and error bars represent the mean and standard deviation of at least five replicates for Fe ratio and six replicates for Δκ. Controls were performed in triplicate. Black circles show biological replicates and white circles show controls.*

.

As expected, the trend in relative magnetic susceptibility changes ∆κ closely followed the changes observed in Fe(II)/Fe(III)total. After the first oxidation ∆κ was –3.86±0.19% for the experimental replicates and only –0.74±0.21% for the controls (Fig. 1b). Possible partial dissolution of the MNPs in the growth medium is a reasonable explanation. For the first reduction, ∆κ greatly increased to +25.42±1.31% and did not change for controls at –0.18± 0.25%. Previous investigations with G. sulfurreducens in cell suspension experiments with magnetite only showed relative increases of ∆κ between 12% (Byrne et al., 2016) and 16.5% (Byrne, Klueglein, Pearce, Rosso, Appel and Kappler, 2015), whereas we showed a much greater increase. This demonstrated that the reduction of MNPs can happen over extended timeframes and to even greater extents than previously demonstrated. While the dissolution of MNPs by G. sulfurreducens was previously reported and correlated with increased concentrations of dissolved Fe2+ (Byrne, Klueglein, Pearce, Rosso, Appel and Kappler, 2015), we could not detect any aqueous Fe. Presumably, the reduction rate plays an essential role in the fate of Fe(II)/Fe2+ produced during the reduction of MNPs by G. sulfurreducens. A lower inoculum concentration (i.e. fewer initial bacteria) could have resulted in lower reduction rates of MNPs, giving produced Fe2+ enough time to interact with the surface of MNPs and, therefore, not remain as dissolved Fe2+.

Notably, during the change from first reduction to second oxidation, one of the experimental replicates was compromised, and the following geochemistry data are calculated with averages and standard deviations of 5 instead of the previous six replicates.

The Fe(II)/Fe(III)total decreased over 13 days to 0.297±0.014 during the second oxidation. Due to an initially high ratio of 0.754, we could determine a much greater change during the second oxidation compared to the first, where the Fe(II)/Fe(III)total decreased from 0.404 to 0.285 (–0.119). The relative change of the Fe(II)/Fe(III)total during the second oxidation, with a decrease of -0.457 from 0.754 to 0.297, was almost four times greater than that of the first oxidation. However, the final Fe(II)/Fe(III)total at the end of both oxidations did not greatly differ (0.285±0.014 after the first and 0.297±0.014 after the second oxidation). This suggests that culture KS oxidized all available Fe(II) of MNPs during both oxidations. Interestingly, this suggests that MNPs

charged with electrons by G. sulfurreducens were a much more accessible and electron-rich source. During the first 28 hours of the second reduction, the Fe(II)/Fe(III)total increased from 0.297±0.014 to 0.383±0.012. Only six hours later the Fe(II)/Fe(III)total was 0.616±0.019. Interestingly, Fe(II)/Fe(III)total continuously increased to a value of 1.64±0.10 at the end of the experiment. This extremely high ratio suggests other processes than the reduction of MNPS occurred. For controls, Fe(II)/Fe(III)total remained at 0.41±0.02, a relative decrease of roughly 5% compared to t = 0.

Magnetic susceptibility measurements showed a relative decrease for the second oxidation of –8.70±1.99% for experimental replicates compared to just –0.94±0.41% for controls. A two times greater $\Delta\kappa$ was achieved during the second oxidation than the first. These results agreed with the findings of ferrozine measurements and again showed that the electrons in the charged MNPs were a better electron source for KS than unaltered MNPs. While Fe(II)/Fe(III)total immediately changed during the second reduction, $\Delta\kappa$ initially showed negligible changes, increasing by 1±0.18% after 31 hours. At this time point, the Fe(II)/Fe(III)total ratio had already reached a value of 0.46±0.01. After that, the magnetic susceptibility increased rapidly to +11.8±0.40% in just 20 hours and eventually plateaued at +14%, which was comparatively low regarding the $\Delta\kappa$ of +25% during the first reduction. The general trends of the $\Delta\kappa$ results differed from Fe(II)/Fe(III)total results. However, it is essential to remember that magnetic susceptibility only measured the magnetic components, whereas Fe(II)/Fe(III)total ratios by ferrozine incorporated all magnetic and non-magnetic components. Magnetic susceptibility values hence exclusively report changes to the MNPs, suggesting that the capacity of MNPs to be reduced by G. sulfurreducens could have been inhibited during the second reduction. An inhibition of reduction could have been caused by surface passivation of MNPs due to microbially derived organic compounds, which have been shown to interact with the surfaces of iron oxides (Eusterhues, Wagner, Häusler, Hanzlik, Knicker, Totsche, Kögel-Knabner and Schwertmann, 2008). However, since we saw a concomitant increase of Fe(II) with ferrozine, another Fe(II) containing phase must have been produced, which increased the Fe(II) but not κ. Additionally, while most of the discussed changes in measured Fe(II)/Fe(III)total and $\Delta\kappa$ were arguably caused by redox changes in MNPs, the high increase of the Fe(II)/Fe(III)total ratio during the second reduction to 1.64 seemed

unrealistic. To explain this, Fe(II) or Fe2+ produced during reductions must have ended in different sinks. Additionally, the ∆κ only increased to +14% during the second reduction, compared to +26% during the first reduction. As the relative change in magnetic susceptibility is linked to a change in the MNPs, these results also suggest the presence of an additional process, and we assume that a partial dissolution of MNPs happened during the long-term incubation with G. sulfurreducens. Since no aqueous Fe phase was detected throughout the experiment, the comparatively slow reduction with 10% inoculum of G. sulfurreducens allowed Fe2+ to associate with MNPs or possibly re-precipitate with available phosphate and carbonate, both present in the microbial growth medium. While the Fe(II)/Fe(III)total would have suggested a continuous reduction of magnetite, the magnetic susceptibility revealed that the reduction must have led to this reductive dissolution of the mineral (Cornell and Schwertmann, 2003), to increase Fe(II) concentration without increasing magnetic susceptibility. As determined by µ-XRD, the Fe(II) phosphate vivianite (FeII3(PO4)2, 8H2O) precipitated. As it has a comparatively low magnetic susceptibility with a peak value of 5.24 × 10–6 m3kg–1 at 37 K (Frederichs, von Dobeneck, Bleil and Dekkers, 2003), which is approximately 300 times smaller than the magnetite magnetic susceptibility of 5.2 × 10–4 m3kg–1 (Heider, Zitzelsberger and Fabian, 1996), it did not interfere with the measurements of κ. Controls of magnetic susceptibility measurements showed no greater change than –1±0.43% throughout the experiment.

Mössbauer spectroscopy

Samples for 57Mössbauer spectroscopy were taken at the start of the experiment and the end of each oxidation/reduction to further investigate the mineral identities and better understand the fate of MNPs. After inoculating with culture KS, the Mössbauer spectrum (Fig. 2a) showed two characteristic sextets that corresponded to the Fe in octahedral (grey) and tetrahedral (light blue) coordination. At 140 K, the two sextets showed some distinct features on the left-hand side and overlapping on the right-hand side, as commonly observed with nanoparticulate magnetite (Gorski and Scherer, 2010). The spectral areas of octahedral and tetrahedral Fe were used to calculate the Fe(II)/Fe(III)mag ratio in magnetite (Gorski and Scherer, 2010). The Fe(II)/Fe(III)mag after addition of culture KS was calculated as 0.44±0.01. Fitting required the incorporation of an additional doublet with a small isomer shift and quadrupole splitting,

which was hence identified as a Fe(III) phase (Fig. 2a, light green). Since no Fe(III) was detected before inoculation, the doublet was exclusively caused by inoculation with the Fe(II)-oxidizing culture KS. As washing the cells resulted in no MNP-oxidation in test experiments, this Fe(III) phase of approximately 1 mM concentration was unavoidable. We calculated the Fe(II)/Fe(III)mag after the first oxidation (Fig. 2b) as 0.39±0.02 (Tables S1-2), showing that MNP oxidation correlated with the change in magnetic susceptibility of –3.86±0.19%, but showed a greater ratio than ferrozine (0.285±0.014). The Mössbauer fit after the first oxidation again required a Fe(III) doublet (Fig. 2b, light green), corresponding to the Fe(III) added with the inoculum.

At the end of the first reduction (Fig. 2c), the two sextets remained, showing the integrity of the MNPs even after reduction. No more Fe(III) was detected, suggesting that if any Fe(III) remained despite the washing, the readily available poorly crystalline ferrihydrite, which is the oxidation product of culture KS (Nordhoff, Tominski, Halama, Byrne, Obst, Kleindienst, Behrens and Kappler, 2017; Bayer, Tomaszewski, Bryce, Kappler and Byrne, 2023) was reduced by G. sulfurreducens. The fit required a doublet with a large isomer shift and quadrupole splitting (Fig. 2c, red), indicative of a newly formed Fe(II) phase. This Fe(II) phase was much more abundant than the previously detected Fe(III), with a relative area of 17.92±0.51%. Even if the washing step did not remove any Fe(III) after oxidation, it could still not explain such a large Fe(II) doublet. Comparing the obtained isomer shift and quadrupole splitting values (Table S2), one of the closest matches was the Fe(II) phosphate vivianite (Wilfert, Dugulan, Goubitz, Korving, Witkamp and Van Loosdrecht, 2018), a reasonable assumption for our system (Miot, Benzerara, Morin, Bernard, Beyssac, Larquet, Kappler and Guyot, 2009). The calculated Fe(II)/Fe(III)mag was 0.42±0.01. Whilst this ratio was much smaller than the determined ratio with ferrozine (0.75±0.023), we could now show that the high ferrozine values were biased by newly formed Fe(II) phases, and we propose that the actual value was closer to the one determined by Mössbauer spectroscopy. Additionally, since $\Delta\kappa$ continuously increased, we assume that the reduction of magnetite and dissolution-reprecipitation happened simultaneously, as formation of vivianite could not have explained the changes in $\Delta\kappa$ values.

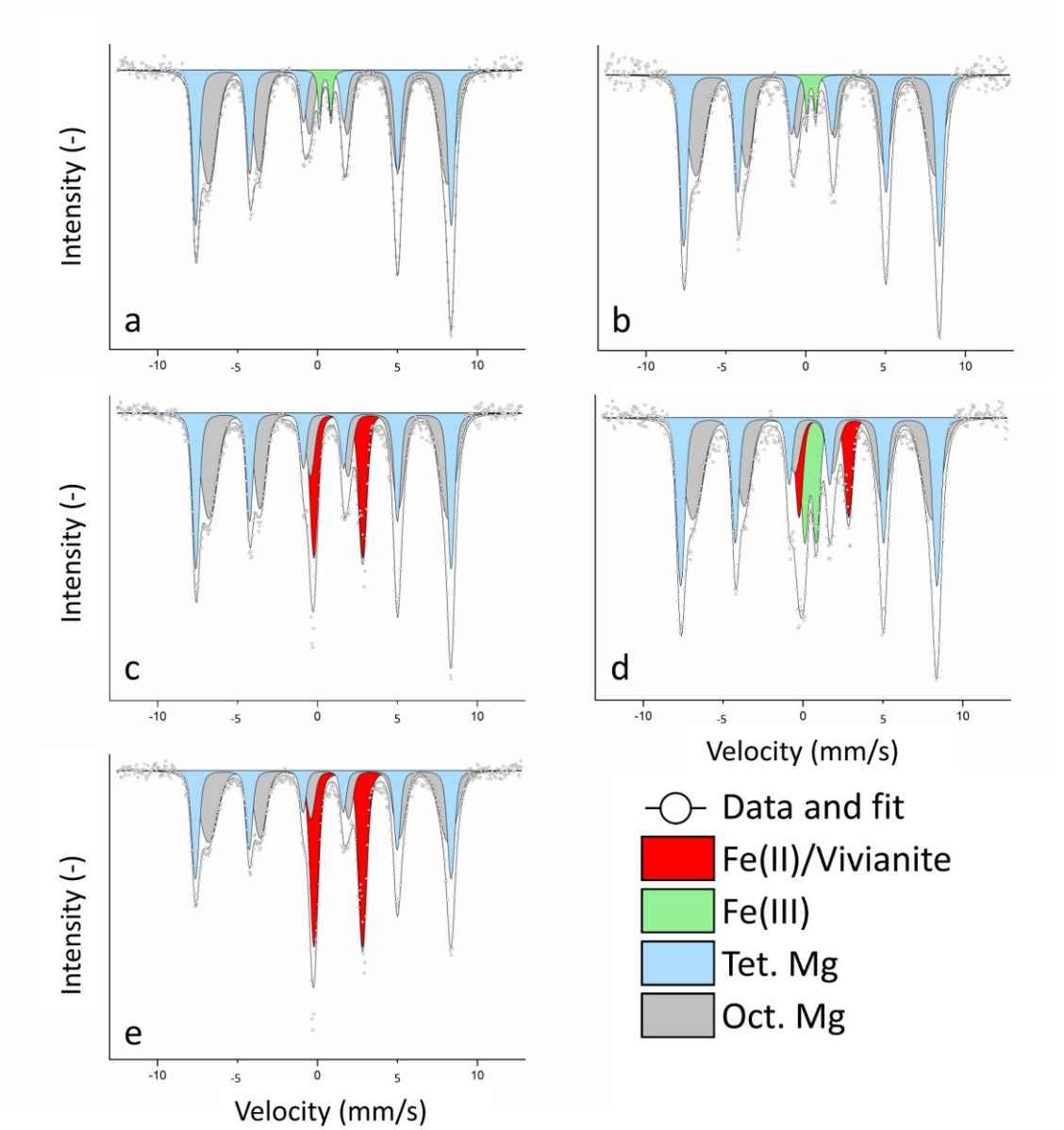

Figure 2. *^{57}Fe Mössbauer spectra of MNPs collected at 140 K at (a) the start and (b) the end of the first oxidation, (c) after the first reduction, (d) after the second oxidation, and (e) after the second reduction. Characteristic sextets of tetrahedral (light blue) and octahedral (grey) magnetite could be observed. We additionally detected a Fe(III) phase (light green) due to inoculation with culture KS and a Fe(II) phase (red), which was confirmed to be (partially) vivianite.*

After the second oxidation, we detected four different phases (Fig. 2d): The two MNPs sextets (light blue, grey), Fe(II) (red), and Fe(III) (light green). The Fe(III) doublet had a much greater spectral area (11.26±0.66%) than for the first oxidation (2.83%). A higher spectral area than roughly 4% for Fe(III) due to inoculum of culture KS was not expected. The high value for Fe(III) indicated that previously formed Fe(II) was not successfully removed by washing and magnetic separation. We suggest that some of the transferred Fe(II) was vivianite, which culture KS was unable to oxidize as previously reported (Tominski, Heyer, Lösekann-Behrens, Behrens and Kappler, 2018; Bayer, Tomaszewski, Bryce, Kappler and Byrne, 2023), while other transferred Fe(II) phases were used as electron sources, resulting in a larger Fe(III) spectral area. Remembering the data shown in Fig. 1, we assume that this oxidation of a non-magnetic bioavailable Fe(II) phase happened towards the end of the second oxidation since $\Delta\kappa$ (Fig. 1b) did not decrease anymore, but the Fe(II)/Fe(III)total ratio did (Fig. 1a). We conclude that reduced MNPs were a preferred electron donor for culture KS, even in the presence of other Fe(II) phases. This could be attributed to a more negative redox potential of highly reduced MNPs, again suggesting that the additional Fe(II) phase was oxidized after MNP oxidation became less favourable (Gorski, Nurmi, Tratnyek, Hofstetter and Scherer, 2010; Dong, Zeng, Sheng, Chen, Yu and Kappler, 2023). The remaining Fe(II) at the end of the second oxidation should have consisted of vivianite. The calculated ratio of the MNPs after the second oxidation was 0.40±0.02.

Finally, after the last reduction, we could determine the two sextets (MNPS) and one Fe(II) doublet (Fig. 2e), which now corresponded to a third of the spectral area (29.94±0.60%). We again assume that most of this Fe(II) phase was vivianite. However, other Fe(II) phases, such as siderite (FeCO3, due to the presence of bicarbonate buffer), were likely since the isomer shift and quadrupole splitting were not conclusive for either vivianite or siderite (Table S2). This large increase of the Fe(II) explained the great increase of the Fe(II)/Fe(III)total ratio as determined by ferrozine (Fig. 1a). During MNPs reduction, dissolved aqueous Fe2+ could have either interacted with magnetite particles or precipitated as a Fe(II) contributing to the doublet that was determined with Mössbauer spectroscopy. Since $\Delta\kappa$ changed much less during the second reduction, we assume that the MNP-dissolution was now more pronounced and that continuous cycling led to an overall loss of mineral, questioning

the biogeobattery capacities of MNPs over many consecutive redox cycles. After the second reduction, the Fe(II)/Fe(III)mag was 0.42±0.01. A control was measured at the end of the second reduction and showed minor changes compared to the control at t = 0 (Fig. S3). The changes in spectral areas are displayed in Fig. S3.

During the first reduction, the trends in ferrozine Fe(II)/Fe(III)total ratios, $\Delta\kappa$ (Fig. 1), and the calculated Mössbauer Fe(II)/Fe(III)mag ratios (Table S2) suggested that the reduction of MNPs could have proceeded for a longer time. Previously, ratios of up to 0.46 after reduction, determined by Mössbauer at 140 K, were described (Byrne, Klueglein, Pearce, Rosso, Appel and Kappler, 2015). The much greater Fe(II)/Fe(III) ratios that we present here and the previous absence of any Fe(II) doublets in Mössbauer spectra imply that the rate and duration of reduction greatly influenced the fate of MNPs. Previously, it was shown that the rate of Fe(II) reduction had consequences for the formation of secondary minerals (Dippon, Schmidt, Behrens and Kappler, 2015) and that the reduction rate of ferrihydrite influenced the formation of magnetite or other Fe minerals (Han, Tomaszewski, Sorwat, Pan, Kappler and Byrne, 2020). We expand on this knowledge by proposing that in a MNP-biogeobattery system, the rate of Fe(II) oxidation and especially Fe(III) reduction is of great importance for the fate of Fe2+/Fe(II). While no newly formed Fe(II) phases could be detected in comparatively short experiments with high cell densities (Byrne, Klueglein, Pearce, Rosso, Appel and Kappler, 2015), we showed that low inoculum and extended timeframe for oxidation/reduction promoted a reductive dissolution and reprecipitation. We conclude that the incubation of MNPs as a biogeobattery will eventually lead to reductive dissolution of the mineral. This dissolution will be more pronounced with an increasing number of redox cycles.

X-ray diffractometry (XRD)

Samples for µXRD were collected at the start of the experiment and after every oxidation and reduction phase for biotic samples and controls (Fig. 3). For the initial phases, only reflections that can be assigned to magnetite were detected with three main reflections at 2θ of: 43.36°, 50.50° and 35.11°. Only magnetite was identified, since the ferrihydrite added with culture KS (see previous discussion) typically does not yield a clear diffraction pattern with the Co-source used for X-ray generation (CoKα radiation, λ = 0.17903 nm). This did not change after the first oxidation.

After the first reduction, we could see the same main reflections caused by magnetite. Additionally, the signal seemed generally noisier between 2θ of 30° to 50°, which we could not identify as a specific mineral phase. Two minor reflections could be seen at 2θ of 15° and 38°, corresponding with the main and an additional reflection of vivianite. µXRD confirmed that vivianite had already formed during the first reduction.

For the second oxidation, both the sample and control showed only the three main reflections of magnetite at 2θ of 43.36°, 50.50° and 35.11°, with some minor reflection

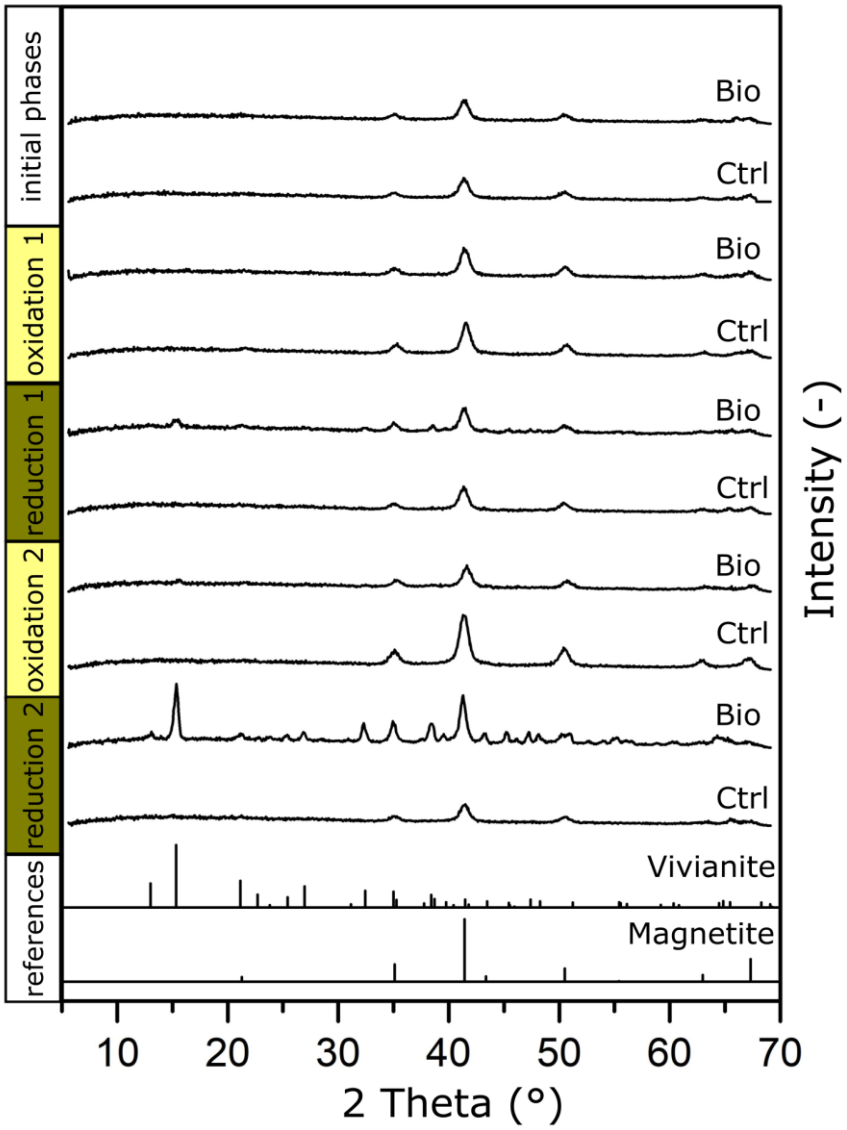

Figure 3. *µXRD patterns of MNPs collected before the experiment (initial phases) and at the end of each oxidation/reduction for the biotic experiments (Bio) and the abiotic controls (Ctrl). References of vivianite and magnetite are shown at the bottom.*

remaining at 2θ of 15.32° (vivianite). This agreed with the Mössbauer measurement, which showed that a Fe(II) phase remained even after the second oxidation. As previously discussed, this Fe(II) phase initially consisted of vivianite and possibly other Fe(II) phases (e.g. siderite). While culture KS could have used additional Fe(II) phases as electron sources, vivianite remained because culture KS could not use it as an electron source (Tominski, Heyer, Lösekann-Behrens, Behrens and Kappler, 2018).
After the second reduction, the most intense reflection (2θ 15.32°) corresponded to the main reflection of vivianite, and further reflections of vivianite were observed (Fig. 3). We could again confirm vivianite as a product during long-term low-volume incubations of MNPs as a biogeobattery in our system.
We additionally compared matches with the reflections of siderite (FeCO3), as it could have precipitated in HCO3–-containing medium. We could show that the first and fourth main reflections (2θ 32.17° and 38.45°) closely matched our diffraction pattern (Fig. S4, black dotted lines). However, since only 2 of the six most intense reflections of siderite could be seen (Fig. S4, grey dotted lines), we cannot confirm its presence with certainty. We again suggest that more than one Fe(II) phase was present in our system, that the main phase was the Fe(II) phosphate vivianite, and that the remainder could have been siderite and other Fe(II)-containing phases.
We calculated the lattice parameters and average crystal diameter (dμXRD in nm) from collected μ-XRD patterns (Table S1). The synthesized MNPs had a size of 10.07 nm and a sample inoculated with culture KS 9.97 nm. The diameter of the abiotic controls showed little change throughout the experiment (dXRD = 10.2120 nm±0.0006 nm). In contrast, the diameters of the biotic samples changed as follows (start ox 1, end ox 1, end red 1, end ox 2, end red 2): 10.07 nm, 9.18 nm, 12.31 nm, 10.88 nm, 17.76 nm. The calculated diameter after reductions (12.31 nm and 17.76 nm) increased by 22% and 76% compared to the initial value. Since we confirmed the presence of vivianite, which has overlapping reflections with magnetite at 2θ of 41.4°, it likely influenced the lattice parameters and average crystal diameter calculation. With increasingly more vivianite present, the calculated crystal size was decreasingly representative of the MNPs.

Infrared spectroscopy

FTIR spectra were collected from 2 biotic samples and one control after the second oxidation and from 3 biotic samples and one control after the second reduction (Fig. 4). All samples showed characteristic vibrations of Fe-O bonds at approximately 565 cm-1, which were mainly caused by the added MNPs. The peaks are widened for the samples collected after the second reduction (Fig. 4c-e), which indicates that additional Fe-O bonds were present in the system (Sklute, Kashyap, Dyar, Holden, Tague, Wang and Jaret, 2018). Since vivianite was abundant, especially after the second reduction, we could see four vibration bands of approx. 819, 939, 975, and 1051 cm-1 corresponding to P-O bonds (Frost, Martens, Williams and Kloprogge, 2002), which only had muted intensities after oxidations and in controls (Fig. 4). Additional vibrations at higher wavenumbers of approx. 1620 cm-1, 3140 cm-1, and 3500 cm-1 were caused by O-H vibrations, which were present in all samples. The increased signals of Fe-O and P-O bonds, especially after the reductions, confirmed the formation of vivianite as a result of Fe reduction and reprecipitation.

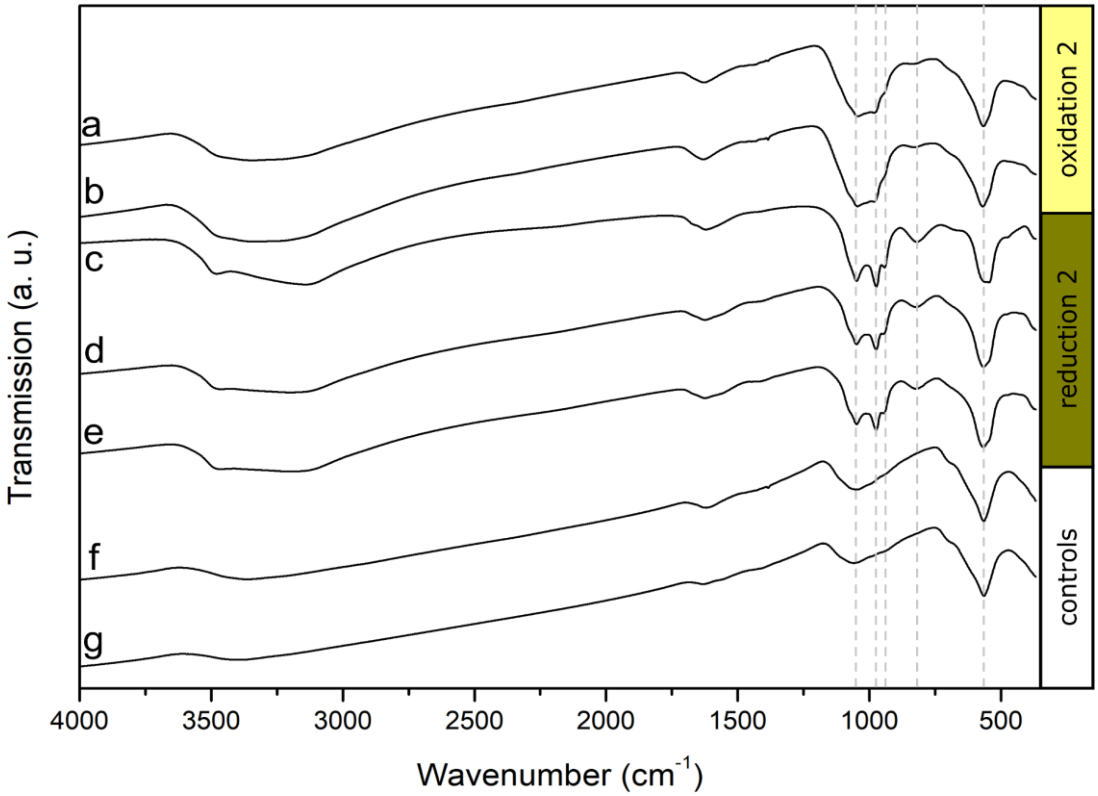

Figure 4. *Fourier-transformed infrared (FTIR) spectra of anoxically dried magnetite samples. (a-b) Biological replicates collected after the second oxidation, (c-e) biological replicates collected after the second reduction, (f) control collected after the second oxidation, (g) control collected after the second reduction.*

Scanning electron microscopy

After the second reduction, samples were prepared for FE-SEM analysis (Fig. 5). Micrographs indicated that MNPs had a diameter of roughly 10 to 12 nm (Fig. 5a),

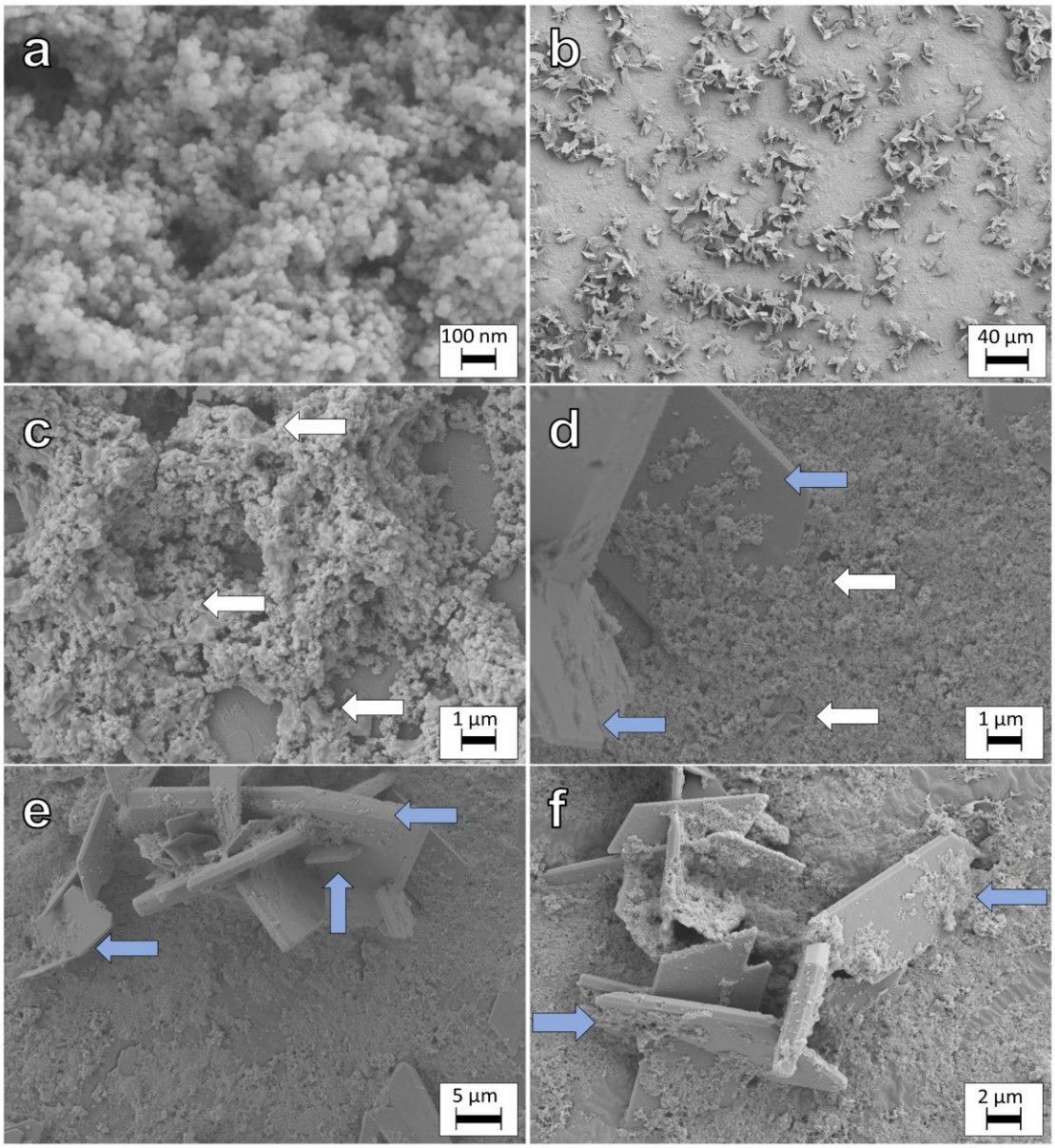

Figure 5. *SEM micrographs of samples collected at the end of the second reduction. (a) High magnification of MNPs, (b) overview of MNPs and newly formed vivianite, (c) remains of biomass/cells (presumably G. sulfurreducens) (cells were not fixed with glutaraldehyde), (d) close contact of MNPs and formed vivianite and cells, (e-f) characteristic twinning of vivianite crystals and close contact with MNPs. White arrows point to cells and blue arrows to MNPs-vivianite associations.*

which agrees with the initial XRD calculated diameter (dXRD = 10.07 for biotic samples and 10.21 nm for controls) and could underline the influence of abundant vivianite on the diameter determination with µXRD after reductions. Vivianite was also observed (Fig. 5b, d-f), agreeing with results from µXRD and 57Fe Mössbauer spectroscopy.
Both almost intact cells and cell fragments of G. sulfurreducens were observed (Fig. 5c-d), as indicated by blue arrows in the respective micrographs. As the samples were not fixed with glutaraldehyde, the cellular structure was not preserved throughout sample preparation and analysis. MNPs appeared to cover the surface of the vivianite crystals in close contact and sometimes nested within vivianite surface defects (Fig. 5b and 5d-f, blue arrows). While sample preparation is essential for SEM analysis, we propose that this close interaction of vivianite and magnetite was not solely a preparation artefact. We hypothesize that the close interactions of vivianite and MNPs caused carry-over of Fe(II)-phases between reduction and oxidation redox half-cycles, despite washings. Additional micrographs are displayed in Fig S5.

2.5 Conclusions

We investigated the viability of magnetite nanoparticles (MNPs) to serve as biogeobatteries in two consecutive redox cycles with growing bacteria and followed changes in biogeochemistry and mineralogy over time. Our results showed that MNPs were successfully used as an electron source and sink over 41 days by the autotrophic nitrate-reducing Fe(II)-oxidizing culture KS and the Fe(III)-reducing Geobacter sulfurreducens. Changes in magnetic susceptibility and Fe(II)/Fe(III) ratio showed successful oxidation of MNPs by culture KS, as previously described (Bayer, Wei, Kappler and Byrne, 2023). The second oxidation resulted in a greater decrease in relative magnetic susceptibility $\Delta\kappa$ than the first (–8.7% vs. –3.9%). This demonstrated that the “charged” MNPs, due to reduction by G. sulfurreducens, were a favourable electron source for culture KS. These findings were supported by the change of the Fe(II)/Fe(III)total ratio, which decreased by –0.119 for the first and by –0.457 for the second oxidation. The lowest measured Fe(II)/Fe(III)total ratio detected during the entire experiment was 0.24, a point where the increasingly positive redox potential of “discharged” MNPs potentially does not allow further oxidation. During reduction of

MNPs by G. sulfurreducens secondary Fe(II) minerals formed, as determined by Mössbauer spectroscopy, µXRD and SEM. Even in the presence of these Fe(II) phases, culture KS prioritized oxidation of MNPs as we showed by comparing changes in Fe(II)/Fe(III)total to ∆κ. Interestingly, the changes in ∆κ were smaller for the second reduction than for the first (+14.3% vs. +25.42%). This suggests that the capacity for MNPs to serve as an electron sink might diminish over time due dissolution of MNPs or further processes like passivation (Byrne et al., 2016). Due to clear evidence of increased vivianite precipitation, we suggest that the second reduction resulted in a more pronounced reductive dissolution followed by re-precipitation. We also suggest that the extent of reductive dissolution and reprecipitation will be increasingly pronounced with every additional redox cycle. The identity of vivianite was confirmed by µXRD and SEM. Additional Fe(II) phases were detected but could not be identified conclusively, likely due to poor crystallinity of these minerals, although some µXRD reflections point towards siderite formation. The demonstrated dissolution and reprecipitation of Fe2+ suggested that the Fe(II)/Fe(III)total ratio determined by the ferrozine assay was influenced by these newly formed Fe(II) phases and that the Fe(II)/Fe(III)mag ratio in MNPs – especially during reductions – was indeed lower than measured by the ferrozine assay.

Finally, while we demonstrated the biogeobattery functioning of MNPs in consecutive redox cycles, prolonged redox cycling did not only greatly influence the Fe(II)/Fe(III) ratio as expected, but resulted in mineral dissolution that represents a loss of MNPs over time. We suggest that, without additional processes that would form MNPs in the environment, like Fe oxidation and reduction, MNPs will be consumed over time. While Fe(II)-oxidizers would greatly benefit from reduced (electron-rich) MNPs, the Fe(III)-reducers would eventually have to rely on a different electron sink. However, the newly formed Fe(II) phases could also result in losing a usable electron source for Fe(II)-oxidizers, as we could show in our experiments with culture KS and the inability to oxidize newly formed vivianite. We suggest that a MNP biogeobattery can support the redox cycling of Fe-metabolizing bacteria, which will, however, disappear over time if no further processes result in the formation of MNPs, which were unlikely in our system. Finally, we show the great importance of contact time between bacteria and Fe-minerals and suggest that the results might be different according to the length of redox cycles, where short-term redox cycles presumably can maintain the integrity of

the MNPs, contrary to the here presented results of long-term incubations. The presented results have significant implications for the (bio)availability of contaminants and nutrients associated with the surface of MNPs. Over time, the remediation capacities of MNPs will decrease during continued redox cycling due to dissolution. The stability of MNPs and the formation and transformation of secondary minerals will determine the fate of contaminants and nutrients and the long-term activity of Fe-metabolizing bacteria.

Supplemental Material

Overview of performed samplings, acetate and nitrate data, Mössbauer relative spectral areas and fitting results, siderite μXRD reflections, additional scanning electron microscopy micrographs, fluorescence microscopy images, and compiled properties of MNPs are available in the supplemental material (PDF). All data (Mössbauer, ferrozine, magnetic susceptibility, μXRD, FTIR, nitrate/acetate) are available as a table (XLSX).

Author Contributions

T.B. and J.M.B. conceived the research. T.B. performed experiments and most analytical measurements. N.J. performed μXRD measurements. J.M.B. and A.K. supervised the research. The research was funded by financial support granted to J.M.B. and A.K. The manuscript was written through the contributions of all authors, and all authors have given their approval to the final version of the manuscript.

Conflict of Interest

The authors declare no competing financial interest.

Acknowledgements

The authors thank the editors and two random reviewers for handling and improving the quality of the manuscript with helpful comments. This work was financed through funding awarded to J.M.B (BY 82/2-1) and A.K. (KA 1736/48-1). The authors thank Lars Grimm for freeze drying and BET analysis, Biao Wan for FTIR measurements, Franziska Schädler for FIA measurements, Verena Nikeleit for HPLC measurements, and Jeremiah Schuster and Stefan Fischer for help with and access to the electron microscopy. We gratefully acknowledge the Tübingen Structural Microscopy Core

Facility, funded by the Excellence Strategy of the German Federal and State Governments, for their support and assistance in this work. J.M.B is supported by a UKRI Future Leaders Fellowship (MR/V023918/1). A.K. acknowledges infrastructural support by the Deutsche Forschungsgemeinschaft (DFG, German Research Foundation) under Germany's Excellence Strategy, Cluster of Excellence EXC2124, project ID 390838134.

2.6 References

1. Amor, M., Tharaud, M., Gélabert, A. and Komeili, A. (2020) Single-cell determination of iron content in magnetotactic bacteria: Implications for the iron biogeochemical cycle. Env. Microbiol., 22, 823-831.
2. Bayer, T., Tomaszewski, E.J., Bryce, C., Kappler, A. and Byrne, J.M. (2023) Continuous cultivation of the lithoautotrophic nitrate-reducing fe (ii)-oxidizing culture ks in a chemostat bioreactor. Env. Microbiol. Rep.
3. Bayer, T., Wei, R., Kappler, A. and Byrne, J.M. (2023) Cu(ii) and cd(ii) removal efficiency of microbially redox-activated magnetite nanoparticles. ACS Earth Space Chem.
4. Bryce, C., Blackwell, N., Schmidt, C., Otte, J., Huang, Y.M., Kleindienst, S., Tomaszewski, E., Schad, M., Warter, V. and Peng, C. (2018) Microbial anaerobic fe(ii) oxidation–ecology, mechanisms and environmental implications. Env. Microbiol., 20, 3462-3483.
5. Byrne, J.M. and Amor, M. (2023) Biomagnetism: Insights into magnetic minerals produced by microorganisms. Elements, 19, 208-214.
6. Byrne, J.M., Klueglein, N., Pearce, C., Rosso, K.M., Appel, E. and Kappler, A. (2015) Redox cycling of fe(ii) and fe(iii) in magnetite by fe-metabolizing bacteria. Sci., 347, 1473-1476.
7. Byrne, J.M., van der Laan, G., Figueroa, A.I., Qafoku, O., Wang, C., Pearce, C.I., Jackson, M., Feinberg, J., Rosso, K.M. and Kappler, A. (2016) Size dependent microbial oxidation and reduction of magnetite nano- and micro-particles. Sci. Rep., 6, 30969.
8. Cornell, R.M. and Schwertmann, U. (2003) The iron oxides: Structure, properties, reactions, occurrences and uses. John Wiley & Sons.
9. Dippon, U., Schmidt, C., Behrens, S. and Kappler, A. (2015) Secondary mineral formation during ferrihydrite reduction by shewanella oneidensis mr-1 depends on incubation vessel orientation and resulting gradients of cells, fe2+ and fe minerals. Geomicrobiol. J., 32, 878-889.
10. Dong, H., Zeng, Q., Sheng, Y., Chen, C., Yu, G. and Kappler, A. (2023) Coupled iron cycling and organic matter transformation across redox interfaces. Nat. Rev. Earth Environ., 4, 659-673.
11. Dong, Y., Sanford, R.A., Boyanov, M.I., Flynn, T.M., O'Loughlin, E.J., Kemner, K.M., George, S., Fouke, K.E., Li, S. and Huang, D. (2020) Controls on iron reduction and biomineralization over broad environmental conditions as suggested by the firmicutes orenia metallireducens strain z6. Environ. Sci. Technol., 54, 10128-10140.
12. Emerson, D. and Moyer, C. (1997) Isolation and characterization of novel iron-oxidizing bacteria that grow at circumneutral ph. Appl. Environ. Microbiol., 63, 4784-4792.
13. Eusterhues, K., Wagner, F.E., Häusler, W., Hanzlik, M., Knicker, H., Totsche, K.U., Kögel-Knabner, I. and Schwertmann, U. (2008) Characterization of ferrihydrite-soil organic matter coprecipitates by x-ray diffraction and mossbauer spectroscopy. Environ. Sci. Technol., 42, 7891-7897.
14. Evans, M. and Heller, F. (2003) Environmental magnetism: Principles and applications of enviromagnetics. Elsevier.
15. Frederichs, T., von Dobeneck, T., Bleil, U. and Dekkers, M.J. (2003) Towards the identification of siderite, rhodochrosite, and vivianite in sediments by their low-temperature magnetic properties. Phys. Chem. Earth, 28, 669-679.

16. Frost, R.L., Martens, W., Williams, P.A. and Kloprogge, J. (2002) Raman and infrared spectroscopic study of the vivianite-group phosphates vivianite, baricite and bobierrite. Mineralogical Magazine, 66, 1063-1073.
17. Gorski, C.A., Nurmi, J.T., Tratnyek, P.G., Hofstetter, T.B. and Scherer, M.M. (2010) Redox behavior of magnetite: Implications for contaminant reduction. Environ. Sci. Technol., 44, 55-60.
18. Gorski, C.A. and Scherer, M.M. (2010) Determination of nanoparticulate magnetite stoichiometry by mossbauer spectroscopy, acidic dissolution, and powder x-ray diffraction: A critical review. Am. Min., 95, 1017-1026.
19. Han, X., Tomaszewski, E.J., Sorwat, J., Pan, Y., Kappler, A. and Byrne, J.M. (2020) Effect of microbial biomass and humic acids on abiotic and biotic magnetite formation. Environ. Sci. Technol., 54, 4121-4130.
20. Heider, F., Zitzelsberger, A. and Fabian, K. (1996) Magnetic susceptibility and remanent coercive force in grown magnetite crystals from 0.1 μm to 6 mm. Phys. Earth and Planetary Interiors, 93, 239-256.
21. Kappler, A., Becker, S. and Enright, A.M.L. (2021) Metals, microbes, and minerals - the biogeochemical side of life. Pp. 185-228. In K. Peter, and T. Martha Sosa, Eds. Living on iron,De Gruyter.
22. Kappler, A., Bryce, C., Mansor, M., Lueder, U., Byrne, J.M. and Swanner, E.D. (2021) An evolving view on biogeochemical cycling of iron. Nat. Rev. Microbiol., 19, 360-374.
23. Kappler, A. and Straub, K.L. (2005) Geomicrobiological cycling of iron. Rev. Min. Geochem., 59, 85-108.
24. Kappler, A., Thompson, A. and Mansor, M. (2023) Impact of biogenic magnetite formation and transformation on biogeochemical cycles. Elements, 19, 222-207.
25. Kendall, B., Anbar, A.D., Kappler, A. and Konhauser, K.O. (2012) The global iron cycle. Fundame. of Geobiol., 1, 65-92.
26. Klug, H.P. and Alexander, L.E. (1974) X-ray diffraction procedures: For polycrystalline and amorphous materials.
27. Lies, D.P., Hernandez, M.E., Kappler, A., Mielke, R.E., Gralnick, J.A. and Newman, D.K. (2005) Shewanella oneidensis mr-1 uses overlapping pathways for iron reduction at a distance and by direct contact under conditions relevant for biofilms. Appl. Environ. Microbiol., 71, 4414-4426.
28. Liu, F., Rotaru, A.E., Shrestha, P.M., Malvankar, N.S., Nevin, K.P. and Lovley, D.R. (2015) Magnetite compensates for the lack of a pilin-associated c-type cytochrome in extracellular electron exchange. Env. Microbiol., 17, 648-655.
29. Lovley, D.R., Stolz, J.F., Nord Jr, G.L. and Phillips, E.J. (1987) Anaerobic production of magnetite by a dissimilatory iron-reducing microorganism. Nat., 330, 252.
30. Lovley, D.R., Ueki, T., Zhang, T., Malvankar, N.S., Shrestha, P.M., Flanagan, K.A., Aklujkar, M., Butler, J.E., Giloteaux, L. and Rotaru, A.-E. (2011) Geobacter: The microbe electric's physiology, ecology, and practical applications. Adv. Microb. Physiol., 59, 1-100.
31. Maher, B.A. (2009) Rain and dust: Magnetic records of climate and pollution. Elements, 5, 229-234.
32. Maher, B.A. and Taylor, R.M. (1988) Formation of ultrafine-grained magnetite in soils. Nat., 336, 368.
33. Miot, J., Benzerara, K., Morin, G., Bernard, S., Beyssac, O., Larquet, E., Kappler, A. and Guyot, F. (2009) Transformation of vivianite by anaerobic nitrate-reducing iron-oxidizing bacteria. Geobiol., 7, 373-384.

34. Miot, J., Li, J., Benzerara, K., Sougrati, M.T., Ona-Nguema, G., Bernard, S., Jumas, J.-C. and Guyot, F. (2014) Formation of single domain magnetite by green rust oxidation promoted by microbial anaerobic nitrate-dependent iron oxidation. Geochim. Cosmochim. Acta, 139, 327-343.
35. Nordhoff, M., Tominski, C., Halama, M., Byrne, J.M., Obst, M., Kleindienst, S., Behrens, S. and Kappler, A. (2017) Insights into nitrate-reducing fe(ii) oxidation mechanisms through analysis of cell-mineral associations, cell encrustation, and mineralogy in the chemolithoautotrophic enrichment culture ks. Appl. Environ. Microbiol., 83, e00752-00717.
36. Notini, L., Byrne, J.M., Tomaszewski, E.J., Latta, D.E., Zhou, Z., Scherer, M.M. and Kappler, A. (2019) Mineral defects enhance bioavailability of goethite toward microbial fe (iii) reduction. Environ. Sci. Technol., 53, 8883-8891.
37. Patterson, A.L. (1939) The scherrer formula for x-ray particle size determination. Phys. Rev., 56, 978-982.
38. Pearce, C.I., Qafoku, O., Liu, J., Arenholz, E., Heald, S.M., Kukkadapu, R.K., Gorski, C.A., Henderson, C.M.B. and Rosso, K.M. (2012) Synthesis and properties of titanomagnetite (fe 3− xtixo 4) nanoparticles: A tunable solid-state fe (ii/iii) redox system. J. Colloid Interface Sci., 387, 24-38.
39. Peterson, M.L., White, A.F., Brown, G.E. and Parks, G.A. (1997) Surface passivation of magnetite by reaction with aqueous cr (vi): Xafs and tem results. Environ. Sci. Technol., 31, 1573-1576.
40. Porsch, K., Dippon, U., Rijal, M.L., Appel, E. and Kappler, A. (2010) In-situ magnetic susceptibility measurements as a tool to follow geomicrobiological transformation of fe minerals. Environ. Sci. Technol., 44, 3846-3852.
41. Schaedler, F., Kappler, A. and Schmidt, C. (2017) A revised iron extraction protocol for environmental samples rich in nitrite and carbonate. Geomicrobiol. J., 35, 23-30.
42. Schüler, D. (2002) The biomineralization of magnetosomes in magnetospirillum gryphiswaldense. International microbiology, 5, 209-214.
43. Sklute, E.C., Kashyap, S., Dyar, M.D., Holden, J.F., Tague, T., Wang, P. and Jaret, S.J. (2018) Spectral and morphological characteristics of synthetic nanophase iron (oxyhydr) oxides. Phys. Chem. Miner., 45, 1-26.
44. Stookey, L.L. (1970) Ferrozine - a new spectrophotometric reagent for iron. Anal. Chem., 42, 779-781.
45. Straub, K.L., Benz, M., Schink, B. and Widdel, F. (1996) Anaerobic, nitrate-dependent microbial oxidation of ferrous iron. Appl. Environ. Microbiol., 62, 1458-1460.
46. Sundman, A., Byrne, J.M., Bauer, I., Menguy, N. and Kappler, A. (2017) Interactions between magnetite and humic substances: Redox reactions and dissolution processes. Geochem. Trans., 18, 1-12.
47. Sundman, A., Vitzhum, A.-L., Adaktylos-Surber, K., Figueroa, A.I., van der Laan, G., Daus, B., Kappler, A. and Byrne, J.M. (2020) Effect of fe-metabolizing bacteria and humic substances on magnetite nanoparticle reactivity towards arsenic and chromium. J. Hazard. Mater., 121450.
48. Tominski, C., Heyer, H., Lösekann-Behrens, T., Behrens, S. and Kappler, A. (2018) Growth and population dynamics of the anaerobic fe(ii)-oxidizing and nitrate-reducing enrichment culture ks. Appl. Environ. Microbiol., 84, e02173-02117.
49. Uebe, R. and Schüler, D. (2016) Magnetosome biogenesis in magnetotactic bacteria. Nat. Rev. Microbiol., 14, 621.

50. Usman, M., Byrne, J., Chaudhary, A., Orsetti, S., Hanna, K., Ruby, C., Kappler, A. and Haderlein, S. (2018) Magnetite and green rust: Synthesis, properties, and environmental applications of mixed-valent iron minerals. Chem. Rev., 118, 3251-3304.
51. Wan, B., Yan, Y., Liu, F., Tan, W., Chen, X. and Feng, X. (2016) Surface adsorption and precipitation of inositol hexakisphosphate on calcite: A comparison with orthophosphate. Chem. Geol., 421, 103-111.
52. Widdel, F., Schnell, S., Heising, S., Ehrenreich, A., Assmus, B. and Schink, B. (1993) Ferrous iron oxidation by anoxygenic phototrophic bacteria. Nat., 362, 834.
53. Wilfert, P., Dugulan, A.I., Goubitz, K., Korving, L., Witkamp, G.J. and Van Loosdrecht, M.C.M. (2018) Vivianite as the main phosphate mineral in digested sewage sludge and its role for phosphate recovery. Water Res., 144, 312-321.

2.7 Supporting Information

Magnetite nanoparticles are metastable biogeobatteries in consecutive redox cycles driven by microbial Fe oxidation and reduction

T. Bayer[1], N. Jakus[1, †], A. Kappler[1,2] and J.M. Byrne[3]

[1]Geomicrobiology Group, Department of Geosciences, University of Tuebingen, Schnarrenbergstrasse 94-96, 72076 Tuebingen, Germany

[†]Current address: Environmental Microbiology Laboratory, École Polytechnique Fédérale de Lausanne, CE1 644, Lausanne CH 1015, Switzerland.

[2]Cluster of Excellence: EXC 2124: Controlling Microbes to Fight Infection, Tuebingen, Germany.

[3]School of Earth Sciences, University of Bristol, Queens Road BS8 1RJ, Bristol, United Kingdom

Number of figures: 6

Number of tables: 2

Total number of pages: 9 (including cover page)

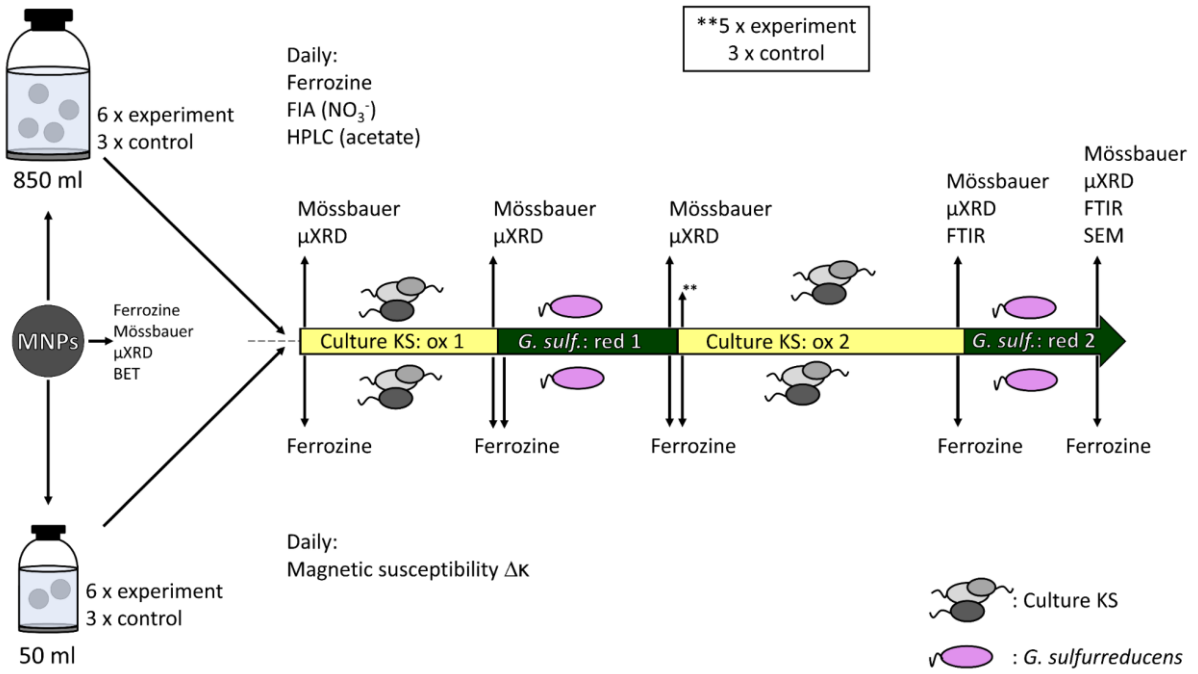

Figure S1. Overview of samplings performed before and during the experiment with magnetite nanoparticles as biogeobattery in two consecutive redox cycles with the nitrate-reducing Fe(II)-oxidizing culture KS and the Fe(III)-reducer *G. sulfurreducens* over 41 days.

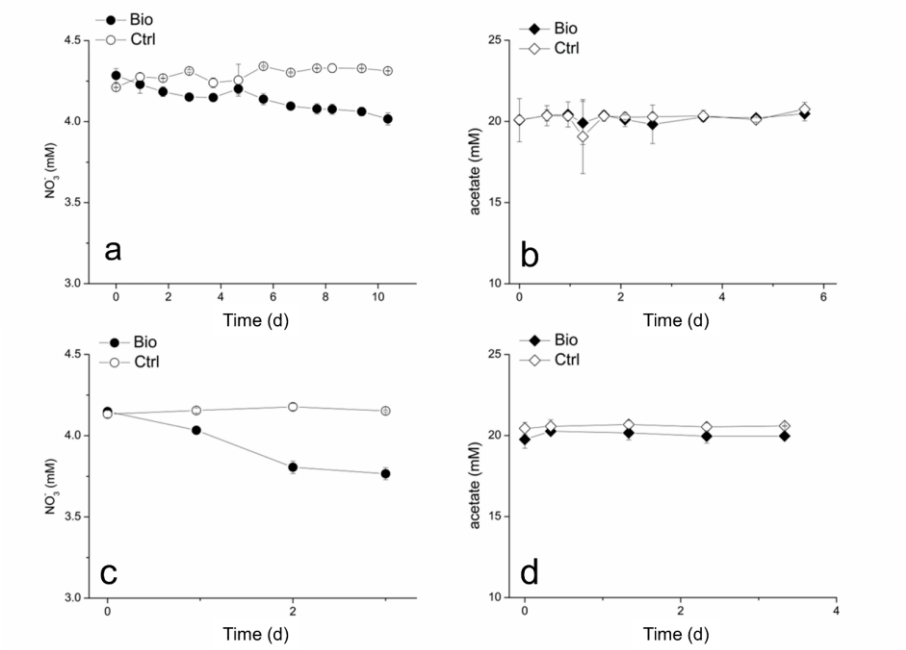

Figure S2. (a+c) Measured changes of nitrate during first and second oxidation, respectively, (b+d) measured acetate during first and second reduction. Not all time points were sampled as Fe(II)/Fe(III) samples were preferentially treated. As expected, NO_3^- decreased during growth of culture KS (a+c). Since acetate was supplied in excess, no changes could be determined via HPLC (b+d, not fully sampled). Please note that the y-axis starts at 3.0 mM for nitrate and 10 mM for acetate.

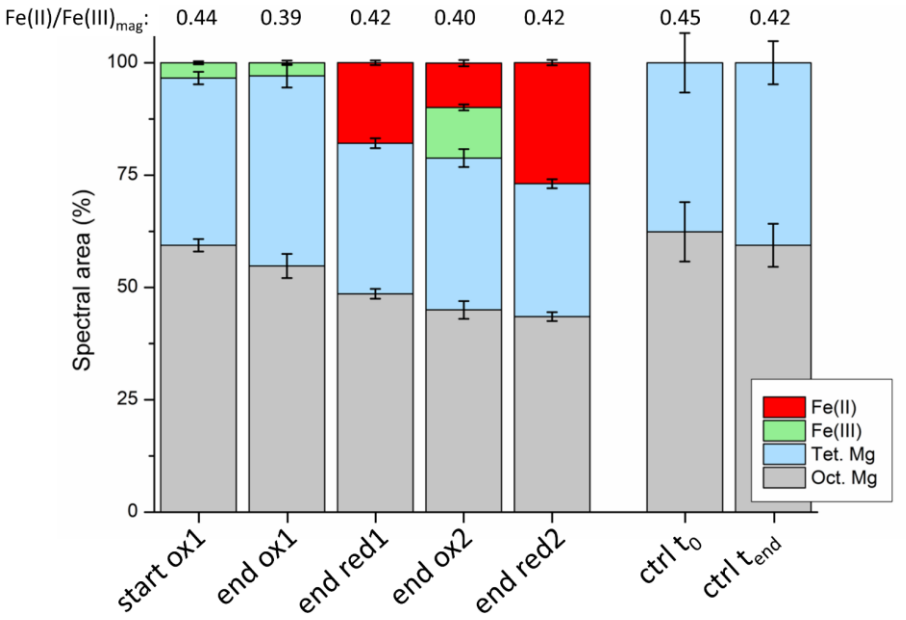

Figure S3. Relative abundances of spectral areas collected with ^{57}Fe Mössbauer spectroscopy. Displayed are octahedral magnetite (Oct. Mg, grey), tetrahedral magnetite (Tet. Mg, light blue), Fe(III) (light green) and Fe(II) (red). The numbers above stacked columns display the determined Fe(II)/Fe(III) ratio of magnetite in the respective sample (Fe(II)/Fe(III)mag).

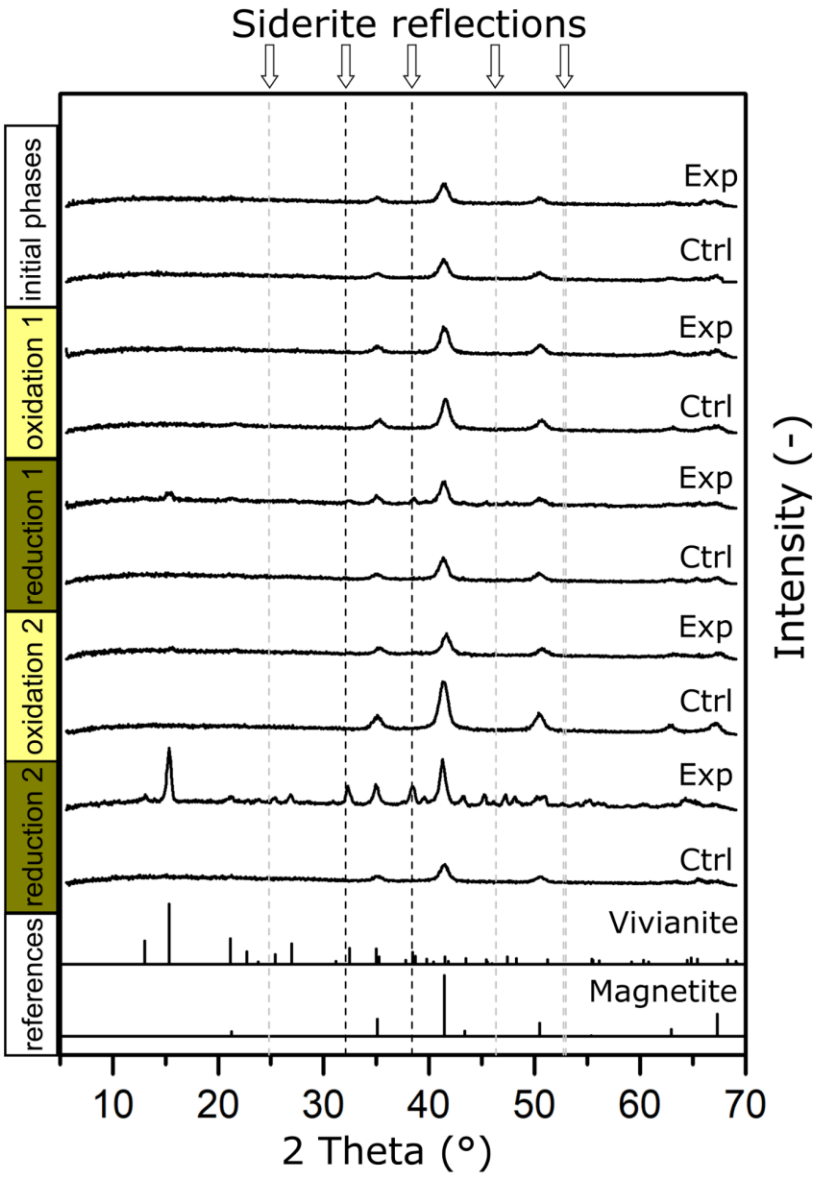

Figure S4. µXRD samples displayed with 6 major reflections of siderite (2θ of 24.85°, 32.12°, 38.45°, 46.33°, 52.92°, 53.1°). Two black dotted lines overlap with samples (32.12°, 38.45°), especially after the second reduction. Additional lines (grey) show major reflections of siderite that were not detected in our samples.

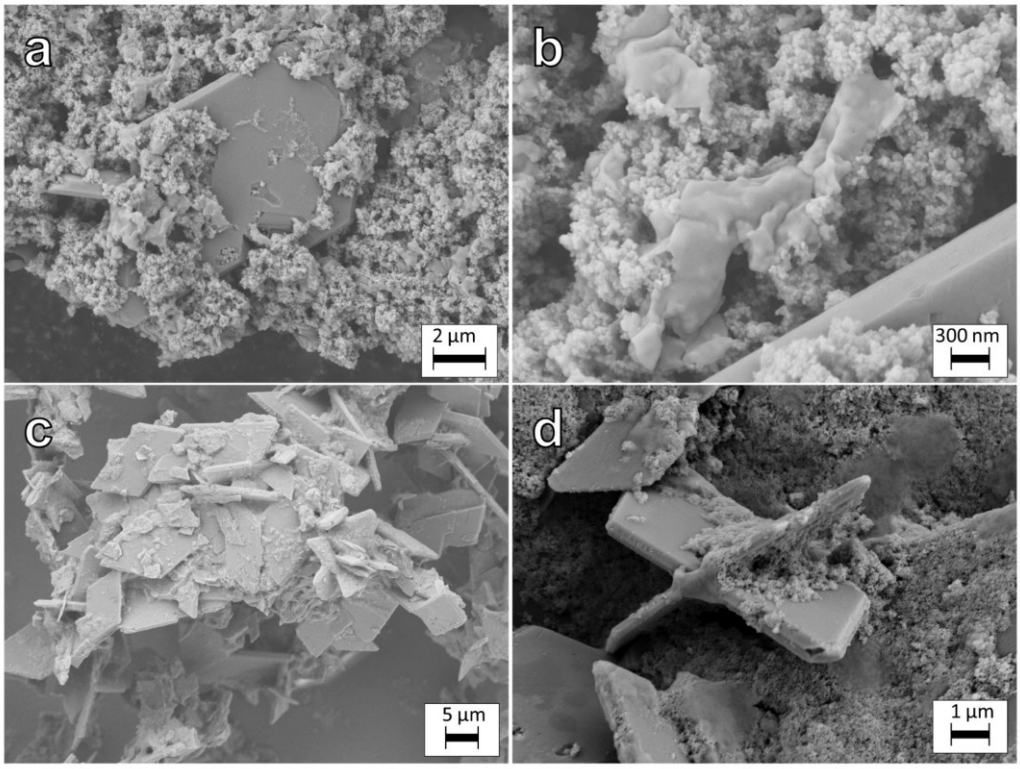

Figure S5. Micrographs from samples taken after the final reduction. (a) vivianite with surface/crystal defects and in close contact with MNPs (b) remains of microbial biomass/cells. (c) Conglomerate of vivianite crystals (d) vivianite crystals with characteristic twinning and in close contact with MNPs.

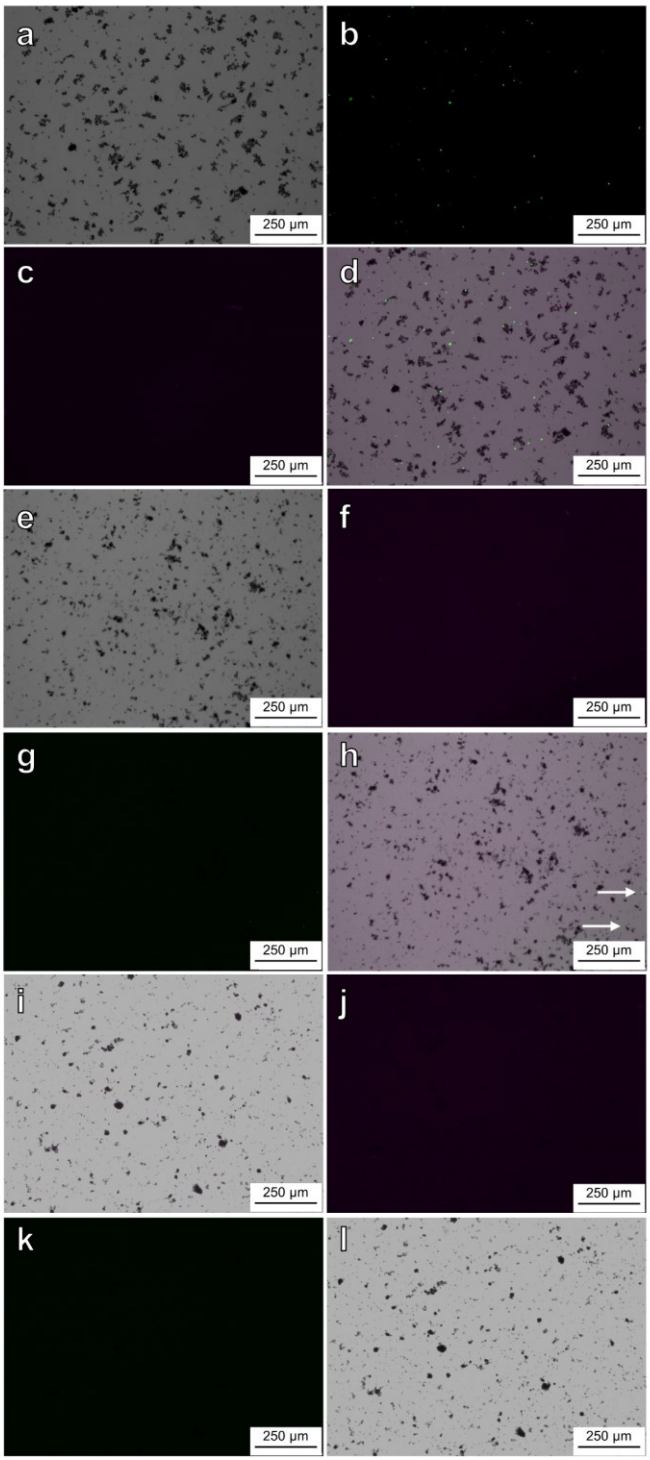

Figure S6. Light/fluorescence microscopy images of culture KS before and after washing steps. (a-d) brightfield, live, dead and overlayed channels of culture KS that was not yet washed. (e-h) brightfield, live, dead and overlayed channels of culture KS that was washed 3 times. Notice that still some cells could be seen (white arrows) (i-l) brightfield, live, dead, and overlayed channels of culture KS that was washed 5 times, no more cells could be detected.

Table S1. Properties of MNPs during incubation with culture KS and *G. sulfurreducens*. Crystal size, lattice parameter and Fe(II)/Fe(III) ratio determined by µXRD. Fe(II)/Fe(III) ratio determined by the spectrophotometric ferrozine assay and Fe(II)/Fe(III) ratio from Mössbauer spectroscopy (both the data presented in the main article (main) and here in the supporting information (SI)).

Sample	**Crystal size d_{XRD},(nm)**	**Lattice parameter (ang)**	**Fe(II)/Fe(III) (µXRD)**	**Fe(II)/Fe(III) (ferrozine)**	**Fe(II)/Fe(III) (Mössbauer, main)**	**Fe(II)/Fe(III) (Mössbauer, SI)**
Initial bio	10.04	8.4009	0.505	0.404 ± 0.005	0.45 ± 0.01	
End ox 1 bio	9.68	8.3838	0.356	0.285 ± 0.014	0.39 ± 0.02	
End red 1 bio	12.31	8.4038	0.532	0.754 ± 0.023	0.42 ± 0.01	
End ox 2 bio	10.88	10.8841	0.152	0.297 ± 0.014	0.40 ± 0.02	
End red 2 bio	17.47	17.4688	0.730	1.636 ± 0.095	0.42 ± 0.01	
Initial abio	10.24	8.4038	0.532	0.434 ± 0.001		0.45 ± 0.01
End ox 1 abio	9.95	8.3891	0.399	0.436 ± 0.003		
End red 1 abio	9.97	8.4065	0.559	0.384 ± 0.006		
End ox 2 abio	10.24	10.2411	0.513	0.375 ± 0.028		
End red 2 abio	10.09	10.0865	0.448	0.410 ± 0.015		0.42 ± 0.02

Table S2. Fitting results of Mössbauer spectroscopy. δ – isomer shift; ΔE_Q – quadrupole splitting; B_{hf} – hyperfine magnetic field; stdev(B_{hf}) – standard deviation of hyperfine magnetic field; R.A. – Relative abundance; red. χ2 – goodness of fit.

Sample	Phase	δ (mm/s)	ΔE_Q (mm/s)	stdev(ΔE_Q) (mm/s)	B_{hf} (T)	stdev(B_{hf}) (T)	R.A. (%)	Error	Red. χ2
Start of ox. 1	Sextet 1	0.382	-0.016		49.6	0.1	37.2	1.4	1.19
	Sextet 2	0.674	-0.018		46.5	2.5	59.4	1.4	
	Doublet F(III)	0.477	0.709	6.5E-09			3.33	0.33	
End of ox. 1	Sextet 1	0.385	-0.023		49.7	0.4	42.3	2.6	0.86
	Sextet 2	0.626	-0.018		46.4	2.9	54.8	2.7	
	Doublet Fe(III)	0.341	0.564	4.5E-09			2.83	0.49	
End of red. 1	Sextet 1	0.379	-0.001		49.5	0.4	33.5	1.1	1.94
	Sextet 2	0.715	-0.043		46.4	2.6	48.6	1.1	
	Doublet Fe(II)	1.309	3.056	0.390			17.92	0.51	
End of ox. 2	Sextet 1	0.385	-0.041		49.7	0.8	33.8	2.0	1.06
	Sextet 2	0.629	-0.062		46.5	2.9	45.0	2.0	
	Doublet Fe(II)	1.309	3.105	0.369			9.87	0.70	
	Doublet Fe(III)	0.468	0.728	0.334			11.26	0.66	
End of red. 2	Sextet 1	0.364	0.0009		49.6	0.69	29.6	1.0	3.28
	Sextet 2	0.729	-0.076		46.6	3.0	43.5	1.1	
	Doublet Fe(II)	1.311	3.020	0.419			26.9	6.0	

Chapter 3 – Personal Contribution

The experiment was conceptualized by myself and Assoc. prof. Dr. James Byrne. The experiments, data collection, and data analysis were carried out by myself. I wrote the manuscript. Ran Wei modelled the kinetic data and helped with data discussion. Prof. Dr**.** Adrian Mellage helped with the modelling of adsorption isotherms. Discussion with Jun. Prof. Dr. E. Marie Muehe improved the methodology of this work. Lars Grimm performed freeze-drying of magnetite particles and BET measurement. Caroline Dreher performed μ-XRD measurements and helped in discussions of the obtained data. All co-authors contributed to the manuscript revision and/or wrote parts of the manuscript.

Chapter 3: Cu(II) and Cd(II) removal efficiency of microbially redox activated magnetite nanoparticles

Timm Bayer[1], Ran Wei[2], Andreas Kappler[1,3], and James M. Byrne[4]

[1]Geomicrobiology Group, Department of Geoscience, University of Tuebingen, Schnarrenbergstraße 94-96, 72076 Tuebingen, Germany

[2]Environmental Systems Analysis, Department of Geoscience, University of Tuebingen, Schnarrenbergstraße 94-96, 72076 Tuebingen, Germany

[3]Cluster of Excellence: EXC 2124: Controlling Microbes to Fight Infection, 72074 Tuebingen, Germany

[4]School of Earth Sciences, University of Bristol, Wills Memorial Building, Queens Road, BS8 1RJ, Bristol, United Kingdom.

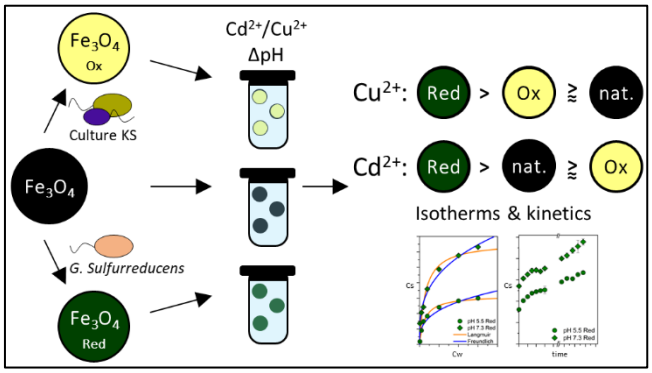

Published in: *ACS Earth and Space Chemistry*

https://doi.org/10.1021/acsearthspacechem.2c00394

3.1 Abstract

Heavy metal pollutants in the environment are of global concern due to their risk of contaminating drinking water and food supplies. Removal of these metals can be achieved by adsorption to mixed-valent magnetite nanoparticles (MNPs) due to their high surface area, reactivity, and ability for magnetic recovery. The adsorption capacity and overall efficiency of MNPs are influenced by redox state as well as surface charge, the latter of which is directly related to solution pH. However, the influence of microbial redox cycling of iron (Fe) in magnetite alongside the change of pH on the metal adsorption process by MNPs remains an open question. Here we investigated adsorption of Cd^{2+} and Cu^{2+} by MNPs at different pH values that were modified by microbial Fe(II) oxidation or Fe(III) reduction. We found that the maximum adsorption capacity increased with pH for Cd^{2+} from 256 µmol/g Fe at pH 5.0 to 478 µmol/g Fe at pH 7.3 and for Cu^{2+} from 229 µmol/g Fe at pH 5.0 to 274 µmol/g Fe at pH 5.5. Microbially reduced MNPs exhibited greatest adsorption for both Cu^{2+} and Cd^{2+} (632 µmol/g Fe at pH 7.3 for Cd^{2+} and 530 µmol/g Fe at pH 5.5 for Cu^{2+}). Magnetite oxidation also enhanced adsorption of Cu^{2+} but inhibited Cd^{2+}. Our results show that microbial modification of MNPs has an important impact on the (im-)mobilization of aqueous contaminations like Cu^{2+} and Cd^{2+}, and that a change in stoichiometry of the MNPs can have a greater influence than a change of pH.

3.2 Introduction

Advancements in industrialization and agriculture have led to increasing heavy metal concentrations in the environment, causing concerns about drinking water quality[1]. Widespread use of cadmium (Cd) in industrial processes such as battery manufacturing and of copper (Cu) in plumbing resulted in increased concentrations of these contaminants in the environment[2, 3]. Removal of these contaminants to achieve safe drinking water and maintain fertile soil is of high interest and continuous investigation[1, 4]. Prolonged ingestion of increased concentrations of heavy metals can lead to adverse effects. Cd is a heavy metal without known metabolic function and is toxic even in very low concentrations[5]. In addition to battery manufacturing and combustion, Cd is widespread as a contaminant in agricultural phosphorus-fertilizers[6, 7]. Cd is considered carcinogenic and prolonged exposure Cd can lead to kidney diseases[5]. In contrast to Cd, Cu is an essential trace metal but high concentrations have been associated with liver damage and possibly gastrointestinal diseases in humans[8]. High Cu concentrations cause oxidative stress through reactive oxygen species on a molecular level[9]. Cu is introduced into the environment through industry and in vineyards and orchards where it is used as a fungicide[10]. Cu and Cd are not biodegradable, accumulate in the environment and ultimately end up in water bodies.

A range of techniques such as membrane filtrations and ion exchange are used to treat heavy metal pollutions[11]. Adsorption is a frequently used method for heavy metal removal due to relative simplicity of implementation and economic efficiency[12, 13]. Iron(III) (Fe(III)) (oxyhydr)oxides are commonly used as adsorbents to remove contaminants from solution and are used commercially[14]. In Vietnam the precipitation of Fe(III) (oxyhydr)oxides in household sand filters has been shown to be highly effective at removing dissolved toxic arsenic (As)[15, 16]. Fe oxides generally have a high surface area and reactivity, which makes them an ideal adsorbent-material[17]. Magnetite is a naturally occurring mixed-valent Fe oxide that contains both Fe(II) and Fe(III) ($Fe(III)_2Fe(II)O_4$). It can be formed abiotically through weathering[18] and biologically through dissimilatory Fe(III) reduction[19] and oxidation[20, 21]. Magnetite nanoparticles (MNPs) especially can be applied in heavy metal remediation since they have high specific surface area, redox reactivity, and can be magnetically extracted. Recent studies investigated the adsorption of chromium (Cr) and As by bioengineered

magnetite[22] and the removal of Cr by magnetite-coated sand[23, 24]. Due to its multivalent nature, unlike most other iron oxides, magnetite can be both oxidized and reduced via microbial activity of Fe(II)-oxidizing and Fe(III)-reducing bacteria respectively. This was previously shown for photoautotrophic Fe(II)-oxidizing bacteria *Rhodopseudomonas palustris* TIE-1 and Fe(III)-reducing bacteria *Geobacter sulfurreducens*[25]. Changing the Fe(II)/Fe(III) ratio in magnetite can ultimately lead to its dissolution through reductive dissolution or transformation to maghemite (maghemitization) through oxidation[26, 27]. However, magnetite can have a wide range of Fe(II)/Fe(III) ratios while not undergoing transformation to a different mineral and maintaining the crystal structure of magnetite[25, 28]. The change of the stoichiometry in MNPs can greatly improve the remediation capacity of magnetite, which was previously shown for Cr[29, 30]. Conversely, it has also been shown that microbial activity decreased the reactivity of MNPs towards As(V)[22] and that magnetite surface passivation can occur through chromium reduction to Cr(III), resulting in a surface layer maghemitization[31]. Studies have shown that increase of Fe^{2+} lead to greater reduction of nitroaromatic compounds[32] and that an increased stoichiometry in magnetite enhanced the capacity to bind antibiotics[33]. Additionally, the recharging of magnetite with Fe^{2+} for increased reactivity has been demonstrated[34]. Previous research investigating removal of Cu^{2+} with magnetite mainly focused on the adsorption process without accounting for the Fe(II)/Fe(III) ratio of magnetite or modified particles with magnetite to obtain magnetic removal[35, 36]. The stoichiometry however directly influences the surface properties of MNPs which are also a consequence of the pH value of the solution.

In this study we consider the impact of microbially mediated redox reactions on the reactivity of MNPs towards two divalent heavy metals. In particular we oxidized MNPs by the autotrophic nitrate-reducing Fe(II)-oxidizing culture KS[37, 38], reduced magnetite by the Fe(III)-reducing bacterium *Geobacter sulfurreducens*, and compare the adsorption of Cu^{2+} and Cd^{2+} against unaltered (native) MNPs. We also tested how changes in pH influence adsorption to the three types of MNPs. The results presented below consider both adsorption isotherms and kinetic experiments of Cd^{2+} and Cu^{2+} on oxidized mag_{ox}, reduced mag_{red}, and native mag_{nat} MNPs.

3.3 Materials and Methods

Safety Statement

No unexpected or unusually high safety hazards were encountered during experiments performed for this research.

Preparation of solutions

For all adsorption experiments, anoxic stock solutions of the adsorbent (mag_{ox}, mag_{red}, or mag_{nat}), adsorbate ($CuNO_3$ or $CdNO_3$) and solvent (0.1 M $NaNO_3$) were adjusted to the desired pH two days prior to the start of the experiment. pH was adjusted with diluted puriss. HNO_3 and NaOH. The pH was checked at least twice per day and corrected accordingly. All solutions were prepared with ultrapure H_2O (Milli-Q, Merck Milli-pore). Glassware and rubber stoppers were soaked for 10 min with 1 M HCl and then rinsed 3 times with MilliQ-H_2O.

Magnetite synthesis, - oxidation, - reduction, and stoichiometry

Magnetite was produced according to Pearce et. al[39] but modified to allow magnetite synthesis outside of the glovebox and on a larger scale. For oxidation, magnetite was incubated with the autotrophic nitrate-reducing iron-oxidizing culture KS as previously described[40] with 4 mM $NaNO_3$ for 7 days, with an increased inoculum of 10% v/v. We previously detected that culture KS can oxidize magnetite. For reduction, magnetite was incubated with 10% v/v of iron-reducing *G. sulfurreducens* with 20 mM sodium acetate for 5 days[25]. After incubation magnetite was washed at least 5 times with 0.1 M $NaNO_3$ to remove all cells and minerals were collected with a strong bar magnet after each washing step. Magnetite stoichiometry was measured by the ferrozine assay[41] adapted to microtiter plates. Removal of biomass was checked by measuring DOC (dissolved organic carbon) (High TOC II, Elementar, Elementar Analysensysteme GmbH, Germany) of a washed sample and via fluorescence microscopy by applying a dead/live stain (BacLight Bacterial Viability Kits, Molecular Probes) to screen for any leftover cells after the washing procedure.

Adsorption isotherms

All experiments were setup in an anoxic glovebox. Triplicate bottles of increasing concentrations of Cu^{2+} or Cd^{2+} and controls (no MNPs/no adsorbate) were prepared

by adding anoxic stock solutions of $NaNO_3$ followed by well mixed MNPs and then Cu^{2+}/Cd^{2+} to obtain a total volume of 5 ml in each bottle. The final concentration of magnetite was 9 mM (as total Fe). Concentration of adsorbate depended on the conducted experiment. The bottles were sealed with rubber stoppers, mixed and then incubated in the dark at 25°C on a rolling shaker. After 24 hours of incubation the bottles were sampled in the glovebox. 2 ml were removed with a pipette, centrifuged for 2 min at 10,000 g and the sample then split into pellet and supernatant fractions. Outside of the glovebox the pellet was dissolved in 2 ml of 6 M puriss. HCl for 15 min. Supernatant and dissolved pellet were diluted in 2% puriss. HNO_3 and measured with microwave plasma-atomic excitation spectroscopy (Agilent 4200 MP-AES, Agilent Technologies). In total, 12 isotherms were obtained for: Cd^{2+} + mag_{nat} at pH 5.0, pH 5.5, pH 6.5 and pH 7.3. Cd^{2+} + mag_{ox} and Cd^{2+} + mag_{red} at pH 5.5 and 7.3. Cu^{2+} + mag_{nat} at pH 5.0 and pH 5.5. Cu^2 + mag_{ox} and Cu^{2+} + mag_{red} at pH 5.5. Experiments with Cu^{2+} were only conducted at pH 5.0 and pH 5.5. The pH was chosen to avoid precipitation of $Cu(OH)_2$ which occurs for concentrations of 2 mM (as present in starting stock. solutions) above pH 5.53, with the solubility product of Cu-hydroxide being $K_{sp}(Cu(OH)_2) = 2.20^{-20}$. While precipitation is a method for remediation purposes, this study focused on adsorption from solution to the magnetite surface, and hence the pH values were not higher than 5.5 for Cu^{2+}.

Kinetic adsorption experiments

For kinetic adsorption experiments, different treatments were prepared as above, in triplicate in the glovebox, but with a total volume of 50 ml. For each timepoint 2 ml of well mixed liquid was removed, centrifuged for 2 min at 10,000 g and then further treated as described above to separate aqueous and solid fractions. Kinetic experiments were performed with 500 µM Cd^{2+} at pH 5.5 and 7.3 for all types of MNPs. For Cu^{2+}, 750 µM was utilized at pH 5.0 with native MNPs only and at pH 5.5 with all types of MNPs. The different initial concentrations of Cd^{2+} and Cu^{2+} were selected based upon their respective adsorption isotherms that led to approximately 50% adsorption in the respective pH ranges.

Metal analyses

Concentrations of Cd, Cu, and Fe were determined with MP-AES, equipped with a SP3 autosampler. Samples were diluted in 2% puris. HNO_3 to obtain a concentration in measurement range of the instrument. The measurement wavelengths were: 371.993 nm for Fe, 228.802 nm for Cd, and 324.754 nm for Cu. The obtained data were first processed by the internal software of the instrument (MP Expert software, 1.5.0.6545).

Specific surface area

Magnetite nanoparticles were anoxically freeze-dried, weighed anoxically, and then the specific surface area (SSA) quantified with a Micromeritics Gemini VII surface area and porosity analyzer (Micromeritics Instrument Cooperation, USA), equipped with a VacPrep 061 and using N_2 as adsorbate. SSA was only determined for mag_{nat} particles.

Mössbauer spectroscopy

One sample of the native magnetite was filtered in a glovebox through a 0.45 µm pore-size syringe filter (Millipore membrane), embedded in Kapton tape and stored at -20°C until measurement. The sample was inserted into a closed-cycle exchange gas cryostat (SHI-650-5; Janis Research, USA). The spectrum was collected at 140 K using a constant acceleration drive system (WissEl, Blieskastel, Germany). Gamma radiation was emitted by a ^{57}Co-source embedded in a rhodium matrix. The sample spectrum was calibrated against a 7-µm-thick Fe(0) foil at room temperature. The software package recoil (University of Ottawa, Canada) was used for fitting using the extended Voigt-based fitting model. The Lorentzian half-width-half-maximum (HWHM) value was kept constant at 0.124 mm/s. The spectrum was analysed with respect to the isomer shift (δ), the quadrupole splitting (ΔE_Q), hyperfine magnetic field (B_{hf}), and the Gaussian width (standard deviation) of the ΔE_Q was used to account for line broadening until the fit was reasonable.

Micro X-ray diffraction

Samples for micro X-ray diffraction (µ-XRD) were washed with anoxic MilliQ and anoxically dried in an Eppendorf tube in the glovebox. µ-XRD was performed with a Bruker's D8 Discover GADDS XRD2 micro-diffractometer equipped with a standard

sealed tube with Cu-cathode (Cu Kα radiation, λ = 0.154 nm, 30 kV/30 mA). The total measurement time was 240 s at two detector positions, 15° and 40°. Phase identification was validated using Match! software version 3.7.1.123 with Crystallography Open Database (COD-Inorg REV211633 2018.19.25).

μ-XRD patterns were utilized to obtain information about mineralogy and crystal size. The Scherrer equation (equation 1) was applied to calculate average crystal size d[42]:

$$d = \frac{K * \lambda}{\beta * \cos\theta} \quad (1)$$

With K = shape factor (0.9), λ = wavelength of the source, β = full width at half maximum (FWHM), and $\cos\theta$ the cosine of the Bragg angle θ.

Data treatment and models of isotherm and kinetic adsorption

The data obtained from MP-AES measurements were evaluated to obtain amount of adsorbed contaminant as Cu/Cd in μmol on mass of Fe in g (μmol/g Fe) by calculating mean and standard deviation of technical triplicates. We used both Langmuir[43] and Freundlich[44] isotherms (equations 2 and 3) for all collected datasets.

$$c_{s,i} = q_{\max,i} \frac{c_{w,i}}{k_{\mathrm{ads},i} + c_{w,i}} \quad (2)$$

$$c_{s,i} = k_i \, c_{w,i}^{n} \quad (3)$$

$c_{s,i}$ [μmol/g] represents the amount of adsorbed Cd^{2+} or Cu^{2+}, $c_{w,i}$ is the concentration in solution [μmol/L], $k_{\mathrm{ads},i}$ [μmol/L] is the binding constant and $q_{\max,i}$ [μmol/g] the maximum adsorption capacity. k_i is the Freundlich adsorption coefficient [(μmol/g)(L/g)^n]and n is the Freundlich coefficient []. Here the subscript *i* always refers to the different experiments (pH/magnetite/heavy metal). Isotherms were fit using the nonlinear least-squares solver *lsqnonlin* (trust region approach)[23, 45] in MATLAB (R2022b) (objective function in *Parameter estimation*). For all the parameterizations we report the fitted parameters values and the goodness of fit of the model as normalized root-mean-square-error (NRMSE) (equation 4)[46] ,

$$NRMSE = \frac{\sqrt{\sum_{i=1}^{n} (y_{\mathrm{model},i} - y_{\mathrm{obs},i})^2 / n}}{y_{\mathrm{obs,max}} - y_{\mathrm{obs,min}}} \quad (4)$$

where *n* is the number of observations; *i* the observation indices.

For kinetic experiments, the rates of adsorption of Cu^{2+} and Cd^{2+} were defined by a linear driving force [24, 44] and a second-order adsorption scheme (equations 5 and 6)[24].

Divalent heavy metals (HM(II)) were assumed to be distributed between equilibrium $S_{\mathrm{HM(II)}}^{\mathrm{EQ}}$ and actual concentration of adsorbed Cu^{2+} or Cd^{2+} ($S_{\mathrm{HM(II)}}$) [µmol/g]. This approach was previously utilized [24, 47]. Here, we applied both Langmuir and Freundlich isotherms (equations 2 and 3) to compute the equilibrium concentration $S_{\mathrm{HM(II)}}^{\mathrm{EQ}}$. The rates of adsorption were finally formulated by multiplying the concentrations differences by the empirical kinetic adsorption rates constants $k_{\mathrm{sorb},1}$ [s^{-1}] and $k_{\mathrm{sorb},2}$ [$\mu mol^{-1}\ g\ s^{-1}$] for equations 5 and 6, respectively.

$$r_{\mathrm{sorb}} = k_{\mathrm{sorb},1}(S_{\mathrm{HM(II)}}^{\mathrm{EQ}} - S_{\mathrm{HM(II)}}) \quad (5)$$

$$r_{\mathrm{sorb}} = k_{\mathrm{sorb},2}(S_{\mathrm{HM(II)}}^{\mathrm{EQ}} - S_{\mathrm{HM(II)}})^2 \quad (6)$$

$$\frac{dS_{HM(II)}}{dt} = r_{\mathrm{sorb}} \quad (7)$$

The ordinary differential equation (ODE) (equation 7) was solved in MATLAB using the ODE solver *ode15s*[48].

Parameter estimation

The model (eqs. 2, 3 and eqs. 5-7) parameters $q_{\max}$, k_{ads}, k, n, $k_{\mathrm{sorb},1}$ and $k_{\mathrm{sorb},2}$ were estimated. The objective function is defined in equation 8,

$$\min_{\theta}\big(f(\boldsymbol{\theta})\big) = \sum_{i=1}^{n}\big(f(\boldsymbol{\theta}, x_i) - y_{\mathrm{obs},i}\big)^2 \quad (8)$$

where $\boldsymbol{\theta}$ is the parameter vector; $y_{\mathrm{obs},i}$ the observations. *lsqnonlin* algorithm in MATLAB was used for optimization by minimizing equation 8. NRMSE was computed to evaluate the goodness of the fit (equation 4).

3.4 Results and discussion

Magnetite characterisation

Synthesized native magnetite mag_{nat} had a Fe(II)/Fe(III) ratio of 0.42±0.01. Microbially oxidized (mag_{ox}) and reduced (mag_{red}) magnetite had ratios of 0.26±0.02 and 0.54±0.03 respectively, suggesting successful magnetite oxidation and reduction by the nitrate-reducing Fe(II)-oxidizing culture KS and Fe(III)-reducer *G. sulfurreducens* respectively. The SSA of the freeze-dried MNPs measured with BET was 92.73 m^2/g, which was comparable with literature[39]. The high SSA is explained by the small size of the particles, as the described synthesis method commonly results in particles in a size order of 10 nm[39]. Calculated apparent diameter d_{app}[49] resulted in 12.49 nm.

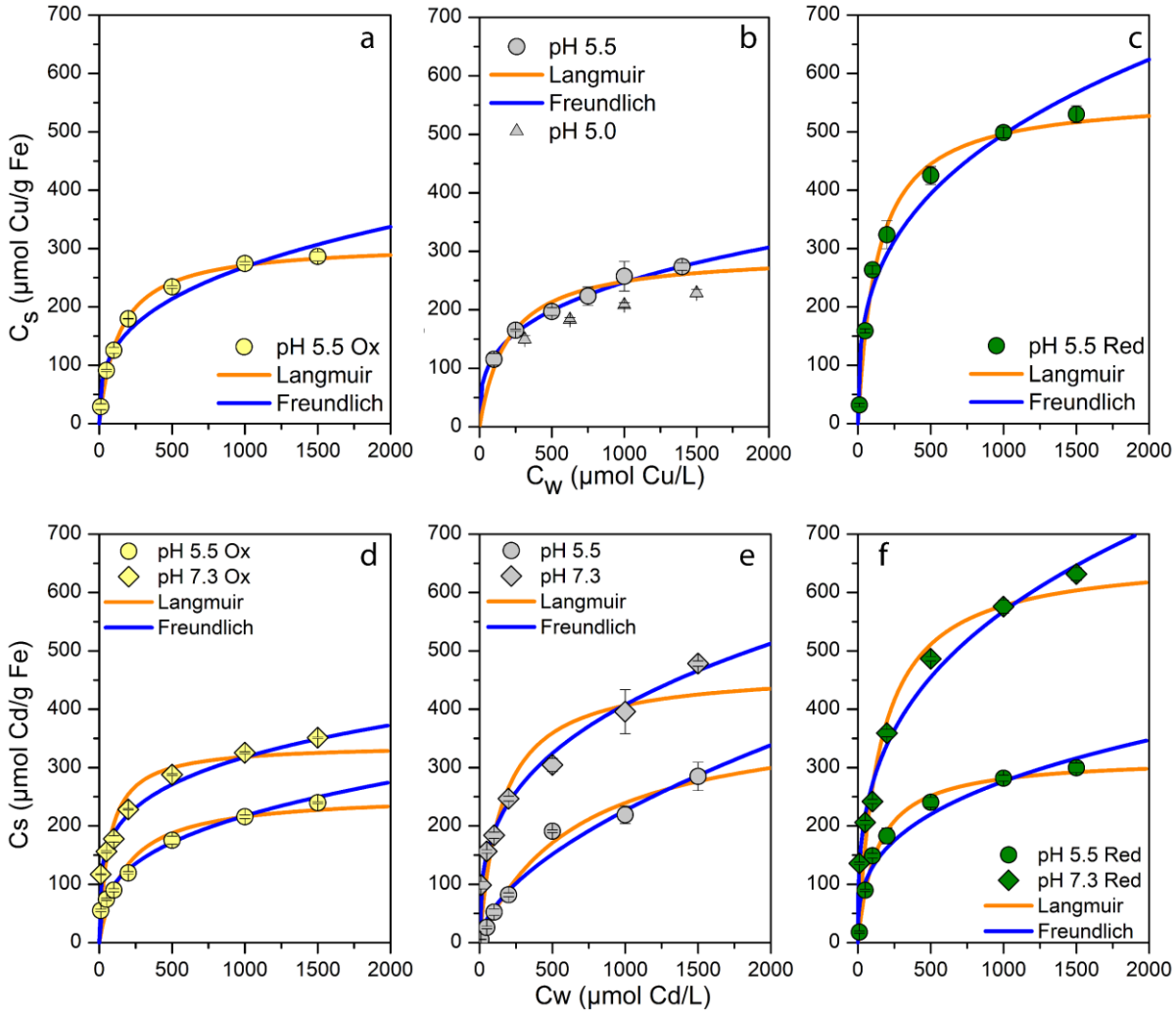

Figure 1. *Measured data and fit isotherms for Cu^{2+} (a−c) and Cd2+ (d−f) adsorption at pH 5.5 (circles) with native (grey), reduced (green), and oxidized (yellow) magnetite nanoparticles. Additionally at pH 7.3 (diamonds) for Cd^{2+}. Triplicate bottles with increasing Cu^{2+}/Cd^{2+} concentrations were incubated for 24 h, and the amount of adsorbed Cu/Cd (in µmol) on mass of magnetite (as g Fe) was determined via MP-AES. Langmuir (orange) and Freundlich (blue) isotherms were modelled. Grey triangles for Cu^{2+} with native magnetite show results of isotherm at pH 5.0.*

^{57}Fe Mössbauer analysis at 140 K confirmed that the prepared mineral was magnetite with two characteristic sextets in the spectrum correlating to Fe in octahedral and Fe in tetrahedral coordination (Figure S1 and Table S1). The Fe(II)/Fe(III) ratio was calculated according to Gorski and Scherer [27] as 0.46±0.024 which was in reasonable

agreement with the ratio determined by the ferrozine assay (0.42±0.01). µ-XRD also confirmed materials used for all adsorption experiments to be magnetite (Figures S2-S4). Minor reflections corresponding to vivianite ($Fe^{II}_3(PO_4)_2$, $8H_2O$) were visible in the pattern for mag_{red} at 2Θ of 15.32°. The reduction of magnetite by *G. sulfurreducens* presumably caused partial dissolution of some Fe^{2+} which precipitated as vivianite in the PO_4^{3-}-rich medium used in this study[50, 51]. Based on the relatively low intensity of the reflections in the XRD patterns, coupled to previous measurements of the SSA of vivianite of 8 to 16 m^2/g[52, 53], we anticipate that the effect of vivianite in this system was minor and did not influence the adsorption experiments. The Scherrer equation (equation 1) was used to calculate the average crystal size[42, 54] of 9.59 nm for mag_{red} and 10.23 nm for mag_{ox} and 10.29 nm for mag_{nat}. The slight decrease of crystal size for the reduced MNPs reflected a relative change of 6.8% (0.699 nm) and of 0.53% (0.055 mm) for mag_{ox}. µ-XRD patterns were collected for native MNPs after kinetic and isotherm experiments, with all results confirming pure magnetite, and no vivianite (Figures S3 and S4).

Using the average crystal size obtained from the Scherrer equation we calculated the theoretical SSA according to Etique et al.[49] to be 107.7 $m^2\ g^{-1}$ for mag_{red}, 101.0 $m^2\ g^{-1}$ for mag_{ox} and 100.4 $m^2\ g^{-1}$for mag_{nat}. This suggests microbial activity influenced the SSA of the MNPs, though the differences are relatively small. Comparison to the BET measured SSA (92.73 $m^2\ g^{-1}$) for mag_{nat} showed that the measurement and calculation are within 10% relative error. Since our calculated SSAs showed small differences overall of less than 7%, the great changes of adsorption properties cannot be explained by the changes in surface area alone.

To confirm the successful removal of biomass, the DOC content of the supernatant of the washed particles was determined. The results yielded a DOC content of 1.28 mg C/L which is just slightly above the MilliQ water used to prepare all solutions (0.95 mg C/L). Representative fluorescence microscopy images, collected after washing oxidized and reduced MNPs five times (Figures S5 and S6), showed no more colored areas, suggesting successful removal of cells. Figure S7 shows the results after washing the reduced MNPs only once which shows many cells remained associated with the MNPs.

Whilst we made every effort to wash the MNPs to be free from bacteria, we cannot guarantee that no residual organic compounds remained. The NO_3^- anion is however not expected to have a significant influence on the magnetite properties because it has been shown before that the binding of metals with nitrate is minor or negligible[55] and the adsorption of nitrate to magnetite is minor[56, 57]. We therefore propose that any influence of NO_3^- on the adsorption of metal cations was systematic and not significant.

Since this study is dealing with adsorption of Cu and Cd onto nanoparticles, particle aggregation is an important process[58, 59] that could influence the available surface area and thus adsorption capacities. If any organic compounds (from biomass) remained in the magnetite solution after washing, particle aggregation could have influenced[60] the adsorption. In a previous study[61] the comparison of abiotically synthesized and biologically induced MNPs showed aggregation differences between biogenic MNPs (larger and less compact). However, in our study the microorganisms were not responsible for the synthesis of the MNPs and as shown above, our MNPs were thoroughly washed and showed little evidence of any associated organic compounds, suggesting that its impact on aggregation and adsorption itself should be minor.

Redox potential and pH_{PZC}

Gorski et. al.[62] empirically derived a linear relationship of the Fe(II)/Fe(III) ratio in magnetite and its' open circuit potential (E_{OCP}) . They showed that an increase in the stoichiometry of magnetite resulted in a decrease of E_{OCP}. Using this expression, we calculated the potential of our MNPs which resulted in -0.54 mV, -0.36 mV and -0.12 mV for mag_{red}, mag_{nat} and mag_{ox} respectively. This suggests that the potential in our MNPs changed over ±0.42 mV from oxidized to reduced magnetite.

Literature described the point of zero charge pH_{PZC} for magnetite at around pH 6.5[17, 63]. Therefore, we can assume that at pH 5.5, 6.5 and 7.3 mag_{nat} should have positive, almost neutral, and negatively charged surface potential at the three different pH values respectively. We can therefore assume that the pH_{PZC} shifted relatively towards lower pH values for mag_{red} and towards higher pH values for mag_{ox}.

Adsorption isotherms and kinetics

*i. Copper.*For mag_{nat}, the maximum concentration of adsorbed Cu^{2+} increased from 228.69±6.25 µmol/g Fe (pH 5.0) to 273.9±6.32 µmol/g Fe (pH 5.5) (Figure 1). Adsorption experiments with oxidized and reduced magnetite were conducted with Cu^{2+} at pH 5.5. Mag_{ox} at pH 5.5 exhibited similar adsorption that was slightly increased (286.44±8.01 µmol Cu/g Fe) as mag_{nat} (273.9±6.32 µmol Cu/g Fe) indicating the effect of microbial oxidation of magnetite was minor. In stark contrast, mag_{red} adsorbed 530.13±14.70 µmol/g Fe, which was roughly twice as much as for mag_{nat} and mag_{ox}.

Reduction of magnetite has been previously described to "charge" particles with electrons[28] for both nano- and micro-scaled particles. This could lead to a corresponding increase in "negative charge" and decrease the point of zero charge of the magnetite, and ultimately lead to a less-positively charged surface. The point of

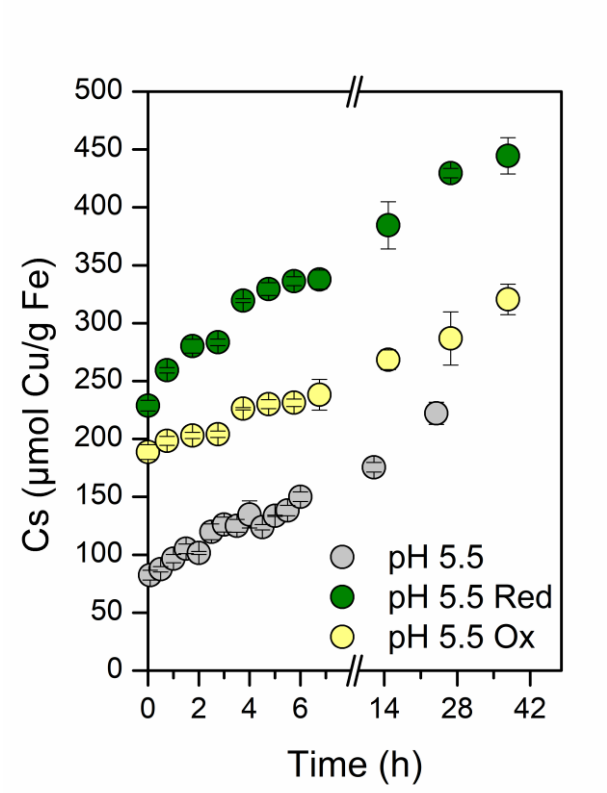

Figure 2. *Kinetic behavior of Cu^{2+} adsorption on magnetite nanoparticles at pH 5.5 with native (grey), reduced (green), and oxidized (yellow) MNPs. Triplicate bottles were incubated with MNPs (as 9 mM Fe) and 750 µM Cu^{2+}. Adsorbed Cu (µmol) on mass of magnetite (as g Fe) was regularly determined via MP-AES.*

zero charge (pH_{PZC}) is defined as pH were the total net charge on the surface is zero[17] as discussed above. Below the pH_{PZC}, the electrostatic repulsion effect of same charges, here positively charged surface of MNPs and divalent cation (Cu^{2+}), decreased as the surface sites of magnetite deviated from a fully protonated surface ($-FeOH_2^+$) towards a more negatively charged surface ($-FeOH^-$)[17]. The more negatively charged the surface, the more positively charged Cu^{2+} can adsorb. Alternatively, the increased adsorption capacity could be due to an increased SSA as a result of microbially induced dissolution. Without further measurements these assumptions are however only speculative, and we suggest that both mechanisms occurred.
Kinetic adsorption experiments were carried out to better understand the time-dependence of Cu^{2+} adsorption to the different types of magnetite. Mag_{nat} was tested at pH 5.0 and 5.5 with little divergence in the concentration of Cu^{2+} adsorption until the final sampling timepoint at 24 h (Figure S8). It was expected, that an increased pH would lead to increased adsorption, since the surface charge of the mineral was less negative[17].

The adsorption on mag_{red} after 5 minutes was already 40 µmol/g Fe greater than mag_{ox} and 146 µmol/g Fe greater than mag_{nat} (Figure 2). After one day 429.56±4.05 µmol Cu/g Fe was adsorbed on mag_{red}, 286.79± 2.97 µmol Cu/g Fe on mag_{ox} and 222.23±9.60 µmol Cu/g Fe on mag_{nat}. The adsorption of Cu^{2+} on MNPs did not reach equilibrium after 24 h for intermediate and higher concentrations of dissolved Cu^{2+}, as adsorption continued onto $mag_{red/ox}$ between hours 26.75 to 37.75. The difference after a few minutes of contact time shows the importance of the stoichiometry of the MNPs (changed through microbial oxidation and reduction) on the rate of adsorption. Both mag_{ox} and mag_{red} adsorbed twice as much Cu^{2+} as mag_{nat} immediately and showed higher capacity even after 2 days.

ii Cadmium. Since Cd^{2+} is more soluble than Cu^{2+} across a wide pH range, Cd^{2+} adsorption isotherms to mag_{nat} were performed at pH 5.0, 5.5, 6.5, and 7.3. As expected, the amount of adsorbed Cd^{2+} on native MNPs increased with pH from 256.95±45.68 µmol/g Fe (pH 5.0), 284.97±24.19 µmol/g Fe (pH 5.5), 417.78±16.08 µmol/g Fe (pH 6.5), to 478.20±4.66 µmol/g Fe (pH 7.3) (see Figure S9). Due to the previously discussed change of positive to negative surface charge across the point of

zero charge, more Cd^{2+} was able to adsorb on the native MNPs with increasing pH. Plotting the maximum of adsorbed Cd^{2+} vs pH (see Figure S10) reveals a linear relationship in the observed pH range. We assumed that further increasing pH will lead to more adsorption of Cd^{2+} onto MNPs. Based on a dissolved Cd^{2+} concentration of 1.5 mM this shows that adsorption could be studied up to pH 8.6 without precipitation of cadmium hydroxide $Cd(OH)_2$ (K_{sp} of $Cd(OH)_2$)= 2.5^{-14}). Using the linear trend shown in Figure S10, we calculated that the maximum possible amount of Cd on mag_{nat} under these conditions as 610.66 µmol Cd/g Fe.

Isotherm (Figure 1) and kinetic (Figure 3) experiments were performed at pH 5.5 and 7.3 for native, oxidized, and reduced MNPs. At pH 5.5 mag_{ox} could adsorb less Cd^{2+} (239.84±1.54 µmol Cd/g Fe) compared to mag_{red} (299.68±8.31 µmol Cd/g Fe) which was slightly above mag_{nat} (284.97±24.19 µmol Cd/g Fe) but within standard deviation of the mean. When comparing results at pH 5.5 for mag_{nat}, mag_{red}, and mag_{ox}, the change in stoichiometry, especially when MNPs were reduced, showed a much greater effect for Cu^{2+} than Cd^{2+}. Even though both Cu^{2+} and Cd^{2+} are divalent cations, Cd^{2+} has a much bigger radius of 109 pm, while Cu^{2+} radius is only 87 pm. Steric interactions

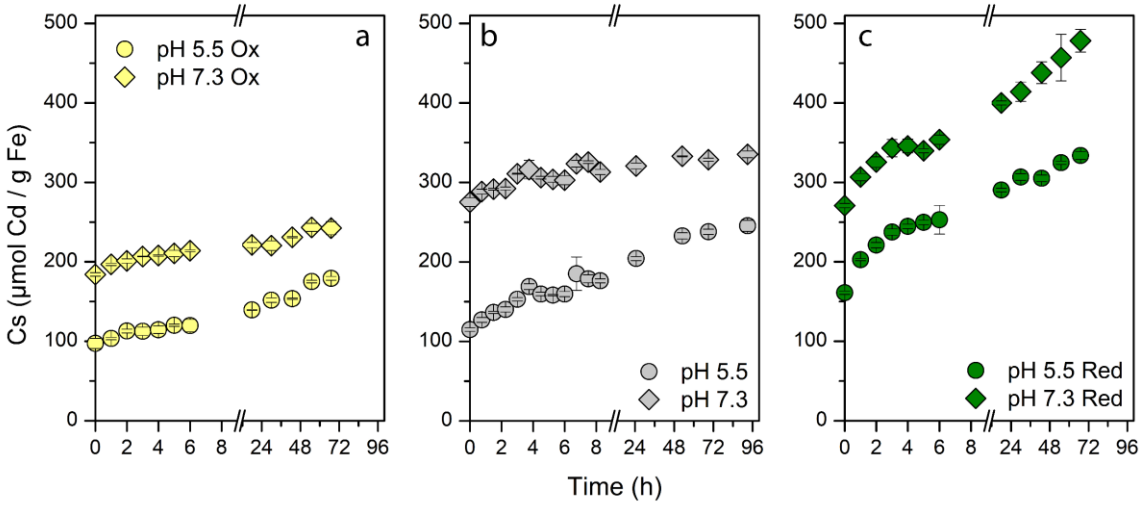

Figure 3. *Kinetic behavior of Cd^{2+} adsorption on magnetite nanoparticles at pH 5.5 (circles) and pH 7.3 (diamonds) with native (grey, panel b),reduced (green, panel c), and oxidized (yellow, panel a) magnetite. Triplicate bottles were incubated with magnetite (as 9 mM Fe) and 500 µM Cd^{2+}. Adsorbed Cd (in µmol) on mass of magnetite (as g Fe) was measured via MP-AES.*

and repulsion of larger Cd^{2+}—Cd^{2+} ions in solution, paired with a still positively charged surface of MNPs even after reduction at low pH, could explain this difference[64-66]

At pH 7.3, mag_{ox} showed the lowest removal capacity towards Cd^{2+} with 351.19±1.14 µmol Cd/g Fe, followed by mag_{nat} with 478.20±4.66 µmol Cd/g Fe, surpassed by mag_{red} with 631.72±11.00 µmol Cd/g Fe., The increased pH led to a less positively charged surface area and hence more divalent cations could adsorb. Interestingly, at pH 7.3 the stoichiometry of MNPs had a greater influence than at pH 5.5 as seen by the greater adsorption by mag_{red}, which was also reflected in the difference between maximum adsorption of Cd at pH 5.5 and pH 7.3 (Figure 4). The increase of adsorbed Cd^{2+} from pH 5.5 to 7.3 was 111.36 µmol Cd/g Fe for mag_{ox}, 193.23 µmol Cd/g Fe for mag_{nat} and 332.04 µmol Cd/g Fe for mag_{red}. At higher pH both the Fe(II)-enriched negatively charged magnetite surface area and the more negatively charged bulk mineral yielded higher Cd^{2+} adsorption. Independently of pH the oxidation of MNPs showed a decrease in adsorption capacity towards Cd^{2+}. We suggest that the increase in positive charge of the MNPs exhibits a repulsive force on the Cd^{2+} ions. The change in stoichiometry of the MNPs played an important role at high pH values for Cd^{2+} and while the effect of pH dominated at pH 5.5 and an influence of the stoichiometry could still be detected at pH 5.5 that resulted in increased adsorption for mag_{red} and decreased adsorption for mag_{ox}. Results from the kinetic experiments for Cd^{2+} ($[Cd^{2+}]$ = 500 µM) performed with all MNPs at pH 5.5 and 7.3 confirmed the previously discussed findings and expanded on them (Figure 3). At both pH values, the adsorption of Cd^{2+} on mag_{ox} showed the slowest rate and achieved the lowest total amount after more than two days. Rate and amount of adsorbed Cd^{2+} on reduced MNPs was greater when compared to native MNPs. Interestingly, the amount of adsorbed Cd^{2+} at this intermediate concentration in solution (initially 500 µM Cd^{2+}) on mag_{red} at pH 5.5 reached roughly the same value (333.84±4.85 µmol Cd/g Fe) after only 67 hours as the adsorbed Cd^{2+} on mag_{nat} at pH 7.3 after 96 hours (335.35±4.23 µmol Cd/g Fe). This showed that for Cd^{2+} adsorption on MNP, the reduction led to an increase of the adsorption rate and capacity. Our results showed the same trends for pH 7.3. Mag_{ox} adsorption was smallest, followed by mag_{nat} and then surpassed by mag_{red}. We can see in Figure 3, that the amount of adsorbed Cd^{2+} on mag_{nat} after 12 hours did not increase much further, while the amount on mag_{red} continued to increase until the last

sampling timepoint. This suggests that independent of the pH the oxidation of MNPs greatly hinders the adsorption of Cd^{2+} while reduction greatly increased it. At low pH there was little difference in the performance of mag_{nat} or mag_{ox} with respect to Cd^{2+}. However, almost immediately 161.15 µmol Cd/g Fe was adsorbed by mag_{red} (Figure 3), which was 1.4x as much as mag_{nat} with 114.88 µmol Cd/g Fe, and 1.7x as much as mag_{ox} with 97.34 µmol Cd/g Fe at the same time point. Therefore, reduced MNPs provide enhanced adsorption even for short contact times and low pH values. Additionally, mag_{red} initially adsorbed 270.86 µmol/g Fe at pH 7.3, which was more than mag_{ox} (184.14 µmol Cd/g Fe) but similar to mag_{nat} with (275.16 µmol Cd/g Fe). Adsorption to mag_{ox} remained low by the end of the study (242.41 µmol Cd/g Fe) whereas adsorption on mag_{nat} increased to 335.35 µmol/g Fe, and to 478.15 µmol/g Fe for mag_{red}.

Figure 4 summarizes the maximum measured adsorbed amount of Cd^{2+}/Cu^{2+} on the different redox MNPs. We show the maximum adsorbed amount for isotherms (left panel, same c_w concentration range for Cu^{2+} and Cd^{2+}) and the kinetic experiments (right two panels, different c_w for Cd^{2+} and Cu^{2+} during kinetic experiments) but only discuss the numbers of the isotherms and use the kinetic data to support these findings. We can see that for mag_{nat} at pH 5.5 the amount of adsorbed Cu^{2+} and Cd^{2+} was within standard deviation, suggesting that at this pH all available surface sites of the unaltered magnetite were saturated for both heavy metals. At pH 7.3 (only Cd^{2+}) about 159 additional µmol Cd/g Fe was adsorbed for mag_{nat}, showing the importance of pH for adsorption processes (see also Figure S9). For mag_{ox}, the adsorption of Cu^{2+} increased slightly compared to mag_{nat}. More Cu^{2+} than Cd^{2+} was adsorbed on mag_{ox}, since the amount of adsorbed Cd^{2+} slightly decreased from mag_{nat} to mag_{ox} which was in contrast with the slight increase for Cu^{2+}. This suggests that previously occupied surfaces sites were not available anymore for Cd^{2+} but remained available for Cu^{2+}. Additionally, a more positively “redox-discharged” mineral (decreased Fe(II)/Fe(III) ratio) likely increased electrostatic repulsion towards the bigger cation Cd^{2+} more profoundly than for smaller Cu^{2+}. Previously the oxidation of magnetite was reported as surface sensitive process[28, 67], and hence this positively charged surface would repel Cd^{2+}. This is reflected in the low adsorption of Cd^{2+} with mag_{ox} at pH 7.3. These findings were supported by kinetic experiments, which consistently showed smaller c_s

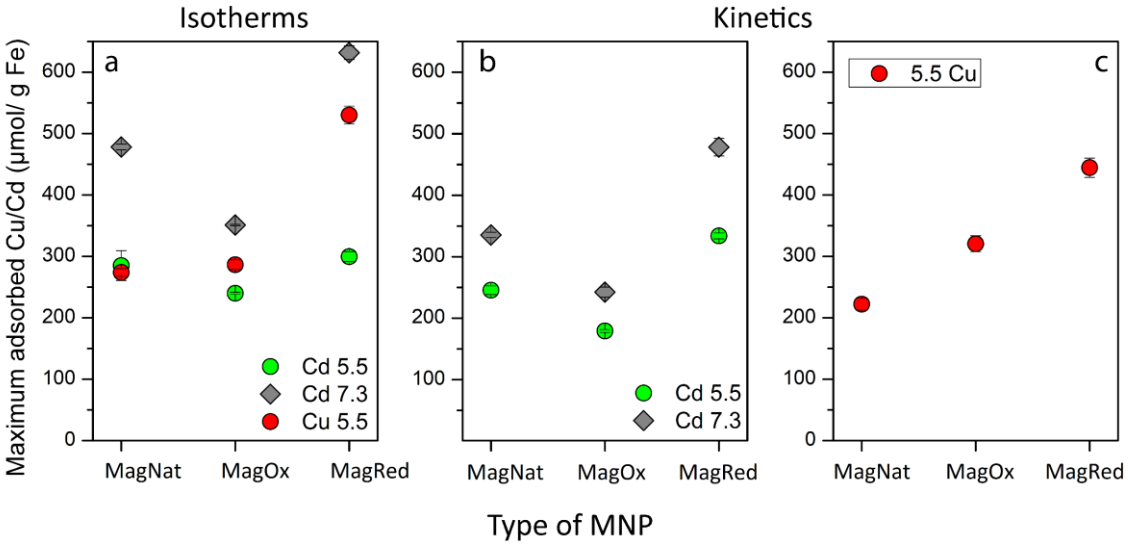

Figure 4. *Summary of maximum adsorbed heavy metal concentrations for isotherm experiments (a) and kinetic experiments (b, c) with MNPs. MNPs were untreated (native: MagNat) or microbially oxidized (MagOx) or reduced (MagOx). Displayed are the results as µmol heavy metal/g Fe ± standard deviation for Cd^{2+} at pH 5.5 (light green circles) and pH 7.3 (dark grey diamonds) and Cu^{2+} at pH 5.5 (red circles).*

values for Cd^{2+} on mag_{ox} than for $mag_{nat,}$ and greater c_s values for Cu^{2+} with mag_{ox} than for mag_{nat}. For Cd^{2+} at pH 7.3, the amount of adsorbed Cd^{2+} on mag_{ox} decreased by roughly 127 µmol Cd/g Fe compared to mag_{nat}, and conclusively only increased by roughly 66 µmol Cd/g Fe compared to pH 5.5 mag_{ox}, showing the importance of the minerals' stoichiometry. Considering Figure S10, the theoretical maximum c_s of Cd^{2+} was calculated as 610.60 µmol Cd/g Fe at pH 8.6, just before precipitation of $Cd(OH)_2$. At pH 7.3, mag_{red} already showed a higher c_s of 631.72±11.00 µmol Cd/g Fe, emphasizing the great importance of MNPs' stoichiometry. The difference at pH 7.3 between mag_{nat} and mag_{ox} was more profound than for pH 5.5, as more Cd^{2+} was adsorbed to the minerals surface at pH 7.3 to begin with. Additionally, it appears that impact of surface charge is more important at low pH than the stoichiometry for Cd^{2+}, and that the stoichiometry gains importance as pH rises. This was also supported by the kinetic experiments (Figure 3) were we consistently measured increasing c_s values of Cd^{2+} in the order of $mag_{ox} < mag_{nat} < mag_{red}$. For mag_{red} the amount of adsorbed Cd^{2+} at pH 5.5 was within error of mag_{ox} and slightly greater than mag_{nat}, supporting the hypothesis that the adsorption process in the system was mostly influenced by pH.

A low pH value lead to a positive surface charge of the MNPs, as the pH_{pzc} was previously reported between 6.1 to 8 for magnetite[17, 67]. Interestingly adsorption of Cu^{2+} on mag_{red} was almost doubled to 530 µmol Cu/g Fe (see also Figure 1) compared to mag_{nat} at pH 5.5. It appears that the net negative charge of the "bulk" magnetite[28] influenced the adsorption of the smaller cation Cu^{2+} at lower pH more intensely than for the bigger Cd^{2+} cation already at pH 5.5. With mag_{red} the amount of adsorbed Cd^{2+} only increased within standard deviation at pH 5.5 while the amount of Cd^{2+} adsorbed on mag_{red} at pH 7.3 increased to 631.72 ±11.00 µmol Cd/g Fe, which was 153 µmol Cd/g Fe greater than on mag_{nat}. While the pH had greater influence on the adsorption of Cd^{2+} onto the MNPs surface at low pH value for Cd^{2+}, increase to pH 7.3 revealed the importance of MNPs stoichiometry as the adsorption capacity was decreased for mag_{ox} and increased for mag_{red}, both compared to mag_{nat}, which was again consistent with the kinetic data (Figure 3, Figure 4 right panels). It was previously reported[33] that the stoichiometry of magnetite is a key parameter for the binding of emerging organic contaminants and naturally ligands as they showed for nalixidic acid the importance of redox for removal of Cr and As was shown[22]. We add on to this knowledge by showing that the stoichiometry of magnetite is crucial for the removal of different divalent heavy metals and that it can have a greater impact than change of pH.

Importance of contact time

While the isotherm experiments with Cu^{2+} (Figure 1) indicated that the timeframe of 24 hours was sufficient, the kinetic experiments revealed that the adsorbed amount of Cu^{2+} still increased, especially for mag_{ox} and mag_{red}, even after 42 hours (Figure 2). Therefore, a longer contact time would be needed in order to obtain equilibrium. The isotherms collected for Cd^{2+} showed that, especially at high pH values and with mag_{nat} and mag_{red}, the contact time of 24 h was insufficient (Figure 1 and Figure 3). As we could show with the kinetics experiment for Cd^{2+} at pH 5.5 and 7.3 for all MNPs, a contact time of 24 h was sufficient for mag_{nat}, but at least 48 h were needed for mag_{red} and mag_{ox}. We therefore recommend a contact time greater than 48 h to explore the future potential of microbially enhanced MNPs for heavy metal removal.

Modelling

Kinetic experiments

The results and corresponding parameters of the kinetic experiments are shown in Figures S11-S12 and Tables S3-S5. Since the experiments with Cu^{2+} were performed in a narrow range of pH, all kinetic experiments could be modelled using a first or second order rate with a NRMSE < 0.06. Data presented in Figure S11 and Table S3-S5 suggested that the collected data could be fitted well with both Langmuir or Freundlich equilibria and first or second order kinetics. However, a second order scheme seemed slightly more suitable for Cu^{2+} with all types of MNPs at both investigated pH values for both equilibrium isotherms (Langmuir or Freundlich). This could indicate that the adsorption of Cu^{2+} onto MNPs is governed by a chemisorption process, which would then have been the rate determining step[68]. Previous studies on adsorption of Cu^{2+} onto magnetite have reported that second order kinetics was a superior model[35]. For Cd^{2+}, no good modelled results were obtained for mag_{nat} at pH 5.5, suggesting that the collected data were of inferior quality compared to the other data set, which could also be implied by (comparatively) large standard deviation of the mean. Additionally, mag_{nat} at pH 7.3 with Cd^{2+} also did not yield a good modelled results; while the model parameters could be bent to fit the data (Figure S12), the parameter results presented in Tables S4 and S5 were not reasonable. Summarized, there was not a clear trend in favour of one specific model, and hence either Langmuir or Freundlich as first or second order kinetics could be used.

Adsorption isotherms

The results of the modelled isotherms can be seen in Table S2 and in Figure 1. The results suggest that for Cu^{2+} a Freundlich model was a better fit for the pH 5.5 isotherms with mag_{nat} while mag_{ox} and mag_{red} were better estimated by a Langmuir equilibrium. Enhanced adsorption due to oxidation and reduction enabled higher c_s (adsorbed amount) values which then allowed better estimation of q_{max}. Freundlich isotherms seemed to overestimate concentrations of Cu^{2+}, if c_w (concentration in solution) would be increased further. For Cd^{2+} with $mag_{nat,}$ a Langmuir model fit better but for pH 7.3, where a Freundlich isotherm was more appropriate (as seen by NRMSE). For Cd^{2+} at pH 5.5 and 7.3 with all types of MNPs, both Langmuir and Freundlich fits were suitable (Figure 1). Most models had a NRMSE of < 0.1. Cd^{2+}

isotherms generally followed a Freundlich model, which showed consistency in increasing *k* (distribution coefficient) for increasing pH of native magnetite (pH 5.0, 5.5, 6.5, 7.3: 2.52, 4.12, 22.20, 41.72 respectively) and for increasing pH for reduced and oxidized magnetite (pH 5.5 and 7.3, max_{red}: 28.28, 62.24, max_{ox}: 20.75, 64.90). Here the model however does not result in appropriate *k* values, where mag_{red} showed much higher total adsorption than mag_{ox}. This was better modelled following the Langmuir equation and we obtained appropriate q_{max} values for Cd at pH 7.3: mag_{red}: 663.7 µmol/g Fe and mag_{ox}: 339.7 µmol/g Fe.

Overall, both heavy metals could be characterized by either Langmuir or Freundlich isotherms at equilibrium. Table S2 shows the NRMSE of all experiments. The goodness of fits at different isotherm varied marginally. For the kinetics, both first and second order rates were tested with both Langmuir and Freundlich equilibrium assumptions, and all combinations could reproduce the dynamics in the data well (NRMSE in Table S3). Finally, while it depended on the investigated experiment which model fit best, we could parameterize a reasonable model that fits (almost) all datasets.

3.5 Conclusions

We investigated native, microbially oxidized and microbially reduced magnetite nanoparticles (MNPs) for the amount and rate of adsorption towards the two divalent heavy metals Cd^{2+} and Cu^{2+}. Our results presented here show that the influence of microbial oxidation and reduction of Fe in these MNPs greatly influences the adsorption behaviour of these environmentally relevant metals. For Cu^{2+} we show that the reduction of MNPs lead to an increase in adsorption capacity. This was expected since the reduction likely led to an increased negative bulk charge of the MNPs as we could show with potential calculations (Table S6). Additionally partial dissolution, as shown by µXRD, led to an increase in SSA of the particles (Table S6). Even the oxidized MNPs showed an increase in adsorption towards dissolved Cu^{2+} with respect to native MNPs, a phenomenon that we are unable to fully explain even when considering the slight differences in calculated SSA. As the redox potential of oxidized MNPs is higher, repulsion due to same charges was expected to be a dominating factor during adsorption. It was assumed that the change in stoichiometry towards Fe(III) (i.e. more positively charged MNPs) would lead to a decrease in adsorption capacity and efficiency through charge repulsion. Our isotherm and kinetic experiments however

showed that the opposite is true. Possibly vacancies in the mineral due to re-organization within the crystal structure[26] could have given smaller Cu^{2+} ions (87 pm ionic radius) more available adsorption sites. On the other hand, we showed that the increase in Fe(II)/Fe(III) ratio in magnetite due to magnetite reduction resulted in almost two-times greater adsorption of 663.7 µmol/g Fe, than for mag_{nat}. For Cd^{2+}, we could see that at low pH values, the stoichiometry of the MNPs had a minor effect on the adsorption behaviour, most likely because the greater ionic radius of Cd^{2+} (109 pm) was repelled due to the same charge from the positively charged magnetite surface, even if the "bulk" was more negatively charged after reduction. This could explain the minor increase of adsorption of MNPs at pH 5.5 for mag_{red} and the detectable decrease for mag_{ox}. At higher pH, we showed that the oxidation of MNPs lead to a more pronounced decreased adsorption capacity and rate even compared to native MNPs. Furthermore, reduction of MNPs led to an increase of adsorbed Cd on mag_{red} compared to mag_{nat} and mag_{ox}. Our results show that ultimately both pH and stoichiometry are highly important parameters for the adsorption processes on MNPs. For relatively small divalent cations like Cu^{2+}, stoichiometry had an impact at low pH values and both microbial oxidation and microbial reduction enhanced the adsorption capacity. For larger ions like Cd^{2+}, electrostatic repulsion seemed to be the dominant process at low pH, where stoichiometry mattered less, but oxidation and reduction had great influences at higher pH values. The MNPs used in this study were cleaned from biomass prior to experiments, however, in nature such "clean" MNPs are not expected to exist. Instead, MNPs are more likely associated with biomass from bacteria (e.g. Fe(II)-oxidizing or Fe(III)-reducing bacteria) or other redox active compounds such as natural organic matter. This associated biomass could potentially have a great influence on the adsorption of Cu^{2+} and Cd^{2+} by, amongst other effects, blocking surface sites[69], changing surface charge[70], or influencing the particle aggregation[61]. Therefore, to better understand the importance of biologically reduced and oxidized MNPs in the environment, further comparative studies should be performed to investigate the role of this naturally occurring biomass and its impact on the ability of bio-reduced and bio-oxidized MNPs to adsorb Cu^{2+}, Cd^{2+}, or other metals. Finally, our results show that the biomodification of magnetite nanoparticles could be of great use for remediation purposes and drinking water purification. However, it seems that not one material can be applied for all contaminations and all conditions, but that the

environment of adsorption (microbial oxidation or reduction) and the pH of the systems must be evaluated and chosen depending on which heavy metal should be remediated most efficiently.

AUTHOR INFORMATION

Corresponding Author

James M. Byrne, School of Earth Sciences, University of Bristol, Queens Road BS8 1RJ, Bristol, United Kingdom. Email: james.byrne@bristol.ac.uk

Authors

Timm Bayer – Geomicrobiology Group, Department of Geoscience, University of Tuebingen, Schnarrenbergstraße 94-96, 72076 Tuebingen, Germany

Ran Wei – Environmental Systems Analysis, Department of Geoscience, University of Tuebingen, Schnarrenbergstraße 94-96, 72076 Tuebingen, Germany

Andreas Kappler – Geomicrobiology Group, Department of Geoscience, University of Tuebingen, Schnarrenbergstraße 94-96, and Cluster of Excellence: EXC 2124: Controlling Microbes to Fight Infection, Tuebingen, Germany

Author Contributions

T.B. and J.M.B. conceived the research. T.B performed the experiments and analytical measurements. R.W. modelled kinetic data. T.B. and J.M.B. modelled isotherms. J.M.B. and A.K. supervised the research. The manuscript was written through contributions of all authors. All authors have given approval to the final version of the manuscript.

Funding

This work was supported via funding awarded to J.M.B (BY 82/2-1) and A.K (KA 1736/48-1). The authors acknowledge infrastructural support by the Deutsche Forschungsgemeinschaft (DFG, German Research Foundation) under Cluster of Excellence, EXC2124. J.M.B is supported by a UKRI Future Leaders Fellowship (MR/V023918/1).

SUPPORTING INFORMATION

Mössbauer spectrum and fitting results, additional μ-XRD patterns of kinetic experiments, fluorescence microscopy images, kinetic and isotherm figures, linear pH-adsorption fit, Matlab data and model of kinetic experiments and their fitting

parameters, and a summary of MNPs properties can be found in the Supporting Information.

Conflict of interest

The authors declare no known conflict of interest.

ACKNOWLEDGEMENTS

This work was supported via funding awarded to J.M.B (BY 82/2-1) and A.K (KA 1736/48-1). The authors acknowledge Prof. Dr. A. Mellage for help with isotherm modelling. We are grateful to Prof. Dr. E. Marie Muehe for help with conceptualization and data discussion. We thank L. Grimm for BET analysis and C. Dreher for µ-XRD measurements and data discussion. J.M.B is supported by a UKRI Future Leaders Fellowship (MR/V023918/1). A.K. acknowledges infrastructural support by the DFG under Germany's Excellence Strategy, Cluster of Excellence EXC2124, project ID 390838134. The authors thank the Editor and anonymous reviewers for their feedback and help in improving the quality of the publication.

3.6 References

1. Ali, H.; Khan, E.; Ilahi, I. Environmental Chemistry and Ecotoxicology of Hazardous Heavy Metals: Environmental Persistence, Toxicity, and Bioaccumulation. *J. Chem.* **2019**, *2019*, 6730305.
2. WHO. Guidelines for drinking-water quality: first addendum to the fourth edition. **2017**.
3. Imseng, M.; Wiggenhauser, M.; Keller, A.; Müller, M.; Rehkämper, M.; Murphy, K.; Kreissig, K.; Frossard, E.; Wilcke, W.; Bigalke, M. Fate of Cd in agricultural soils: a stable isotope approach to anthropogenic impact, soil formation, and soil-plant cycling. *Environ. Sci. Technol.* **2018**, *52* (4), 1919-1928.
4. Rozada, F.; Otero, M.; Morán, A.; García, A. Adsorption of heavy metals onto sewage sludge-derived materials. *Bioresour. Technol.* **2008**, *99* (14), 6332-6338.
5. Young, S. D. Chemistry of heavy metals and metalloids in soils. In *Heavy metals in soils*, Springer, 2013; pp 51-95.
6. Grant, C. A.; Sheppard, S. C. Fertilizer Impacts on Cadmium Availability in Agricultural Soils and Crops. *Hum. ecol. risk assess.* **2008**, *14* (2), 210-228.
7. Hutton, M. Sources of cadmium in the environment. *Ecotoxicol. Environ. Saf.* **1983**, *7* (1), 9-24.
8. Nolan, K. R. Copper toxicity syndrome. *J. of Orthomolecular Psychiatry* **1983**, *12* (4), 270-282.
9. Gaetke, L. M.; Chow, C. K. Copper toxicity, oxidative stress, and antioxidant nutrients. *Toxicology* **2003**, *189* (1-2), 147-163.
10. Brun, L.; Maillet, J.; Hinsinger, P.; Pepin, M. Evaluation of copper availability to plants in copper-contaminated vineyard soils. *Environ. Pollut.* **2001**, *111* (2), 293-302.
11. Shannon, M. A.; Bohn, P. W.; Elimelech, M.; Georgiadis, J. G.; Mariñas, B. J.; Mayes, A. M. Science and technology for water purification in the coming decades. *Nat.* **2008**, *452* (7185), 301-310. DOI: 10.1038/nature06599.
12. Crini, G. Non-conventional low-cost adsorbents for dye removal: a review. *Bioresour. Technol.* **2006**, *97* (9), 1061-1085.
13. Fu, F.; Wang, Q. Removal of heavy metal ions from wastewaters: a review. *J. Environ. Manage.* **2011**, *92* (3), 407-418.
14. Driehaus, W.; Jekel, M.; Hildebrandt, U. Granular ferric hydroxide—a new adsorbent for the removal of arsenic from natural water. *J. Water Supply Res. T.* **1998**, *47* (1), 30-35.
15. Berg, M.; Luzi, S.; Trang, P. T. K.; Viet, P. H.; Giger, W.; Stüben, D. Arsenic removal from groundwater by household sand filters: comparative field study, model calculations, and health benefits. *Environ. Sci. Technol.* **2006**, *40* (17), 5567-5573.
16. Van Le, A.; Straub, D.; Planer-Friedrich, B.; Hug, S. J.; Kleindienst, S.; Kappler, A. Microbial communities contribute to the elimination of As, Fe, Mn, and NH4+ from groundwater in household sand filters. *Sci. Total Environ.* **2022**, 156496.
17. Cornell, R. M.; Schwertmann, U. *The iron oxides: structure, properties, reactions, occurrences and uses*; John Wiley & Sons, 2003.
18. Evans, M.; Heller, F. *Environmental magnetism: principles and applications of enviromagnetics*; Elsevier, 2003.
19. Lovley, D. R.; Stolz, J. F.; Nord Jr, G. L.; Phillips, E. J. Anaerobic production of magnetite by a dissimilatory iron-reducing microorganism. *Nat.* **1987**, *330* (6145), 252.
20. Dippon, U.; Pantke, C.; Porsch, K.; Larese-Casanova, P.; Kappler, A. Potential function of added minerals as nucleation sites and effect of humic substances on

mineral formation by the nitrate-reducing Fe (II)-oxidizer Acidovorax sp. BoFeN1. *Environ. Sci. Technol.* **2012**, *46* (12), 6556-6565.
21. Jiao, Y.; Kappler, A.; Croal, L. R.; Newman, D. K. Isolation and characterization of a genetically tractable photoautotrophic Fe(II)-oxidizing bacterium, Rhodopseudomonas palustris strain TIE-1. *Appl. Environ. Microbiol.* **2005**, *71* (8), 4487-4496.
22. Sundman, A.; Vitzhum, A.-L.; Adaktylos-Surber, K.; Figueroa, A. I.; van der Laan, G.; Daus, B.; Kappler, A.; Byrne, J. M. Effect of Fe-metabolizing bacteria and humic substances on magnetite nanoparticle reactivity towards arsenic and chromium. *J. Hazard. Mater.* **2020**, 121450.
23. Sorwat, J.; Mellage, A.; Kappler, A.; Byrne, J. M. Immobilizing magnetite onto quartz sand for chromium remediation. *J. Hazard. Mater.* **2020**, *400*, 123139.
24. Sorwat, J.; Mellage, A.; Maisch, M.; Kappler, A.; Cirpka, O. A.; Byrne, J. M. Chromium (VI) removal kinetics by magnetite-coated sand: small-scale flow-through column experiments. *J. Hazard. Mater.* **2021**, *415*, 125648.
25. Byrne, J. M.; Klueglein, N.; Pearce, C.; Rosso, K. M.; Appel, E.; Kappler, A. Redox cycling of Fe(II) and Fe(III) in magnetite by Fe-metabolizing bacteria. *Sci.* **2015**, *347* (6229), 1473-1476.
26. Usman, M.; Byrne, J.; Chaudhary, A.; Orsetti, S.; Hanna, K.; Ruby, C.; Kappler, A.; Haderlein, S. Magnetite and green rust: synthesis, properties, and environmental applications of mixed-valent iron minerals. *Chem. Rev.* **2018**, *118* (7), 3251-3304.
27. Gorski, C. A.; Scherer, M. M. Determination of nanoparticulate magnetite stoichiometry by Mossbauer spectroscopy, acidic dissolution, and powder X-ray diffraction: A critical review. *Am. Min.* **2010**, *95* (7), 1017-1026.
28. Byrne, J. M.; van der Laan, G.; Figueroa, A. I.; Qafoku, O.; Wang, C.; Pearce, C. I.; Jackson, M.; Feinberg, J.; Rosso, K. M.; Kappler, A. Size dependent microbial oxidation and reduction of magnetite nano- and micro-particles. *Sci. Rep.* **2016**, *6*, 30969.
29. He, Y. T.; Traina, S. J. Cr(VI) reduction and immobilization by magnetite under alkaline pH conditions: the role of passivation. *Environ. Sci. Technol.* **2005**, *39* (12), 4499-4504.
30. Crean, D. E.; Coker, V. S.; van der Laan, G.; Lloyd, J. R. Engineering Biogenic Magnetite for Sustained Cr(VI) Remediation in Flow-through Systems. *Environ. Sci. Technol.* **2012**, *46* (6), 3352-3359.
31. Peterson, M. L.; White, A. F.; Brown, G. E.; Parks, G. A. Surface passivation of magnetite by reaction with aqueous Cr (VI): XAFS and TEM results. *Environ. Sci. Technol.* **1997**, *31* (5), 1573-1576.
32. Klausen, J.; Troeber, S. P.; Haderlein, S. B.; Schwarzenbach, R. P. Reduction of substituted nitrobenzenes by Fe (II) in aqueous mineral suspensions. *Environ. Sci. Technol.* **1995**, *29* (9), 2396-2404.
33. Cheng, W.; Marsac, R.; Hanna, K. Influence of magnetite stoichiometry on the binding of emerging organic contaminants. *Environ. Sci. Technol.* **2018**, *52* (2), 467-473.
34. Gorski, C. A.; Scherer, M. M. Influence of magnetite stoichiometry on FeII uptake and nitrobenzene reduction. *Environ. Sci. Technol.* **2009**, *43* (10), 3675-3680.
35. Zhang, J.; Lin, S.; Han, M.; Su, Q.; Xia, L.; Hui, Z. Adsorption properties of magnetic magnetite nanoparticle for coexistent Cr (VI) and Cu (II) in mixed solution. *Water* **2020**, *12* (2), 446.

36. Kim, Y.; Lee, B.; Yi, J. Preparation of functionalized mesostructured silica containing magnetite (MSM) for the removal of copper ions in aqueous solutions and its magnetic separation. *Sep. Sci. T.* **2003**, *38* (11), 2533-2548.
37. Straub, K. L.; Benz, M.; Schink, B.; Widdel, F. Anaerobic, nitrate-dependent microbial oxidation of ferrous iron. *Appl. Environ. Microbiol.* **1996**, *62* (4), 1458-1460.
38. Nordhoff, M.; Tominski, C.; Halama, M.; Byrne, J. M.; Obst, M.; Kleindienst, S.; Behrens, S.; Kappler, A. Insights into nitrate-reducing Fe(II) oxidation mechanisms through analysis of cell-mineral associations, cell encrustation, and mineralogy in the chemolithoautotrophic enrichment culture KS. *Appl. Environ. Microbiol.* **2017**, *83* (13), e00752-00717.
39. Pearce, C. I.; Qafoku, O.; Liu, J.; Arenholz, E.; Heald, S. M.; Kukkadapu, R. K.; Gorski, C. A.; Henderson, C. M. B.; Rosso, K. M. Synthesis and properties of titanomagnetite (Fe 3− xTixO 4) nanoparticles: A tunable solid-state Fe (II/III) redox system. *J. Colloid Interface Sci.* **2012**, *387* (1), 24-38.
40. Tominski, C.; Heyer, H.; Lösekann-Behrens, T.; Behrens, S.; Kappler, A. Growth and population dynamics of the anaerobic Fe(II)-oxidizing and nitrate-reducing enrichment culture KS. *Appl. Environ. Microbiol.* **2018**, *84* (9), e02173-02117.
41. Stookey, L. L. Ferrozine - a new spectrophotometric reagent for iron. *Anal. Chem.* **1970**, *42* (7), 779-781.
42. Patterson, A. L. The Scherrer Formula for X-Ray Particle Size Determination. *Phys. Rev.* **1939**, *56* (10), 978-982.
43. Langmuir, I. The constitution and fundamental properties of solids and liquids. Part I. Solids. *J. Am. Chem. Soc.* **1916**, *38* (11), 2221-2295.
44. El Bardiji, N.; Ziat, K.; Naji, A.; Saidi, M. Fractal-like kinetics of adsorption applied to the solid/solution interface. *ACS omega* **2020**, *5* (10), 5105-5115.
45. Coleman, T. F.; Li, Y. An interior trust region approach for nonlinear minimization subject to bounds. *SIAM Journal on optimization* **1996**, *6* (2), 418-445.
46. Liu, H.; Maghoul, P.; Shalaby, A.; Bahari, A.; Moradi, F. Integrated approach for the MASW dispersion analysis using the spectral element technique and trust region reflective method. *Computers and Geotechnics* **2020**, *125*, 103689.
47. Mikutta, C.; Wiederhold, J. G.; Cirpka, O. A.; Hofstetter, T. B.; Bourdon, B.; Von Gunten, U. Iron isotope fractionation and atom exchange during sorption of ferrous iron to mineral surfaces. *Geochim. Cosmochim. Acta* **2009**, *73* (7), 1795-1812.
48. Shampine, L. F.; Reichelt, M. W. The matlab ode suite. *SIAM journal on scientific computing* **1997**, *18* (1), 1-22.
49. Etique, M.; Jorand, F. P.; Ruby, C. Magnetite as a precursor for green rust through the hydrogenotrophic activity of the iron-reducing bacteria Shewanella putrefaciens. *Geobiol.* **2016**, *14* (3), 237-254.
50. Miot, J.; Benzerara, K.; Morin, G.; Bernard, S.; Beyssac, O.; Larquet, E.; Kappler, A.; Guyot, F. Transformation of vivianite by anaerobic nitrate-reducing iron-oxidizing bacteria. *Geobiol.* **2009**, *7* (3), 373-384.
51. Hegler, F.; Posth, N. R.; Jiang, J.; Kappler, A. Physiology of phototrophic iron (II)-oxidizing bacteria: implications for modern and ancient environments. *FEMS Microbiol. Ecol.* **2008**, *66* (2), 250-260.
52. Luna Zaragoza, D.; Romero Guzmán, E. T.; Reyes Gutiérrez, L. R. Surface and physicochemical characterization of phosphates vivianite, Fe2(PO4)3 and hydroxyapatite, Ca5(PO4)3OH. *J. Min. Mat. Char. Eng.* **2009**, *Vol. 8* (No 8), pp591-609.

53. Eynard, A. d.; Del Campillo, M.; Barrón, V.; Torrent, J. Use of vivianite (Fe3 (PO4) 2.8 H2O) to prevent iron chlorosis in calcareous soils. *Fertilizer Research* **1992**, *31* (1), 61-67.
54. Borchert, H.; Shevchenko, E. V.; Robert, A.; Mekis, I.; Kornowski, A.; Grübel, G.; Weller, H. Determination of nanocrystal sizes: a comparison of TEM, SAXS, and XRD studies of highly monodisperse CoPt3 particles. *Langmuir* **2005**, *21* (5), 1931-1936.
55. Criscenti, L. J.; Sverjensky, D. A. The role of electrolyte anions (ClO 4-, NO 3-, and Cl-) in divalent metal (M 2+) adsorption on oxide and hydroxide surfaces in salt solutions. *Am. J. Sci.* **1999**, *299* (10), 828-899.
56. Leitzke, T. J.; Downey, J.; LaDouceur, R. M.; Margrave, D. M.; Wallace, G. C.; Hutchins, D. L. Water Treatment Method for Removal of Select Heavy Metals and Nutrient Ions Through Adsorption by Magnetite. *ACS ES&T Water* **2022**, *2* (9), 1584-1592.
57. Dhakal, P.; Matocha, C.; Huggins, F.; Vandiviere, M. Nitrite reactivity with magnetite. *Environ. Sci. Technol.* **2013**, *47* (12), 6206-6213.
58. Hotze, E. M.; Phenrat, T.; Lowry, G. V. Nanoparticle aggregation: challenges to understanding transport and reactivity in the environment. *J. Environ. Qual.* **2010**, *39* (6), 1909-1924.
59. Liu, W.-T. Nanoparticles and their biological and environmental applications. *J. Biosci. Bioeng.* **2006**, *102* (1), 1-7.
60. Baalousha, M. Aggregation and disaggregation of iron oxide nanoparticles: influence of particle concentration, pH and natural organic matter. *Sci. Total Environ.* **2009**, *407* (6), 2093-2101.
61. Mansor, M.; Drabesch, S.; Bayer, T.; Van Le, A.; Chauhan, A.; Schmidtmann, J.; Peiffer, S.; Kappler, A. Application of Single-Particle ICP-MS to Determine the Mass Distribution and Number Concentrations of Environmental Nanoparticles and Colloids. *Environ. Sci. Technol. Lett.* **2021**, *8* (7), 589-595.
62. Gorski, C. A.; Nurmi, J. T.; Tratnyek, P. G.; Hofstetter, T. B.; Scherer, M. M. Redox behavior of magnetite: Implications for contaminant reduction. *Environ. Sci. Technol.* **2010**, *44* (1), 55-60.
63. Milonjić, S.; Kopečni, M.; Ilić, Z. The point of zero charge and adsorption properties of natural magnetite. *J. Radioanal. Nucl.* **1983**, *78* (1), 15-24.
64. Anson, F. C.; Barclay, D. J. Anion induced adsorption of cadmium (II) on mercury from iodide and bromide media. *Anal. Chem.* **1968**, *40* (12), 1791-1798.
65. Liu, J.-F.; Zhao, Z.-s.; Jiang, G.-b. Coating Fe3O4 magnetic nanoparticles with humic acid for high efficient removal of heavy metals in water. *Environ. Sci. Technol.* **2008**, *42* (18), 6949-6954.
66. Vermeer, A. W. P.; van Riemsdijk, W. H.; Koopal, L. K. Adsorption of Humic Acid to Mineral Particles. 1. Specific and Electrostatic Interactions. *Langmuir* **1998**, *14* (10), 2810-2819. DOI: 10.1021/la970624r.
67. Jolsterå, R.; Gunneriusson, L.; Holmgren, A. Surface complexation modeling of Fe3O4–H+ and Mg (II) sorption onto maghemite and magnetite. *J. Colloid Interface Sci.* **2012**, *386* (1), 260-267.
68. Ho, Y.; McKay, G. The sorption of lead (II) ions on peat. *Water Res.* **1999**, *33* (2), 578-584.
69. Swindle, A. L.; Cozzarelli, I. M.; Elwood Madden, A. S. Using Chromate to Investigate the Impact of Natural Organics on the Surface Reactivity of Nanoparticulate Magnetite. *Environ. Sci. Technol.* **2015**, *49* (4), 2156-2162.

70. Hu, J.-D.; Zevi, Y.; Kou, X.-M.; Xiao, J.; Wang, X.-J.; Jin, Y. Effect of dissolved organic matter on the stability of magnetite nanoparticles under different pH and ionic strength conditions. *Sci. Total Environ.* **2010**, *408* (16), 3477-3489.

3.7 Supporting Information

Cu(II) and Cd(II) removal efficiency of microbially redox-activated magnetite nanoparticles

Timm Bayer[1], Ran Wei[2], Andreas Kappler[1,3], and James M. Byrne[4]

[1]Geomicrobiology Group, Department of Geoscience, University of Tuebingen, Schnarrenbergstraße 94-96, 72076 Tuebingen, Germany

[2]Environmental Systems Analysis, Department of Geoscience, University of Tuebingen, Schnarrenbergstraße 94-96, 72076 Tuebingen, Germany

[3]Cluster of Excellence: EXC 2124: Controlling Microbes to Fight Infection, 72074 Tuebingen, Germany

[4]School of Earth Sciences, University of Bristol, Wills Memorial Building, Queens Road, BS8 1RJ, Bristol, United Kingdom.

Number of tables in supporting information: 6

Number of figures in supporting information: 12

Total number of pages in supporting information: 16 (including cover page)

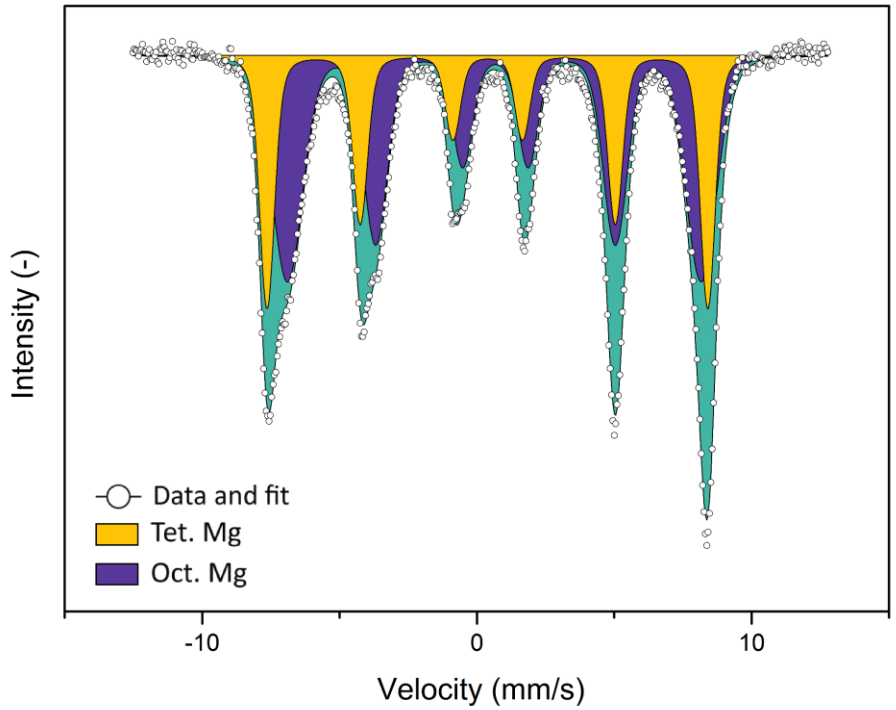

Figure S1: *Mössbauer spectrum of unmodified magnetite before start of experiments, collected at 140 K. Circles correspond to raw data. Yellow sextet Fe in magnetite in tetrahedral coordination, and purple sextet Fe in magnetite in octahedral coordination.*

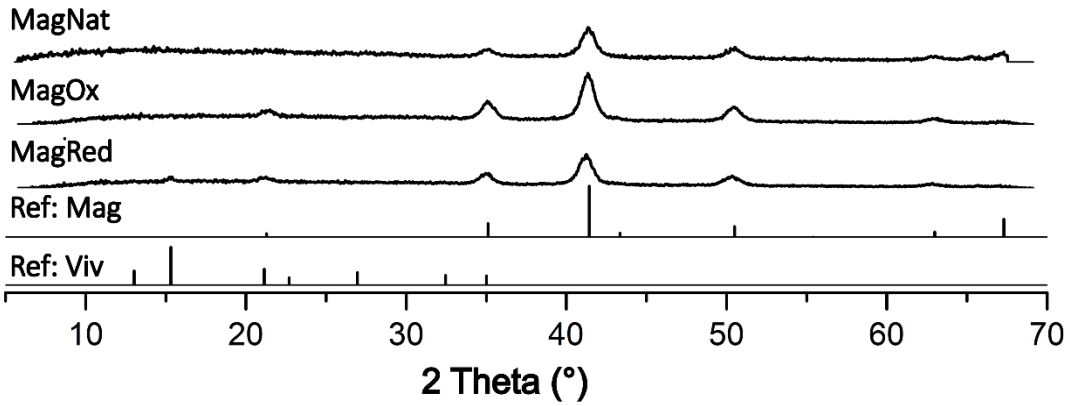

Figure S2: *µXRD patterns collected from microbially oxidized and microbially reduced magnetite. References shown for magnetite and vivianite (Ref: Mag and Ref: Viv).*

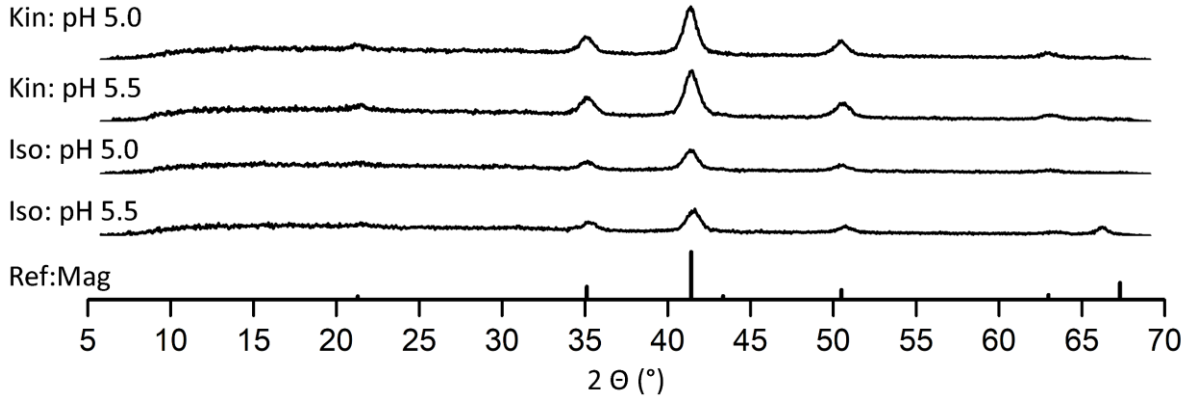

Figure S3: *μXRD patterns collected of native magnetite and Cu^{2+}: kinetic experiments (Kin) at pH 5.0 and pH 5.5 and isotherm experiments (Iso) at pH values 5.0, 5.5, 6.5, and 7.3. Bottom bars show reference for magnetite (Ref: Mag).*

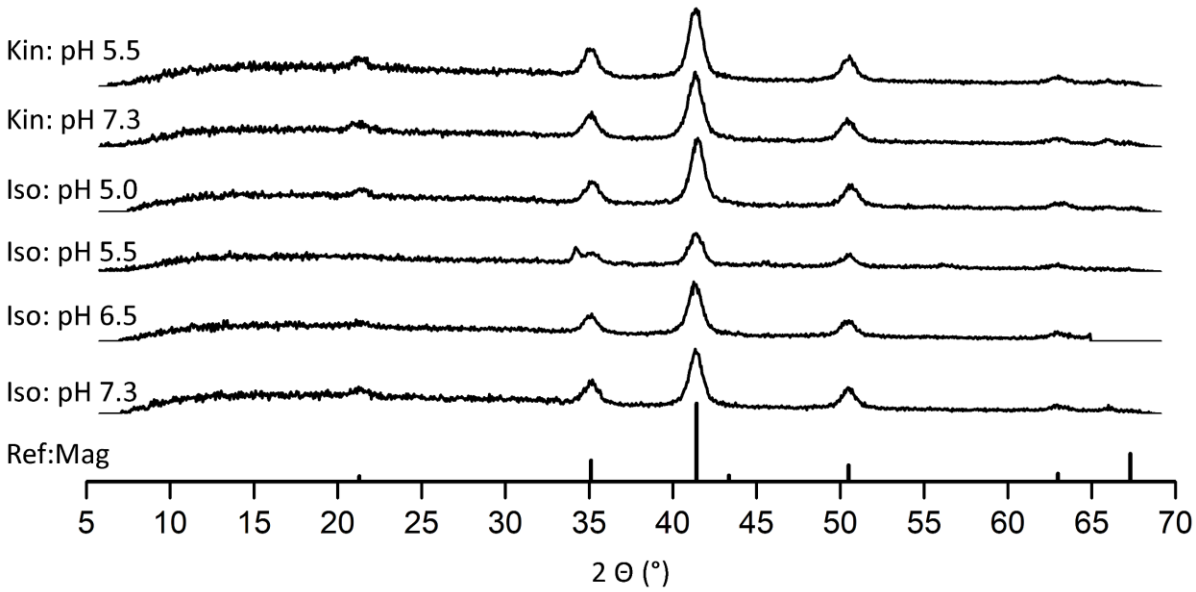

Figure S4: *μXRD patterns collected of native magnetite and Cd^{2+}. Kinetic experiments (Kin) at pH 5.5 and pH 7.3 and Isotherm experiments (Iso) at pH values 5.0, 5.5, 6.5, and 7.3 Bottom bars show reference for magnetite (Ref: Mag).*

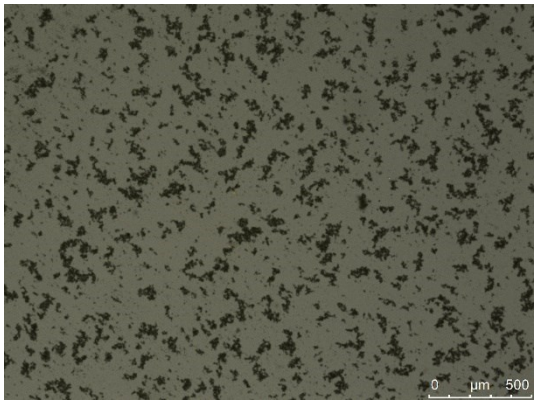

Figure S5: *Washed MNPs (overlayed image) - After oxidation MNPs were washed with anoxic $NaNO_3$ five times.*

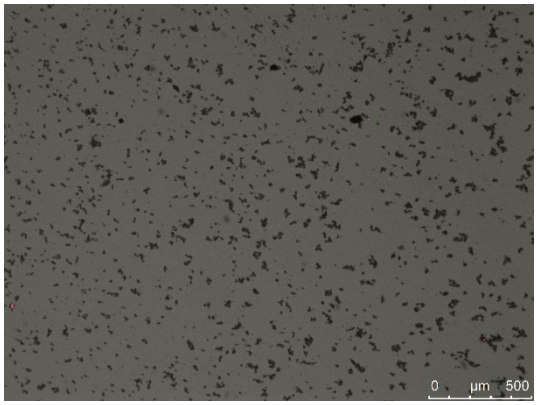

Figure S6: *Washed MNPs (overlayed image) - After reduction MNPs were washed with anoxic $NaNO_3$ five times.*

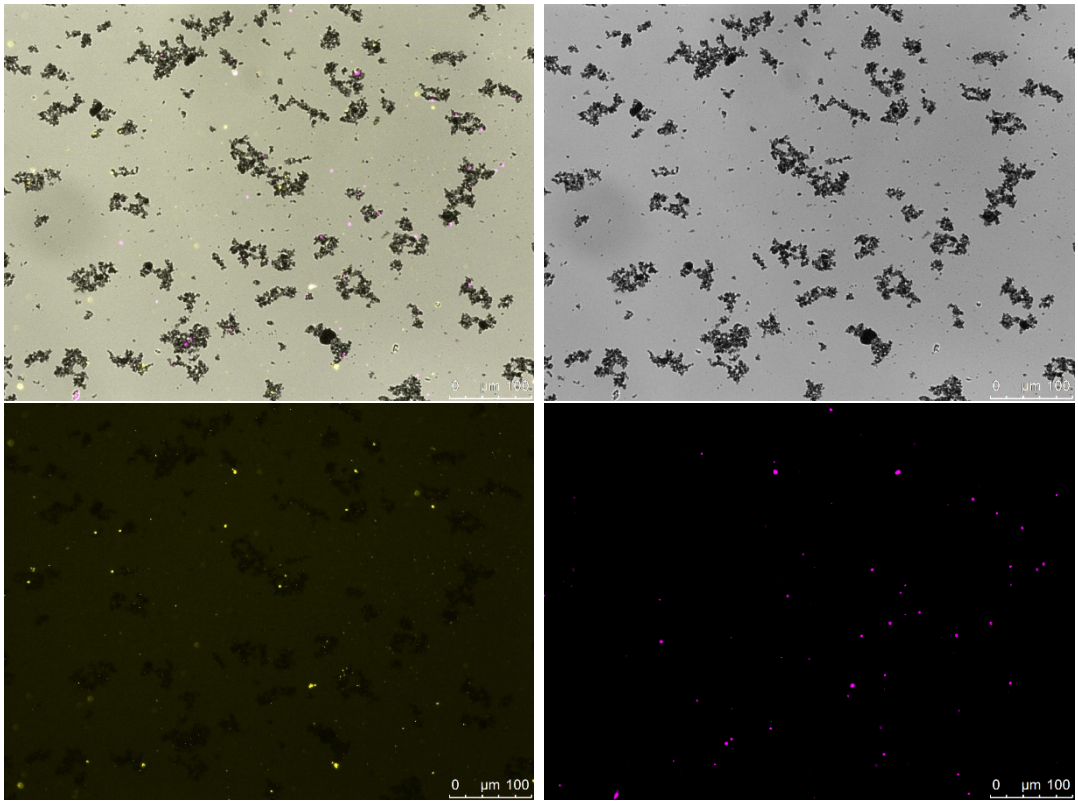

Figure S7: *Partially washed MNPs - After reduction MNPs were washed with $NaNO_3$ once. Colours indicate presence of bacteria (top left - Overlay, top right – brightfield, bottom left – living cells, bottom right – dead cells).*

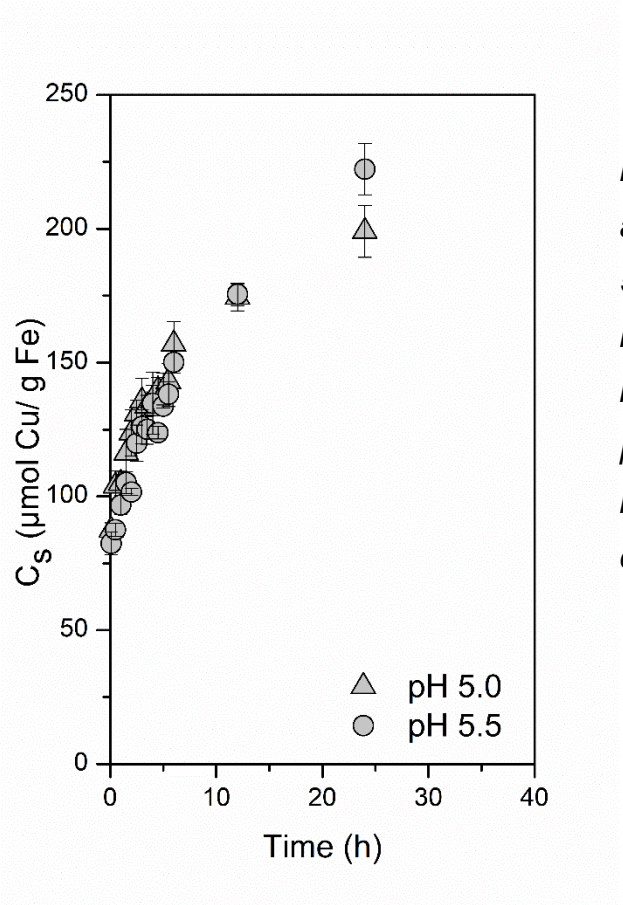

Figure S8: *Kinetic behaviour of Cu^{2+} adsorption on magnetite nanoparticles at pH 5.0 (triangles) and pH 5.5 (circles) with native MNPs (grey). Triplicate bottles were incubated with magnetite (9 mM Fe) and 750 µM Cu^{2+}. Adsorbed Cu (µmol) on mass of magnetite (as g Fe) was regularly determined via MP-AES.*

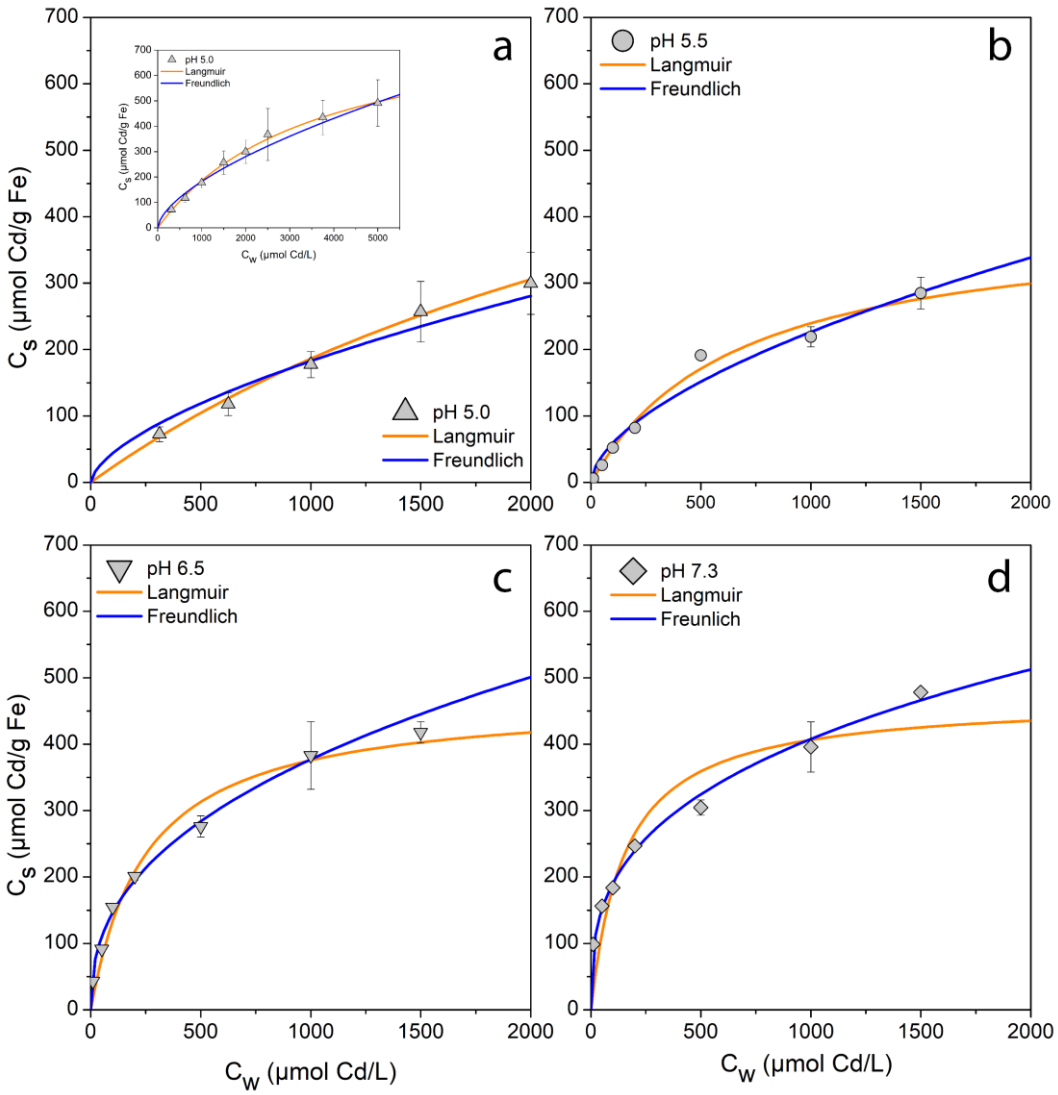

Figure S9: *Measured data and fit isotherms for Cd^{2+} pH 5.0 (pyramids, panel a), 5.5 (circles panel b), 6.5 (triangles, panel c) and 7.3 (diamonds, panel d) with native (grey). Triplicate bottles with increasing Cd^{2+} concentrations were incubated for 24h and the amount of adsorbed Cu (in µmol) on mass of magnetite (as g Fe) was determined via MP-AES. Langmuir (orange) and Freundlich (blue) isotherms were fit to the data. The inset for pH 5.0 in panel a shows the entire range of the performed isotherm.*

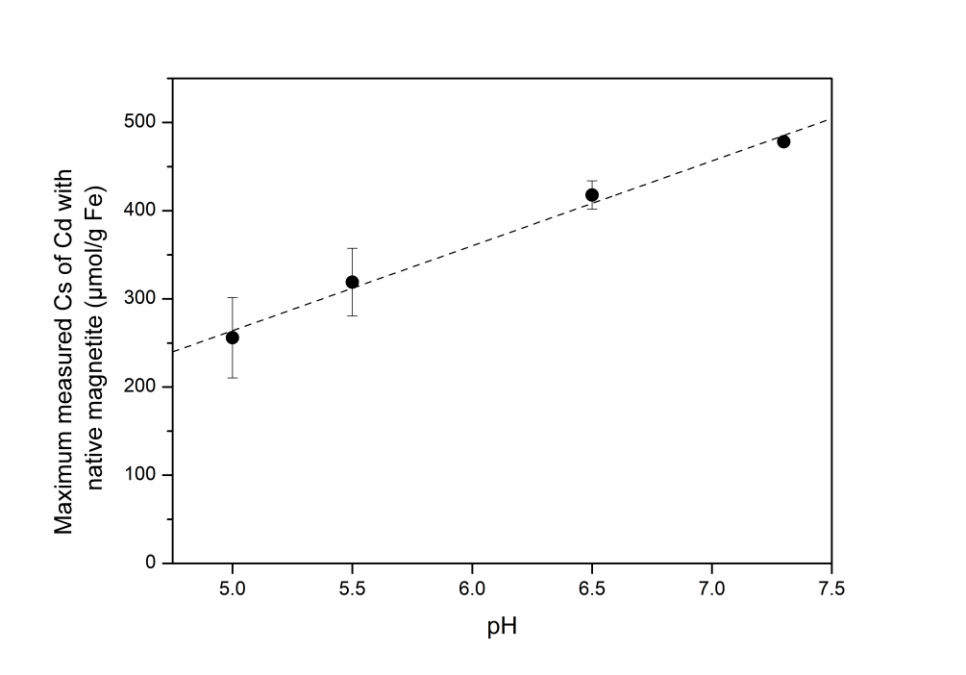

Figure S10: *Linear relationship between increased pH of performed isotherms and maximum adsorbed Cd^{2+} for experiments performed with native magnetite.*

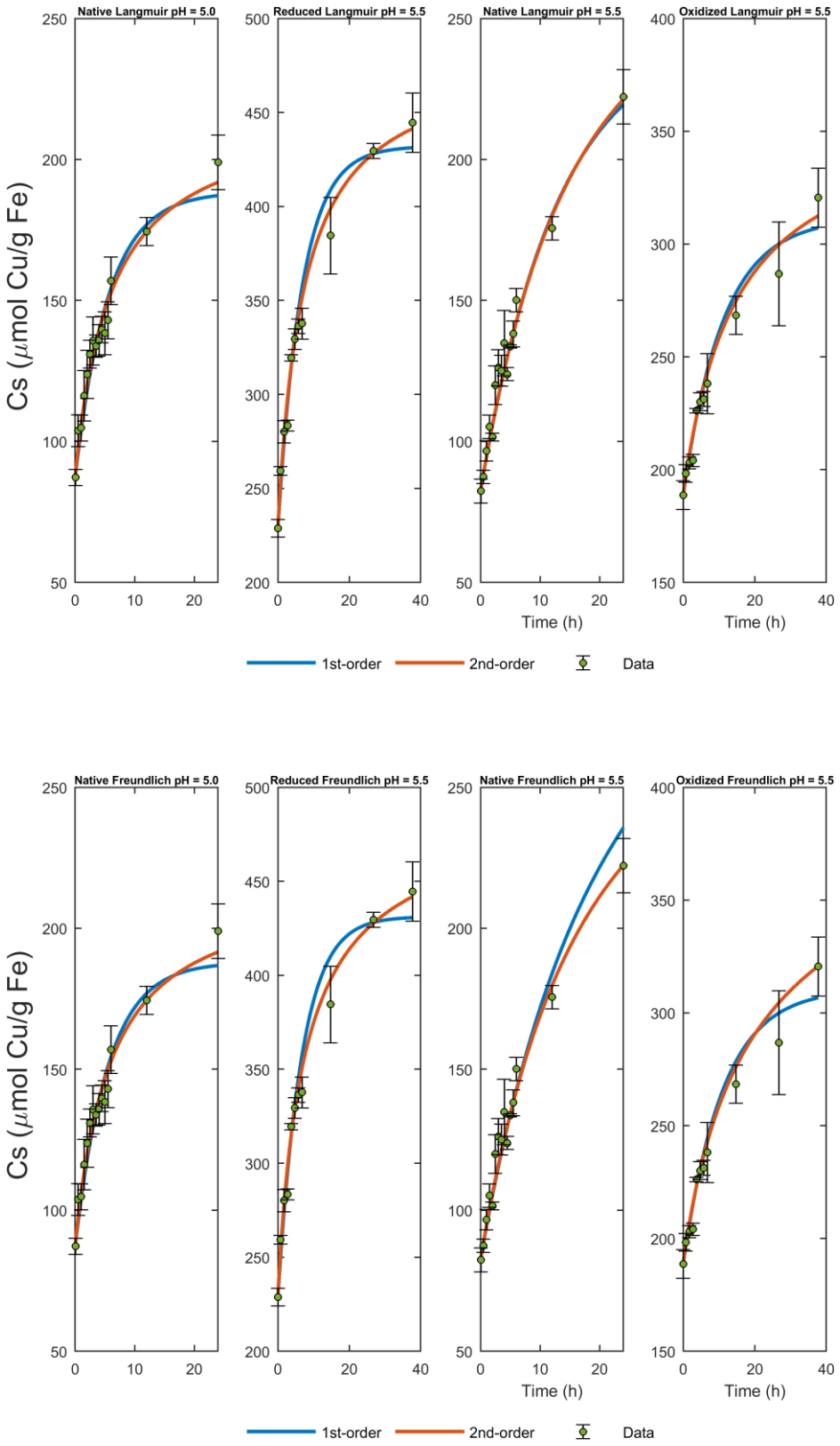

Figure S11: *Data and fit model of kinetic experiments for Cu at pH 5.5 with first and second order (blue and orange) kinetics parameter derived from either Langmuir or Freundlich isotherms for equilibrium concentration.*

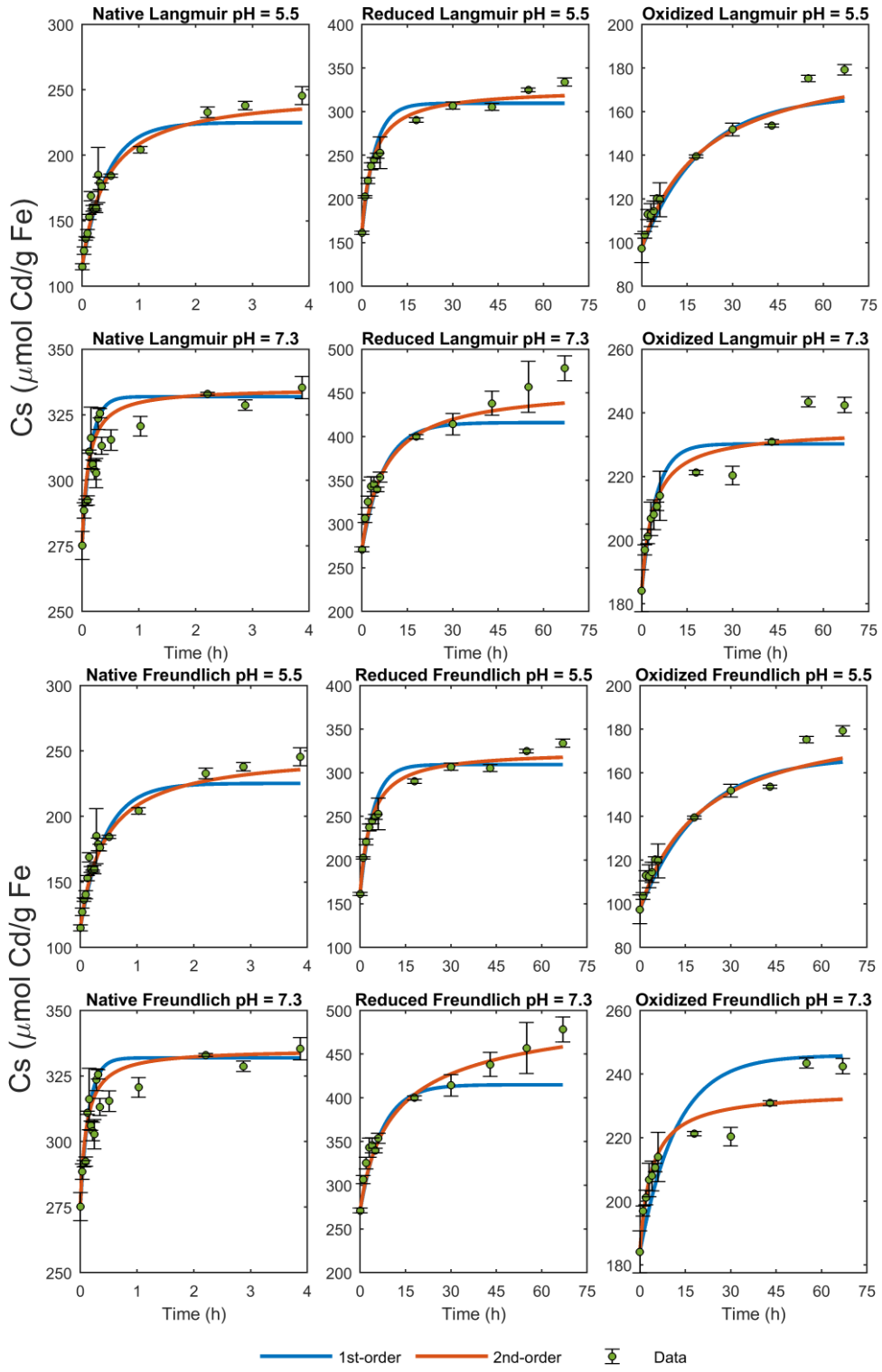

Figure S12: *Data and fit model of kinetic experiments for Cu at pH 5.5 and 7.3 with first and second order (blue and orange) kinetics parameter with either Langmuir or Freundlich isotherm for equilibrium concentration.*

Table S1: *Fitting results of Mössbauer spectroscopy. δ – isomer shift; ΔE_Q – quadrupole splitting; B_{hf} – hyperfine magnetic field; stdev(B_{hf}) – standard deviation of hyperfine magnetic field; R.A. – Relative abundance; red. χ2 – goodness of fit.*

	δ (mm/s)	ΔE_Q (mm/s)	B_{hf} (T)	stdev (B_{hf}) (T)	R.A. (%)	Error	Red. χ2
Sextet 1	0.655	-0.042	46.725	2.52547	62.6	1.4	1.49
Sextet 2	0.388	-0.011	49.756	3.87E-07	37.4	1.4	

Table S2: *Fitting parameters for magnetite isotherms collected with Cd^{2+} and Cu^{2+} contacted with native, reduced, and oxidized magnetite at different pH values. Upper part showing Freundlich fitting parameters and lower part showing Langmuir fitting parameters. Fits with * at pH 5.0 indicate that a narrower range of values were used to fit the range of the other pH values.*

Isotherms fit to Freundlich model

Magnetite	Element	pH	k ((µmol g^{-1})(L g^{-1})^n)	SD	rel. err.	n	SD	rel. err.	NRMSE
native	Cd	5.00	2.52	0.61	1.84	0.62	0.12	1.13	0.0460
	Cd	5.50	4.12	0.75	2.11	0.58	0.12	1.20	0.0603
	Cd	6.50	22.20	0.25	1.29	0.41	0.09	1.10	0.3454
	Cd	7.30	41.72	0.17	1.18	0.33	0.08	1.08	0.0293
reduced	Cd	5.50	28.28	0.68	1.98	0.33	0.31	1.37	0.0790
oxidized	Cd	5.50	20.75	0.25	1.29	0.34	0.11	1.12	0.0333
reduced	Cd	7.30	62.24	0.29	1.33	0.32	0.14	1.15	0.0396
oxidized	Cd	7.30	64.90	0.16	1.17	0.23	0.10	1.11	0.0322
native*	Cd	5*	0.51	0.27	1.31	0.85	0.05	1.05	0.1995
native	Cu	5.00	23.81	0.18	1.19	0.32	0.07	1.07	0.0303
native	Cu	5.50	28.62	0.18	1.20	0.31	0.09	1.09	0.0368
reduced	Cu	5.50	50.02	0.48	1.62	0.33	0.22	1.25	0.0790
oxidized	Cu	5.50	27.66	0.41	1.50	0.33	0.19	1.21	0.0709
native*	Cu	5.0*	32.30	0.07	1.07	0.27	0.04	1.04	0.0196

Isotherms fit to Langmuir model

Magnetite	Element	pH	q_{max} (µmol g^{-1})	SD	rel. err.	k_{ads} (µmol L^{-1})	SD	rel. err.	NRMSE
native	Cd	5.00	851.2	0.1	1.1	3572.6	0.2	1.2	0.0120
	Cd	5.50	399.1	0.2	1.2	666.6	0.4	1.5	0.0426
	Cd	6.50	470.1	0.1	1.1	251.1	0.3	1.4	0.0549
	Cd	7.30	468.4	0.2	1.2	152.4	0.6	1.9	0.1125
reduced	Cd	5.50	317.6	0.1	1.3	131.6	0.2	1.3	0.0276
oxidized	Cd	5.50	254.2	0.2	2.1	177.6	0.8	2.1	0.1043
reduced	Cd	7.30	663.7	0.2	1.9	149.6	0.6	1.9	0.0864
oxidized	Cd	7.30	339.7	0.2	2.4	66.9	0.9	2.4	0.1407
native*	Cd	5*	1231.6	0.4	1.5	5761.9	0.5	1.7	0.2973
native	Cu	5.00	375.0	0.11	1.11	692.10	0.37	1.45	0.0903
native	Cu	5.50	297.1	0.08	1.08	195.66	0.31	1.36	0.0747
reduced	Cu	5.50	561.7	0.04	1.04	131.60	0.16	1.18	0.0276
oxidized	Cu	5.50	308.8	0.03	1.04	138.32	0.13	1.14	0.0233
native*	Cu	5.0*	262.4	0.03	1.03	247.71	0.13	1.14	0.4409

Table S3: *Fitting parameters for magnetite kinetic experiments Cu^{2+} contacted with native, reduced, and oxidized magnetite at different pH values.*

Kinetics fit to Langmuir model							
Magnetite	Element	pH	$k_{sorb,1}$ (s^{-1}) or $k_{sorb,2}$ (μmol^{-1} g s^{-1})	order	q_{max} (μmol g^{-1})	k_{ads} (μmol L^{-1})	NRMSE
native	Cu	5.0	5.00e-05	first	188.53	0.0006924232	0.0559
native	Cu	5.5	6.32e-06	first	4301582.11	5119248.0615	0.0428
reduced	Cu	5.5	4.08e-05	first	432.03	0.0001317265	0.0541
oxidized	Cu	5.5	2.47e-05	first	311.43	0.0001387612	0.0596
native	Cu	5.0	5.20e-08	second	7517257.53	13173464.532	0.0443
native	Cu	5.5	9.17e-09	second	1175.49	507.42192	0.0421
reduced	Cu	5.5	1.51e-07	second	482.23	0.0001317433	0.0372
oxidized	Cu	5.5	4.74e-09	second	640723.00	472627.2032	0.0504

Kinetics fit to Freundlich model							
Magnetite	Element	pH	$k_{sorb,1}$ (s^{-1}) or $k_{sorb,2}$ (μmol^{-1} g s^{-1})	order	k ((μmol g^{-1})(L g^{-1})^n)	n	NRMSE
native	Cu	5.0	3.10e-05	first	4.76	0.60	0.0566
native	Cu	5.5	3.88e-08	first	2.86	1.56	0.0512
reduced	Cu	5.5	6.66e-06	first	5.00	0.86	0.0561
oxidized	Cu	5.5	9.67e-06	first	2.77	0.79	0.0602
native	Cu	5.0	2.43e-07	second	71.43	0.19	0.0449
native	Cu	5.5	1.04e-08	second	35.80	0.44	0.0417
reduced	Cu	5.5	1.39e-13	second	163.24	1.12	0.0561
oxidized	Cu	5.5	1.45e-13	second	2.77	1.65	0.0551

Table S4: *Fitting parameters for magnetite kinetic experiments Cd^{2+} with Freundlich equilibrium, contacted with native, reduced, and oxidized magnetite at different pH values.*

Kinetics fit to Freundlich model							
Magnetite	Element	pH	$k_{sorb,1}$ (s^{-1}) or $k_{sorb,2}$ (μmol^{-1} g s^{-1})	order	k ((µmol g^{-1})(L g^{-1})^n)	n	NRMSE
native	Cd	7.3	1.39e-03	first	75.90	0.23	0.1473
native	Cd	5.5	2.47e-4	first	0.31	1.08	0.0795
reduced	Cd	5.5	5.83e-05	first	210.44	0.07	0.0744
reduced	Cd	7.3	3.37e-05	first	285.12	0.06	0.1224
oxidized	Cd	5.5	9.04e-06	first	2.08	0.70	0.0856
oxidized	Cd	7.3	1.39e-05	first	6.49	0.57	0.1569
native	Cd	7.3	1.67e-05	second	27.60	0.39	0.1206
native	Cd	5.5	4.51e-07	second	0.31	1.13	0.0595
reduced	Cd	5.5	3.68e-07	second	223.40	0.06	0.0462
reduced	Cd	7.3	1.39e-13	second	6.22	1.58	0.0594
oxidized	Cd	5.5	1.35e-07	second	123.42	0.07	0.0733
oxidized	Cd	7.3	1.30e-06	second	174.13	0.05	0.0927

Table S5: *Fitting parameters for magnetite kinetic experiments Cd^{2+} with Langmuir equilibrium, contacted with native, reduced, and oxidized magnetite at different pH values.*

Kinetics fit to Langmuir model							
Magnetite	Element	pH	$k_{sorb,1}$ (s^{-1}) or $k_{sorb,2}$ (μmol^{-1} g s^{-1})	order	q_{max} (μmol L^{-1})	k_{ads} (μmol L^{-1})	NRMSE
native	Cd	7.3	7.23e-04	first	80048645.81	142458828.1852	0.1468
native	Cd	5.5	2.64e-04	first	468902468.63	919212790.2676	0.0800
reduced	Cd	5.5	6.5e-05	first	309.62	0.0001316016	0.0735
reduced	Cd	7.3	3.86e-05	first	416.00	0.000149647	0.1201
oxidized	Cd	5.5	1.41e-05	first	167.28	0.0001795486	0.0853
oxidized	Cd	7.3	5.93e-05	first	230.23	7.023212e-05	0.1125
native	Cd	7.3	1.62e-05	second	591.33	444.7175	0.1210
native	Cd	5.5	5.91e-07	second	19999474.62	30140634.7864	0.0601
reduced	Cd	5.5	4.69e-07	second	326.69	0.0001316818	0.0448
reduced	Cd	7.3	1.94e-07	second	457.55	0.0001496525	0.0784

Table S6: *Summary of properties of MNPs*

Type	Fe(II)/Fe(III)	Open circuit potential E_{OCP} [mV][62]	*Average crystal size d [nm][42]*	BET SSA [$m^2 g^{-1}$]	Calculated SSA from *d* [$m^2 g^{-1}$][49]
oxidized	0.26 ± 0.02	-0.12	10.23		101.0
native	0.42 ± 0.01	-0.36	10.29 (12.49*)	92.73	100.4
reduced	0.54 ± 0.03	-0.54	9.59		107.7

*calculated from BET measurement[49]

References

1. Gorski, C. A.; Nurmi, J. T.; Tratnyek, P. G.; Hofstetter, T. B.; Scherer, M. M. Redox behavior of magnetite: Implications for contaminant reduction. *Environ. Sci. Technol.* **2010**, 44 (1), 55-60.

2 Patterson, A. L. ThEnviron. Sci. Technol. Scherrer Formula for X-Ray Particle Size Determination. *Phys. Rev.* **1939**,56 (10), 978-982. DOI: 10.1103/PhysRev.56.978.

3 Etique, M.; Jorand, F. P.; Ruby, C. Magnetite as a precursor for green rust through thehydrogenotrophic activity of the iron-reducing bacteria Shewanella putrefaciens. *Geobiol.* **2016**,14 (3), 237-254.

Contribution to other works

Chapter 4 – Personal Contribution

This work was conceptualized and written by Dr. Muammar Mansor. For the *magnetite* part, I contributed to data analysis, discussion, display, and writing. All co-authors helped by providing samples, preparing samples, and revision of the manuscript.

Chapter 4: Application of single particle ICP-MS to determine mass distribution and number concentrations of environmental nanoparticles and colloids.

Muammar Mansor[1], Sören Drabesch[1], **Timm Bayer[1]**, Anh Van Le[1], Ankita Chauhan[1], Johanna Schmidtmann[2], Stefan Peiffer[2], Andreas Kappler[1]*

[1]Geomicrobiology, Center for Applied Geosciences, University of Tuebingen, 72076 Tuebingen, Germany; [2]Department of Hydrology, University of Bayreuth, 95447 Bayreuth, Germany.

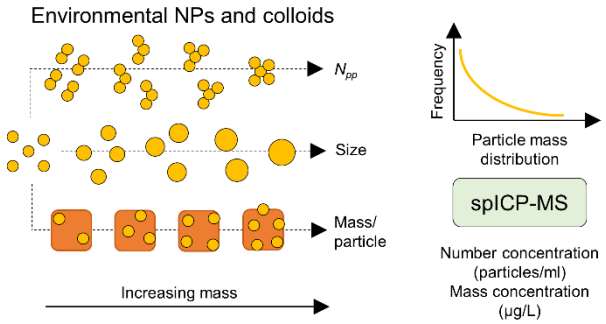

Published in: *Environmental Science and Technology Letters*

https://doi.org/10.1021/acs.estlett.1c00314

4.1 Abstract

Analyzing the elemental compositions and size distributions of nanoparticles, colloids and their aggregates in environmental samples represents a key task in understanding contaminant, substrate, and nutrient cycling. Single particle ICP-MS (spICP-MS) is a high-throughput method that is capable of providing the elemental mass of thousands of particles within minutes. The challenge however lies in data analysis and interpretation especially for complex environmental samples. Here we present successful applications of spICP-MS for environmental samples. We first analyzed the homoaggregation behavior of synthetic microplastic and magnetite (abiogenic and biogenic) nanoparticles. The measured distribution of aggregate mass was described as a function of the number of primary particles/aggregate (N_{pp}) parameter. In tandem with dynamic light scattering data, differences in aggregates' compactness (primary particles/nm unit) between samples can be determined. Second, we showed how sequential elemental analysis allows to evaluate the mobility of toxic arsenic metalloid and its inferred association with colloidal Fe(III) (oxyhydr)oxides. Finally, we investigated the composition of heterogenous iron-carbon-rich colloidal flocs, highlighting distinct colloidal Fe and C distributions and C/Fe ratios between samples from different permafrost thawing stages. Based on our results we provide guidelines for successful sample preparation and promising future spICP-MS opportunities/applications on environmental samples.

4.2 Introduction

Nanoparticles (NPs; ≤100 nm diameter) and colloids (≤1,000 nm) constitute a highly dynamic environmental pool of elements with a wide continuum in size, reactivity, aggregation and transport properties. Natural NPs have always been part of the Earth's biogeochemical cycling, while engineered and incidental NPs are increasingly released to the environment due to anthropogenic activities[1]. Our understanding of particle-driven processes is limited by the analytical techniques available at our disposal. Electron microscopy is the standard technique for providing mineralogical and elemental information at the single particle-level, but suffers from the high cost, time and effort needed to translate this information to the whole particle population, as well as artifacts during sample preparation. In contrast, sequential filtration (coupled to subsequent elemental/mineralogical analyses) provides population-level information

on particles separated into discrete size classes, but fails to treat them as a continuum of size and reactivity. Field-flow fractionation can also separate particles based on their properties (e.g., size) but separation parameters are highly sample-specific[2]. A combination of all these techniques is ideal to characterize NPs and colloids, but there remains a gap on how to combine the information gained from single particle up to the population level.

Single particle inductively coupled plasma mass spectrometry (spICP-MS) has the potential to become the method of choice to fill this technical gap. In spICP-MS, single particles are channeled to the instrument and detected as separate pulses in a time-resolved mode[3,4]. The intensity of each pulse is proportional to the element mass per particle, and can be converted to particle size given prior knowledge on the particle's density, shape and element mass fraction (**Fig. 1**). Sample preparation is comparatively simple – often requiring only dilutions – and thousands of particles can be analyzed within minutes. Simultaneous information is obtained at the single particle level (particle mass distribution) as well as the population level (particle number and mass concentrations). However, the use of spICP-MS for characterization of natural colloids has lagged behind engineered NPs[5–7], largely due to the inherent complexity of the former. spICP-MS is also limited to the analysis of one element per particle, but elemental association can be inferred by sequential elemental analysis of the same sample. The lack of element- and size-specific reference materials is another complication, although so far commonly-used calibration techniques are suitable for most particles[5,8,9] (except for selenium NPs[10]).

Here we detail approaches towards characterizing and interpreting spICP-MS data from environmental samples to facilitate the adoption of this technique. We present examples ranging from relatively simple aggregation of lab-synthesized particles (microplastics and abiogenic versus biogenic magnetite nanoparticles), to particle-facilitated mobilization of the toxic metalloid arsenic, and characterization of iron-carbon-rich colloids from a thawing permafrost.

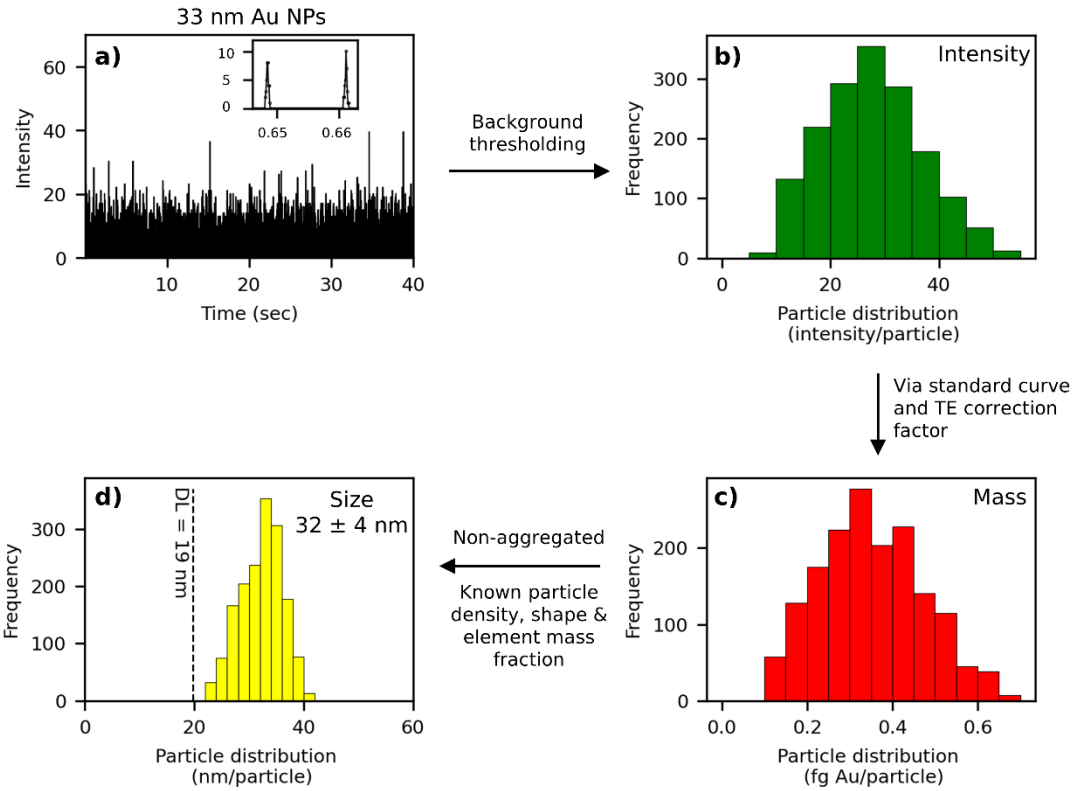

Figure 1: Illustration of data processing steps for spICP-MS. (a) Au nanoparticle (NP) standard is analyzed in single-particle mode, yielding a time-series consisting of pulses corresponding to particle detection events. Inset shows two adjoining pulses within a timeframe of ~0.02 sec, with a background intensity of 0. (b) After applying background thresholding (typically mean + 3 standard deviations), intensities corresponding to particle pulses are collected to generate a histogram. (c) Particle intensities are converted to the element mass per particle using a standard curve from dissolved elements and a transport efficiency (TE) correction factor (to account for different efficiency for the detection of dissolved elements versus particles). The masses can be summed to obtain the total mass or concentration in a sample. (d) Mass distribution can be converted to particle size distribution if the particles are non-aggregated and if the particle density, shape and metal mass fraction are known.

4.3 Materials and Methods

All samples were analyzed in time-resolved analysis mode on the Agilent 7900 ICP-MS (Agilent Technologies, Santa Clara, CA) with RF power = 1550 V and sampling depth = 8 mm. Samples and standards were prepared and measured as detailed in

Table S1 and **Table S2**, with results from standards shown in **Table S3**. Acid and water rinses were monitored in-between samples to ensure no carry-over. The transport efficiency (TE) was determined daily by comparing the median intensity of 50 nm Au NPs to dissolved Au standards using the particle mass method, which is less susceptible to dilution errors compared to the particle number method[3,11]. Over 6 separate days, the TE was comparable and averaged 0.037 ± 0.001. Masses at ^{12}C, ^{27}Al, ^{56}Fe, ^{75}As or ^{197}Au were monitored using integration time = 0.1 ms, acquisition time = 40-60 seconds, sample flow rate = 0.466 mL/min, and either in NoGas (argon only) or Gas mode (helium flow = 1 mL/min). Sequential analysis with a time gap of 10 seconds between elements was employed for multi-element analysis of the same sample. Data analysis was performed via a custom Python script following the approaches of Pace et al. (2011) and described in detail in **SI Data Analysis**. Lower detection limits with increasing element mass were observed (**Table S2**), consistent with previous studies[12,13].

4.4 Results and Discussion

Example 1: Aggregation of microplastic beads and magnetite nanoparticles

Aggregation of nanoparticles and colloids greatly affects their reactivity (surface area loss) and mobility (settling velocity)[14]. With spICP-MS, the particle mass distribution can be directly measured as a parameter to quantify the state of aggregation. An example is presented for the aggregation of synthetic polystyrene microplastic beads, which affects the sedimentation and mobilization of microplastics in aquatic systems[15,16]. Here we introduce the term N_{pp} (number of primary particles per aggregate), which can be obtained by dividing the mass of the measured aggregate (determined via spICP-MS) to the mass of the primary particle (calculable for particles of known size and composition; **SI Data Analysis**). **Figure 2a** showed that particle signals consisting of isolated microplastic beads (N_{pp} = 1) to aggregates composed of 5 beads (N_{pp} = 5) were readily distinguished based on their relative masses. Furthermore, the number frequency of each aggregate can be summed and compared to yield their relative frequencies and aggregation pattern. The combination of spICP-MS with ongoing work on microplastic aggregation holds promise to shed light on their fate in the environment[9,17–19].

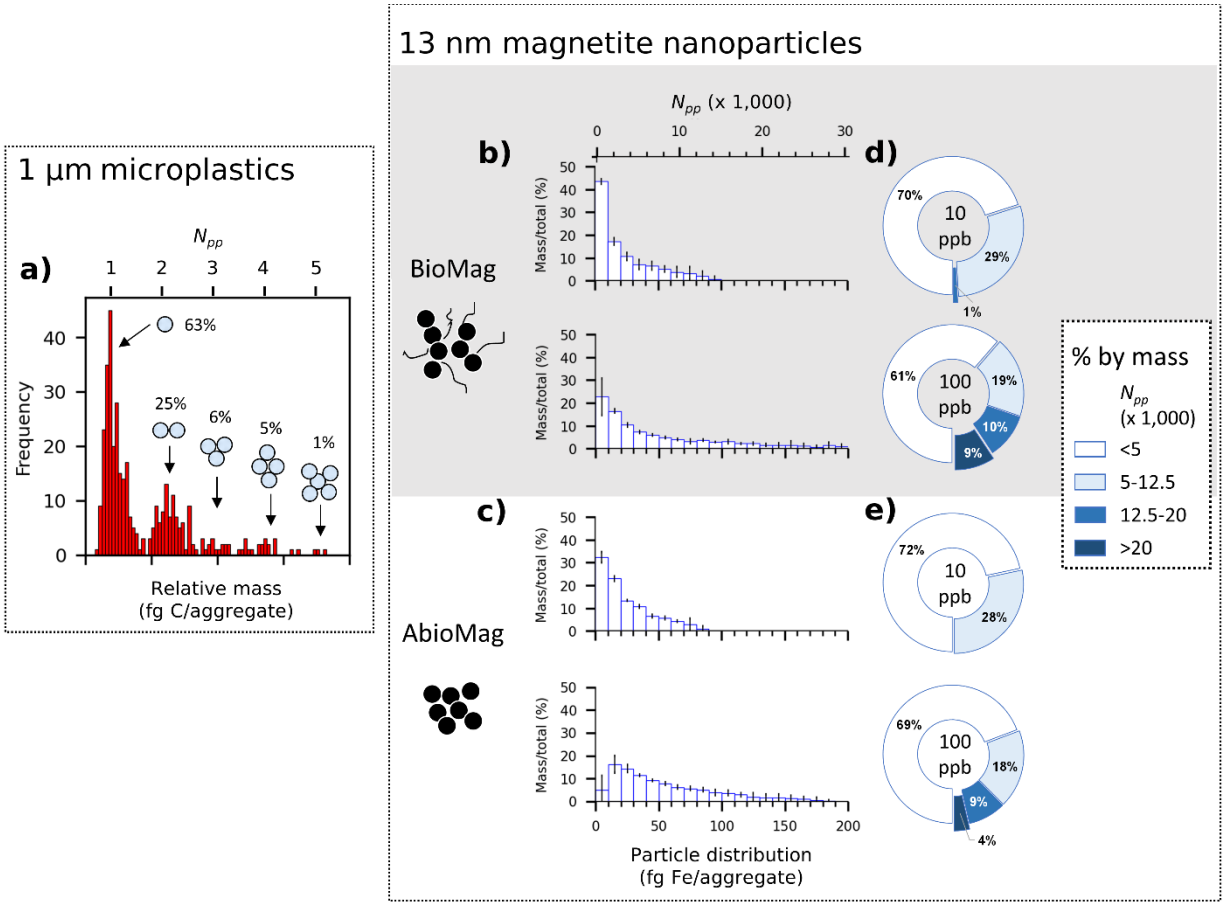

Figure 2: Examples on the usage of spICP-MS to quantify particle aggregation. (a) Frequency-based particle distribution (fg C/aggregate) of unsonicated 1 µm microplastic beads. The detected particles cluster based on their relative masses, which varies according to their corresponding N_{pp} (number of primary particles per aggregate; formula in SI Data Analysis). The use of the term N_{pp} allows for the description of particle distribution based on their masses, remaining true to the parameter actually measured by spICP-MS. The percentages of each aggregate can be quantified based on their relative detection frequencies with typical reproducibility of < 1%. (b-c) Mass-based particle distribution of (b) biogenic (BioMag) and (c) abiogenic (AbioMag) magnetite NPs at 10 and 100 ppb total Fe. The y-axis is converted from frequency to mass (% mass within a bin relative to total particle mass) so as to be more environmentally-relevant. Error bars correspond to standard deviations from triplicate measurements. (d-e) Mass-based percentages of the magnetite aggregates. Most of the particle masses are contributed by aggregates with N_{pp} < 5,000 (these include mass of particles smaller than spICP-MS' detection limit, assuming no dissolved Fe in the samples). The mass distribution changes depending

on the total NP concentration (10 vs 100 ppb Fe) and the sample type (BioMag vs AbioMag).

The technique was further developed through the analysis of ~13 nm-sized NPs of abiogenic and biogenic magnetite[20–22]. The detection limit for spICP-MS is 0.9 fg Fe/particle, which means that only aggregates larger than 140 N_{pp} can be detected. **Figure 2b-c** showed that magnetite aggregates with up to 30,000 N_{pp} were detectable. Due to the smaller sizes, the separation of signals for nanoparticle aggregates was not as clear as the larger microplastics, but differences in aggregation patterns were still distinguishable. Analyzing the same samples at higher particle concentrations lead to the formation of larger aggregates and a more positively skewed particle distribution, because aggregation increases with increasing total primary particles in suspension[23,24]. Between samples, biogenic magnetite was observed to form larger aggregates compared to abiogenic magnetite at the same concentration. This result was consistent with measurements of hydrodynamic diameter (D_H) via dynamic light scattering; biogenic magnetite displayed a D_H of 3,671 ± 670 nm (n = 9) compared to a smaller D_H of 1,567 ± 192 nm (n = 8) for abiogenic magnetite.

By combining measurements of N_{pp} from spICP-MS and D_H from DLS[25], we can calculate the Compaction Factor (CF; primary particles/nm unit) of a sample:

$$CF = N_{pp} / D_H \quad (1)$$

We determined CF for biogenic magnetite to be 2 to 6 times smaller than abiogenic magnetite, depending on the measurement dilutions and statistics used to describe skewed particle distributions (**Table S4**). Therefore, biogenic magnetite formed less compact aggregates than abiogenic magnetite. Overall, the data suggest that biogenic magnetite aggregation was enhanced via bridging by associated organic matter, but they were not packed as tightly as in the case of abiogenic magnetite. This in turn would affect the particle reactivity, that depends on the degree of reactive sites lost due to surface area decrease (as well as organic matter coverage) upon aggregation. Note however that CF values are dependent on the sample concentrations used for

both DLS (ppm level required due to lower sensitivity) and spICP-MS (ppb level), but can be applied to compare different samples as long as the same concentrations are used.

Example 2: Colloid-facilitated mobilization of As contaminant from used sand filters

In Asia, household sand-based filters are used regularly to treat arsenic-contaminated groundwater for drinking. Oxidation of dissolved Fe(IIin the sand filter results in the formation of solid-phase Fe(III) (oxyhydr)oxides that sequester toxic As and remove it from solution[26]. After being used up, the contaminated sand filter material is often dumped in the backyard garden, thus potentially acting as point sources that will channel As back into the pore water or enter the human food chain.

Our ongoing research has shown limited release of dissolved As from the used sand even as Fe(III) reduction occurs extensively in anoxic microcosms (**Table S1**). However, we noticed that the microcosms also produced colloids that remain stably suspended in solution for weeks. We therefore to investigate through spICP-MS if colloid-facilitated mobilization of As could be an important mechanism for As release, similar to in acid mine drainage[27].

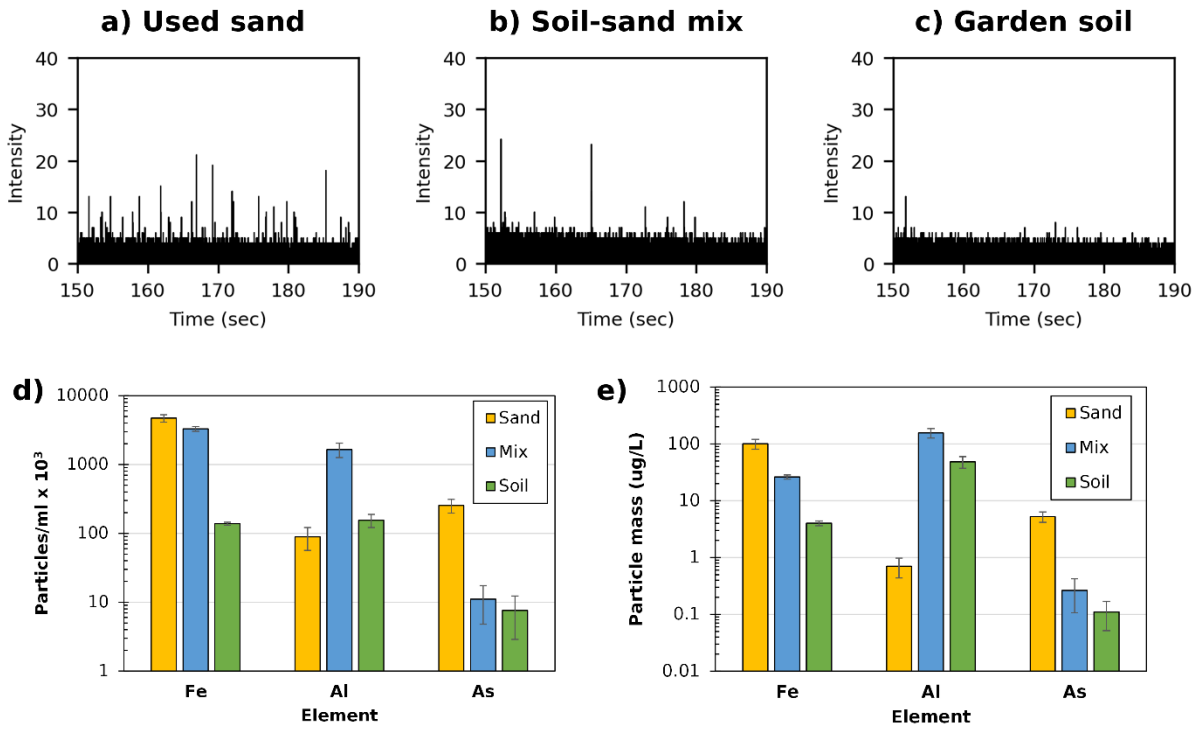

Figure 3: Example of spICP-MS usage to quantify colloidal contaminant mobilization. (a-c) Raw spICP-MS time series for arsenic (As) in used As-rich sand filters (left), sand-soil mix (middle) and uncontaminated garden soil (right). The used sand filters show elevated frequency of colloidal As. (d-e) Particle number concentrations (left) and particulate mass concentrations (right) of Fe, Al and As-containing colloids. The two parameters show the same trend between samples but with different relative values depending on the particle number frequency in each mass bin, highlighting the need to compare both number and mass concentrations side-by-side. Error bars represent standard deviations from measurements of three separate microcosm bottles.

Colloids from three microcosm samples were analyzed: As-rich used sand, uncontaminated garden soil, and 1:1 mixture of the two. The results were stark: As-containing colloids were detectable and most abundant from the used sand (~50), followed by the sand-soil mix (~10), while very low As-containing colloids were detected from the uncontaminated soil (≤ 2; comparable to H_2O blank) (**Fig. 3a-c**). After accounting for dilution, colloids from used sand were found to contain ~10^5 As-containing particles/ml with a collective mass of ~10 µg/L As, close to the World Health Organization's drinking water limit for dissolved As (**Fig. 3d-e**). The bioavailability of these colloids is an open question. Nonetheless, this result indicated that colloid-

facilitated mobilization of As from used sand could indeed be an important point source contamination.

We sought to understand the particle association of As by monitoring colloidal Fe and Al (**Fig. 3e-f**). The used sand contained higher colloidal Fe but lower colloidal Al than soil and the sand-soil mix. This trend was consistent regardless if the particle number or particle mass concentration was used as a comparison metric. Given the concurrent elevated Fe and As levels, we hypothesize that As was mobilized in the form of colloidal Fe(III) (oxyhydr)oxides, consistent with their known associations[28]. Future work using (sub)micron visualization of elemental distribution will help to evaluate this hypothesis.

Example 3: Colloidal Fe-carbon flocs released from thawing permafrost

Permafrost regions store a significant amount of organic carbon that are becoming increasingly bioavailable due to increasing global temperature[29]. Thawing of permafrost leads to the release of organic carbon that interacts with iron to form Fe-organic rich aggregates (flocs). These flocs are composed of heterogenous mixtures of amorphous Fe (oxyhydr)oxides with humic acids, microbial cells and plant detritus that are likely to be highly reactive and mobile[30,31]. Characterizing these flocs is vital towards understanding the role that they will play in greenhouse gas formation and climate change.

We analyzed the flocs collected from an intermediately-thawed bog and a fully-thawed fen from the Stordalen Mire (Abisko, Sweden). Bog and fen represent two distinct stages of thawing permafrost with different biogeochemical characteristics (e.g., E_h-pH, microbial communities)[32]. **Figure 4** illustrates the colloidal C and Fe distribution. A significant difference was apparent between the two samples: flocs from bog were characterized by high colloidal C and low colloidal Fe, while flocs from fen were characterized by low colloidal C (~1.5x lower) and high colloidal Fe (~15x higher). Correspondingly, the total colloidal C/Fe ratio (mass/mass) decreased from 14.3 ± 3.7 (n = 8) to 0.7 ± 0.5 (n = 7; replicates including different treatments in **Figure S1**) from bog to fen.

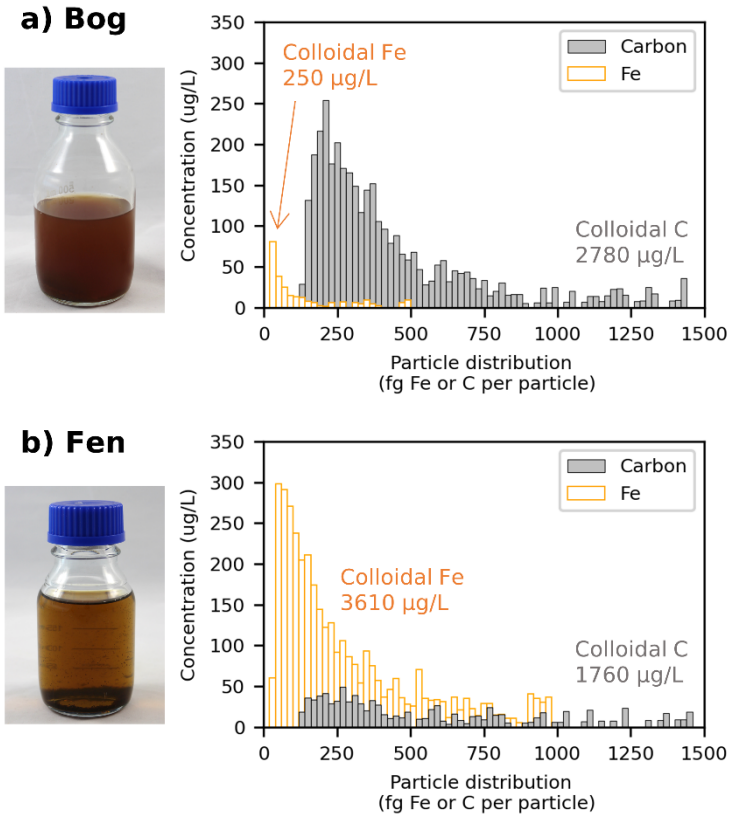

Figure 4: Results of spICP-MS analysis from colloidal Fe-C flocs from site (a) bog and (b) fen. The y-axis is shown in concentration (µg/L) by converting from frequency to mass to concentration after correcting for the sample volume analyzed (see **SI Data Analysis)**. The lack of smaller colloidal Fe (<20 fg Fe/particle) and C particles (<140 fg/particles) are not due to their absence, but are rather due to the detection limit of spICP-MS. Replicate samples show the same trend even after different treatments (**Figure S1**).

The increase in colloidal Fe may be explained by microbial Fe cycling that weathers large particles to form smaller colloidal particles that were detectable by spICP-MS, while the decrease in colloidal C was consistent with inferred organic C degradation during bog-to-fen transition[32]. Smaller colloidal Fe and C were also likely present but they were not detectable due to the detection limit of spICP-MS (**Table S2**).

Guidelines and future opportunities

The presented examples highlight the utility of spICP-MS in providing new insights into particle aggregation, adsorption and mobilization of toxic elements and their mass

distributions in environmental samples. The given examples are only snapshots and further analysis will undoubtedly provide more information on particle-driven biogeochemical cycling as a function of time or reaction progress. Sample preparation and interpretation are vital for spICP-MS, and here we present several guidelines:

- Remove large particles (>5 μm) by filtration, centrifugation or gravitational settling to avoid clogging in the tubings. When using gravitational settling, always use the same container type, sample volume and height, settling time, and sampling depth.

- Dilute samples to particle number concentration ≤10^6 particles/ml or to low ppb levels to reduce coincidence (two particles reaching the plasma at the same time) and particle carry-over effects[3]. Optimal dilution for unknown environmental samples should be determined via trial-and-error. The diluent choice is a compromise between ease of use and minimization of background and elemental interferences (MQ H_2O) to maintaining environmentally-relevant pH and ionic strength (e.g., filtered environmental water).

- Consciously select your mixing methods. Sonication for 5-10 minutes followed by brief mixing by inversion is recommended for analysis of irreversibly-bonded aggregates. Weaker mixing methods such as hand shaking and gas bubbling can be used to analyze weakly-bonded agglomerates.

- Choose appropriate sample container, tubings and reagents to minimize background and adsorptive losses. Reagents can be filtered beforehand to remove colloids. Fe and Al colloids are especially common in blank reagents but they can be statistically removed by conservative background thresholding.

- Particle distribution for complex environmental samples should be reported with element mass per particle as the primary x-axis as this parameter is directly measured by spICP-MS. Derived parameters (N_{pp} and size) should be plotted on the secondary x-axis.

Variants of spICP-MS are increasingly finding environmental applications[7]. Single cell ICP-MS has been used successfully to quantify metal content of single cells[33,34].

Recent development of *dual element* spICP-MS and time-of-flight (TOF)-spICP-MS can identify elemental association at the single particle level[35–38]. We expect spICP-MS to be an essential tool in environmental research in upcoming years.

SUPPORTING INFORMATION

SI Data Analysis.pdf – Thorough overview of the data analysis steps.
SI Tables-Figures.pdf – Table S1: Preparation steps of sample and standards, Table S2: Measurement details and detection limits for each element, Table S3: Size and particle number concentration of standards, Table S4: Determination of compaction factors from associated D_H and N_{pp} of magnetite, Figure S1: spICP-MS results of bog and fen samples after treated with N_2 degassing or sonication.

AUTHOR INFORMATION

Corresponding Author

*Muammar Mansor - Geomicrobiology, Center for Applied Geosciences, University of Tuebingen, 72076 Tuebingen, Germany; orcid.org/0000-0001-7830-650X; Email: muammar.muammar-bin-mansor@uni-tuebingen.de

Author Contributions

MM adapted the spICP-MS technique with a focus on environmental applications, supported and encouraged by AK. SD provided invaluable support with ICP-MS analysis. AC, AVL, JS, and TB provided samples. TB performed zetasizer measurements. All authors contributed to data interpretation and manuscript revisions.

Funding Sources

This work was supported by the Deutsche Forschungsgemeinschaft (DFG, German Research Foundation) project number 391977956 (SFB 1357) as well as DFG-funding provided to AK (KA 1736/66-1, KA 1736/51-1, KA 1736/48-1 and Cluster of Excellence: EXC 2124: Controlling Microbes to Fight Infection, Tübingen, Germany).

ACKNOWLEDGMENT

MM thanks Jie Xu for initial support in encouraging him to learn new techniques, Jim Ranville and Manuel Montaño for teaching spICP-MS, Saurav Kumar for building the original Python framework for data analysis, Weinan Leng and Frank Wackenhut for supplying Au NPs, Peter Kühn for supplying noble metal standards, and Christoph Glotzbach for easy access to the ICP-MS. AC would like to acknowledge Monique Patzner and Erik Lundin (Abisko Research Station, Abisko, Sweden) for their help in sampling and providing floc samples. The authors acknowledge infrastructural support by the Deutsche Forschungsgemeinschaft (DFG, German Research Foundation) under Germany's Excellence Strategy, cluster of Excellence EXC2124, project ID 390838134.

4.5 References

1. Hochella, M. F.; Mogk, D. W.; Ranville, J.; Allen, I. C.; Luther, G. W.; Marr, L. C.; McGrail, B. P.; Murayama, M.; Qafoku, N. P.; Rosso, K. M.; Sahai, N.; Schroeder, P. A.; Vikesland, P.; Westerhoff, P.; Yang, Y. Natural, Incidental, and Engineered Nanomaterials and Their Impacts on the Earth System. *Science (80-.).* **2019**, *363* (6434). https://doi.org/10.1126/science.aau8299.
2. Moens, C.; Waegeneers, N.; Fritzsche, A.; Nobels, P.; Smolders, E. A Systematic Evaluation of Flow Field Flow Fractionation and Single-Particle ICP-MS to Obtain the Size Distribution of Organo-Mineral Iron Oxyhydroxide Colloids. *J. Chromatogr. A* **2019**, *1599*, 203–214. https://doi.org/10.1016/j.chroma.2019.04.032.
3. Montaño, M. D.; Olesik, J. W.; Barber, A. G.; Challis, K.; Ranville, J. F. Single Particle ICP-MS: Advances toward Routine Analysis of Nanomaterials. *Anal. Bioanal. Chem.* **2016**, *408* (19), 5053–5074. https://doi.org/10.1007/s00216-016-9676-8.
4. Degueldre, C.; Favarger, P. Y. Colloid Analysis by Single Particle Inductively Coupled Plasma-Mass Spectroscopy: A Feasibility Study. *Colloids Surfaces A Physicochem. Eng. Asp.* **2003**, *217* (1–3), 137–142. https://doi.org/10.1016/S0927-7757(02)00568-X.
5. Mozhayeva, D.; Engelhard, C. A Critical Review of Single Particle Inductively Coupled Plasma Mass Spectrometry-A Step towards an Ideal Method for Nanomaterial Characterization. *J. Anal. At. Spectrom.* **2020**, *35* (9), 1740–1783. https://doi.org/10.1039/c9ja00206e.
6. Peters, R.; Herrera-Rivera, Z.; Undas, A.; Van Der Lee, M.; Marvin, H.; Bouwmeester, H.; Weigel, S. Single Particle ICP-MS Combined with a Data Evaluation Tool as a Routine Technique for the Analysis of Nanoparticles in Complex Matrices. *J. Anal. At. Spectrom.* **2015**, *30* (6), 1274–1285. https://doi.org/10.1039/c4ja00357h.
7. Flores, K.; Turley, R. S.; Valdes, C.; Ye, Y.; Cantu, J.; Hernandez-Viezcas, J. A.; Parsons, J. G.; Gardea-Torresdey, J. L. Environmental Applications and Recent Innovations in Single Particle Inductively Coupled Plasma Mass Spectrometry (SP-ICP-MS). *Appl. Spectrosc. Rev.* **2021**, *56* (1), 1–26. https://doi.org/10.1080/05704928.2019.1694937.
8. Montaño, M. D.; Majestic, B. J.; Jämting, Å. K.; Westerhoff, P.; Ranville, J. F. Methods for the Detection and Characterization of Silica Colloids by Microsecond SpICP-MS. *Anal. Chem.* **2016**, *88* (9), 4733–4741. https://doi.org/10.1021/acs.analchem.5b04924.
9. Laborda, F.; Trujillo, C.; Lobinski, R. Analysis of Microplastics in Consumer Products by Single Particle-Inductively Coupled Plasma Mass Spectrometry Using the Carbon-13 Isotope. *Talanta* **2021**, *221* (July 2020), 121486. https://doi.org/10.1016/j.talanta.2020.121486.
10. Jiménez-Lamana, J.; Abad-Álvaro, I.; Bierla, K.; Laborda, F.; Szpunar, J.; Lobinski, R. Detection and Characterization of Biogenic Selenium Nanoparticles in Selenium-Rich Yeast by Single Particle ICPMS. *J. Anal. At. Spectrom.* **2018**, *33* (3), 452–460. https://doi.org/10.1039/c7ja00378a.
11. Pace, H. E.; Rogers, N. J.; Jarolimek, C.; Coleman, V. A.; Higgins, C. P.; Ranville, J. F. Determining Transport Efficiency for the Purpose of Counting and Sizing Nanoparticles via Single Particle Inductively Coupled Plasma Mass Spectrometry. *Anal. Chem.* **2011**, *83* (24), 9361–9369. https://doi.org/10.1021/ac201952t.
12. Lee, S.; Bi, X.; Reed, R. B.; Ranville, J. F.; Herckes, P.; Westerhoff, P. Nanoparticle Size Detection Limits by Single Particle ICP-MS for 40 Elements. *Environ. Sci. Technol.* **2014**, *48* (17), 10291–10300. https://doi.org/10.1021/es502422v.

13. Laborda, F.; Gimenez-Ingalaturre, A. C.; Bolea, E.; Castillo, J. R. About Detectability and Limits of Detection in Single Particle Inductively Coupled Plasma Mass Spectrometry. *Spectrochim. Acta - Part B At. Spectrosc.* **2020**, *169* (November 2019), 105883. https://doi.org/10.1016/j.sab.2020.105883.
14. Hotze, E. M.; Phenrat, T.; Lowry, G. V. Nanoparticle Aggregation : Challenges to Understanding Transport and Reactivity in the Environment. *J. Environ. Qual.* **2010**, *39* (6), 1909–1924. https://doi.org/10.2134/jeq2009.0462.
15. Li, Y.; Wang, X.; Fu, W.; Xia, X.; Liu, C.; Min, J.; Zhang, W.; Crittenden, J. C. Interactions between Nano/Micro Plastics and Suspended Sediment in Water: Implications on Aggregation and Settling. *Water Res.* **2019**, *161*, 486–495. https://doi.org/10.1016/j.watres.2019.06.018.
16. Michels, J.; Stippkugel, A.; Lenz, M.; Wirtz, K.; Engel, A. Rapid Aggregation of Biofilm-Covered Microplastics with Marine Biogenic Particles. *Proc. R. Soc. B Biol. Sci.* **2018**, *285* (1885). https://doi.org/10.1098/rspb.2018.1203.
17. Alimi, O. S.; Farner Budarz, J.; Hernandez, L. M.; Tufenkji, N. Microplastics and Nanoplastics in Aquatic Environments: Aggregation, Deposition, and Enhanced Contaminant Transport. *Environ. Sci. Technol.* **2018**, *52* (4), 1704–1724. https://doi.org/10.1021/acs.est.7b05559.
18. Oriekhova, O.; Stoll, S. Heteroaggregation of Nanoplastic Particles in the Presence of Inorganic Colloids and Natural Organic Matter. *Environ. Sci. Nano* **2018**, *5* (3), 792–799. https://doi.org/10.1039/c7en01119a.
19. Bolea-Fernandez, E.; Rua-Ibarz, A.; Velimirovic, M.; Tirez, K.; Vanhaecke, F. Detection of Microplastics Using Inductively Coupled Plasma-Mass Spectrometry (ICP-MS) Operated in Single-Event Mode. *J. Anal. At. Spectrom.* **2020**, *35* (3), 455–460. https://doi.org/10.1039/c9ja00379g.
20. Sundman, A.; Vitzthum, A. L.; Adaktylos-Surber, K.; Figueroa, A. I.; van der Laan, G.; Daus, B.; Kappler, A.; Byrne, J. M. Effect of Fe-Metabolizing Bacteria and Humic Substances on Magnetite Nanoparticle Reactivity towards Arsenic and Chromium. *J. Hazard. Mater.* **2020**, *384* (July 2019). https://doi.org/10.1016/j.jhazmat.2019.121450.
21. Pearce, C. I.; Qafoku, O.; Liu, J.; Arenholz, E.; Heald, S. M.; Kukkadapu, R. K.; Gorski, C. A.; Henderson, C. M. B.; Rosso, K. M. Synthesis and Properties of Titanomagnetite ($Fe_{3-x}Ti_xO_4$) Nanoparticles: A Tunable Solid-State Fe(II/III) Redox System. *J. Colloid Interface Sci.* **2012**, *387* (1), 24–38. https://doi.org/10.1016/j.jcis.2012.06.092.
22. Byrne, J. M.; Telling, N. D.; Coker, V. S.; Pattrick, R. A. D.; Van Der Laan, G.; Arenholz, E.; Tuna, F.; Lloyd, J. R. Control of Nanoparticle Size, Reactivity and Magnetic Properties during the Bioproduction of Magnetite by *Geobacter Sulfurreducens*. *Nanotechnology* **2011**, *22* (45). https://doi.org/10.1088/0957-4484/22/45/455709.
23. Baalousha, M. Aggregation and Disaggregation of Iron Oxide Nanoparticles: Influence of Particle Concentration, PH and Natural Organic Matter. *Sci. Total Environ.* **2009**, *407* (6), 2093–2101. https://doi.org/10.1016/j.scitotenv.2008.11.022.
24. Vikesland, P. J.; Rebodos, R. L.; Bottero, J. Y.; Rose, J.; Masion, A. Aggregation and Sedimentation of Magnetite Nanoparticle Clusters. *Environ. Sci. Nano* **2016**, *3* (3), 567–577. https://doi.org/10.1039/c5en00155b.
25. Li, Z.; Shakiba, S.; Deng, N.; Chen, J.; Louie, S. M.; Hu, Y. Natural Organic Matter (NOM) Imparts Molecular-Weight-Dependent Steric Stabilization or Electrostatic Destabilization to Ferrihydrite Nanoparticles. *Environ. Sci. Technol.* **2020**, *54*, 6761–6770. https://doi.org/10.1021/acs.est.0c01189.

26. Nitzsche, K. S.; Weigold, P.; Lösekann-Behrens, T.; Kappler, A.; Behrens, S. Microbial Community Composition of a Household Sand Filter Used for Arsenic, Iron, and Manganese Removal from Groundwater in Vietnam. *Chemosphere* **2015**, *138*, 47–59. https://doi.org/10.1016/j.chemosphere.2015.05.032.
27. Gomez-Gonzalez, M. A.; Bolea, E.; O'Day, P. A.; Garcia-Guinea, J.; Garrido, F.; Laborda, F. Combining Single-Particle Inductively Coupled Plasma Mass Spectrometry and X-Ray Absorption Spectroscopy to Evaluate the Release of Colloidal Arsenic from Environmental Samples. *Anal. Bioanal. Chem.* **2016**, *408* (19), 5125–5135. https://doi.org/10.1007/s00216-016-9331-4.
28. Wallis, I.; Prommer, H.; Berg, M.; Siade, A. J.; Sun, J.; Kipfer, R. The River–Groundwater Interface as a Hotspot for Arsenic Release. *Nat. Geosci.* **2020**, *13* (4), 288–295. https://doi.org/10.1038/s41561-020-0557-6.
29. Estop-Aragonés, C.; Cooper, M. D. A.; Fisher, J. P.; Thierry, A.; Garnett, M. H.; Charman, D. J.; Murton, J. B.; Phoenix, G. K.; Treharne, R.; Sanderson, N. K.; Burn, C. R.; Kokelj, S. V.; Wolfe, S. A.; Lewkowicz, A. G.; Williams, M.; Hartley, I. P. Limited Release of Previously-Frozen C and Increased New Peat Formation after Thaw in Permafrost Peatlands. *Soil Biol. Biochem.* **2018**, *118* (December 2017), 115–129. https://doi.org/10.1016/j.soilbio.2017.12.010.
30. Zak, D.; Gelbrecht, J. The Mobilisation of Phosphorus, Organic Carbon and Ammonium in the Initial Stage of Fen Rewetting (a Case Study from NE Germany). *Biogeochemistry* **2007**, *85* (2), 141–151. https://doi.org/10.1007/s10533-007-9122-2.
31. Pokrovsky, O. S.; Shirokova, L. S.; Kirpotin, S. N.; Audry, S.; Viers, J.; Dupré, B. Effect of Permafrost Thawing on Organic Carbon and Trace Element Colloidal Speciation in the Thermokarst Lakes of Western Siberia. *Biogeosciences* **2011**, *8* (3), 565–583. https://doi.org/10.5194/bg-8-565-2011.
32. Patzner, M. S.; Mueller, C. W.; Malusova, M.; Baur, M.; Nikeleit, V.; Scholten, T.; Hoeschen, C.; Byrne, J. M.; Borch, T.; Kappler, A.; Bryce, C. Iron Mineral Dissolution Releases Iron and Associated Organic Carbon during Permafrost Thaw. *Nat. Commun.* **2020**, *11* (1), 1–11. https://doi.org/10.1038/s41467-020-20102-6.
33. Amor, M.; Tharaud, M.; Gélabert, A.; Komeili, A. Single-Cell Determination of Iron Content in Magnetotactic Bacteria: Implications for the Iron Biogeochemical Cycle. *Environ. Microbiol.* **2020**, *22* (3), 823–831. https://doi.org/10.1111/1462-2920.14708.
34. Gomez-Gomez, B.; Corte-Rodríguez, M.; Perez-Corona, M. T.; Bettmer, J.; Montes-Bayón, M.; Madrid, Y. Combined Single Cell and Single Particle ICP-TQ-MS Analysis to Quantitatively Evaluate the Uptake and Biotransformation of Tellurium Nanoparticles in Bacteria. *Anal. Chim. Acta* **2020**, *1128*, 116–128. https://doi.org/10.1016/j.aca.2020.06.058.
35. Montaño, M. D.; Badiei, H. R.; Bazargan, S.; Ranville, J. F. Improvements in the Detection and Characterization of Engineered Nanoparticles Using SpICP-MS with Microsecond Dwell Times. *Environ. Sci. Nano* **2014**, *1* (4), 338–346. https://doi.org/10.1039/c4en00058g.
36. Bevers, S.; Montaño, M. D.; Rybicki, L.; Hofmann, T.; von der Kammer, F.; Ranville, J. F. Quantification and Characterization of Nanoparticulate Zinc in an Urban Watershed. *Front. Environ. Sci.* **2020**, *8*, 1–16. https://doi.org/10.3389/fenvs.2020.00084.
37. Praetorius, A.; Gundlach-Graham, A.; Goldberg, E.; Fabienke, W.; Navratilova, J.; Gondikas, A.; Kaegi, R.; Günther, D.; Hofmann, T.; Von Der Kammer, F. Single-Particle Multi-Element Fingerprinting (SpMEF) Using Inductively-Coupled Plasma Time-of-Flight Mass Spectrometry (ICP-TOFMS) to Identify Engineered Nanoparticles

against the Elevated Natural Background in Soils. *Environ. Sci. Nano* **2017**, *4* (2), 307–314. https://doi.org/10.1039/c6en00455e.
38. Naasz, S.; Weigel, S.; Borovinskaya, O.; Serva, A.; Cascio, C.; Undas, A. K.; Simeone, F. C.; Marvin, H. J. P.; Peters, R. J. B. Multi-Element Analysis of Single Nanoparticles by ICP-MS Using Quadrupole and Time-of-Flight Technologies. *J. Anal. At. Spectrom.* **2018**, *33* (5), 835–845. https://doi.org/10.1039/c7ja00399d.

4.6 Supporting Information

Application of single particle ICP-MS to determine mass distribution and number concentrations of environmental nanoparticles and colloids.

Muammar Mansor[1], Sören Drabesch[1], **Timm Bayer[1]**, Anh Van Le[1], Ankita Chauhan[1], Johanna Schmidtmann[2], Stefan Peiffer[2], Andreas Kappler[1]*

[1]Geomicrobiology, Center for Applied Geosciences, University of Tuebingen, 72076 Tuebingen, Germany; [2]Department of Hydrology, University of Bayreuth, 95447 Bayreuth, Germany.

Number of tables in supporting information: 1

Number of figures in supporting information: 3

Total number of pages in supporting information: 10 (including cover page)

Data Analysis

Here we detail the step-by-step approach for data analysis from spICP-MS time series1,2.

First, determine the average background intensity (σdiss) by an iterative approach

Average the whole dataset.

Remove datapoints that are higher than σdiss + x standard deviation (SD). See step 2 for discussions on the appropriate value of x.

Repeat the first two steps until there is no significant change in σdiss.

The dissolved element concentration in the sample can be calculated by using σdiss and the slope and intercept of the standard curve of the dissolved element. However, one must keep in mind that the determined value includes contribution from particles that are below the particle detection limit (see step 4 on how to determine detection limit).

Matrix effect caused by insufficient dilutions may cause an increasing or decreasing background signal over time. A linear background correction can be applied without severely impacting particle signals. However, this will increase the error for measurements of dissolved concentrations.

Collect all the datapoints corresponding to particle events (i.e. datapoints higher than σdiss + xSD) and subtract the background

The appropriate value of x can be anywhere from 3 to 8 (references compiled in Laborda et al., 2020), depending on the element and the noisiness of the background signal.

Optimal value of x aims to minimize false positives i.e., the signals detected as “particles” from rinse acids or dissolved element standards compared to real particle-containing samples. Aim to achieve a false positive value of < 3% by systematically varying x.

Proper tuning of the instrument to maximize stability and reduction of background signals (from contamination/residues) will help in improving particle detection limit.

After collecting the datapoints, subtract each one with the average background intensity determined in step 1.

Sum up the intensity of all datapoints that constitute a particle event

Depending on the signal integration time, each particle event may consist of several consecutive datapoints. For example, a particle event with 5 datapoints has a transit time of 500 µs with an integration time of 100 µs. Longer transit times are observed for larger particles and with measurements using He in Gas mode4.

To reduce false positives, we can further implement a minimum consecutive point (MCP) threshold, in which a particle event must contain a minimum number of consecutive datapoints to be considered as real. We found that MCP implementation significantly decreased the number of false positives, likely due to the statistical elimination of short-lived instrument shot noise.

We advise using MCP = 1 to 3 with SD = 3 to 5.

For each particle event, sum up the intensity of the consecutive datapoints. The summed intensity of each particle can be tabulated and used to generate a frequency-based particle intensity distribution.

Convert intensity to element mass per particle and subsequently to other derived parameters (particle mass, particle size, number of primary particles per aggregate)

First, calculate the slope of the standard curve of element mass per particle (mp) based on the pre-determined transport efficiency (TE)2 and the slope of the standard curve of the dissolved element (mdiss):

mp = mdiss / TE / flow rate / integration time (1)

Determine the detection limit (DL) of element mass per particle:

DL= (〖(σ〗 _diss+ xSD)*MCP)/(IE*m_p) (2)

where IE = particle ionization efficiency (often assumed to be equal to 1, but can be less than 1 especially for elements with low ionization efficiencies such as selenium and carbon (Jiménez-Lamana et al., 2018; this study)).

Then, calculate the element mass per particle (ME) for each detected particle event:

M_E=I_(sum)/(IE*m_p) (3)

where Isum = summed particle intensity from step 3.

Data for all particles can be tabulated and used to generate a frequency-based particle distribution with element mass per particle on the x-axis.

If the element mass fraction (f) of the particle is known, the whole mass of a particle (Mp) can be calculated as following:

$$Mp = ME / f \quad (4)$$

If the particle is not aggregated, is spherical in shape and has a known density (ρ), particle size (D) can be calculated as following:

$$D = \sqrt[3]{((6*M_p)/(\rho*\pi))} \quad (5)$$

For the analysis of aggregates, if the size (Dpp), density (ρ) and mass fraction (f) of the primary particle are known, then the number of primary particles per aggregate (Npp) can be calculated:

$$M_{pp} = (〖D_{pp}〗^3*\rho*\pi)/6 \quad (6)$$

$$Npp = ME / Mpp \quad (7)$$

where Mpp = element mass per primary particle. Due to analytical error and natural size variation, the determined Npp values are usually non-integers but can be rounded for simplicity.

Particle distribution data can then be expressed in terms of element mass per particle, particle mass, particle size or Npp. We recommend always reporting element mass per particle on the primary x-axis as this parameter is directly measured by spICP-MS. Other derivative parameters can be reported on the secondary axis depending on the information of interest.

Population-level information – particle number and mass concentration

Particle number concentration (PNC) and particle element mass concentration (PMC) can be calculated with the following:

$$PNC = Fevent / acquisition\ time / flow\ rate / TE / IE \quad (8)$$

$$PMC = \Sigma ME / acquisition\ time / flow\ rate / TE \quad (9)$$

where Fevent = frequency of the particle event over the period of the acquisition time and ΣME = sum of the element mass per particle for all particles.

References

1. Montaño, M. D.; Olesik, J. W.; Barber, A. G.; Challis, K.; Ranville, J. F. Single Particle ICP-MS: Advances toward Routine Analysis of Nanomaterials. *Anal. Bioanal. Chem*. **2016**, 408 (19), 5053–5074. https://doi.org/10.1007/s00216-016-9676-8.
2. Pace, H. E.; Rogers, N. J.; Jarolimek, C.; Coleman, V. A.; Higgins, C. P.; Ranville, J. F. Determining Transport Efficiency for the Purpose of Counting and Sizing Nanoparticles via Single Particle Inductively Coupled Plasma Mass Spectrometry. *Anal. Chem.* **2011**, 83 (24), 9361–9369. https://doi.org/10.1021/ac201952t.
3. Laborda, F.; Gimenez-Ingalaturre, A. C.; Bolea, E.; Castillo, J. R. About Detectability and Limits of Detection in Single Particle Inductively Coupled Plasma

Mass Spectrometry. *Spectrochim. Acta - Part B At. Spectrosc*. **2020**, 169 (November 2019), 105883. https://doi.org/10.1016/j.sab.2020.105883.
4. Bolea-Fernandez, E.; Leite, D.; Rua-Ibarz, A.; Liu, T.; Woods, G.; Aramendia, M.; Resano, M.; Vanhaecke, F. On the Effect of Using Collision/Reaction Cell (CRC) Technology in Single-Particle ICP-Mass Spectrometry (SP-ICP-MS). *Anal. Chim. Acta* **2019**, 1077, 95–106. https://doi.org/10.1016/j.aca.2019.05.077.
5. Jiménez-Lamana, J.; Abad-Álvaro, I.; Bierla, K.; Laborda, F.; Szpunar, J.; Lobinski, R. Detection and Characterization of Biogenic Selenium Nanoparticles in Selenium-Rich Yeast by Single Particle ICPMS. *J. Anal. At*. Spectrom. **2018**, 33 (3), 452–460. https://doi.org/10.1039/c7ja00378a

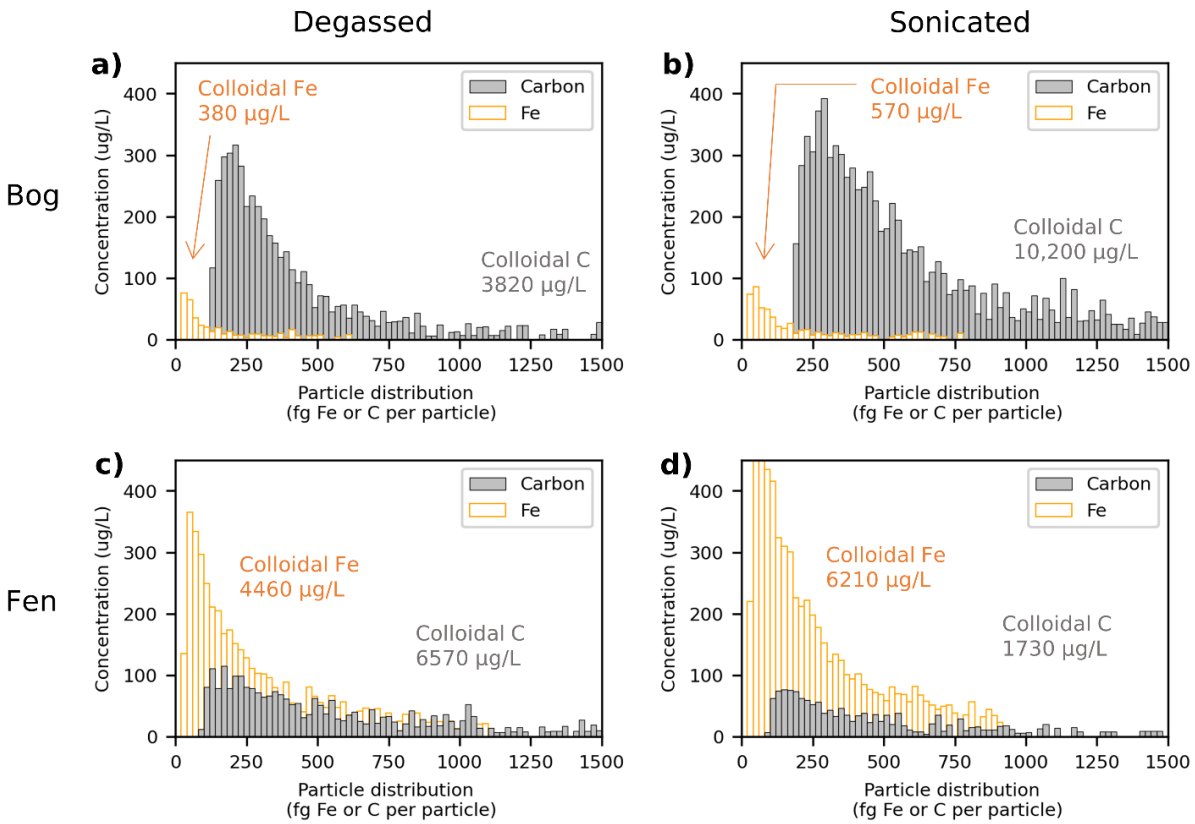

Figure S1: Selected replicate analysis of colloidal flocs. The samples came from either (a-b) bog or (c-d) fen. They were treated by degassing for 5 minutes with N_2 (to remove CO_2) or sonicated to break weakly-bonded agglomerates. Compared to untreated samples (Figure 4 in the main text), degassed and sonicated samples had a lower C detection limit, more detection of smaller colloids, and overall higher concentrations of colloidal C and Fe. Irrespective of treatments, the particle distribution trends are similar and bog samples always have higher C/Fe than fen.

Table S1: Details for sample and standard preparation methods

Material	Source	Sample preparation
Dissolved Fe, Al & As standards	Agilent Environmental Calibration Standard, product #5183-4688	Diluted in 1% HCl to 0-1,000 ppb
Dissolved Au standards	LGC noble metal standard, product #SM40-100	Diluted in 1% HCl to 0-50 ppb
Dissolved C standards	Potassium hydrogen phthalate	Diluted in 1% HCl to 0-20 ppm
30 nm Au NPs	NanoPartz, product # A11-30-Cit	Sonication for 10 minutes, diluted to ~10^5 particles/ml in MQ H_2O
33 nm Au NPs	In-house standard from NanoEarth*, confirmed by TEM	Sonication for 10 minutes, diluted to ~10^5 particles/ml in MQ H_2O
50 nm Au NPs	Sigma Aldrich, product #742007	Sonication for 10 minutes, diluted to ~10^5 particles/ml in MQ H_2O
1 µm polystyrene microplastic beads	microParticles GmbH, product # PS-F-KM392-2	Unsonicated/sonication for 10 minutes, diluted to 1 ppm in MQ H_2O or 1% HCl
2.5 µm polystyrene microplastic beads	Fluidigm, product #201078	Vortexed vigorously for 1 minute and analyzed immediately undiluted
13 nm biogenic (BioMag) and abiogenic (AbioMag) magnetite NPs	BioMag synthesized via microbial reduction of ferrihydrite by *Geobacter sulfurreducens*[1] and washed 3 times with H_2O. AbioMag synthesized abiotically via co-precipitation of Fe(II) and Fe(III)[2]. Size and shape had been previously characterized[3].	Total Fe concentration first determined via spectrophotometric ferrozine assay[4]. Samples then serially diluted in MQ H_2O with 5-10 seconds of vortexing in-between dilutions
As-containing colloids from microcosm experiments	Household sand filter and garden soils were collected from Hanoi, Vietnam (20.848518 N; 105.919483 E). Sand, soil or 1:1 mixture of the two (2.5 g) was then incubated at 28°C in the dark in the presence of 125 ml of anoxic artificial rainwater (in 225 cm^3 serum bottles).	Microcosms were shaken and large particles were allowed to settle for 24 hrs while standing. About 1 ml of suspensions were sampled directly from the top and diluted 100-fold in anoxic MQ H_2O. All sampling performed in an anoxic glovebox.
Fe-C-rich flocs	Flocs were collected from bog and fen in Stordalen Mire, Abisko, Sweden[5]. The flocs were collected in a sterilized HPDE 1L bottle, immediately put in dry ice, transported to the station, and stored at 4°C in the dark.	1 L Schott bottles containing ~1 L of samples were briefly shaken by inversion and then left standing for 30 minutes. About 10 ml of suspensions were sampled directly from the top and diluted 100-fold in MQ H_2O. Samples were then analyzed untreated, with 5 minutes of N_2 degassing or with 5 minutes of sonication

*Virginia Tech National Center for Earth and Environmental Nanotechnology Infrastructure.

Table S2: Measurement details and detection limits for the measured elements

Mass	Measurement mode	DL element mass per particle (fg)	DL size (nm)	Assumptions for size calculation
^{12}C	NoGas	91	564	Polystyrene microplastic, f_C = 0.923, ρ = 1.05 g/cm^3
^{27}Al	He = 1 ml/min	1.4	109	Al_2O_3, f_{Al} = 0.529, ρ = 3.95 g/cm^3
^{56}Fe	He = 1 ml/min	0.9	66	Magnetite, f_{Fe} = 0.724, ρ = 7.87 g/cm^3
			94	Ferrihydrite, f_{Fe} = 0.523, ρ = 3.8 g/cm^3
^{75}As	He = 1 ml/min	0.4	-	-
^{197}Au	He = 1 ml/min	0.06	18	Au NPs, f_{Au} = 1 , ρ = 19.3 g/cm^3

Values shown correspond to ideal condition determined from blanks (rinse acids or MQ H_2O). Background thresholding was applied using SD = 3 and MCP = 3 for all elements. For ^{12}C, an additional correction factor we attributed to low ionization efficiency (IE = 0.1) was applied following determination via analysis of microplastic standards. Analysis on ^{13}C was also tested based on previous recommendation[6] but was found to be less sensitive compared to ^{12}C. DL = detection limit; f = element mass fraction; ρ = particle density.

Table S3: Size and particle number concentration of particle standards

Material	Measured size (nm)	Particle number concentration (particles/ml)	
		Measured	Expected[a]
33 nm Au NPs	32 ± 4	1 x 10^5	10^5
30 nm Au NPs	32 ± 5	8 x 10^5	10^6
	31 ± 5	8 x 10^5	
	29 ± 3	8 x 10^4	10^5
	30 ± 3	9 x 10^4	
50 nm Au NPs	50 ± 10	6 x 10^4	10^5
	50 ± 10	2 x 10^5	
	49 ± 10	4 x 10^4	
1 µm polystyrene microplastic beads[b]	992 ± 167	4 x 10^6	5 x 10^6
	1,068 ± 200	4 x 10^6	5 x 10^6
	1,008 ± 136	2 x 10^6	2 x 10^6
2.5 µm polystyrene microplastic beads	2,707 ± 470	3 x 10^5	3 x 10^5
	2,460 ± 691	6 x 10^4	3 x 10^5

[a]Expected values calculated assuming no errors in dilution. Different stocks of diluted standards are prepared for each analysis day. All samples were dispersed via 10 minutes of sonication or vigorous vortexing for 1 minute.

Table S4: Compaction factor and associated parameters for magnetite aggregates

Sample	D_H (nm)[a]	spICP-MS concentration (ppb Fe)	Number-weighted mean		Number-weighted median		Mass-weighted mean	
			N_{pp}	CF[b]	N_{pp}	CF[b]	N_{pp}	CF[b]
BioMag	3671 ± 670	10	1230 ± 6	0.34	580 ± 17	0.16	3840 ± 91	1.05
AbioMag	1567 ± 192	10	1540 ± 70	0.98	832 ± 11	0.53	3797 ± 324	2.42
BioMag	3671 ± 670	100	2251 ± 479	0.61	978 ± 216	0.27	8101 ± 1650	2.21
AbioMag	1567 ± 192	100	4477 ± 1177	2.86	2691 ± 887	1.72	8263 ± 1674	5.27

[a]Z-average hydrodynamic diameters (D_H) obtained from DLS measurements at 100 ppm Fe.

[b]CF = Compaction Factor = N_{pp}/D_H. N_{pp} was determined from spICP-MS dataset.

References

1. Byrne, J. M.; Telling, N. D.; Coker, V. S.; Pattrick, R. A. D.; Van Der Laan, G.; Arenholz, E.; Tuna, F.; Lloyd, J. R. Control of Nanoparticle Size, Reactivity and Magnetic Properties during the Bioproduction of Magnetite by Geobacter Sulfurreducens. *Nanotechnol.* **2011**, 22 (45).
2. Pearce, C. I.; Qafoku, O.; Liu, J.; Arenholz, E.; Heald, S. M.; Kukkadapu, R. K.; Gorski, C. A.; Henderson, C. M. B.; Rosso, K. M. Synthesis and Properties of Titanomagnetite (Fe3-xTixO4) Nanoparticles: A Tunable Solid-State Fe(II/III) Redox System. *J. Colloid Interface Sci.* **2012**, 387 (1), 24–38.
3. Sundman, A.; Vitzthum, A. L.; Adaktylos-Surber, K.; Figueroa, A. I.; van der Laan, G.; Daus, B.; Kappler, A.; Byrne, J. M. Effect of Fe-Metabolizing Bacteria and Humic Substances on Magnetite Nanoparticle Reactivity towards Arsenic and Chromium. *J. Hazard. Mater*. **2020**, 384.
4. Hegler, F.; Posth, N. R.; Jiang, J.; Kappler, A. Physiology of Phototrophic Iron(II)-Oxidizing Bacteria: Implications for Modern and Ancient Environments. *FEMS Microbiol. Ecol*. **2008**, 66 (2), 250–260.
5. Patzner, M. S.; Mueller, C. W.; Malusova, M.; Baur, M.; Nikeleit, V.; Scholten, T.; Hoeschen, C.; Byrne, J. M.; Borch, T.; Kappler, A.; Bryce, C. Iron Mineral Dissolution Releases Iron and Associated Organic Carbon during Permafrost Thaw. *Nat. Commun.* **2020**, 11 (1), 1–11.
6. Bolea-Fernandez, E.; Rua-Ibarz, A.; Velimirovic, M.; Tirez, K.; Vanhaecke, F. Detection of Microplastics Using Inductively Coupled Plasma-Mass Spectrometry (ICP-MS) Operated in Single-Event Mode. *J. Anal. At. Spectrom*. **2020**, 35 (3), 455–460.

Chapter 5: Summary, general conclusions and outlook

Iron (Fe) is a redox-active compound that interacts with elemental cycles such as carbon, nitrogen, and oxygen in the environment and hence plays a key role. As Fe (oxyhydr)oxide minerals, Fe interacts with nutrients like phosphate and heavy metal contaminants such as cadmium, influencing their mobility, (bio)availability, and hence toxicity, through adsorption interactions and redox reactions[1]. Fe-metabolizing microorganisms can use Fe as an electron donor or acceptor. Therefore, studying the effect of Fe-metabolizing microorganisms on the identity, stoichiometry, crystallinity, and redox potential of Fe minerals will help to comprehend the fate of these minerals and their interactions with associated compounds like nutrients and contaminants.

Magnetite (Fe_3O_4) is a ubiquitous mixed-valent Fe mineral[2], containing Fe(II) and Fe(III) within the mineral structure ($Fe(III)_2Fe(II)O_4$), that was shown to be used as an electron donor and acceptor for Fe-oxidizing and Fe-reducing microorganisms respectively, and therefore named biogeobattery[3]. However, most evidence of Fe(II) oxidation in magnetite has been demonstrated for the phototrophic Fe(II)-oxidizing microorganism *Rhodopseudomonas palustris* TIE-1, limiting the implications to specific environments that allow for phototrophic Fe(II)-oxidation. Additionally, successive redox cycles of magnetite have been performed using cell suspension experiments[3]. The methodology used, and the results obtained, may hence not be fully representative of natural environments, as biogeochemical factors, such as cell density, redox potential, presence of cations and anions, and utilization of different pH buffer systems, play a significant role in the formation and transformation of Fe minerals[4-6].

Previously, effects of magnetite oxidation or reduction and the fate of contaminants were mainly studied with magnetite modified by cell suspensions[7, 8], or on unchanged magnetite particles[9, 10]. To better comprehend the potential of magnetite as a remediation agent, and as a continuous electron source or sink, it is crucial to consider the effect of lower cell density incubations on its properties. This understanding can help us determine the subsequent (bio)availability for Fe-metabolizing microorganisms and the adsorption mechanisms of toxic compounds. This knowledge can be applied to improve the use of magnetite in groundwater decontamination (as in reactive barriers[11]) and wastewater treatment processes[12] as an adsorbent for contaminations.

The aim of this PhD project was to study the impact of Fe-metabolizing microorganisms on magnetite nanoparticles, acting as biogeobatteries, in conditions that are one step closer to closer to environmental conditions.

A method was established to produce high amounts of magnetite nanoparticles outside of a glovebox, while being comparable with previously published methods[13]. This ensured that there were enough nanoparticles for all experiments, making the research consistent and comparable throughout all the presented chapters. The identity and stoichiometry of magnetite nanoparticles was studied to determine their ability to serve as a biogeobattery during continuous redox cycles. This was achieved by establishing the oxidation of magnetite nanoparticles by the nitrate-reducing Fe(II)-oxidizing enrichment culture "culture KS"[14] and coupling it to the reduction by *G. sulfurreducens* in four consecutive oxidation/reduction half-cycles (**Chapter 2**). Nitrate-reducing microorganisms have been found in various environments like lakes, freshwater ponds, marine sediments, and aquifers[15-17], suggesting the ubiquitous importance of magnetite as a biogeobattery, that can be driven by the oxidation of these microorganisms. We could show that the synthesized magnetite nanoparticles served as biogeobatteries for 41 consecutive days, as displayed by changes in Fe(II)/Fe(III) stoichiometry determined by the ferrozine assay, µ-XRD, and ^{57}Fe Mössbauer spectroscopy. Additionally, reductive dissolution of magnetite followed by reprecipitation to vivianite was shown through a combination of ferrozine, Mössbauer, µ-XRD, FTIR and magnetic susceptibility measurements. This reductive dissolution was more pronounced during the second reduction. Finally, these findings were supported by investigation of the different morphologies of minerals with scanning electron microscopy. During oxidations, the lowest determined Fe(II)/Fe(III) ratio was 0.297, which could have represented a thermodynamic limitation of magnetite oxidation in our system.

Afterwards, magnetite nanoparticles that were oxidized or reduced by culture KS or *G. sulfurreducens,* respectively, were utilized to investigate differences in the adsorption efficiency and capacity towards heavy metal contaminants. For this, Cadmium (Cd^{2+}) and (Cu^{2+}) were selected, two relevant metals that are increasingly introduced to the environment due to agriculture (Cd^{2+})[18, 19] and viticulture (Cu^{2+})[20].

It could be demonstrated for both metals, that a greater amount was adsorbed at elevated pH values, presumably due to a less positively charged mineral surface at

increased pH values[21, 22]. For example, additional 330 µmol Cd/g Fe were adsorbed on reduced magnetite nanoparticles at pH 7.3 compared to pH 5.5. Furthermore, 280 µmol Cd/g Fe more were removed by reduced magnetite nanoparticles compared to the oxidized counterpart at pH 7.3. These results showed that the stoichiometry, and therefore the redox state[23], of magnetite nanoparticles greatly influences the adsorption interactions with contaminants (**Chapter 3**).

Lastly, the aggregation of magnetite nanoparticles derived from abiotic synthesis and from dissimilatory Fe(III) reduction of ferrihydrite by *G. sulfurreducens* was investigated. The particle aggregation could play a crucial role for the bioavailability of magnetite to Fe-metabolizing microorganisms and greatly influencing adsorption properties due to the loss of (reactive) surface area[24]. It was revealed that biogenic magnetite nanoparticles tend to form larger aggregates compared to abiotic magnetite at the same concentrations. Abiotic magnetite also formed more compact particles. These findings suggest that biotic magnetite, despite undergoing washing steps, showed increased aggregation and less compaction due to the presence of associated biomass (**Chapter 4**). Therefore, depending on the type of associated biomass, magnetite biogeobattery cycling and adsorption interactions could be improved or deteriorated.

Here, these findings, potential future experiments, and proposed outcomes are discussed.

5.1 Is magnetite a biogeobattery in consecutive redox cycles indefinitely?

Research on the long-term effects of the magnetite biogeobattery are scarce. It is therefore considered prudent to conduct further studies to gain a better understanding of the durability and about potential environmental implications of (magnetite) biogeobatteries. This PhD work presents the first study that investigated the consequences on magnetite when serving as a biogeobattery for two full redox cycles over 41 days by nitrate-reducing Fe(II)-oxidizing culture KS and Fe(III)-reducing *G. sulfurreducens* in non-suspension experiments. In environments with changing redox conditions (i.e. fluctuations in the water table that result in a shift between oxidizing and reducing conditions), it is possible that magnetite is cycled continuously. Magnetic susceptibility profiles were collected from cores taken from a rice paddy field in Vercelli, Italy, and from a soil located near Bebenhausen in the Schönbuch forest, Tübingen. The profiles consistently showed a peak of magnetic susceptibility between 2 to 10 cm, representing the layer of active magnetite biogeobattery cycling, if the core responded to magnetic susceptibility measurements (see also Figure 3 in Chapter 1).

The results presented in this work suggest that magnetite cycling as a biogeobattery will lead to mineral loss due to reductive dissolution during activity of *G. sulfurreducens*. This would lead to a depletion of magnetite, which would essentially represent the loss of the entire magnetite biogeobattery system. The influence of the specific lengths of individual redox cycles should be further investigated. Shortening the reduction period in lab experiments, which corresponds to briefer periods of water logging and reduced redox potential in the environment, may decrease or even mitigate the reductive dissolution of magnetite. On the other hand, prolonged oxidation might cause surface passivation due to maghemitization[1, 7].

Lastly, Byrne et al (2016)[7] demonstrated that magnetite-biogeobattery-properties could be altered by changes in particle size of the magnetite mineral due to size-dependent oxidation/reduction processes and therefore implications of different particle sizes on the biogeobattery process need to be investigated.

Therefore, the following open research questions remain:

(1) For how many redox cycles can magnetite (nanoparticles) serve as a biogeobattery?

The here presented work suggests that magnetite nanoparticles will not serve as a biogeobattery indefinitely, as reductive dissolution followed by re-precipitation to secondary Fe(II) minerals like vivianite occurred.

(2) How does the particle size affect the biogeobattery properties and the possible number of redox cycles?

Previous work investigated the impact on particle size of magnetite on microbially mediated redox reactions with the mineral. However, it was so far not investigated how the particle size will influence consecutive redox cycles.

(3) What are the ultimate consequences for the mineral during continued redox cycles?

The presented work showed for the first-time extensive dissolution of magnetite nanoparticles during Fe-redox reactions in a biogeobattery redox cycling setting. Our data suggest that magnetite nanoparticles will eventually dissolve when exposed to continued reduction by *G. sulfurreducens,* therefore leading to a complete mineral transformation. Additionally, surface passivation due to maghemitization could lead to loss of reactive surface are and decrease the biogeobattery capacities of magnetite (now maghemite γ-Fe_2O_3).

A series of laboratory experiments should be conducted to investigate individual factors that impact the magnetite biogeobattery.
By performing selected experiments batch incubation experiments with magnetite of different particle sizes as electron source and sink for Fe-metabolizing microorganisms, after careful determination of the different properties (crystallinity, aggregation, redox potential), the differences caused by particle size could be determined (**Figure 1**). To remain consistent with the here presented work and the previously reported data[7] magnetite nanoparticles should be precipitated by the well-

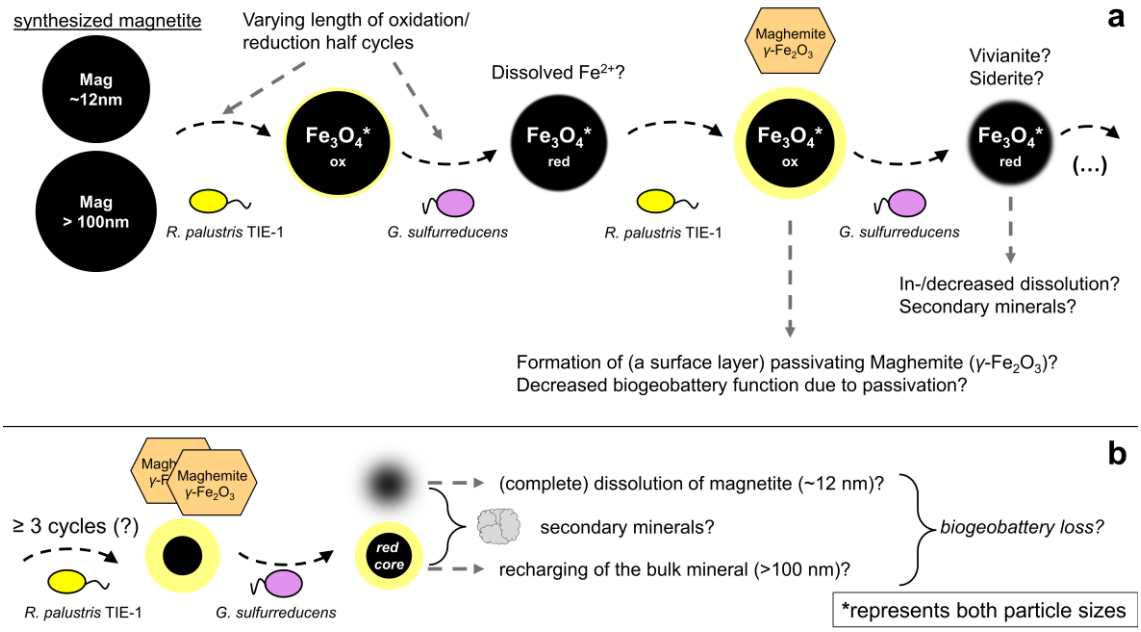

Figure 1. Proposed mechanism during long term incubation of magnetite particles as biogeobatteries. *In the presented work we have demonstrated that magnetite nanoparticles will be dissolved during reduction phases that lasted for more than 5 days. Here we propose experiments that a) would be performed with synthesized magnetite nano- and microparticles in separate batch experiments. These experiments will involve varying lengths of oxidation and reduction half-cycles. The differences in particle size are suggested to lead to great differences during the redox cycles. b) Namely, the formation of a passivating surface layer of maghemite (large particles) and the reductive dissolution followed by reprecipitation of secondary Fe(II) minerals (small & large particles), when performing experiments for ≥3 redox cycles. The ability of Fe(III)-reducing microorganisms to induce electron hopping throughout the magnetite crystal lattice could allow continued reduction of larger particles that display a maghemite surface layer. Combining the different types of particles sizes with different incubation periods for redox cycles would therefore yield great insights into the biogeobattery mechanisms of magnetite.*

established protocols that yield sizes of about 12 nm diameter[13] and 100~200 nm diameter[25]. Firstly, *R. palustris* TIE-1 could be utilized as Fe(II)-oxidizer.

Since culture KS must be grown with Fe(II)/Fe^{2+} and washing cells w stopped Fe(II) oxidation of the thereafter transferred culture (unpublished data), introduction of an

additional Fe(III) could not be avoided. Therefore, to minimise the influencing factors, *R. palustris* TIE-1 could be pre-cultivated on sodium acetate, which was shown to be a suitable electron donor[26]. The redox cycling should then be repeated for ≥3 cycles to unravel the long-term properties of the magnetite biogeobatteries and differences caused by particle size. These experiments will reveal how long-term redox cycling will change the mineral identity, stoichiometry, composition, and crystallinity.

Preliminary experiments could be performed by tracking only the relative changes in magnetic susceptibility, as these measurements are quick and no sample removal is necessary[27]. Therefore, first results that give insights on the length of redox cycles could be obtained i) by allowing one set of replicates to be oxidized/reduced until no more changes of magnetic susceptibility occur and ii) by pre-determining the length of redox cycles for another set of replicates. For detailed investigations, the mineralogical changes could be traced with ^{57}Fe Mössbauer spectroscopy, with an emphasize for measurements at 140 K, targeting magnetite. These results will reveal the changes induced by the redox cycles and differences due to incubation times and particles sizes. To identify secondary products, ^{57}Fe Mössbauer profiles down to 5 K could be performed , which will allow to also identify low amorphous ferrihydrite[28]. Additionally, X-ray diffractometry ([µ-]XRD) for additional mineralogical identification and determination of lattice parameters[29] could be utilized. During further experiments, that need to include regular geochemical sampling, detailed measurements like ferrozine[30] for determination of aqueous and solid Fe concentrations, scanning electron microscopy for morphological information of microbial cells and minerals, transmission electron microscopy for small scale mineralogical information and particle associations, and X-ray magnetic circular dichroism (XMCD) for a more surface sensitive analysis of the particles are needed.

The following hypotheses are expected results, however high dependence on the biogeochemical settings must be considered for interpretation of results:

- The magnetite biogeobattery cannot serve indefinitely as a biogeobattery for Fe-metabolizing microorganisms.

- Depending on the particle size and length of redox incubation periods, magnetite can function as electron donor and acceptor for a varying number of

redox cycles. For smaller particles, reductive dissolution can shorten the availability of magnetite as a biogeobattery, while larger particles may undergo surface passivation due to maghemitization, which would change surface properties but potentially not stop electron transfer by Fe(III)-reducing microorganisms.

- Reductive dissolution will initiate precipitation of secondary Fe(II) minerals. The Fe(II) oxidation will ultimately lead to a mineral transformation of the magnetite particles to maghemite, either as a surface or bulk process, and possibly oxidize the previously precipitated secondary Fe(II) minerals. These newly formed products will decrease biogeobattery interactions of remaining magnetite particles or even lead to the complete loss of it.

5.2 Magnetite as a sustainable agent for nitrate removal

This work described oxidation of magnetite coupled to nitrate reduction by the autotrophic enrichment culture “culture KS” which was then also utilized to produce bioengineered oxidized magnetite for the removal of heavy metals from solution. This nitrate-reducing Fe-oxidizing (NRFeOx) mechanism could be utilized for the efficient and sustainable removal of nitrate, which is found in increasing concentrations in water bodies, including wastewater treatment plants, due to increased use of N-fertilization for food production[31, 32]. During magnetite oxidation, nitrate is reduced to harmless dinitrogen gas (N_2) which will be released into the atmosphere. The feasibility of this process is supported by research that demonstrated the abundance of nitrate reducing Fe(II)-oxidizing microorganisms like *Acidovorax* sp. Strains 2AN and BoFeN1, *Paracoccus denitrificans* Pd 1222 and *Pseudogulbenkiania* sp. Strain 2022[33]. In comparison to the autotrophic culture KS, these organisms could not undoubtedly be cultivated without an additional source of organic carbon. As this additional carbon may interfere with the biogeobattery nitrate removal interactions, autotrophic microorganisms should preferentially be utilized, as they do not require an additional carbon source. If NRFeOx microorganisms can access the electrons of magnetite particles, and therefore using it in the sense of a biogeobattery when coupled with Fe(III)-reducers, this would open the possibility to use magnetite as sustainable agent for the removal of nitrate[34]. The demonstration of nitrate reduction coupled to magnetite oxidation by yet another autotrophic NRFeOx enrichment culture, culture AG[17] (Figure 2, unpublished data) suggests likelihood of this mechanism.

The following open questions remain:

(1) Is the utilization of the magnetite biogeobattery concept feasible for the purpose of coupling NRFeOx with Fe(III) reduction to achieve prolonged nitrate removal?

Since the redox potential of magnetite can be in a range of ~ –500 to +500 mV[35], depending on the Fe(II)/Fe(III)[23] or incorporation of foreign divalent ions[36] , it should allow the coupling to nitrate reduction with a redox potential of approx. 0.4 mV[37]. Thermodynamically, the coupling of the here presented microbially reduced magnetite nanoparticles would become increasingly beneficial with additional reduction and

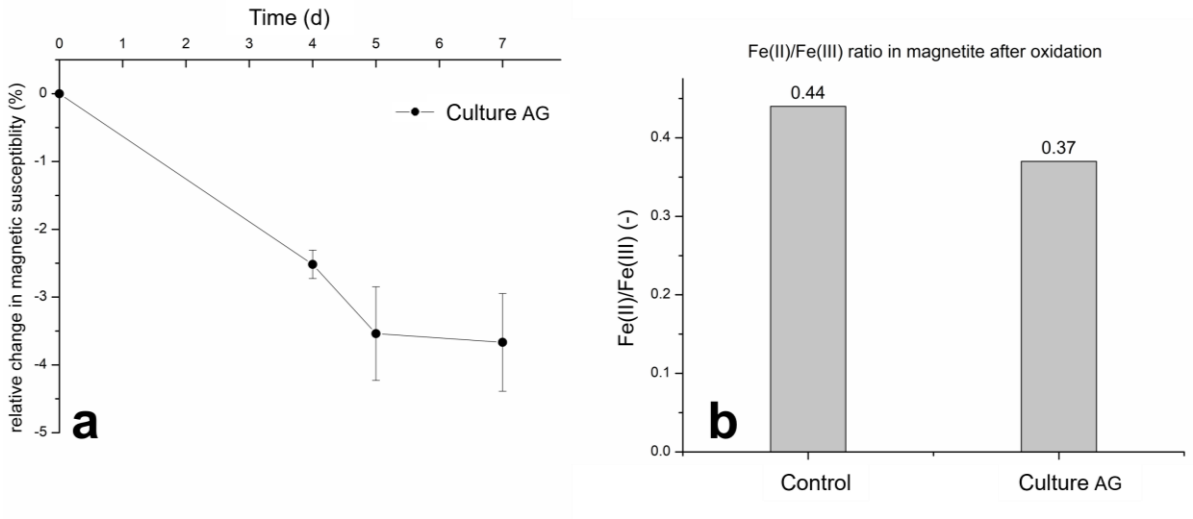

Figure 2. Magnetic susceptibility changes and stoichiometry of magnetite nanoparticles incubated with nitrate-reducing Fe(II)-oxidizing "culture AG". a) *Relative decrease in magnetic susceptibility over time and b) decrease in the Fe(II)/Fe(III) ratio determined by the ferrozine assay, indicated successful oxidation of magnetite nanoparticles by culture AG.*

would even be feasible with oxidized magnetite nanoparticles: We calculated redox potentials of -0.12 V for microbially oxidized and -0.54 V for microbially reduced magnetite nanoparticles (Chapter 3). Therefore, prolonged nitrate reduction should be achievable by re-charging magnetite with electrons through the activity of Fe(III)-reducers such as *Geobacter* or *Shewanella*.

(2) Can magnetite (nano)particles be applied as a sustainable biogeobattery for nitrate decontamination by (autotrophic) NRFeOx?

We confirmed the magnetite oxidation of the autotrophic NRFeOx culture KS and culture AG[38, 39]. The benefit of autotrophic NRFeOx is the possibility to be active in oligotrophic environments low in organic carbon and could therefore be applied in organic carbon poor groundwaters or in wastewater treatment plants after carbon removal. Additionally, low amounts of C_{org} would prevent carbon-magnetite interactions, that could influence the biogeobattery-redox reactions[8, 40].

With the knowledge gained from previously suggested research (see Figure 1) the oxidation/reduction phases could be optimized to allow maximal nitrate removal and lifetime of the magnetite biogeobattery. Additionally, when the capacity of cycled

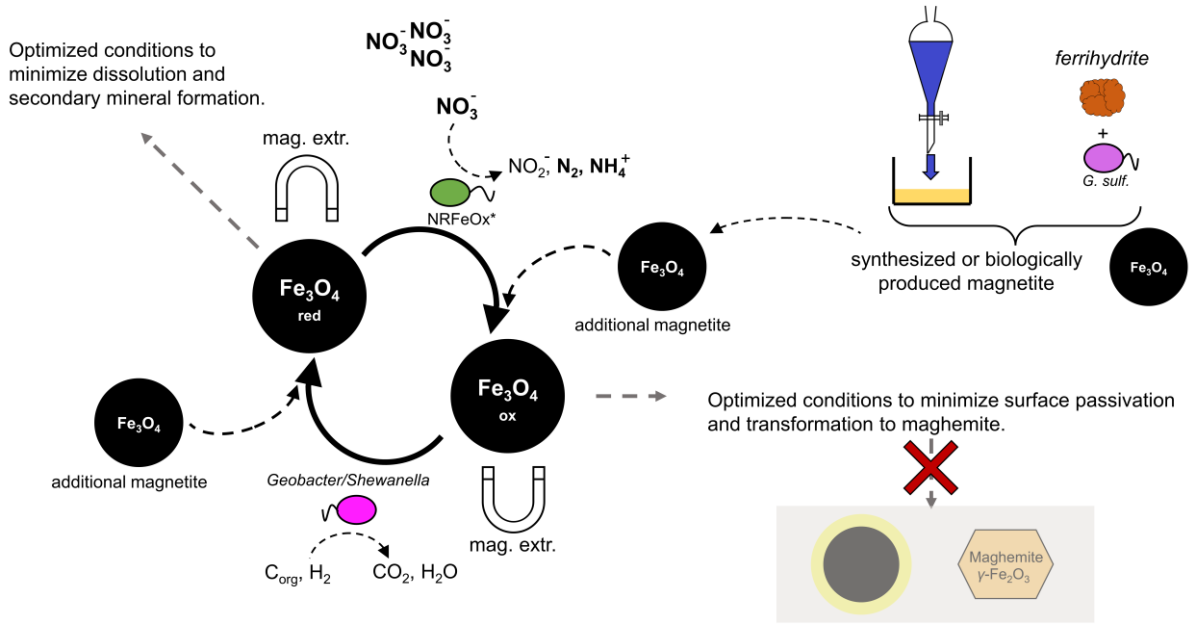

Figure 3. Nitrate removal with help of the magnetite biogeobattery. *Nitrate-reducing Fe(II)-oxidizing NRFeOx microorganisms (i.e. culture KS, culture AG) can use magnetite (Fe_3O_4) as an electron acceptor to reduce nitrate to dinitrogen gas (N_2) or ammonia (NH_4^+). The magnetite biogeobattery can thereafter be recharged by Fe(III)-reducing organisms. The optimized biogeobattery-cycling can help to maintain integrity of magnetite particles due to minimizing oxidation to maghemite and reductive dissolution processes. Additional magnetite, from abiotic or biogenic origins, could be introduced during or after reduction/oxidation phases to improve the rates and extend of nitrate removal. Additionally, magnetite can be magnetically extracted (mag. extr.) before/after oxidations/reductions or before introduction of new magnetite particles.*

magnetite particles to act as electron source or sink decreases, amendment of additional magnetite could increase the biogeobattery capacities again.

This additional magnetite could be of abiotic origin (chemically synthesized or commercially available) or produced due to the activity of Fe-metabolizing microorganisms (Figure 3).

By following the N-speciation during incubation experiments from NO_3^- to N_2/NH_4^+ (with intermediates NO_2^-, NO, and N_2O[14, 41, 42]) with continuous flow analysis for dissolved

species or with gas chromatography for gaseous phases, the nitrate removal capacity with help of the magnetite biogeobattery could be revealed.

When autotrophic NRFeOX enrichment cultures (i.e. culture KS or culture AG) are utilized for the nitrate removal, following changes of the microbial community could reveal changes in the community composition in order to adapt to magnetite oxidation. *Gallionellaceae* spp[39, 43]. are expected to dominate the community composition with 16S r-NA analysis during NRFeOx with magnetite as electron acceptor. However, a change in the community composition due to extended incubation with magnetite could be revealed.

The following hypotheses are expected due to the results presented in this PhD work, they are however highly dependent on the biogeochemical settings and need to be demonstrated by experimental work:

(1) The magnetite biogeobattery will allow nitrate removal in consecutive redox cycles.

(2) Autotrophic NRFeOx should be preferred for nitrate removal due to decreased influences of biomass, which is needed for growth of heterotrophic NRFeOx microorganisms.

(3) Even in optimized conditions (pH, temperature, particle size, time periods for oxidation/reduction) the magnetite biogeobattery will eventually be consumed and must be re-supplied by addition of more magnetite.

(4) Autotrophic NRFeOx cultures will enrich in *Gallionellacea* spp. when utilized for nitrate removal by magnetite oxidation.

5.3 Is the magnetite biogeobattery a sustainable solution for heavy metal remediation from contaminated water and soil?

As presented in Chapter 3 of this work, the redox cycling of magnetite can have great impacts on the adsorption of contaminants found in waters (like rivers and wastewater) and soils (agricultural or viticultural). Just like the increased nitrate concentrations due to N-fertilization of food crops, heavy metal concentrations continuously increased in the recent decades. Magnetite nanoparticles could help improving water quality in wastewater treatment plants or in soils by interacting with these compounds. This work has shown that the change in Fe(II)/Fe(III) in magnetite will greatly influence adsorption of heavy metals onto magnetite nanoparticles.
Redox modification of the magnetite biogeobattery can therefore increase water and soil quality, and allow magnetic recovery of these compounds, which might even be used for further processes[44].

Concerning the application of magnetite and its redox properties for the remediation of heavy metals the open research questions are:

(1) How will redox cycling of magnetite influence the interactions with previously adsorbed compounds?

Magnetite has been shown to interact with contaminants due to adsorption and reduction mechanisms[45-47]. As demonstrated in this work, the adsorption capacity for the heavy metals Cu^{2+} and Cd^{2+} greatly differed depending on the redox state (Fe(II)/Fe(III) ratio) of the magnetite nanoparticles. This suggests that ions in solution will compete for available adsorption sites on the mineral[6] depending on the Fe(II)/Fe(III) in magnetite and surface attraction will change with redox and pH changes.
Looking into a singular compound specifically (i.e. Cd^{2+}, see Chapter 3), a change from reduced to oxidized magnetite (due to i.e. NRFeOx, Figure 3) would lead to a release of between approximately 60 to 280 µmol Cd/g Fe, which corresponds to 6.7 to 31 mg Cd/g Fe. Since Cadmium is toxic in low concentrations[48], oxidation of cadmium loaded

magnetite must be avoided in the environment, or could be utilized for cadmium recovery.

(2) Can adsorbed compounds be recovered while preserving magnetite for further utilization as adsorbing agent?

After magnetic extraction, changes in redox and pH, which can decrease the surface affinity of contaminants towards magnetite, could be applied to release and recover the previously adsorbed compounds. Additionally, magnetite could be treated with strong chelating agents such as EDTA[49] for competitive removal of the adsorbed compounds. The solubilized compounds could then be easily separated from the magnetite by filtration, centrifugation, and decanting while magnetically withholding the magnetite particles. The magnetite particles would not have to be treated anoxically, as atmospheric magnetite oxidation could be neglected[50] for this recovery process. Additionally, minor oxidation to maghemite could possibly be irrelevant for further redox interactions of the magnetite particles (Figure 1).

(3) Could magnetite particles be biomodified to selectively target specific compounds?

Selective targeting of specific compounds would be desirable, especially for targeting the most toxic compounds or the compound with the highest return value, like rare earth elements. However, complex aqueous solutions in wastewater treatment plants or complex environmental interactions in soils will make it very difficult to achieve this. As tuning magnetite towards one specific compound likely results in additional affinity towards further compounds, and fine tuning likely requires more effort than profit.
Alternatively, magnetite could be applied in heavily contaminated field sites where specific compounds are targeted, put simply, because they are most abundant. Examples of this could be the high concentration of arsenic in the groundwater in Vietnam[51, 52], cadmium contaminated agricultural soils due to Cd-containing PO_4^{3-} fertilizers[18], or copper contaminated orchards and vineyards due to Cu-containing fungicides[20].
Preliminary results (data not published) of copper-enriched vineyard soils collected from Wurmlingen, Tübingen, showed that the amount of Cu^{2+} extracted in two hours

was decreased by 25 mg/kg, 0.98 mg/kg, 0.37 mg/kg, 0.5 mg/kg for extractions performed with EDTA, citric acid, malic acid, and artificial rainwater, respectively, when soil was amended with not redox modified magnetite nanoparticles. These results suggest that synthesized magnetite nanoparticles will adsorb contaminants even in complex environmental systems like a vineyard soil, and combination with results of Chapter 3 would suggest that a change of the redox potential of magnetite (Fe(II)/Fe(III)) ratio might further increase this removal.

Small scale adsorption experiments with different types biomodified magnetite (oxidized/reduced for 1/2/3 redox cycles) particles with individual compounds will reveal the individual adsorption affinities. Mineralogical techniques (Mössbauer, [μ-]XRD) will reveal changes to the mineral identity, crystallinity, and stoichiometry. Synchrotron based techniques like X-ray adsorption spectroscopy (XAS), X-ray adsorption near edge spectroscopy (XANES) and extended X-ray adsorption fine structure (EXAFS) could be utilized to understand if the contaminant is incorporated into the magnetite or adsorbed at the surface, for the Fe-redox state of the mineral, and for understanding the binding environment of the contaminant and the magnetite particles, respectively. The determination of dissolved and magnetite associated contaminant concentrations by spectroscopic methods like MP-AES (Microwave Plasma Atomic Emission Spectroscopy) or ICP-OES (Inductively Coupled Plasma Optical Emission Spectroscopy) will allow to understand the adsorption mechanisms and reveal the differences caused by redox cycling.

The hypotheses are:

(1) Redox cycling of magnetite will have significant influences on the adsorption of contaminants and nutrients.
- Previously surface associated compounds could be released due to change in redox potential and adsorption of further compounds might be dampened due to a combination of unfavourable pH and redox values.

(2) After magnetic extraction from water/soil, the associated contaminants can be removed due to competition with chelating/complexing agents and redox or pH

changes. Magnetite particles can then be re-utilized for further redox-driving remediation cycles.

- If the compounds can not be removed from the surface, magnetite can be dissolved in acidic solutions and the surface associated compounds recovered.

(3) (Bio)modification of magnetite to target certain compounds is a tedious process with minor returning benefits. “Targeting” compounds by utilizing magnetite in highly contaminated sites increases removal efficiency.

Lastly, the described adsorption processes could also be investigated for nutrients like phosphate or sulfate, as these anions can also be adsorbed by the surface are of magnetite particles[6].

5.4 How does organic matter influence the magnetite biogeobattery?

Natural organic matter (NOM) is omnipresent in the environment[53], stemming from decaying plants and animals, from microbiological sources when cells reach the end of their life span, or from human sources. Different types of natural organic matter will interact with the surface of magnetite and with the contaminants via their functional groups[54]. Exemplary compounds of NOM are humic acids (HS)[55]. These commonly contain quinone, phenol, and catechol moieties or carboxyl groups[35]. Therefore, the interactions of NOM with magnetite will influence the biogeobattery redox cycling (Fe bioavailability for Fe-metabolizing microbes) and the interactions of contaminants with the magnetite's surface, possibly de-/increasing the adsorption. Organic matter itself can inherit biogeobattery properties (storing or transferring electrons)[56, 57], emphasizing the importance of the possible synergistic or antagonistic interactions with the magnetite biogeobattery.

Open research questions are:

(1) Will NOM enhance or hinder the redox processes of the magnetite biogeobattery?

It was shown that NOM can influence the electron redox interactions of Fe minerals due to the presence of electron accepting/donating moieties[35] . Humic compounds were shown to reduce Fe(III) and to reduce magnetite in laboratory experiments[8, 55]. Therefore, interactions of NOM during magnetite biogeobattery cycling could have either beneficial or non-favourable consequences on the redox cycling of magnetite and the adsorption of heavy metals/nutrients.

Additionally, NOM can block surface sites that would otherwise be available for contaminant/nutrient adsorption. However, if the NOM itself has surface sites that can complex/chelate or adsorb compounds, the total removal from solution might stay the same or even increase. If the only NOM interaction is coverage of adsorption surface sites, the removal of heavy metals will decrease. Similarly, if NOM contains charged moieties, they will either repel or attract ions in solution due to same or opposite charge and electrostatic interactions.

Additionally, NOM will influence the particle aggregation of the magnetite particles. In chapter 4 it was shown that biogenic magnetite particles (from ferrihydrite reduction by *G. sulfurreducens*) formed larger, less compacted, particles. Therefore, NOM interacting with magnetite could furthermore increase the adsorption capacity due to increased surface area and less compaction.

To further understand the consequences NOM can have on the redox and adsorption properties of the magnetite biogeobattery, the following experimental procedures are proposed:

(1) Evaluate magnetite biogeobattery cycling in the presence of NOM.

For this purpose, well characterized humic acids that are commercially available from the *International Humic Substance Society* can be utilized. After an equilibration phase of 24 hours for magnetite (nano)particles and humic acid mixture, excess humic acids (i.e. not associated with the surface of magnetite) should be separated from the particles by gentle washing while withholding the magnetite with a strong bar magnet during decanting. Afterwards, the previously suggested experiments (Figure 1) could be repeated in a comparative manner, which then allows for understanding the changes that were caused by addition of NOM.
Control experiments without humic acids need to be performed to fully understand the impact of the additional organic matter. Tracing of dissolved organic and inorganic carbon throughout the experiment will give an indication of the dis-/association of NOM and magnetite throughout the redox cycling. Finally, changes of the composition of NOM should be followed via HPLC and possibly gas formation via GC.

(2) Isotherm and kinetic adsorption experiments with redox cycled NOM-magnetite and compounds of interest.

Previously described adsorption reactions should be repeated with oxidized/reduced NOM-magnetite to investigate the influence of additional NOM.

The following hypotheses are postulated:

(1) NOM will influence the redox reactions of magnetite and Fe-metabolizing microorganisms. Increasing the redox extend if the NOM can help in extracellular electron transport between the minerals and cells but decreasing it if the hinder electron transfer between minerals and cells.

(2) Charged NOM decreases the adsorption capacity and efficiency of redox modified magnetite if a) the NOM displays the same charge as dissolved ions due to electrostatic repulsion b) it covers surface adsorption sites of the mineral. However, NOM might increase adsorption capacity and efficiency if they display opposite charge of the dissolved species (electrostatic attraction) and if they offer new adsorption, complexation, or chelating moieties that will interacting with contaminants or nutrients.

Finally, the here described experiments could be repeated for biologically formed magnetite nanoparticles (biologically induced or biologically controlled mineralization). Magnetite through biologically induced mineralization will be naturally associated with more natural organic matter than biologically controlled mineralized magnetize, and could therefore be studied to further understand the influences of NOM.

5.5 Magnetosomes of magnetotactic bacteria are magnetite biogeobatteries

Magnetotactic bacteria are prokaryotes that can form single domain magnetite particles inside of the cell, the so called magnetosomes[58]. This process is genetically controlled to optimize magnetic properties of the formed magnetite or greigite ($Fe(II)Fe(III)S_4$[59]) crystals. Magnetosomes are formed in vesicle-like compartments[60] which align themselves due to magnetic moments, helping to navigate along the earth magnetic field to find the optimal biogeochemical conditions[59]. After the cells decay, magnetosomes are a source of magnetite (or greigite) for the sediments and soils of MTB habitats. Here, the magnetosomes could possibly serve as a biogeobattery. Additionally, magnetosomes can be preserved in these environments and act as magnetofossils[61]. Due to the widespread presence of MTB, the utilization of magnetosomes by Fe-metabolizing microorganisms seems feasible. Additionally, the use of magnetosomes as an internal biogeobattery to store electrons for MTB themselves was discussed[62, 63].

Therefore, the following research questions remain:

(1) Can MTB use magnetosomes as an internal biogeobattery?

The storage of electrons, that are later used in favourable redox conditions as electron source, could allow MTB the utilization of magnetosomes as biogeobatteries. Cultivation of MTB in different redox conditions, followed by extraction of magnetosomes and analysis of their redox properties, will give insights into the possibility of MTB using the magnetosomes as an intracellular electron storage. Investigating of magnetosomes collected from MTB at specific redox conditions could display a linear relationship between redox potential and Fe(II)/Fe(III) ratio in magnetosomes, similarly as previously described for magnetite particles[23].

(2) Do magnetosomes act as a (magnetite/greigite) biogeobattery for Fe-metabolizing bacteria and can they remediate soils by binding nutrients and contaminants?

Magnetosome collected from scaled up growth vessels like fermenters[64] or continuous flow systems[65] could provide sufficient amounts to study the redox cycling of magnetite (greigite) by Fe-metabolizing bacteria as described in this work (Chapter 2; Figure 1). Differences between abiogenic or biotic particles as biogeobatteries, as previously discussed, could show an importance of magnetosomes as biogeobatteries, or disprove their importance. For the investigation of magnetite particles derived from magnetosomes as internal biogeobatteries, high resolution techniques like TEM in combination with EELS (electron energy loss spectroscopy), ^{57}Fe Mössbauer spectroscopy, and synchrotron-based analysis will help to answer the questions.

This research might ultimately allow for the determination of the environmental relevance of the magnetosome biogeobattery.

Thy hypotheses are:

(1) As no researched so far has shown that magnetosomes can act as electron storage in MTB it is unlikely that they serve as an intracellular biogeobattery – which however would make the discovery of this process even more important.

(2) Omnipresent magnetosomes can be used by Fe-metabolizing bacteria similarly to the abiogenic biogeobattery and will interact with contaminants/nutrients in the environment.

5.6 Further mechanism of the magnetite biogeobattery

The redox storing and transporting mechanisms of magnetite could be applied to achieve novel remediation methods. Previously described application of NRFeOx microorganisms could be coupled to Fe-ammox through (direct) inter-species electron transfer ([D]IET) that allows electron exchange across larger distances through the natural conductivity of e.g. magnetite. It was described, that the extracellular electron transfer mechanisms between microorganisms and minerals are mediated by molecules like c-type cytochromes and microbial nanowires[66]. It was demonstrated that magnetite could allow electron flow between species, i.e. the coupling of magnetite-reducing methane-oxidizers to denitrifying microorganisms[67] and methanogens that obtain electrons from magnetite after it was reduced by *Geobacter*[68]. Fe-ammox (iron-reducing anaerobic oxidation of ammonium)[69] is a process that couples the nitrogen and Fe cycles, and is suggested, like NRFeOx, to possibly be performed autotrophic[70]. Possibly, NRFeOx could be coupled to Fe-ammox with the help of the biogeobattery through an electron transfer through space and electron storage through time. While nitrite (NO_2^-) might abiotically oxidize magnetite and other present Fe(oxyhydr)oxides[71-74], ammonia produced during NRFeOx and nitrite produced during Fe-ammox might be used as a educt for the reaction of the DIET partner, suggesting improved nitrate and ammonium removal (Figure 4).

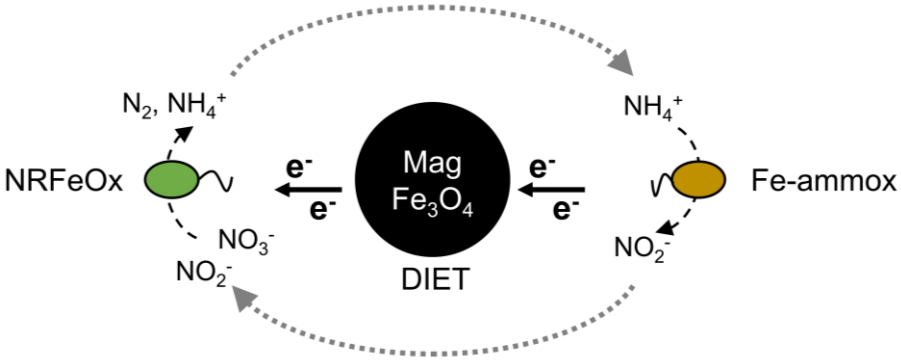

Figure 4. Nitrate-reducing Fe(II) oxidation (NRFeOx) coupled to Fe-reducing ammonium oxidation (Fe-ammox) by magnetite via DIET. *The Fe and nitrogen cycle could be closely linked through the magnetite biogeobattery by transferring electrons from ammonium oxidation coupled to Fe(III) reduction, to nitrate-reducing Fe(II) oxidation.*

5.7 References

1. Peterson, M. L.; White, A. F.; Brown, G. E.; Parks, G. A. Surface passivation of magnetite by reaction with aqueous Cr (VI): XAFS and TEM results. *Environ. Sci. Technol.* **1997**, *31* (5), 1573-1576.
2. Maher, B. A.; Taylor, R. M. Formation of ultrafine-grained magnetite in soils. *Nat.* **1988**, *336* (6197), 368.
3. Byrne, J. M.; Klueglein, N.; Pearce, C.; Rosso, K. M.; Appel, E.; Kappler, A. Redox cycling of Fe(II) and Fe(III) in magnetite by Fe-metabolizing bacteria. *Sci.* **2015**, *347* (6229), 1473-1476.
4. Dippon, U.; Pantke, C.; Porsch, K.; Larese-Casanova, P.; Kappler, A. Potential function of added minerals as nucleation sites and effect of humic substances on mineral formation by the nitrate-reducing Fe (II)-oxidizer Acidovorax sp. BoFeN1. *Environ. Sci. Technol.* **2012**, *46* (12), 6556-6565.
5. Dippon, U.; Schmidt, C.; Behrens, S.; Kappler, A. Secondary Mineral Formation During Ferrihydrite Reduction by Shewanella oneidensis MR-1 Depends on Incubation Vessel Orientation and Resulting Gradients of Cells, Fe^{2+} and Fe Minerals. *Geomicrobiol. J.* **2015**, *32* (10), 878-889.
6. Cornell, R. M.; Schwertmann, U. *The iron oxides: structure, properties, reactions, occurrences and uses*; John Wiley & Sons, 2003.
7. Byrne, J. M.; van der Laan, G.; Figueroa, A. I.; Qafoku, O.; Wang, C.; Pearce, C. I.; Jackson, M.; Feinberg, J.; Rosso, K. M.; Kappler, A. Size dependent microbial oxidation and reduction of magnetite nano- and micro-particles. *Sci. Rep.* **2016**, *6*, 30969.
8. Sundman, A.; Byrne, J. M.; Bauer, I.; Menguy, N.; Kappler, A. Interactions between magnetite and humic substances: redox reactions and dissolution processes. *Geochem. Trans.* **2017**, *18* (1), 1-12.
9. Sorwat, J.; Mellage, A.; Kappler, A.; Byrne, J. M. Immobilizing magnetite onto quartz sand for chromium remediation. *J. Hazard. Mater.* **2020**, *400*, 123139.
10. Sorwat, J.; Mellage, A.; Maisch, M.; Kappler, A.; Cirpka, O. A.; Byrne, J. M. Chromium (VI) removal kinetics by magnetite-coated sand: small-scale flow-through column experiments. *J. Hazard. Mater.* **2021**, *415*, 125648.
11. Bartzas, G.; Komnitsas, K. Solid phase studies and geochemical modelling of low-cost permeable reactive barriers. *J. Hazard. Mater.* **2010**, *183* (1), 301-308.
12. Zhang, Y.; Xu, S.; Luo, Y.; Pan, S.; Ding, H.; Li, G. Synthesis of mesoporous carbon capsules encapsulated with magnetite nanoparticles and their application in wastewater treatment. *J. Mater. Chem.* **2011**, *21* (11), 3664-3671.
13. Pearce, C. I.; Qafoku, O.; Liu, J.; Arenholz, E.; Heald, S. M.; Kukkadapu, R. K.; Gorski, C. A.; Henderson, C. M. B.; Rosso, K. M. Synthesis and properties of titanomagnetite (Fe 3− xTixO 4) nanoparticles: A tunable solid-state Fe (II/III) redox system. *J. Colloid Interface Sci.* **2012**, *387* (1), 24-38.
14. Straub, K. L.; Benz, M.; Schink, B.; Widdel, F. Anaerobic, nitrate-dependent microbial oxidation of ferrous iron. *Appl. Environ. Microbiol.* **1996**, *62* (4), 1458-1460.
15. Emmerich, M.; Bhansali, A.; Lösekann-Behrens, T.; Schröder, C.; Kappler, A.; Behrens, S. Abundance, distribution, and activity of Fe(II)-oxidizing and Fe(III)-reducing microorganisms in hypersaline sediments of Lake Kasin, southern Russia. *Appl. Environ. Microbiol.* **2012**, *78* (12), 4386-4399.
16. Hafenbradl, D.; Keller, M.; Dirmeier, R.; Rachel, R.; Roßnagel, P.; Burggraf, S.; Huber, H.; Stetter, K. O. Ferroglobus placidus gen. nov., sp. nov., a novel

hyperthermophilic archaeum that oxidizes Fe2+ at neutral pH under anoxic conditions. *Arch. Microbiol.* **1996**, *166* (5), 308-314.
17. Jakus, N.; Blackwell, N.; Osenbrück, K.; Straub, D.; Byrne, J. M.; Wang, Z.; Glöckler, D.; Elsner, M.; Lueders, T.; Grathwohl, P.; et al. Nitrate removal by a novel lithoautotrophic nitrate-reducing iron(II)-oxidizing culture enriched from a pyrite-rich limestone aquifer. *Appl. Environ. Microbiol.* **2021**, *87* (16), e00460-00421.
18. Grant, C. A.; Sheppard, S. C. Fertilizer Impacts on Cadmium Availability in Agricultural Soils and Crops. *Hum. ecol. risk assess.* **2008**, *14* (2), 210-228.
19. Hutton, M. Sources of cadmium in the environment. *Ecotoxicol. Environ. Saf.* **1983**, *7* (1), 9-24.
20. Brun, L.; Maillet, J.; Hinsinger, P.; Pepin, M. Evaluation of copper availability to plants in copper-contaminated vineyard soils. *Environ. Pollut.* **2001**, *111* (2), 293-302.
21. Schwertmann, U.; Fechter, H. The Influence of Aluminum on Iron Oxides: XI. Aluminum-Substituted Maghemite in Soils and Its Formation 1. *Soil Sci. Soc. Am. J.* **1984**, *48* (6), 1462-1463.
22. Milonjić, S.; Kopečni, M.; Ilić, Z. The point of zero charge and adsorption properties of natural magnetite. *J. Radioanal. Nucl.* **1983**, *78* (1), 15-24.
23. Gorski, C. A.; Nurmi, J. T.; Tratnyek, P. G.; Hofstetter, T. B.; Scherer, M. M. Redox behavior of magnetite: Implications for contaminant reduction. *Environ. Sci. Technol.* **2010**, *44* (1), 55-60.
24. Hotze, E. M.; Phenrat, T.; Lowry, G. V. Nanoparticle aggregation: challenges to understanding transport and reactivity in the environment. *J. Environ. Qual.* **2010**, *39* (6), 1909-1924.
25. Schwertmann, U.; Cornell, R. M. *Iron oxides in the laboratory: preparation and characterization*; John Wiley & Sons, 2008.
26. Jiao, Y.; Kappler, A.; Croal, L. R.; Newman, D. K. Isolation and characterization of a genetically tractable photoautotrophic Fe(II)-oxidizing bacterium, Rhodopseudomonas palustris strain TIE-1. *Appl. Environ. Microbiol.* **2005**, *71* (8), 4487-4496.
27. Porsch, K.; Dippon, U.; Rijal, M. L.; Appel, E.; Kappler, A. In-situ magnetic susceptibility measurements as a tool to follow geomicrobiological transformation of Fe minerals. *Environ. Sci. Technol.* **2010**, *44* (10), 3846-3852.
28. Byrne, J. M.; Kappler, A. A revised analysis of ferrihydrite at liquid helium temperature using Mössbauer spectroscopy. *Am. Min.* **2022**, *107* (8), 1643-1651.
29. Patterson, A. L. The Scherrer Formula for X-Ray Particle Size Determination. *Phys. Rev.* **1939**, *56* (10), 978-982.
30. Stookey, L. L. Ferrozine - a new spectrophotometric reagent for iron. *Anal. Chem.* **1970**, *42* (7), 779-781.
31. Kim, H.; Kaown, D.; Mayer, B.; Lee, J.-Y.; Hyun, Y.; Lee, K.-K. Identifying the sources of nitrate contamination of groundwater in an agricultural area (Haean basin, Korea) using isotope and microbial community analyses. *Sci. of the tot. Environ.* **2015**, *533*, 566-575.
32. Visser, A.-N.; Lehmann, M. F.; Rügner, H.; D'Affonseca, F. M.; Grathwohl, P.; Blackwell, N.; Kappler, A.; Osenbrück, K. Fate of nitrate during groundwater recharge in a fractured karst aquifer in Southwest Germany. *Hydrogeol. J.* **2021**, *29* (3), 1153-1171.
33. Bryce, C.; Blackwell, N.; Schmidt, C.; Otte, J.; Huang, Y. M.; Kleindienst, S.; Tomaszewski, E.; Schad, M.; Warter, V.; Peng, C. Microbial anaerobic Fe(II)

oxidation–Ecology, mechanisms and environmental implications. *Env. Microbiol.* **2018**, *20* (10), 3462-3483.
34. Li, S.; Kappler, A.; Haderlein, S. B.; Zhu, Y.-G. Powering biological nitrogen removal from the environment by geobatteries. *Trends. Biotechnol.* **2022**.
35. Dong, H.; Zeng, Q.; Sheng, Y.; Chen, C.; Yu, G.; Kappler, A. Coupled iron cycling and organic matter transformation across redox interfaces. *Nat. Rev. Earth Environ.* **2023**, *4* (9), 659-673.
36. Sidhu, P.; Gilkes, R.; Posner, A. The behavior of Co, Ni, Zn, Cu, Mn, and Cr in magnetite during alteration to maghemite and hematite. *Soil Sci. Soc. Am. J.* **1980**, *44* (1), 135-138.
37. Borch, T.; Kretzschmar, R.; Kappler, A.; Cappellen, P. V.; Ginder-Vogel, M.; Voegelin, A.; Campbell, K. Biogeochemical redox processes and their impact on contaminant dynamics. *Environ. Sci. Technol.* **2009**, *44* (1), 15-23.
38. Jakus, N.; Blackwell, N.; Osenbruck, K.; Straub, D.; Byrne, J. M.; Wang, Z.; Glockler, D.; Elsner, M.; Lueders, T.; Grathwohl, P.; et al. Nitrate Removal by a Novel Lithoautotrophic Nitrate-Reducing, Iron(II)-Oxidizing Culture Enriched from a Pyrite-Rich Limestone Aquifer. *Appl. Environ. Microbiol.* **2021**, *87* (16), e00460-00421.
39. Huang, Y.-M.; Jakus, N.; Straub, D.; Konstantinidis, K. T.; Blackwell, N.; Kappler, A.; Kleindienst, S. 'Candidatus ferrigenium straubiae' sp. nov., 'Candidatus ferrigenium bremense' sp. nov., 'Candidatus ferrigenium altingense' sp. nov., are autotrophic Fe(II)-oxidizing bacteria of the family Gallionellaceae. *Syst. Appl. Microbiol.* **2022**, *45* (3), 126306.
40. Fimmen, R. L.; Cory, R. M.; Chin, Y.-P.; Trouts, T. D.; McKnight, D. M. Probing the oxidation–reduction properties of terrestrially and microbially derived dissolved organic matter. *Geochim. Cosmochim. Acta* **2007**, *71* (12), 3003-3015.
41. Canfield, D. E.; Glazer, A. N.; Falkowski, P. G. The evolution and future of Earth's nitrogen cycle. *Sci.* **2010**, *330* (6001), 192-196.
42. Tiedje, J. M. Ecology of denitrification and dissimilatory nitrate reduction to ammonium. *Biol. Anaer. Micro.* **1988**, *717*, 179-244.
43. He, S.; Tominski, C.; Kappler, A.; Behrens, S.; Roden, E. E. Metagenomic Analyses of the Autotrophic Fe(II)-Oxidizing, Nitrate-Reducing Enrichment Culture KS. *Appl. Environ. Microbiol.* **2016**, *82* (9), 2656-2668.
44. Gandarias, L.; Kimber, R. L.; Ona-Nguema, G. Environmental, biomedical, and industrial applications of biogenic magnetite nanoparticles. *Elements* **2023**, *19* (4), 228-233.
45. Scott, T.; Allen, G.; Heard, P.; Randell, M. Reduction of U (VI) to U (IV) on the surface of magnetite. *Geochim. Cosmochim. Acta* **2005**, *69* (24), 5639-5646.
46. He, Y. T.; Traina, S. J. Cr(VI) reduction and immobilization by magnetite under alkaline pH conditions: the role of passivation. *Environ. Sci. Technol.* **2005**, *39* (12), 4499-4504.
47. Crean, D. E.; Coker, V. S.; van der Laan, G.; Lloyd, J. R. Engineering Biogenic Magnetite for Sustained Cr(VI) Remediation in Flow-through Systems. *Environ. Sci. Technol.* **2012**, *46* (6), 3352-3359.
48. Young, S. D. Chemistry of heavy metals and metalloids in soils. In *Heavy metals in soils*, Springer, 2013; pp 51-95.
49. Oviedo, C.; Rodríguez, J. EDTA: the chelating agent under environmental scrutiny. *Quim. Nova* **2003**, *26*, 901-905.

50. Schwaminger, S.; Bauer, D.; Fraga-García, P.; Wagner, F.; Berensmeier, S. Oxidation of magnetite nanoparticles: impact on surface and crystal properties. *Cryst. Eng. Comm.* **2017**, *19* (2), 246-255.
51. Berg, M.; Luzi, S.; Trang, P. T. K.; Viet, P. H.; Giger, W.; Stüben, D. Arsenic removal from groundwater by household sand filters: comparative field study, model calculations, and health benefits. *Environ. Sci. Technol.* **2006**, *40* (17), 5567-5573.
52. Berg, M.; Tran, H. C.; Nguyen, T. C.; Pham, H. V.; Schertenleib, R.; Giger, W. Arsenic contamination of groundwater and drinking water in Vietnam: a human health threat. *Environ. Sci. Technol.* **2001**, *35* (13), 2621-2626.
53. LaRowe, D. E.; Van Cappellen, P. Degradation of natural organic matter: a thermodynamic analysis. *Environ. Sci. Technol.* **2011**, *75* (8), 2030-2042.
54. Sutton, R.; Sposito, G. Molecular structure in soil humic substances: the new view. *Environ. Sci. Technol.* **2005**, *39* (23), 9009-9015.
55. Sundman, A.; Vitzhum, A.-L.; Adaktylos-Surber, K.; Figueroa, A. I.; van der Laan, G.; Daus, B.; Kappler, A.; Byrne, J. M. Effect of Fe-metabolizing bacteria and humic substances on magnetite nanoparticle reactivity towards arsenic and chromium. *J. Hazard. Mater.* **2020**, 121450.
56. Sun, T.; Levin, B. D.; Guzman, J. J.; Enders, A.; Muller, D. A.; Angenent, L. T.; Lehmann, J. Rapid electron transfer by the carbon matrix in natural pyrogenic carbon. *Nat. Commun.* **2017**, *8* (1), 14873.
57. Bai, Y.; Sun, T.; Angenent, L. T.; Haderlein, S. B.; Kappler, A. Electron hopping enables rapid electron transfer between quinone-/hydroquinone-containing organic molecules in microbial iron (III) mineral reduction. *Environ. Sci. Technol.* **2020**, *54* (17), 10646-10653.
58. Faivre, D.; Schuler, D. Magnetotactic bacteria and magnetosomes. *Chem. Rev.* **2008**, *108* (11), 4875-4898.
59. Amor, M.; Tharaud, M.; Gélabert, A.; Komeili, A. Single-cell determination of iron content in magnetotactic bacteria: implications for the iron biogeochemical cycle. *Env. Microbiol.* **2020**, *22* (3), 823-831.
60. Uebe, R.; Schüler, D. Magnetosome biogenesis in magnetotactic bacteria. *Nat. Rev. Microbiol.* **2016**, *14* (10), 621.
61. Amor, M.; Wan, J.; Egli, R.; Carlut, J.; Gatel, C.; Andersen, I. M.; Snoeck, E.; Komeili, A. Key signatures of magnetofossils elucidated by mutant magnetotactic bacteria and micromagnetic calculations. *J. Geophys. Res. Solid Earth* **2022**, *127* (1), e2021JB023239.
62. Simmons, S. L.; Edwards, K. J. Geobiology of magnetotactic bacteria. In *Magnetoreception and magnetosomes in bacteria*, Springer, 2006; pp 77-102.
63. Vali, H.; Kirschvink, J. L. Observations of magnetosome organization, surface structure, and iron biomineralization of undescribed magnetic bacteria: evolutionary speculations. In *Iron biominerals*, Springer, 1991; pp 97-115.
64. Heyen, U.; Schüler, D. Growth and magnetosome formation by microaerophilic Magnetospirillum strains in an oxygen-controlled fermentor. *Appl. Microbiol. Biotechnol.* **2003**, *61* (5-6), 536-544.
65. Bayer, T.; Tomaszewski, E. J.; Bryce, C.; Kappler, A.; Byrne, J. M. Continuous cultivation of the lithoautotrophic nitrate-reducing Fe (II)-oxidizing culture KS in a chemostat bioreactor. *Env. Microbiol. Rep.* **2023**.
66. Shi, L.; Dong, H.; Reguera, G.; Beyenal, H.; Lu, A.; Liu, J.; Yu, H.-Q.; Fredrickson, J. K. Extracellular electron transfer mechanisms between microorganisms and minerals. *Nat. Rev. Microbiol.* **2016**, *14* (10), 651-662.

67. Liang, L.; Sun, C.; Jin, Z.; Wang, M.; Yu, Q.; Zhao, Z.; Zhang, Y. Magnetite-mediated electrically connected community for shortening startup of methane-dependent denitrification in a membrane biofilm reactor. *J. Chem. Eng.* **2022**, *428*, 132004.
68. Dong, G.; Chen, Y.; Yan, Z.; Zhang, J.; Ji, X.; Wang, H.; Dahlgren, R. A.; Chen, F.; Shang, X.; Chen, Z. Recent advances in the roles of minerals for enhanced microbial extracellular electron transfer. *Renew. Sustain. Energy Rev.* **2020**, *134*, 110404.
69. Clément, J.-C.; Shrestha, J.; Ehrenfeld, J. G.; Jaffé, P. R. Ammonium oxidation coupled to dissimilatory reduction of iron under anaerobic conditions in wetland soils. *Soil Biol. Biochem.* **2005**, *37* (12), 2323-2328.
70. Huang, S.; Jaffé, P. R. Isolation and characterization of an ammonium-oxidizing iron reducer: Acidimicrobiaceae sp. A6. *PLoS One* **2018**, *13* (4), e0194007.
71. Dhakal, P.; Matocha, C.; Huggins, F.; Vandiviere, M. Nitrite reactivity with magnetite. *Environ. Sci. Technol.* **2013**, *47* (12), 6206-6213.
72. Klueglein, N.; Kappler, A. Abiotic oxidation of Fe(II) by reactive nitrogen species in cultures of the nitrate-reducing Fe(II) oxidizer Acidovorax sp. BoFeN1 - questioning the existence of enzymatic Fe(II) oxidation. *Geobiol.* **2013**, *11* (2), 180-190.
73. Klueglein, N.; Picardal, F.; Zedda, M.; Zwiener, C.; Kappler, A. Oxidation of Fe(II)-EDTA by nitrite and by two nitrate-reducing Fe(II)-oxidizing Acidovorax strains. *Geobiol.* **2015**, *13* (2), 198-207.
74. Klueglein, N.; Zeitvogel, F.; Stierhof, Y. D.; Floetenmeyer, M.; Konhauser, K. O.; Kappler, A.; Obst, M. Potential role of nitrite for abiotic Fe(II) oxidation and cell encrustation during nitrate reduction by denitrifying bacteria. *Appl. Environ. Microbiol.* **2014**, *80* (3), 1051-1061.

Statement of personal contribution

The work presented in this PhD Thesis was funded by grants from the Deutsche Forschungsgemeinschaft (DFG) to Assoc. Prof. Dr. James Byrne (applicant) and Prof. Dr. Andreas Kappler (co-applicant), DFG references BY 82/2-1 and KA 1736/48-1, respectively.

The conceptual background to this project was designed by Assoc. Prof. Dr. James Byrne and Prof. Dr. Andreas Kappler. Assoc. Prof. Dr. James Byrne was the first supervisor throughout the project, and Prof. Dr. Andreas Kappler was the second supervisor. Unless stated otherwise, the experiments were conceptualized by me or together with Assoc. Prof. Dr. James Byrne and/or Prof. Dr. Andreas Kappler.

I carried out the experiments. The general discussions, analysis of the data collected, and writing of all manuscripts were performed by me and Assoc. Prof. Dr. James Byrne and Prof. Dr. Andreas Kappler; for chapter 2 in cooperation with Dr. Natalia Jakus; and for chapter 3 with Ran Wei.

Exceptions for Chapter 4: This work conceptualized by Dr. Muammar Mansor and extended to include magnetite particles after discussions with me. Discussion and analysis of the collected data for *magnetite particles* was performed by Dr. Muammar Mansor and me. All co-authors contributed for writing of the manuscript.

In detail, the contributions of people other than Assoc. Prof. Dr. James Byrne, Prof. Dr. Andreas Kappler or myself were:

Field Work. Lea Baier and Paola Hernandez helped collect soil samples from vineyards in Wurmlingen, Tübingen (48°30'21.3"N 8°58'54.4"E). The access was kindly granted by Daniel Böckle. Presented core magnetic susceptibility profiles (Figure 3 in Chapter 1) were collected by myself for soils from Bebenhausen and by Hannah Grimm for Vercelli paddy soil.

Chapter 2. Dr. Natalia Jakus performed µ-XRD measurements and helped with the data analysis and interpretation. Discussions with Jun. Prof. Dr. E. Marie Muehe improved the methodology of this work. Lars Grimm performed freeze-drying of magnetite particles and BET measurement. Dr. Bio Wan performed FTIR measurements and helped with data discussion. Franziska Schädler performed flow injection analysis (FIA) measurements for nitrate and nitrite data. Verena Nikeleit performed high-pressure liquid chromatography (HPLC) for acetate data. Dr. Jeremiah Schuster and Dr. Stefan Fischer enabled access to electron microscopy infrastructure.

All co-authors contributed to the manuscript revisions and/or wrote parts of the manuscript. Infrastructural support of this work included the Deutsche Forschungsgemeinschaft (DFG) under Germany's Excellence Strategy, cluster of Excellence EXC2124, project ID 390838134; and the Tübingen Structural Microscopy Core Facility (Funded by the Federal Ministry of Education and Research (BMBF) and the Baden-Württemberg Ministry of Science as part of the Excellence Strategy of the German Federal and State Governments).

Chapter 3. Ran Wei modelled the kinetic data and helped with data discussion. Prof. Dr**.** Adrian Mellage helped with the modelling of adsorption isotherms. Discussion with Jun. Prof. Dr. E. Marie Muehe improved the methodology of this work. Lars Grimm performed freeze-drying of magnetite particles and BET measurement. Caroline Dreher performed µ-XRD measurements and helped in discussions of the obtained data. All co-authors contributed to the manuscript revision and/or wrote parts of the manuscript. Infrastructural support of this work included the Deutsche Forschungsgemeinschaft (DFG) under Germany's Excellence Strategy, cluster of Excellence EXC2124, project ID 390838134.

Chapter 4. This work was conceptualized and written by Dr. Muammar Mansor. For the *magnetite* part, I contributed to data analysis, discussion, display, and writing. All co-authors helped by providing samples, preparing samples, and revision of the manuscript. Infrastructural support of this work included the Deutsche Forschungsgemeinschaft (DFG) under Germany's Excellence Strategy, cluster of Excellence EXC224, Project 390828134. This work was funded by the DFG Project 391977956 (SFB 1357) and KA 1736/66-1, KA 1736/51-1 and KA 1736/48-1 and Cluster of Excellence: EXC 2124: Controlling Microbes to Fight Infection, Tübingen, Germany.

I hereby state that I have not plagiarized or copied any of the text. Chapter 3 has been published in ACS Earth and Space Chemistry, and Chapter 4 has been published in Environmental Science and Technology Letters. Chapter 2 has been submitted for publication in Geo-Bio Interfaces and might be published in a slightly modified version elsewhere.

Acknowledgements

I want to thank everyone that was a part during my PhD and Tübingen time and helped me to finish this work in one way or another with: supervision, ZAG stairs and GUZ sofa coffee breaks, encouragement, tough questions, chips & beer, extended office cooking sessions, garage plum wine, trust, car repair sessions, time at or on the Neckar, Lagerfeuer, support in times of need, card and boardgames, Van-life, shelter, breakfasts, music, all-nighters, and friendship.

Danke an meine Omas, Emma Bayer und Elsbeth Franz, die immer an mich geglaubt haben, ihr fehlt uns.
Danke an meinen Opa, Ewald Franz, den stärksten und fürsorglichsten Mann.